

12

AD A 053671

DDC FILE COPY

AFGL-TR-78-0019

REENTRY DESIGN HANDBOOK FOR
SOUNDING ROCKET PAYLOADS

James V. McAnally
Carl D. Engel
Judy K. Lapointe

REMTECH, Inc.
2603 Artie Street, Suite 21
Huntsville, Alabama 35805

Final Report
May 1977 - December 1977

December 1977

Approved for public release; distribution unlimited.

DDC
MAY 9 1978
F

AIR FORCE GEOPHYSICS LABORATORY
AIR FORCE SYSTEMS COMMAND
UNITED STATES AIR FORCE
HANSCOM AFB, MASSACHUSETTS 01731

Qualified requestors may obtain additional copies from the Defense Documentation Center. All others should apply to the National Technical Information Service.

Unclassified

SECURITY CLASSIFICATION OF THIS PAGE (When Data Entered)

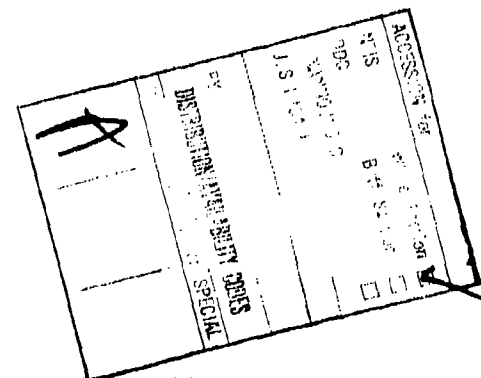
REPORT DOCUMENTATION PAGE		READ INSTRUCTIONS BEFORE COMPLETING FORM
1. REPORT NUMBER AFGL-TR-78-0019	2. GOVT ACCESSION NO.	3. RECIPIENT'S CATALOG NUMBER
4. TITLE (and Subtitle) REENTRY DESIGN HANDBOOK FOR SOUNDING ROCKET PAYLOADS		5. TYPE OF REPORT & PERIOD COVERED Final Report, Nov 1977
7. AUTHOR(s) James V. McAnally, Carl D. Engel, Judy K. Lapointe		6. PERFORMING ORG. REPORT NUMBER RTR-927-1
8. PERFORMING ORGANIZATION NAME AND ADDRESS REMTECH, Inc. 2603 Artie Street, Suite 21 Huntsville, Alabama 35805		9. CONTRACT OR GRANT NUMBER(s) F19628-77-C-0022
10. PROGRAM ELEMENT, PROJECT, TASK AREA & WORK UNIT NUMBERS PE 62101F 7659 04		11. CONTROLLING OFFICE NAME AND ADDRESS Air Force Geophysics Laboratory Monitor: E. F. McKenna/LCR Hanscom AFB, Mass. 01731
12. MONITORING AGENCY NAME & ADDRESS (if different from Controlling Office)		13. REPORT DATE Dec. 1977
		14. NUMBER OF PAGES 186 P.
		15. SECURITY CLASS. (of this report) Unclassified
		16. DECLASSIFICATION/DOWNGRADING SCHEDULE
16. DISTRIBUTION STATEMENT (of this Report) Approved for public release; distribution unlimited		
17. DISTRIBUTION STATEMENT (of the abstract entered in Block 20, if different from Report)		
18. SUPPLEMENTARY NOTES		
19. KEY WORDS (Continue on reverse side if necessary and identify by block number) Aerodynamic Coefficients Sounding Rockets Aerodynamic Heating Reentry Dynamics		
20. ABSTRACT (Continue on reverse side if necessary and identify by block number) A reentry design handbook has been developed which will assist the sounding rocket payload integration engineer in determining potential reentry dynamics and heating problems in small fineness ratio (2.5 to 7) cylinders and cone-cylinders.		

D D C
RECEIVED
MAY 9 1978
RECEIVED

41856-1

TABLE OF CONTENTS

<u>Section</u>	<u>Page</u>
ACKNOWLEDGEMENTS	v
LIST OF FIGURES	vi
LIST OF TABLES	xi
NOMENCLATURE	xii
1 INTRODUCTION	1
2 AERODYNAMIC CHARACTERISTICS	14
3 INTEGRATED HEATING LOADS	26
4 OSCILLATING AND TUMBLE CORRECTION FACTORS	43
5 SURFACE TEMPERATURE CALCULATIONS	60
6 PAYLOAD REENTRY DYNAMICS	67
7 CONVECTIVE HEATING RATES	86
8 REENTRY GUIDELINES	106
9 REFERENCES	116
 <u>Appendix</u>	
A METHODS AND PROCEDURES FOR CALCULATING AERODYNAMIC COEFFICIENTS	A1
B 6 DOF TRAJECTORY PROGRAM DESCRIPTION (Program REENTR)	B1
C REENTRY HEATING METHODOLOGY	C1
D CONDUCTION HEAT TRANSFER ANALYSIS	D1



ACKNOWLEDGEMENTS

This report was prepared under Air Force Contract F 19628-77-C-0022 by REMTECH Inc. The technical monitors for the contract were Mr. Edward McKenna and Capt. Alan Williams of the Geophysics Laboratory.

The authors wish to acknowledge D. W. Shuford and R. E. Somers for their contributions.

LIST OF FIGURES

<u>FIGURE</u>		<u>PAGE</u>
1.1	Flow diagram for handbook usage	9
2.1	Cone-cylinder configuration with cone nose bluntness	14
2.2	Volumetric C. G. location versus vehicle fineness ratio and nose bluntness ratio	18
2.3	Ratio of the planform areas of a blunt cone-cylinder geometry to that of a sharp cone-cylinder geometry	19
2.4	Aerodynamic force center versus C. G. location and fineness ratio for constant trim attitudes (Cone-cylinder configurations)	20
2.5	Drag coefficient versus trim attitude and fineness ratio for cone-cylinder configurations	22
2.6	Aerodynamic force center versus C. G. location and fineness ratio for constant trim attitudes (Cylinder configurations)	23
2.7	Drag coefficient versus trim attitude and fineness ratio for cylinder configurations	25
3.1	Heating Loads for $\alpha_T = 90^\circ$	33
3.2	Heating Loads for $\alpha_T = 100^\circ$	34
3.3	Heating Loads for $\alpha_T = 110^\circ$	35
3.4	Heating Loads for $\alpha_T = 120^\circ$	36
3.5	Heating Loads for $\alpha_T = 130^\circ$	37
3.6	Heating Loads for $\alpha_T = 140^\circ$	38
3.7	Heating Loads for $\alpha_T = 150^\circ$	39
3.8	Heating Loads for $\alpha_T = 160^\circ$	40
3.9	Heating Loads for $\alpha_T = 170^\circ$	41
3.10	Heating Loads for $\alpha_T = 180^\circ$	42

<u>FIGURE</u>		<u>PAGE</u>
4.1	Tumble correction factors, Q_t/Q_{ct} , for base and cylindrical sections of cone-cylinder configuration fineness ratio, λ/d , of 7, fwd C.G. offset, versus offset parameter, P.	46
4.2	Tumble correction factors, Q_t/Q_{ct} , for base and cylindrical sections of cone-cylinder configuration fineness ratio, λ/d , of 5, fwd C.G. offset, versus attitude offset parameter, P.	47
4.3	Tumble correction factors, Q_t/Q_{ct} , for base and cylindrical sections of cone-cylinder configuration fineness ratio, λ/d , of 4, fwd C.G. offset, versus attitude offset parameter, P.	48
4.4	Tumble correction factors, Q_t/Q_{ct} , for base and cylindrical sections of cone-cylinder configuration fineness ratio, λ/d , of 3, fwd C. G. offset, versus attitude offset parameter, P.	49
4.5	Tumble correction factors, Q_t/Q_{ct} , for base and cylindrical sections of cone cylinder configuration fineness ratio, λ/d , of 7, aft C. G. offset, versus attitude offset parameter, P.	50
4.6	Tumble correction factors, Q_t/Q_{ct} , for base and cylindrical sections of cone-cylinder configuration fineness ratio, λ/d , of 5, aft C. G. offset, versus offset parameter, P.	51
4.7	Tumble correction factors, Q_t/Q_{ct} , for base and cylindrical sections of cone-cylinder configuration fineness ratio, λ/d , of 4, aft C. G. offset, versus offset parameter, P.	52
4.8	Tumble correction factors, Q_t/Q_{ct} , for base and cylindrical sections of cone-cylinder configuration fineness ratio, λ/d , of 3, aft C G. offset, versus attitude offset parameter, P.	53
4.9	Tumble correction factors, Q_t/Q_{ct} , for base and cylindrical sections of cylinder configuration fineness ratio, λ/d , of 2.5, fwd C. G. offset, versus attitude offset parameter, P.	54
4.10	Tumble correction factors, Q_t/Q_{ct} , for base and cylindrical section of cylinder configuration fineness ratio, λ/d , of 4, fwd C. G. offset, versus attitude offset parameter, P.	55

<u>FIGURE</u>		<u>PAGE</u>
4.11	Tumble correction factors, Q_t/Q_{ct} , for base and cylindrical sections of cylinder configuration fineness ratio, λ/d , of 5, fwd C.G. offset, versus attitude offset parameter, P.	56
4.12	Tumble correction factors, Q_t/Q_{ct} , for base and cylindrical sections of cylinder configuration fineness ratio, λ/d , of 2.5, aft of C.G. offset, versus attitude offset parameter, P.	57
4.13	Tumble correction factors, Q_t/Q_{ct} , for base and cylindrical sections of cylinder configuration fineness ratio, λ/d , of 4, aft C.G. offset, versus attitude offset parameter, P.	58
4.14	Tumble correction factors, Q_t/Q_{ct} , for base and cylindrical sections of cylinder configuration fineness ratio, λ/d , of 5, aft C.G. offset, versus attitude offset parameter, P.	59
5.1	Variable surface temperature correction of constant wall temperature load, Q_{swo} , for three wall thicknesses (δ).	63
5.2	Cylinder diameter adjustment factor for heating.	64
5.3	Roll averaged heat transfer coefficient ratio for circular cylinders.	64
5.4	Surface temperature, T_{sc} , versus heating load, Q.	65
5.5	Variable heat capacity adjustment to constant heat capacity surface temperature, T_{sc} .	66
6.1	Ballistic trajectories for an initial release altitude (H_i) of 75 miles.	76
6.2	Ballistic trajectories for an initial release altitude (H_i) of 100 miles.	77
6.3	Ballistic trajectories for an initial release altitude (H_i) of 150 miles.	78
6.4	Ballistic trajectories for an initial release altitude (H_i) of 175 miles.	79
6.5	Ballistic trajectories for an initial release altitude (H_i) of 200 miles.	80
6.6	Ballistic trajectories for an initial release altitude (H_i) of 225 miles.	81
6.7	Ballistic trajectories for an initial release altitude (H_i) of 250 miles.	82

<u>FIGURE</u>		<u>PAGE</u>
6.8	Ballistic trajectories for an initial release altitude (H_4) of 300 miles.	83
6.9	Ballistic trajectories for an initial release altitude (H_4) of 350 miles.	84
6.10	Maximum descent velocity versus ballistic coefficient and release altitude at two vehicle recovery altitudes.	85
7.1	Convection heating rates for $\alpha_T = 90$ degrees.	91
7.2	Convection heating rates for $\alpha_T = 100$ degrees.	92
7.3	Convection heating rates for $\alpha_T = 110$ degrees.	93
7.4	Convection heating rates for $\alpha_T = 120$ degrees.	94
7.5	Convection heating rates for $\alpha_T = 130$ degrees.	95
7.6	Convection heating rates for $\alpha_T = 140$ degrees.	96
7.7	Convection heating rates for $\alpha_T = 150$ degrees.	97
7.8	Convection heating rates for $\alpha_T = 160$ degrees.	98
7.9	Convection heating rates for $\alpha_T = 170$ degrees.	99
7.10	Convection heating rates for $\alpha_T = 180$ degrees	100
7.11	End of positive heating altitude versus ballistic coefficient.	101
7.12	Flow regime transition criterion for cone-cylinders at large angle of attack.	102
7.13a	Turbulent Recovery Factor	103
7.13b	Laminar Recovery Factor	103
7.14	1962 Standard Atmosphere Temperature	104
7.15	Free stream density versus altitude	105

LIST OF TABLES

<u>TABLE</u>		<u>PAGE</u>
1.1	Range of Applicability of the Handbook Results	2
3.1	Cone Heating Loads	30
3.2	Base Heating Load Magnitude Chart (H = 200 mi.)	31
3.3	Cylinder Heating Load Magnitude Chart (H = 200 mi.)	32
6.1a	Information for Determining the Ballistic Trajectories for Particular Cone-Cylinder Configurations	72
6.1b	Information for Determining the Ballistic Trajectories for Particular Cylinder Configurations	73
6.2	The Percent Variation of an Equivalent Ballistic Coefficient from a Constant Trim Entry Ballistic Coefficient Versus Initial Attitude and C. G. Offset	74
6.3	Vehicle Attitude Dynamics Versus C. G. Location and Release Attitude	75
7.1	Cone Heating Rates	90
8.1	Typical Heat Sink Materials	113
8.2	Initial Surface Temperatures on an Aries I Payload for Three Ascent Trajectories	114

NOMENCLATURE

W	weight of payload, lb.
A	cylinder cross section area, ft.
l/d	fineness ratio
x/l	C. G. location
d	cylinder diameter, ft.
P	attitude offset parameter
T_{sc}	constant heat capacity, °R
X_{ac}	aerodynamic force center, ft.
X_m	pitching moment reference point, ft.
V_{rel}	relative free stream velocity vector, ft/sec
M_∞	-free-stream Mach number
$W/C_D A$	ballistic coefficient, lb/ft ²
R	recovery factor
Re_∞	free-stream Reynolds number per foot, 1/ft
C_D	drag coefficient based on cylinder cross-section area
C_m	pitching moment coefficient
C_N	normal force coefficient
C_p	specific heating, Btu/lbm°R
Q	convection heating load, Btu/ft ²
Q_{660}	convection heating load at $T_s = 660$ R, Btu/ft ²
q	convection heating rate, Btu/ft ² -sec
Q_{ct}	constant trim heating load, Btu/ft ²
Q_t	oscillating or tumbling heating load, Btu/ft ²
T_∞	free-stream temperature, °R
T_s	surface temperature, °R
T_{aw}	adiabatic wall temperature °R

H_i	initial release altitude, statute mi.
h_r	roll averaged heat transfer coefficient, $\text{Btu/ft}^2\text{-sec}^\circ\text{R}$
h_{s1}	stagnation line heat transfer coefficient, $\text{Btu/ft}^2\text{-sec}^\circ\text{R}$
g	gravitational constant, 32.17 ft/sec^2
J	$778.22 \text{ Btu/ft.lb.}$
α_i	release attitude, degrees
α_T	trim attitude or angle of attack, degrees
δ	vehicle skin thickness, in.
ρ	material density, lbm/ft^3

SECTION 1 INTRODUCTION

The purpose of this document is to provide the design engineer with the information required to determine the heating environments and certain dynamic characteristics of sounding rocket payloads prior to launch. Depending upon the particular mission, there are certain modifications that can be made to an existing design. These modifications could possibly eliminate or at least considerably reduce certain dynamics and heating problems associated with the reentry payload. The ability to determine these potential problems prior to launch gives the engineer a certain amount of time and flexibility in considering possible design change to the vehicle to prevent these problems from occurring during flight.

The reentry problem that must be addressed by the design engineer is complex. Various center of gravity locations combined with certain release attitudes can often result in complex payload attitude dynamics which have a pronounced effect on the reentry heating environment. Because of these variations in attitude, constant trim methods cannot be used alone to adequately predict the trajectory or the heating environment for the vehicle. This makes it necessary to use a combined sophisticated analysis to obtain the vehicle dynamics and heating environment. The results from these types of sophisticated methods in many cases are too complex to use effectively and apply only in particular situations. A considerable amount of effort was spent to assure that the results presented could be easily used and general enough to be applicable to numerous reentry heating problems.

1.1 Scope of Contents

The results presented in the following sections are applicable to the geometric configurations and range of parameters shown in Table 1.1. The results are directly applicable only to cylinder and cone-cylinder configurations with a C.G. offset range of 10% of the vehicle length forward and aft of the volumetric C.G. location. The initial release attitude or angle of attack range is from 90 to 180 degrees referenced to the earth's local vertical vector. The handbook results cover a range of 75 to 350 statute miles in release altitude and consider cylinder diameters from 22 to 38 inches. The skin material is considered to be aluminum with skin thicknesses of .125, .250 and .500 inches. Vehicle fineness ratios of 2.5 to 5 are considered for the cylinder configurations while fineness ratios of 3 to 7 are considered for cone-cylinder configurations. The resultant ballistic coefficient range for the vehicles is between 10 and 250 lb/ft². The results presented in the following sections consider neither roll nor tumble moments imparted to the vehicle at release.

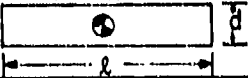

GEOMETRIC CONFIGURATION	CYLINDER 	CONE-CYLINDER 
C. G. Offset Fineness Ratio Release Attitude Release Altitude Diameter Skin Thickness Cone Half Angle	$-.10 < \text{C.G.} < .10$ $2.5 < l/d < 5$ $90^\circ < \alpha_i < 180^\circ$ $75 \text{ mi.} < H_i < 350 \text{ mi.}$ $22 \text{ in.} < d < 38 \text{ in.}$ $.125 \text{ in.} < \delta < .500 \text{ in.}$	$-.10 < \text{C.G.} < .10$ $3 < l/d < 7$ $90^\circ < \alpha_i < 180^\circ$ $75 \text{ mi.} < H_i < 350 \text{ mi.}$ $.22 \text{ in.} < d < 38 \text{ in.}$ $.125 \text{ in.} < \delta < .500 \text{ in.}$ $12^\circ < \theta < 18^\circ$

Table 1.1 Range of applicability of the handbook results

The handbook is comprised of essentially eight separate sections and four appendices. A concise description will be given for each section and appendix:

- Section 1, in addition to the Scope of Contents Section, contains the procedures to be followed when solving a problem with the handbook. The solution to a sample problem is presented and can be followed as an example when solving a reentry for an actual flight case.
- Section 2 provides all the necessary information required to determine the trim attitude and ballistic coefficient for the reentry payload. This assumes, of course, that the configuration type, cross-sectional area, weight and C.G. location have already been specified for the vehicle.
- Section 3 contains the results from the constant trim integrated heating load analysis. This heating load must be determined in order to obtain the surface temperatures of the reentry vehicle.
- Section 4 presents the oscillation and tumble correction factors. These factors are multiplied by the constant trim heating loads presented in Section 3 to correct for vehicle oscillations and tumbling during reentry.
- Section 5 provides all the necessary information required to determine the surface temperature of the reentry vehicle once the tumble corrected heating load has been obtained.
- Section 6 deals specifically with the dynamics of the reentry vehicle. Two distinct types of reentry trajectories are considered, i.e., the trajectories which exhibit normal stable flight at a constant trim attitude and those which consider vehicle oscillations

and tumbling. Methods and procedures are presented in order to determine both types of trajectories.

- Section 7 presents the heating rates versus altitude and velocity for the configuration types being considered. From the figures presented in Section 7, the heating history for the reentry vehicle can be determined once the trajectory for the vehicle has been specified.
- Section 8 presents the reentry guidelines that should be followed when using the handbook to solve a vehicle heating or dynamics problem.
- Appendices A-D discuss all the theoretical methods and procedures used in determining the results presented in the following sections.

1.2 Handbook Usage Procedures

There are basically three types of analyses which can be performed with the handbook. In addition to the heating load and surface temperature analysis which will undoubtedly be the most important to the design engineer, trajectory and heating rate analyses can also be performed. The basic procedures involved in using the handbook are outlined by the flowchart presented in Fig. 1.1

A certain amount of required information is needed to begin a reentry analysis. This information includes:

- (1) The payload geometric configuration type and fineness ratio
- (2) Cone nose bluntness ratio if cone-cylinder geometry
- (3) The weight of the payload

- (4) The C. G. location and cylinder cross-sectional area
- (5) The initial surface temperature of the vehicle at release
- (6) The initial attitude and altitude of the payload at release
- (7) Initial roll, tumble or yaw moments imparted to the vehicle at release

The initial attitude of a reentry vehicle may not be known with any degree of confidence for certain missions. In these situations, engineering judgement and knowledge of the problem must be used to come up with the best estimate of this attitude since it is an important factor in the analysis.

The figures in Section 2 are to be used to determine the trim attitude and the resultant drag coefficient for the vehicle type, fineness ratio and C. G. location given. Once the drag coefficient has been established, compute the ballistic coefficient using Eqn. 1.1.

$$\text{Ballistic Coefficient} = W/C_D A \quad 1.1$$

where

W = weight of payload

C_D = drag coefficient based on cylinder cross-sectional area

A = cylinder cross-sectional area

In order to determine the surface temperature on a vehicle, the integrated heating load must be obtained. With the constant trim ballistic coefficient, vehicle trim attitude, and release altitude already established at this point, determine the heating load from Figs. 3.1 - 3.10 for the base and cylinder regions of the vehicle. Table 3.1 is provided in order to determine the heating load for the cone section when considering a cone-cylinder geometry. Heating load magnitude charts are presented in Tables 3.2 and 3.3 for the configurations, C. G. locations, and release attitudes considered in the 6 DOF trajectory and tumble heating analyses. The heating levels presented are for

a release altitude of 200 miles. While the magnitude of the heating loads presented in Tables 3.2 and 3.3 change with altitude, the distribution does not. From Tables 3.2 and 3.3 the engineer can determine what C. G. offset and release attitude combinations promote the highest levels of heating in relation to other C. G. offsets and release attitudes.

The heating loads obtained in Section 3 are for a constant trim reentry situation. A tumble correction factor must be applied to the load to account for vehicle oscillations and tumbling. Determine this tumble correction factor from Figs. 4.1 - 4.14 for the configuration and initial conditions being considered. This factor is multiplied times the load obtained in Section 3 to determine a tumble corrected heating load. If this factor is less than 1, it should not be applied unless the initial release attitude is known with a high degree of certainty.

The tumble corrected heating loads obtained in Section 4 will be used along with the figures presented in Section 5 to determine the surface temperature of the reentry vehicle. Adjust the tumble corrected heating load for surface temperature variations using Fig. 5.1. If the cylinder diameter for the configuration varies from 24 inches, correct the heating load for diameter change using Fig. 5.2. If the vehicle is rolling, correct the stagnation line heating load on cylinder section by the roll average heat transfer coefficient using Fig. 5.3. Determine the vehicle surface temperature using this corrected load and Fig. 5.4. The surface temperature obtained from Fig. 5.4 considers a constant heat capacity for the vehicle material. Correct this surface temperature for variable heat capacity using Fig. 5.5.

The results presented in Section 6 are used to determine the vehicle trajectory once the ballistic coefficient has been established. The ballistic

coefficient for the mission can be compared to those presented in Table 6.1 in order to have a check on the ballistic coefficient calculation. The next step in determining the vehicle trajectory is to consider the results in Table 6.2. A tumbling or oscillating trajectory can be related to a constant trim trajectory using these results. Determine the percent of variation from Table 6.2 for the configuration type and initial conditions being considered. Calculate an equivalent ballistic coefficient using the constant trim ballistic coefficient and this percent of variation. This calculation can be performed by considering the following relationship.

$$\left(\frac{W}{C_{DA}}\right)_{eq} = \left(\frac{W}{C_{DA}}\right)_{CT} + \frac{V}{100} \left(\frac{W}{C_{DA}}\right)_{CT} \quad 1.2$$

where

$\left(\frac{W}{C_{DA}}\right)_{eq}$ = The equivalent ballistic coefficient for an oscillating or tumbling trajectory

$\left(\frac{W}{C_{DA}}\right)_{CT}$ = Constant trim ballistic coefficient

V = Percent of variation (from Table 6.2)

The smaller the percent of variation the more closely the trajectory resembles a constant trim trajectory. The reentry trajectory of the vehicle can now be determined by using the equivalent ballistic and the release altitude (from Figs. 6.1 - 6.9). The attitude dynamics for the reentry vehicle can be established for the particular configuration and set of initial conditions by considering the information provided in Table 6.3. From Table 6.3 it is possible to determine if the vehicle is oscillating or tumbling or whether it is trimmed during reentry. It is also possible to determine if these oscillations are small in amplitude or whether they are large and unstable. Fig. 6.10 has been provided in order for the engineer to be able to determine the maximum descent velocity for the vehicle. The equivalent ballistic coefficient along with the release attitude can be used in Fig. 6.10 to obtain the maximum

descent velocity of the reentry vehicle at two selected recovery altitudes.

Section 7 deals specifically with the heating rate environments for the reentry payloads. If a heating rate analysis is being considered, examine the magnitude of the percent of variation determined in Section 6. If the absolute value of this percentage is greater than 5%, this is an indication that vehicle oscillations or tumbling will occur. The heating rates presented in Figs. 7.1 - 7.10 are for constant trim attitudes. The heating rate history for a vehicle cannot be determined using these figures if the vehicle attitude is not known at each specific time point which is the case in an oscillating or tumbling trajectory. If the percent of variation is larger than 5% and the heating rate history of the vehicle is required, a complete 6 DOF trajectory analysis and a tumbling heating analysis must be performed for these results. If, however, the absolute value of the percentage is less than 5%, this means that the vehicle is essentially trimmed at a constant attitude. For these types of situations, select a heating rate plot from Figs. 7.1 - 7.10 which is closest to the trim attitude of the vehicle and superimpose the reentry trajectory that was determined in Section 6. The heating rate history can then be determined for both the cylinder and base regions of the payload. Table 7.1 is provided in order to determine heating rates on the cone section for the cone-cylinder configurations. Fig. 7.11 is also presented in order to show the altitude cutoff limits for the heating rate analysis. These are the altitudes at which aerodynamic heating ends and cooling begins.

The reentry guidelines are presented in Section 8. When potential heating or dynamic problems are indicated for a particular flight case, follow the recommendations presented in Section 8 prior to changing the vehicle design.

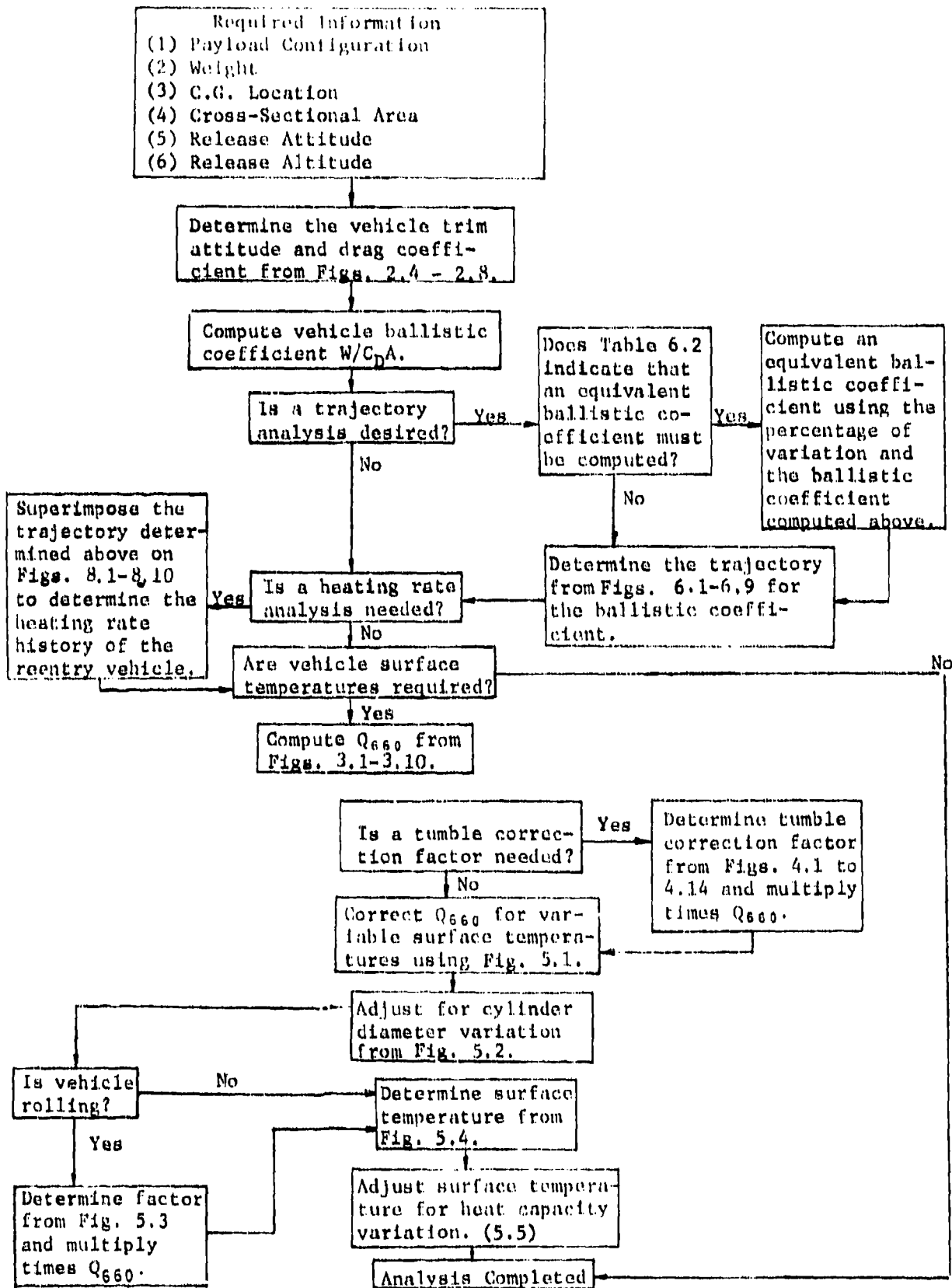


Fig. 1.1. Flow diagram for handbook usage.

1.3 Sample Problem

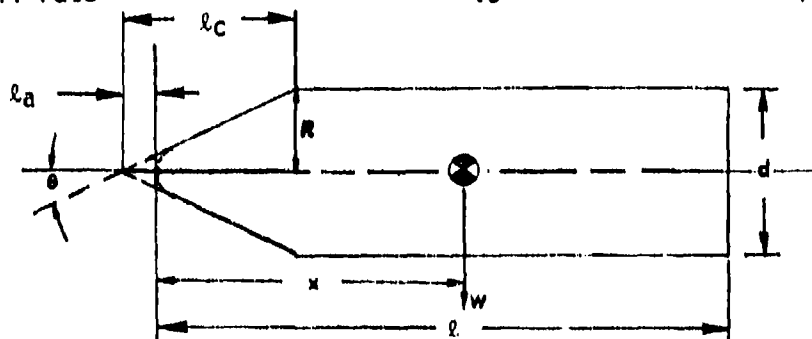
A detailed step by step solution to a sample problem is presented in this section. The problem illustrates the techniques and procedures that a user should follow in solving a problem. This problem is representative of the types of problems which will most likely be encountered while performing a flight reentry heating analysis.

PROBLEM:

Determine the maximum descent velocity at 60K feet, the attitude dynamics, maximum heating rate and surface temperature on the cylinder region of a blunt cone-cylinder configuration.

CONFIGURATION AND MISSION CHARACTERISTICS:

<u>Item</u>	<u>Symbol</u>	<u>Value</u>	<u>Units</u>
Configuration type		cone-cylinder	
Cylinder diameter	d	37.5	in.
Vehicle length	l	158	in.
Vehicle weight	w	1742	lbs.
Nose bluntness ratio	l_a/l_c	0.132	
Skin thickness	δ	0.250	in.
Release altitude	H_f	175	statute miles
C. G. location	x/l	.645	
Release attitude	α_f	90	degrees
cone half angle	θ	14	degrees
Vehicle roll rate		.5	rps



SOLUTION FOR SURFACE TEMPERATURE:

Step No.

1	Calculate fineness ratio	$\lambda/d = 4.21$
2	From Fig. 2.2 determine volumetric C. G. location	$\bar{x}/\lambda = .620$
3	Calculate vehicle C. G. offset from volumetric C. G.	C. G. Offset = .025 λ AFT of Vol. C.G.
4	From Fig. 2.3 determine planform area ratio	$A_{bc}/A_{sc} = .99$ Handbook results are valid (Section 2)
5	From Fig. 2.4 determine trim attitude	$\alpha_T = 161^\circ$
6	From Fig. 2.5 determine drag coefficient	$C_D = 1.9$
7	Calculate cylinder cross-sectional area	$A = 7.67 \text{ ft}^2$
8	Calculate ballistic coefficient	$W/C_D A = 119.5 \text{ lbm/ft}^2$
9	From Fig. 3.8 and 3.9 linearly interpolate for heating load	$Q_{660} = 207 \text{ Btu/ft}^2$
10	Calculate attitude offset parameter	$P = -.441$
*11	Calculate vehicle fineness ratio as if the vehicle were a sharp cone-cylinder geometry, $\lambda_a = 0$	$\lambda/d = 4.48$
12	Determine from Fig. 4.6 and 4.7 tumble correction factor (linearly interpolate with vehicle fineness ratio from Step 11)	$Q_t/Q_{ct} = 1.87$
13	Calculate tumble corrected heating load	$Q_{660} = 387 \text{ Btu/ft}^2$
14	Determine from Fig. 5.1 variable surface temperature corrected load	$Q = 360 \text{ Btu/ft}^2$
15	Determine diameter adjustment factor from Fig. 5.2	Factor = .915
16	Adjust load from Step 14 for diameter change	$Q = 329 \text{ Btu/ft}^2$
17	Determine the factor \bar{h}_r/h_{se} from Fig. 5.3 for α_T and multiply times Q_{660}	$Q_{660} = 145$
18	Determine constant heat capacity surface temperature from Fig. 5.4	$T_{sc} = 843^\circ\text{R}$

SOLUTION FOR SURFACE TEMPERATURE (Continued):

Step No.

**19 Correct surface temperature for variable heat capacity using Fig. 5.5 $T_s = 833^\circ R$

SOLUTION FOR MAXIMUM VELOCITY AT 60K FEET:

Step No.

20 Determine percent of variation from Table 6.2 (linearly interpolate between fineness ratios using fineness ratio from Step 11) Percent = -7.8%

21 Calculate equivalent ballistic coefficient (use Eq. 1.2) $(W/C_D A)_{eq} = 110$

22 From Fig. 6.4 determine maximum velocity at 60K feet Maximum velocity = 4000 ft/sec

SOLUTION FOR ATTITUDE DYNAMICS:

Step No.

23 From Table 6.3 determine attitude dynamics Vehicle oscillations are less than 25° about α_T . Vehicle is re-entering aft end first

SOLUTION FOR MAXIMUM HEATING RATE:

Step No.

24 The percent of variation from Step 19 is 7.8% which is greater than the 5% limit imposed. An approximate maximum heating rate will try to be obtained even though the vehicle is not at constant trim

25 Superimpose the trajectories from Fig. 6.4 onto the heating rate plots for the cylinder section in Fig. 7.8

26 Determine maximum heating rate Maximum heating rate = 20 Btu/ft²-sec

*This calculation must be performed since the results in Section 4 were determined for sharp cone-cylinder geometries and blunt cylinder geometries only. Determine the length of the cone-section from its theoretical apex (see Fig. 3.1 and Eq. 2.1).

$$l_c = \frac{R}{\tan \theta} = 75.20 \text{ in.}$$

Calculate cone length

$$l_a = .132 l_c = 9.926 \text{ in.}$$

Determine vehicle length from theoretical apex

$$l + l_a = 158 + 9.926 = 167.926 \text{ in.}$$

Calculate fineness ratio from theoretical apex

$$f = 167.926/37.5 = 4.48$$

**This is the final estimate of the surface temperature on the cylinder section. This value assumes an initial surface temperature at apogee of 660°R.

SECTION 2

AERODYNAMIC CHARACTERISTICS

The data based theoretical methods discussed in Appendix A provide the necessary aerodynamic coefficients used in both the six-degree-of-freedom trajectory simulation analysis and the three-degree-of-freedom ballistic reentry analysis. The normal force, axial force, and pitching moment coefficients were computed using these methodologies. The damping coefficients which were an integral part of the 6 DOF trajectory analysis were computed using Ref. 1. The aerodynamics computed using these theoretical methods consider a sharp cone geometry for the cone section of the cone-cylinder configurations. The sharp cone geometry considered in the handbook analysis can be defined as one in which the cone tip and theoretical apex coincide. While it is true that the aerodynamics are not directly applicable to blunt cone-cylinder geometries, there are certain degrees of nose bluntness for which the handbook results are valid. In order to define nose bluntness consider the schematic in Fig. 2.1.

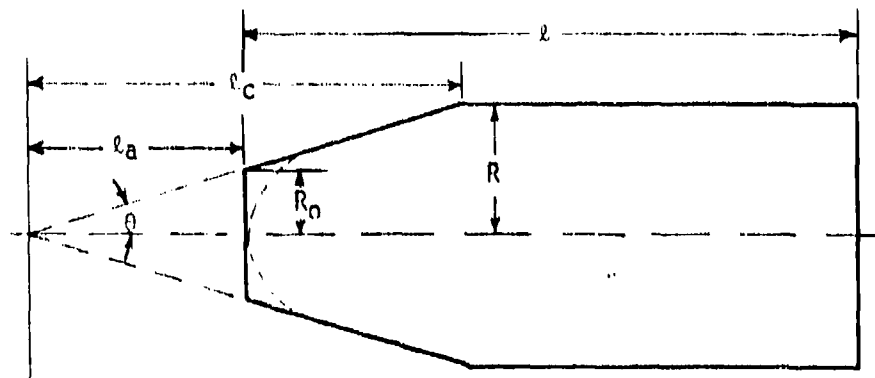


Fig. 2.1 Cone-cylinder configuration with cone nose bluntness

The nose bluntness ratio will be defined as the distance from the theoretical apex to the actual nose ratioed to the distance from the theoretical apex to the cone base.

$$\frac{R_0}{R} = \frac{\lambda_a}{\lambda_c} = \frac{\lambda_a \tan \theta}{R} \quad 2.1$$

where

- λ_c = distance from the theoretical apex of the cone to the cone base
- λ_a = distance from the theoretical apex to the hemisphere-flat face tangent point

In order to maintain consistency in the application of the handbook results to both sharp and blunt cone cylinder geometries, the vehicle fineness ratio will always be defined unless otherwise stated as the distance from the nose of the vehicle to the base of the cylinder afterbody.

A volumetric C. G. location must be determined for the reentry vehicle as a first step in the reentry analysis regardless of the vehicle geometry. Fig. 2.2 presents the volumetric C. G. locations for cone-cylinder geometries with nose bluntness ratios ranging from zero for a sharp cone-cylinder geometry to one for a cylinder geometry. When a blunt nose cone geometry is being considered in a reentry analysis, the nose bluntness ratio is first determined by using equation 2.1. The volumetric C. G. location can then be determined for the vehicle fineness ratio and specific nose bluntness ratio using Fig. 2.2.

As the cone nose bluntness increases the vehicle aerodynamics begin to change. There are certain nose bluntness cutoff limits that must be considered. Beyond these limits the vehicle aerodynamics have changed to the extent that

the handbook results are no longer valid for the particular geometry. When considering a blunt cone-cylinder configuration, the bluntness ratio determines whether the aerodynamics are more closely associated with those of a sharp cone geometry or those of a cylinder geometry. Therefore, basically two cutoff limits exist. One limit would be the bluntness ratio that would render the sharp cone-cylinder results invalid, and the other limit would be that bluntness which would make the cylinder results invalid. These limits will change, of course, with vehicle fineness ratio. It is not possible to determine these exact limits without performing an in-depth analysis. It is possible, however, to make some generalized approximate statements regarding these limits. The aerodynamics for a vehicle are direct functions of the planform area of that vehicle. As the planform area changes there are corresponding changes in the aerodynamics. Fig. 2.3 presents the planform area for a blunt cone-cylinder geometry ratioed to the planform area of a sharp cone-cylinder geometry. This ratio (A_{bc}/A_{sc}) is presented versus fineness ratio and nose cone bluntness ratio. The fineness ratio for this specific case will be the distance from the theoretical cone apex to the base of the cylinder afterbody. When considering a blunt nose cone-cylinder geometry for a specific flight case, it is generally felt that the handbook results should be valid and accurate if the planform area ratio is greater than 0.95. The data book will become less and less accurate for planform area ratios less than 0.95. A generalized statement regarding a practical cutoff limit for a cylinder configuration cannot be made as easily however. It has been experimentally determined and theoretically verified that the addition of a hemispherical cap to one end of a cylinder can greatly alter the aerodynamics of the cylinder. For this reason, it is recommended that blunt cylinder configurations be separately analyzed as to their reentry characteristics.

A trim attitude is established for a reentry vehicle when its C. G. location and aerodynamic force center coincide. This is the point at which there are zero moments and torques on the reentry body. The aerodynamic force center versus angle of attack can be computed using the following equation.

$$\frac{X_{ac}}{l} = \left(\frac{X_m}{d} - \frac{C_m}{C_N} \right) \frac{d}{l} \quad 2.2$$

where

$\frac{X_{ac}}{l}$ = Aerodynamic force center location non-dimensionalized by the vehicle length

$\frac{X_m}{d}$ = Pitching moment reference point location non-dimensionalized by the vehicle diameter

C_m = Pitching moment coefficient

C_N = Normal force coefficient

$\frac{d}{l}$ = Vehicle diameter to length ratio

Aerodynamic force centers were computed using Equation 2.2 for the configuration types and range of fineness ratios presented in Table 1.1. An angle of attack range of 5 to 175 degrees was considered in the calculations. The aerodynamic force center is undefined at 0° and 180° when Equation 2.2 is used. This is due to the fact that both the normal force and pitching moment coefficients are zero at these angles of attack. The aerodynamic force centers versus fineness ratio for constant trim attitudes are presented in Fig. 2.4 for the cone-cylinder configurations. The same results are presented in Fig. 2.6 for the cylinder configurations. Aerodynamic drag coefficients for the cone-cylinder configuration versus trim attitude and fineness ratio are given in Fig. 2.5 while similar results are presented for the cylinder configuration in Fig. 2.7.

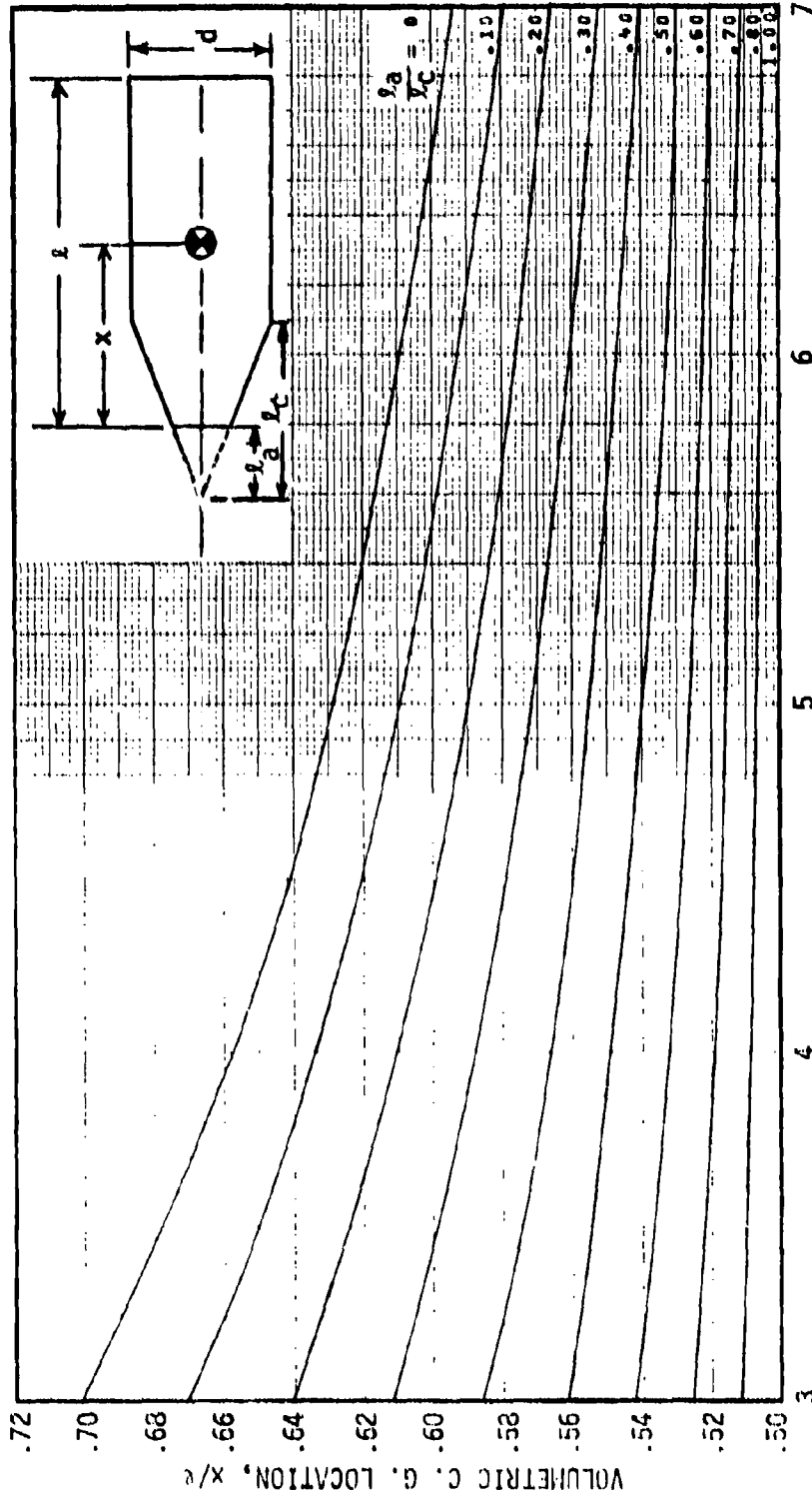


Fig. 2.2 Volumetric C. G. location versus vehicle fineness ratio and nose bluntness ratio.

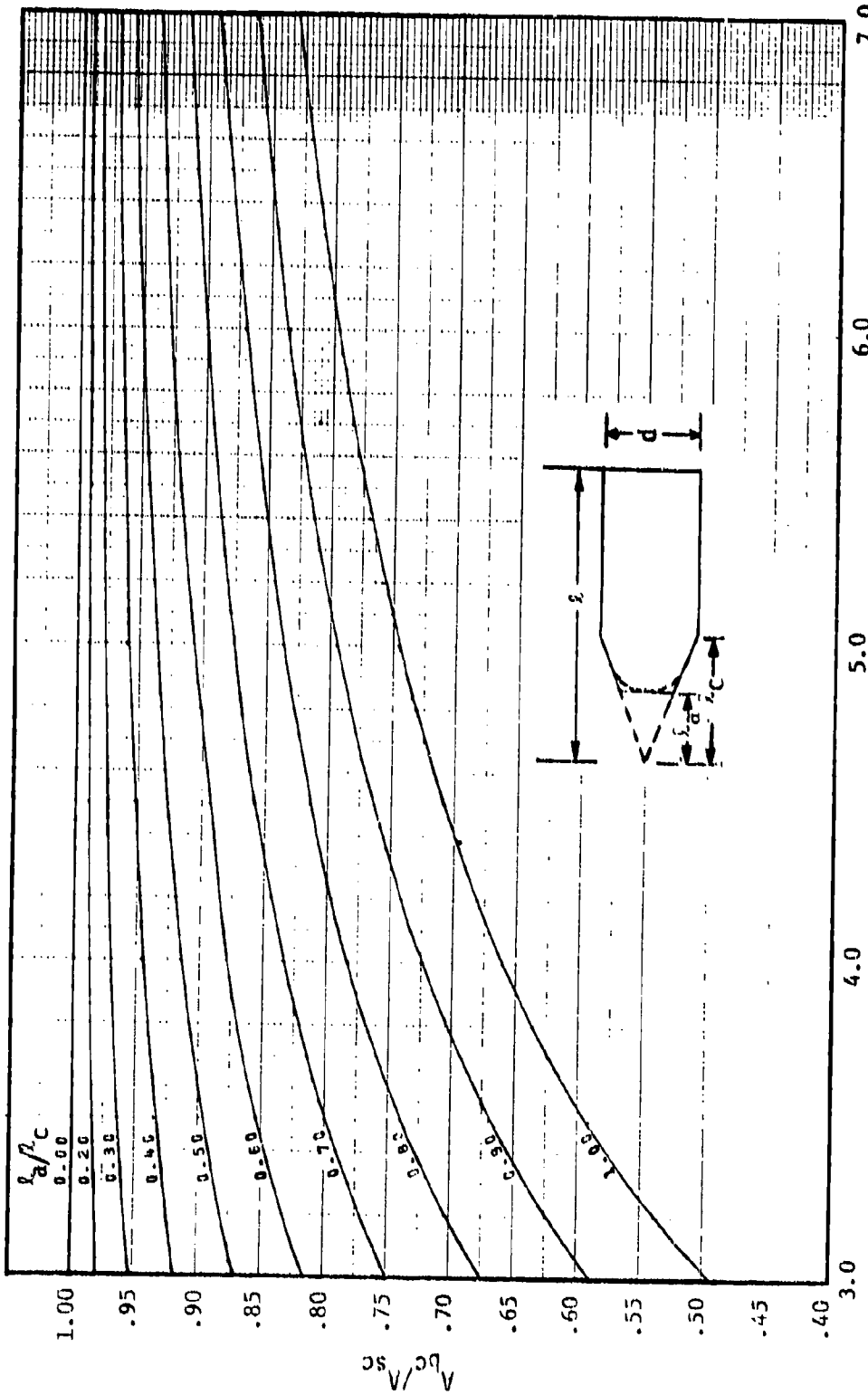


Fig. 2.3 Ratio of the planform areas of a blunt cone-cylinder geometry to that of a sharp cone-cylinder geometry.

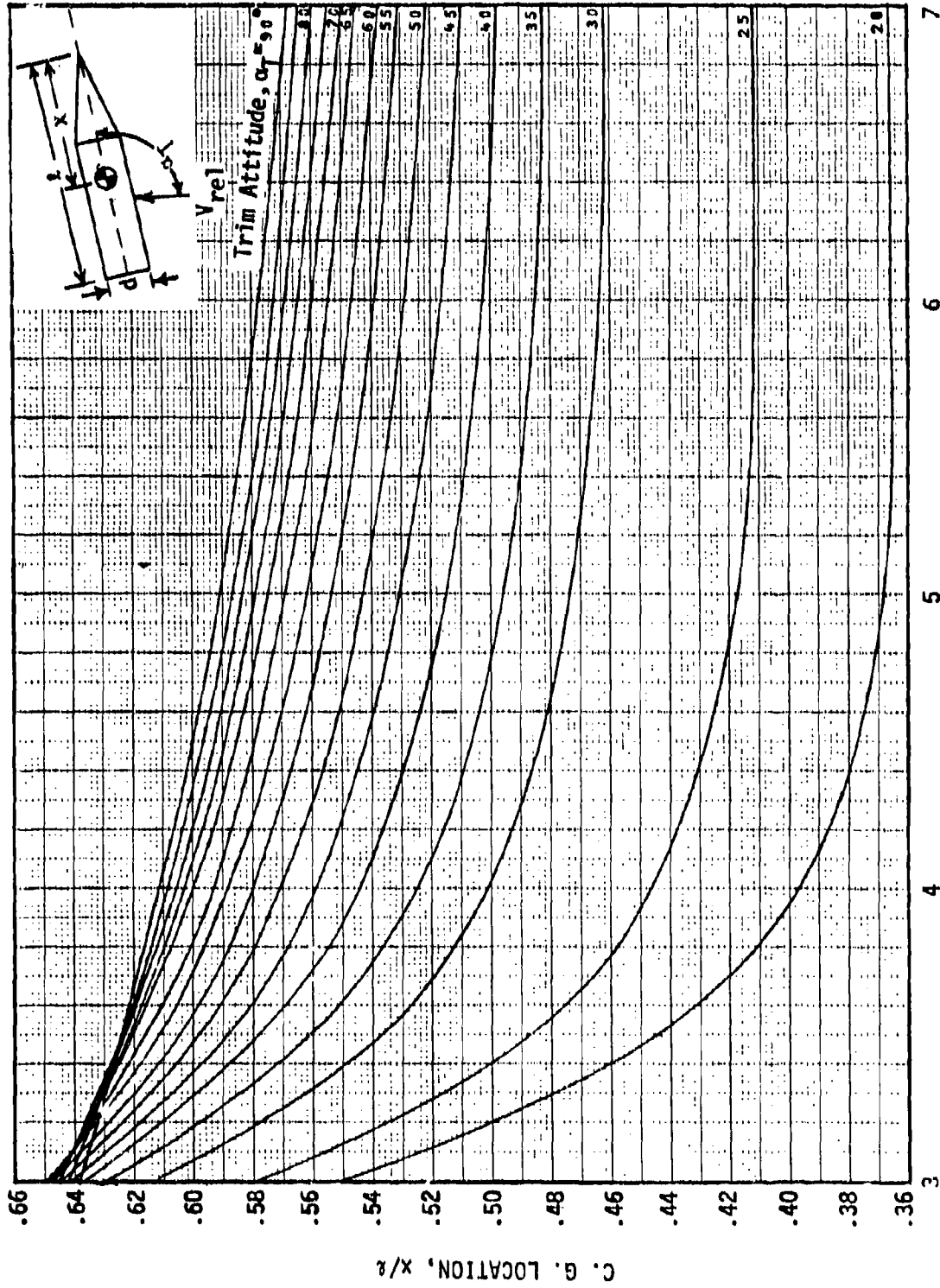
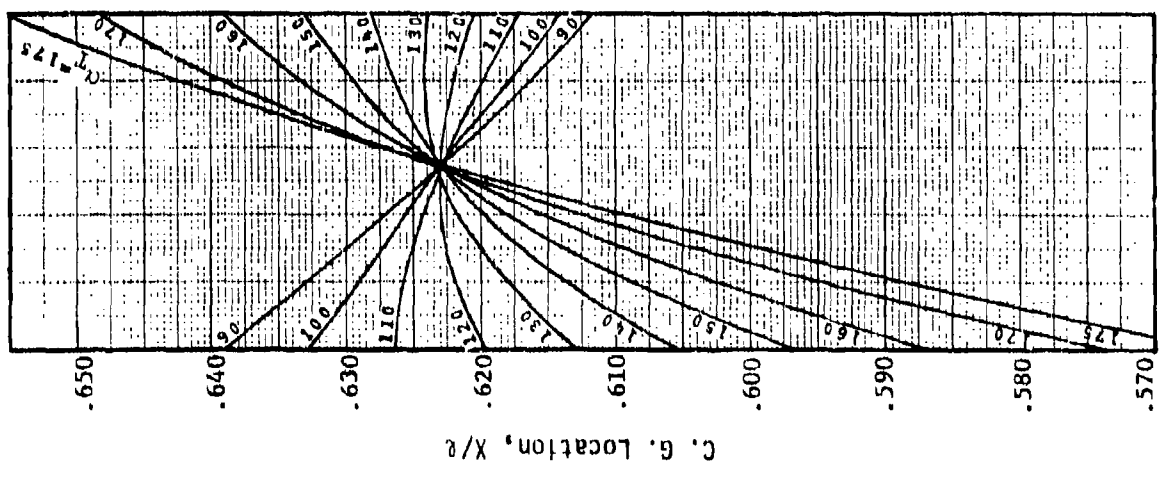
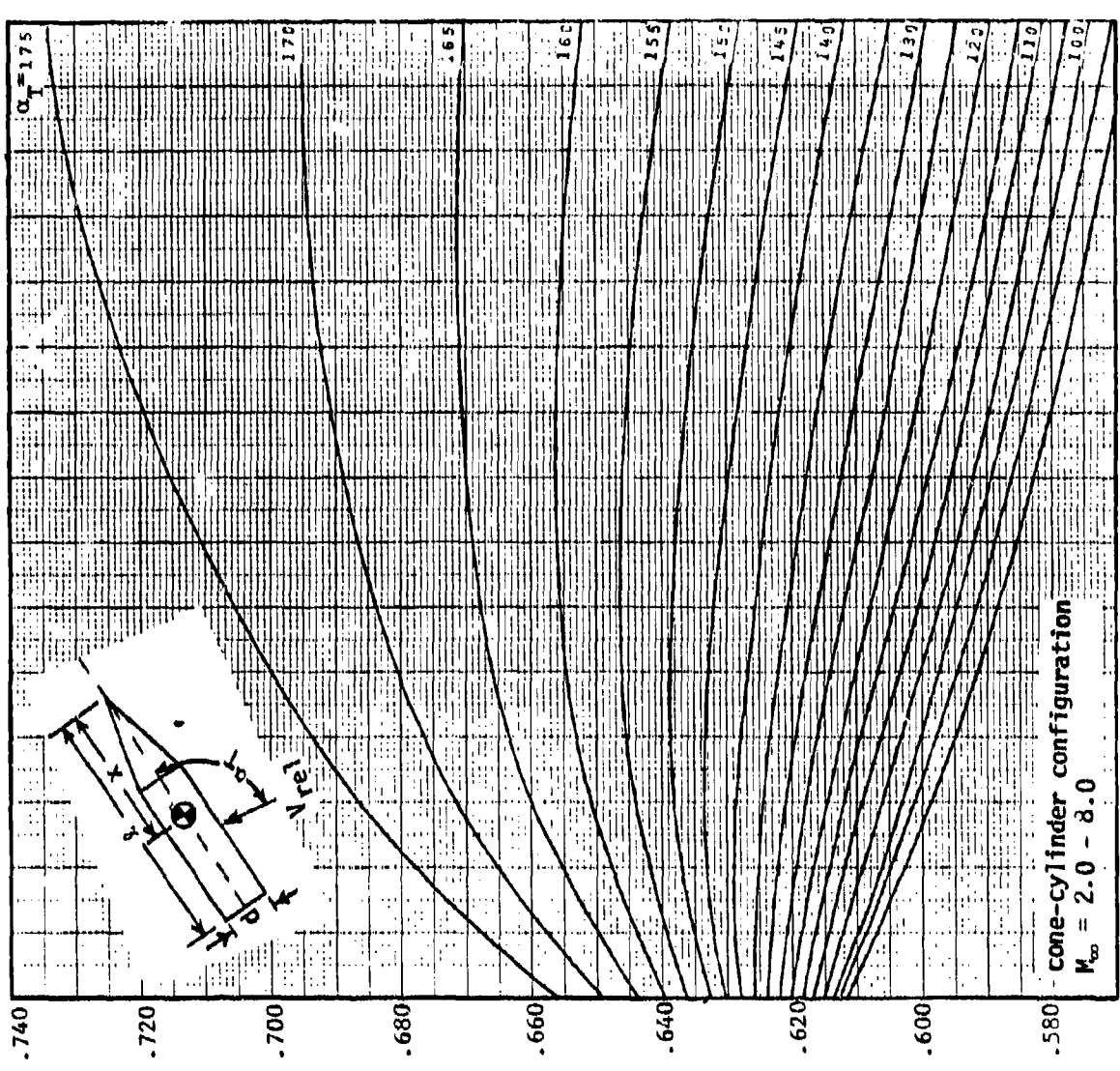


Fig. 2.4 Aerodynamic force center versus C. G. location and fineness ratio for constant trim attitudes. (Cone-cylinder configurations)



3.0 3.2 3.4 3.6 3.8 4.0 4.2 4.4 4.6 4.8 5.0 5.2 5.4 5.6 5.8 6.0 6.2 6.4 6.6 6.8 7.0

Fineness Ratio, l/d

Fig. 2.4 Continued

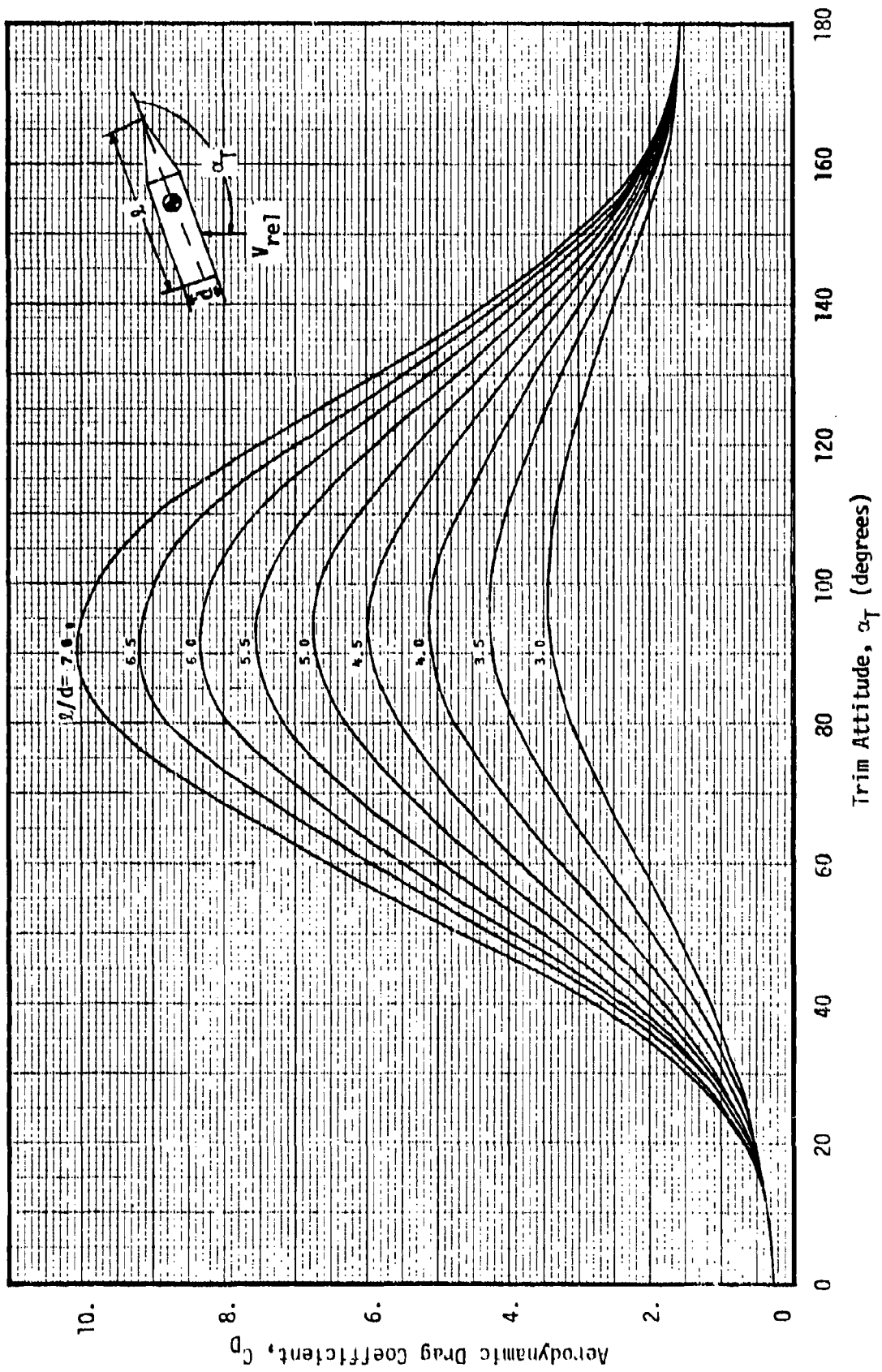


Fig. 2.5 Drag coefficient versus trim attitude and fineness ratio for cone-cylinder configurations.

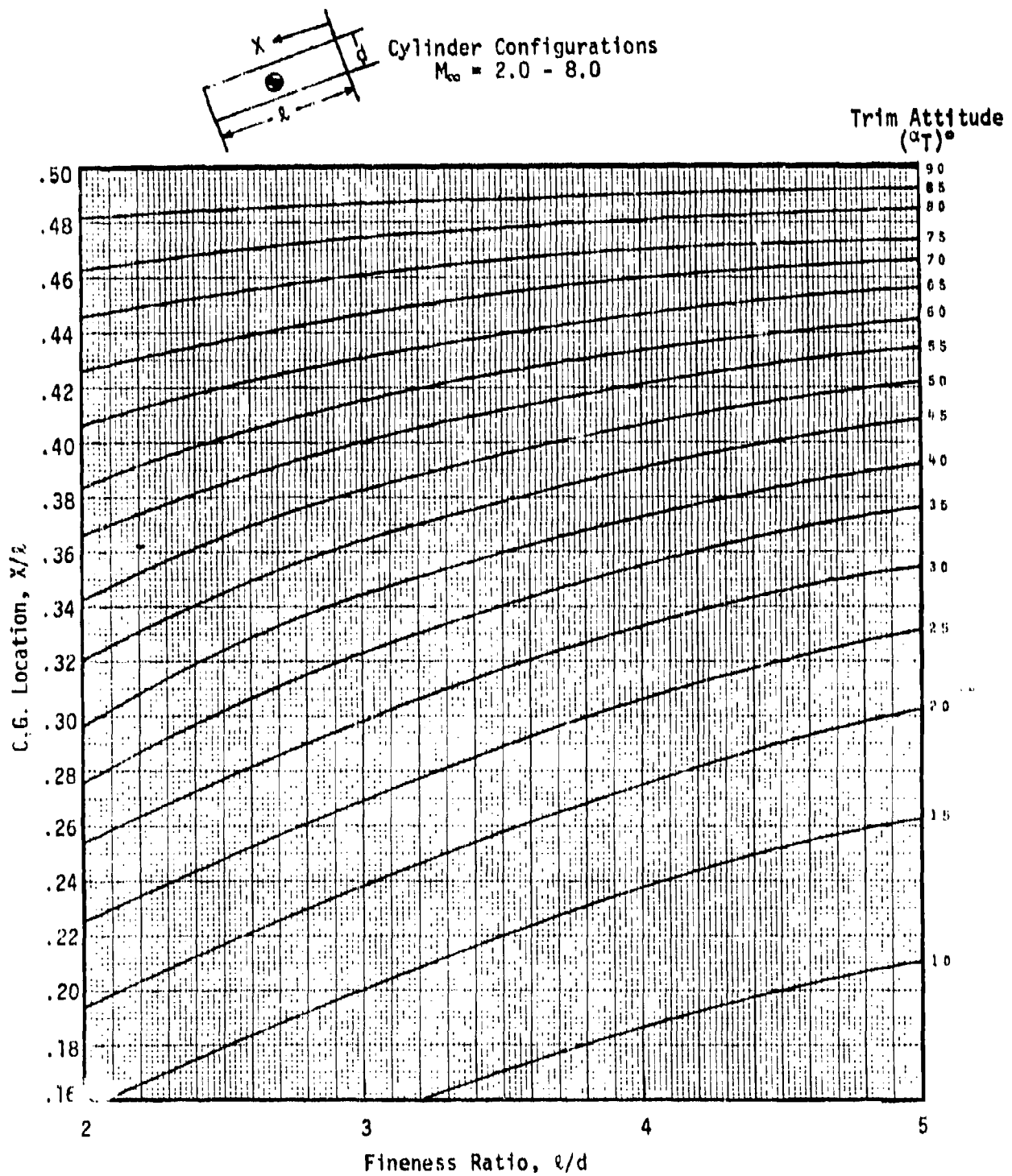


Fig. 2.6 Aerodynamic Force Center Versus C. G. Location and Fineness Ratio for Constant Trim Attitudes (Cylinder Configurations)

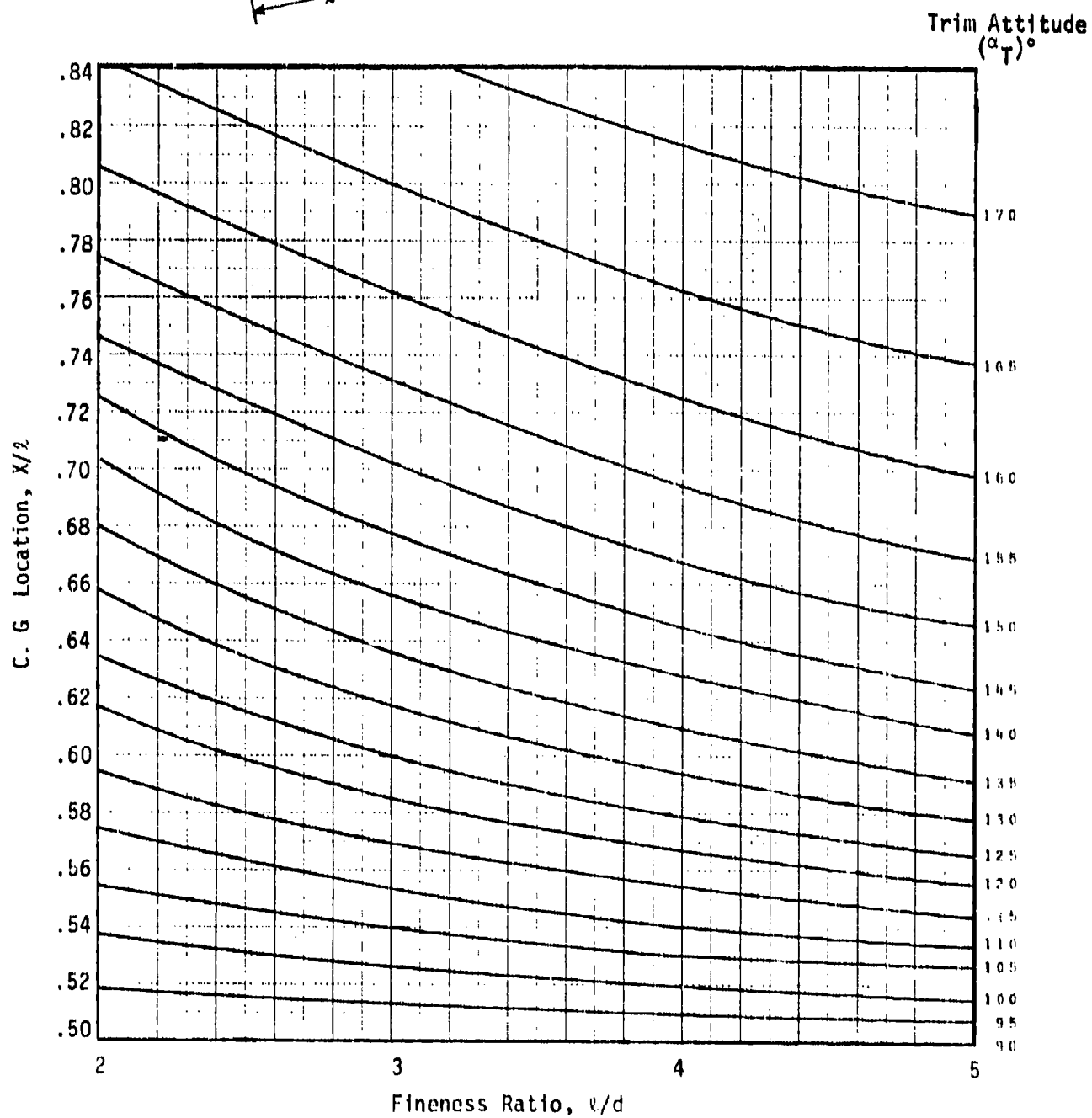
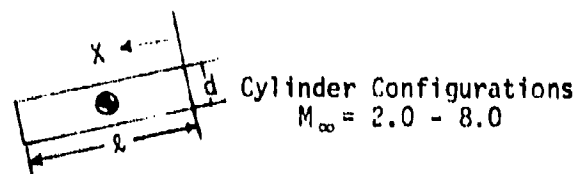


Fig. 2.6 Continued

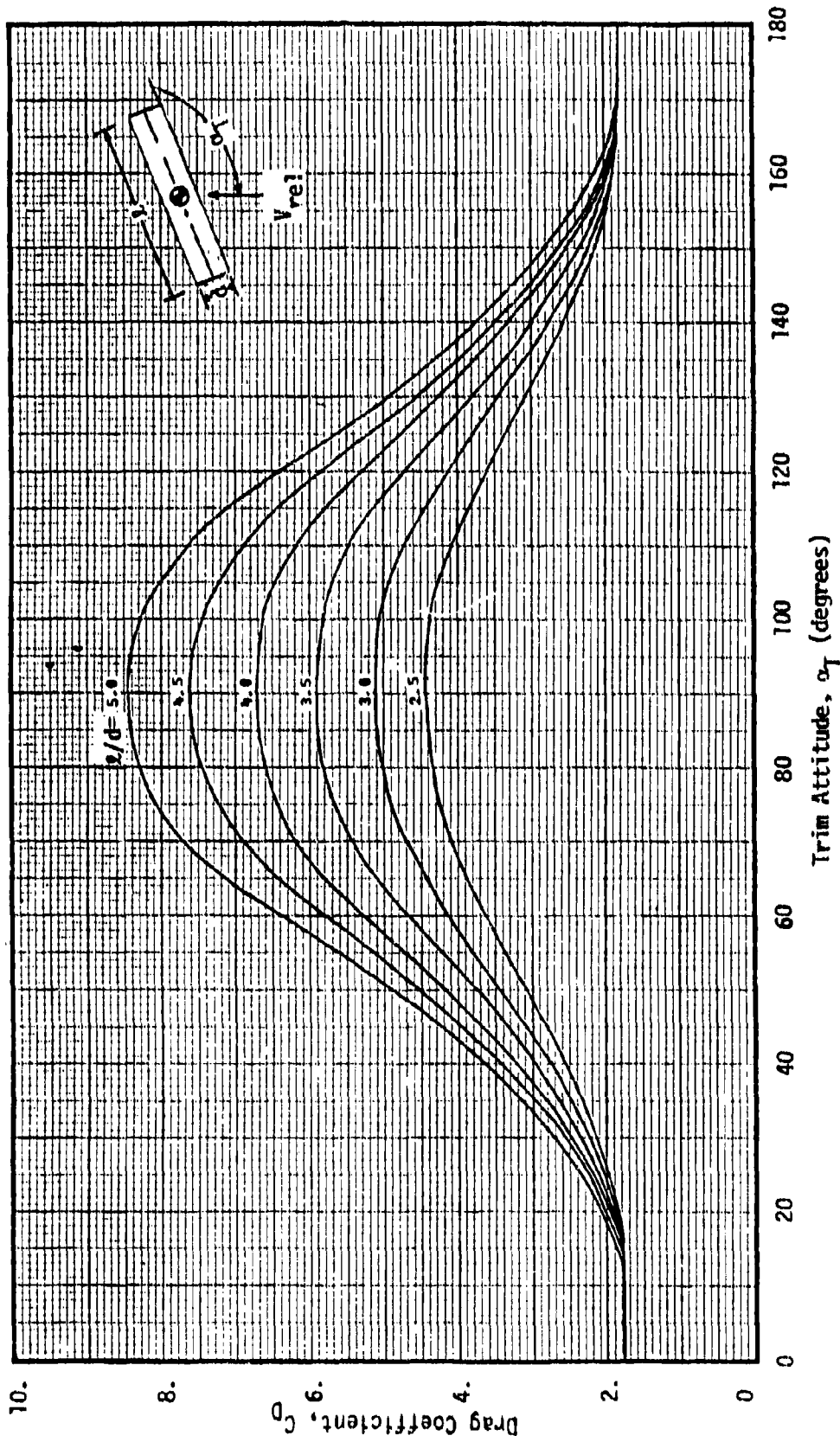


Fig. 2.7 Drag coefficient versus trim attitude and fineness ratio for cylinder configurations.

SECTION 3 INTEGRATED HEATING LOADS

The heating loads discussed in this section fall basically into two categories. Ballistic, or constant trim entry heating loads, are discussed in Section 3.1. Relative heating load magnitudes for a number of trajectories which include, not only constant trim entries, but also oscillating and tumbling type entries are discussed in Section 3.2.

3.1 Constant Trim Entry Loads

Integrated heating loads were computed using the Bentry Computer Program (Ref. C.1 - Appendix C) for each of the constant trim ballistic trajectories presented in Figs. 6.1 - 6.9 of Section 6. The heating loads were computed for a release altitude range of 50 to 350 statute miles. The results, presented in Figs. 3.1 - 3.10, are applicable to the base and cylindrical sections of both the cylinder and cone-cylinder configurations.

The heating load results presented in Figs. 3.1 to 3.10 were calculated for a reference diameter of 24 inches, for angles of attack of 90 to 180 degrees using a reference temperature of 660°R.* The heating load may be adjusted for diameter variations using Fig. 5.2. To compute a load for trim angles between 0 and 90 degrees use the following relations:

$$\text{Cylinder: } \alpha_T = 180 - \alpha$$

$$\text{Base: } \alpha_T = 90$$

A wall temperature adjustment to the heating load is provided in Section 7 by Fig. 7.1.

*660°R was assumed to be a nominal estimate of the wall temperature at apogee. Differences in wall temperatures at apogee are discussed in Section 8.

The heating load to the cone section of a cone-cylinder body may be calculated using the algorithm given in Table 3.1 where the cylinder is used as a reference.

3.2 Oscillating and Tumbling Entry Heating Levels

The Bentry program has the capability of determining heating rates and integrated loads on tumbling reentry bodies once the trajectory for the tumbling body has been established. The matrix of runs considered in the 6 DOF trajectory analysis is presented in Table 6.2 of Section 6. Integrated heating loads were computed using the Bentry program for each of these trajectories which included those with vehicle oscillations and tumbling, as well as the constant trim reentries. While these Bentry runs for heating loads were performed mainly for determining the oscillating and tumbling correction factors presented in Section 4, they are also used in determining relative heating load magnitudes for various combinations of C.G. offsets and initial release attitudes for the payload configurations considered in the analysis. These results are shown in the heating load magnitude charts presented in Tables 3.2 and 3.3. A number of trajectories were determined with the 6 DOF analysis for initial release altitudes other than 200 miles. From these trajectory runs, it was determined that the vehicle dynamics with respect to the attitude of the vehicle during an oscillating or tumbling reentry were essentially constant for the release altitudes examined. The extensive trajectory analysis in which C.G. locations and release attitudes were varied and for which the heating load calculations were performed considered a 200 mile release altitude. Therefore, only the overall magnitude of the heating loads presented in Tables 3.2 and 3.3 would change with release altitude and not the distribution since the vehicle attitude dynamics are essentially constant with release altitude.

A number of trends can be established and a number of conclusions made regarding the results presented in Tables 3.2 and 3.3. It is obvious from Table 3.2 that the base load environment is considerably higher in practically all cases where the C.G. offset is aft of the volumetric C.G. location. This occurs since the base region is subjected to the flow in situations where the vehicle is trimmed or is oscillating aft end first during reentry. Notice that the maximum loads on the base occur for the 4, 5 and 7 fineness ratio cone-cylinder configurations at C.G. offsets of 2.5% forward, 2.5% aft and 5% aft, respectively. These maximum levels are essentially independent of initial release attitude. For the cylinder section of the cone-cylinder configuration, a totally different heating load level distribution is observed. The 10% forward location gives the highest load levels and the distribution is highly dependent on the initial release attitude, but essentially independent of fineness ratio. For the base and cylinder regions of the cylinder configurations, the maximum load levels occur for a 10% C.G. aft offset. Notice the difference in the load levels on the base region between the cone-cylinder configurations of fineness ratios 4 and 5 and the same fineness ratio cylinder configurations. Maximum heating loads occur on the base region of both types of configurations when the vehicle is trimmed aft at 140° angle of attack. This is not necessarily the case, however, when a vehicle is oscillating about a 140° trim point since the base may be subjected to flow more often at angles of attack which vary from 140°. These variations are dependent upon the amplitude of the oscillations. It is entirely possible during an oscillating trajectory that oscillations about a 130° or 150° trim attitude, for instance, could give the highest heating levels since the base would then be subjected more often during the trajectory to the 140° maximum load attitude. For the cone-cylinder configurations with fineness ratios of 4 and 5, with C.G. offsets of 2.5% forward and 2.5% aft,

respectively, the constant trim attitudes (from Figs. 2.2 and 2.4 in Section 2) are 147° and 158° . These C.G. offsets result in the highest load levels for the 4 and 5 fineness ratio cone-cylinder configurations. Similarly, constant trim attitudes of 132° and 138° for 10% aft offsets in C.G. give the largest loads for the 4 and 5 fineness ratio cylinder configurations.

A number of other comparisons can be made and trends established concerning relative heating levels with Tables 3.2 and 3.3 for each of the cases and configurations considered in the analysis. The results presented in Tables 3.2 and 3.3 should prove to be valuable to the engineer in that he can determine very quickly and without any calculations the relative magnitude of the heating levels anticipated for his particular mission.

TABLE 3.1
CONE HEATING LOADS

The procedure for computing heating loads to the cone of a cone-cylinder configuration is as follows:

- (1) Determine the angle of attack of the cone's windward surface

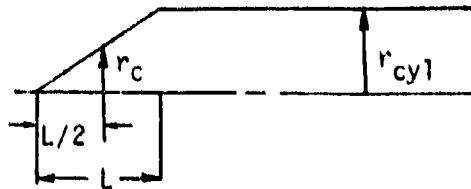
$$\alpha_{\text{cone}} = \alpha_{\text{cyl}} + \theta_c$$

α_{cyl} = Angle of attack of cylinder

θ_c = Semi-vertex angle of the cone

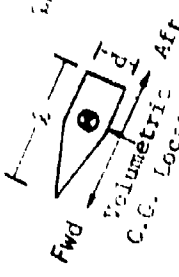
NOTE: If $\alpha_{\text{cone}} > 180^\circ$, $\alpha_{\text{cone}} = 180^\circ$

- (2) Determine the heating load for a cylinder at α_{cone} from Figs. 3.1 to 3.10.
- (3) Determine the cone radius at the midlength of the cone.



- (4) Determine the load adjustment factor for the equivalent cone diameter, $2r_c$, by using Fig. 5.2.
- (5) Make additional adjustments as required for a cylinder calculation.

C.G. (%) α_1	Fwd					Aft				
	15	10	5	2.5	0	2.5	5	10	15	20
90	2	2	3	3	3	3	3	3	3	3
120	2	2	2	2	2	2	2	2	2	2
135	2	2	2	2	2	2	2	2	2	2
150	2	2	2	2	2	2	2	2	2	2
165	2	2	2	2	2	2	2	2	2	2
180	2	2	2	2	2	2	2	2	2	2



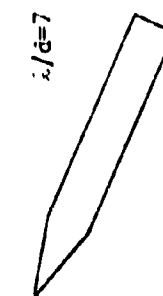
$l/d=3$

C.G. (%) α_1	Fwd					Aft				
	10	5	2.5	0	2.5	5	10	15	20	
90	1	1	1	1	1	4	4	4	4	
120	1	1	1	1	1	4	5	4	4	
135	1	1	1	1	1	4	5	4	3	
150	1	1	1	1	1	4	5	3	3	
165	1	1	2	4	5	3	3	3	3	
180	1	2	2	4	5	3	3	3	3	



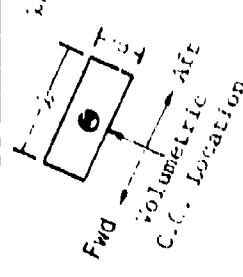
$l/d=5$

C.G. (%) α_1	Fwd					Aft				
	10	5	2.5	0	2.5	5	10	15	20	
90	1	1	1	1	1	3	5	6	6	
120	1	1	1	1	1	3	6	7	5	
135	1	1	1	1	1	3	6	6	5	
150	1	1	1	1	1	3	6	7	4	
165	1	1	1	1	1	3	6	7	3	
180	1	2	2	3	6	7	3	3	3	



$l/d=7$

C.G. (%) α_1	Fwd					Aft				
	10	5	2.5	0	2.5	5	10	15	20	
90	N _D	N _D	N _D	N _D	N _D	N _D	1	1	2	
120	1	1	1	1	1	1	1	2	4	
135	N _D	N _D	N _D	N _D	N _D	1	1	2	5	
150	1	1	1	1	1	1	1	2	5	
165	N _D	N _D	N _D	N _D	N _D	1	2	2	5	
180	1	1	1	1	1	1	2	2	5	



$l/d=2.5$

C.G. (%) α_1	Fwd					Aft				
	10	5	2.5	0	2.5	5	10	15	20	
90	N _D	N _D	N _D	N _D	N _D	1	1	2	3	
120	1	1	1	1	1	1	1	2	4	
135	N _D	N _D	N _D	N _D	N _D	1	1	2	4	
150	1	1	1	1	1	1	1	2	4	
165	N _D	N _D	N _D	N _D	N _D	1	1	2	4	
180	1	1	1	1	1	1	1	2	4	



$l/d=4$

C.G. (%) α_1	Fwd					Aft				
	10	5	2.5	0	2.5	5	10	15	20	
90	N _D	N _D	N _D	N _D	N _D	N _D	1	1	2	
120	1	1	1	1	1	1	1	2	4	
135	N _D	N _D	N _D	N _D	N _D	1	1	2	5	
150	1	1	1	1	1	1	1	2	5	
165	N _D	N _D	N _D	N _D	N _D	1	2	2	5	
180	1	1	1	1	1	1	2	2	5	



$l/d=5$

* C. G. (%) - The percentage of the vehicle's axial length that the C. G. location is offset from the volumetric center of gravity.

** α_1 (degrees) - The initial vehicle release attitude.

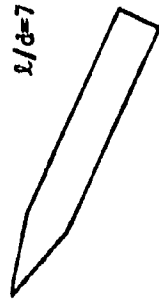
On Base

No.	(0.666) $\frac{BTU}{ft^2}$	No.	(0.666) $\frac{BTU}{ft^2}$
1	0-100	5	400-500
2	100-200	6	500-600
3	200-300	7	600-700
4	300-400	N _D	No Data Available

Table 3.2 Base Heating Load Magnitude Chart (H = 200 mi.)

$l/d=7$

C.G. (%) $q_1(\%)$	Fwd					Aft					
	10	5	2.5	0	2.5	5	10	15	20	25	30
90	6	5	2	4	4	3	2	2	4	3	2
120	6	4	3	4	5	4	2	2	4	2	2
135	5	4	3	4	5	4	2	2	4	2	2
150	4	3	3	4	5	4	2	2	4	2	2
165	3	3	3	4	5	4	2	2	4	2	2
180	2	2	4	3	4	4	1	1	4	1	1



* C. G. (Z) - The percentage of the vehicle's axial length that the C. G. location is offset from the volumetric center of gravity.

** α_i (degrees) - The initial vehicle release attitude.

No.	Cylinder		No.	(Q ₆₅₀) BTU/ft ²	(Q ₆₅₀) BTU/ft ²
	(Q ₆₅₀) BTU/ft ²	No.			
1	0-100	5	5	400-500	
2	100-200	6	6	500-600	
3	200-300	7	7	600-700	
4	300-400	N/D	N/D	No Data Available	

$l/d=5$

C.G. (%) $q_1(\%)$	Fwd					Aft					
	10	5	2.5	0	2.5	5	10	15	20	25	30
90	6	4	3	3	2	2	2	2	2	2	2
120	5	3	3	4	3	2	2	2	2	2	2
135	5	3	3	4	2	1	1	1	1	1	1
150	4	3	3	4	3	1	1	1	1	1	1
165	3	3	3	4	3	1	1	1	1	1	1
180	2	2	3	4	2	1	1	1	1	1	1



$l/d=5$

C.G. (%) $q_1(\%)$	Fwd					Aft					
	10	5	2.5	0	2.5	5	10	15	20	25	30
90	N/D	N/D	N/D	2	3	3	4	4	4	4	4
120	4	4	3	2	2	2	4	5	5	5	5
135	N/D	N/D	N/D	2	3	4	5	5	5	5	5
150	3	3	3	3	3	4	5	5	5	5	5
165	N/D	N/D	N/D	3	3	3	4	5	5	5	5
180	2	2	2	3	3	3	4	5	5	5	5



$l/d=4$

C.G. (%) $q_1(\%)$	Fwd					Aft					
	10	5	2.5	0	2.5	5	10	15	20	25	30
90	6	2	3	2	2	2	1	1	1	1	1
120	5	3	3	1	1	1	1	1	1	1	1
135	5	3	3	1	1	1	1	1	1	1	1
150	4	3	3	1	1	1	1	1	1	1	1
165	2	3	3	1	1	1	1	1	1	1	1
180	2	3	3	1	1	1	1	1	1	1	1



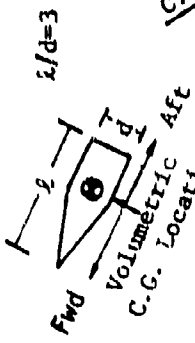
$l/d=4$

C.G. (%) $q_1(\%)$	Fwd					Aft					
	10	5	2.5	0	2.5	5	10	15	20	25	30
90	N/D	N/D	N/D	2	3	3	4	4	4	4	4
120	3	3	3	2	2	3	4	4	4	4	4
135	N/D	N/D	N/D	2	3	3	4	4	4	4	4
150	3	3	3	3	3	3	4	4	4	4	4
165	N/D	N/D	N/D	3	3	3	4	4	4	4	4
180	2	2	3	3	3	3	4	4	4	4	4



$l/d=3$

C.G. (%) $q_1(\%)$	Fwd					Aft					
	10	5	2.5	0	2.5	5	10	15	20	25	30
90	1	1	1	1	1	1	1	1	1	1	1
120	1	1	1	1	1	1	1	1	1	1	1
135	1	1	1	1	1	1	1	1	1	1	1
150	1	1	1	1	1	1	1	1	1	1	1
165	1	1	1	1	1	1	1	1	1	1	1
180	1	1	1	1	1	1	1	1	1	1	1



$l/d=3$

C.G. (%) $q_1(\%)$	Fwd					Aft					
	10	5	2.5	0	2.5	5	10	15	20	25	30
90	N/D	N/D	N/D	2	2	2	3	3	3	3	3
120	3	2	2	2	2	2	3	3	3	3	3
135	N/D	N/D	N/D	2	2	2	3	3	3	3	3
150	2	2	2	2	2	2	3	3	3	3	3
165	N/D	N/D	N/D	2	2	2	3	3	3	3	3
180	2	2	3	2	2	2	3	3	3	3	3

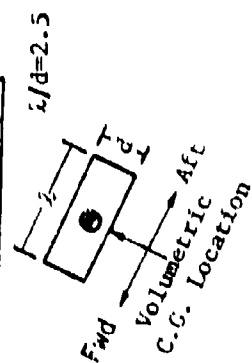
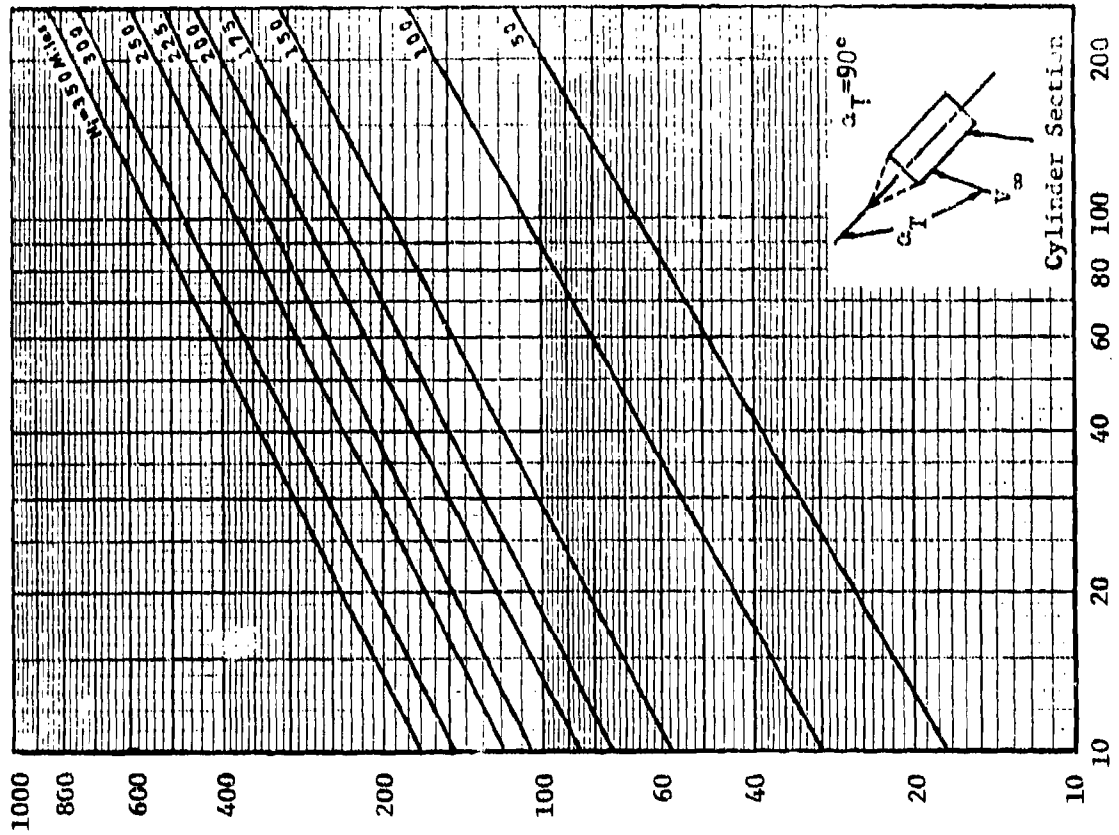
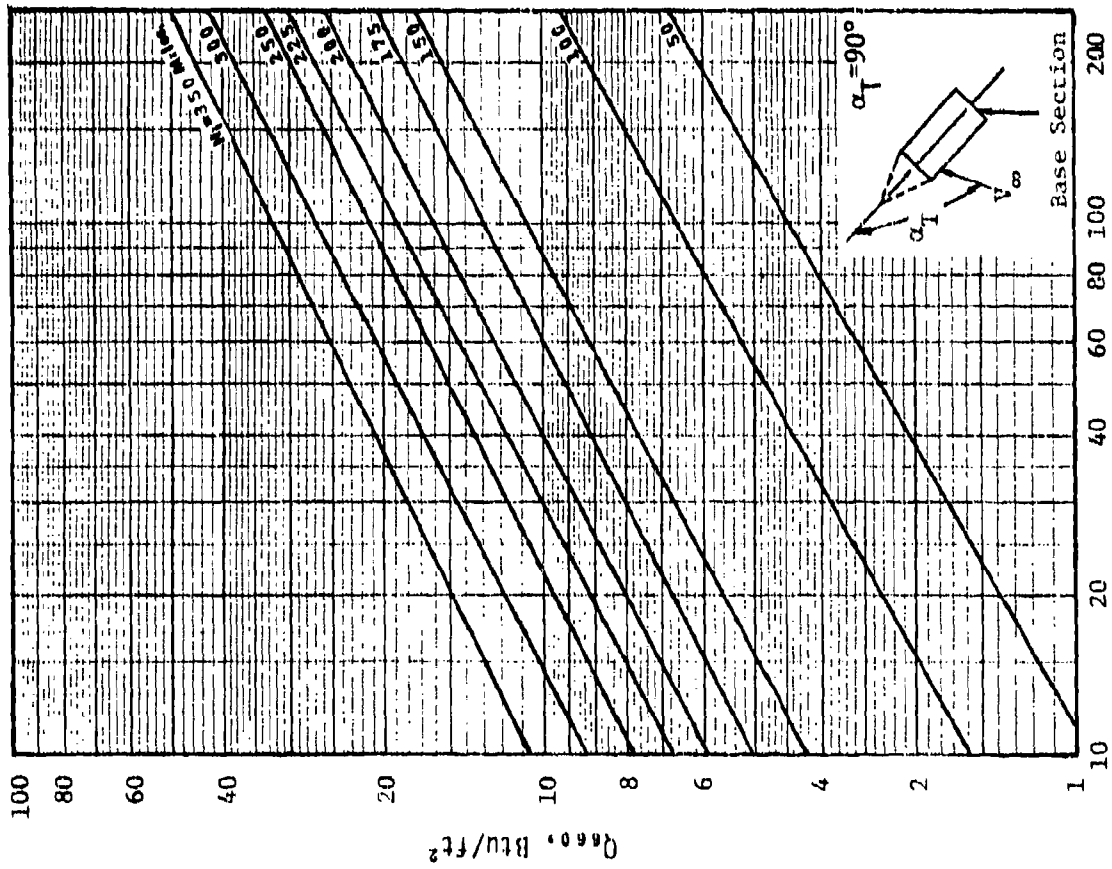


Table 3.3 Cylinder Heating Load Magnitude Chart (H = 200 mi.)



W/C_{DA} , lb/ft^2



W/C_{DA} , lb/ft^2

Fig. 3.1 Heating Loads for $\alpha_T = 90^\circ$

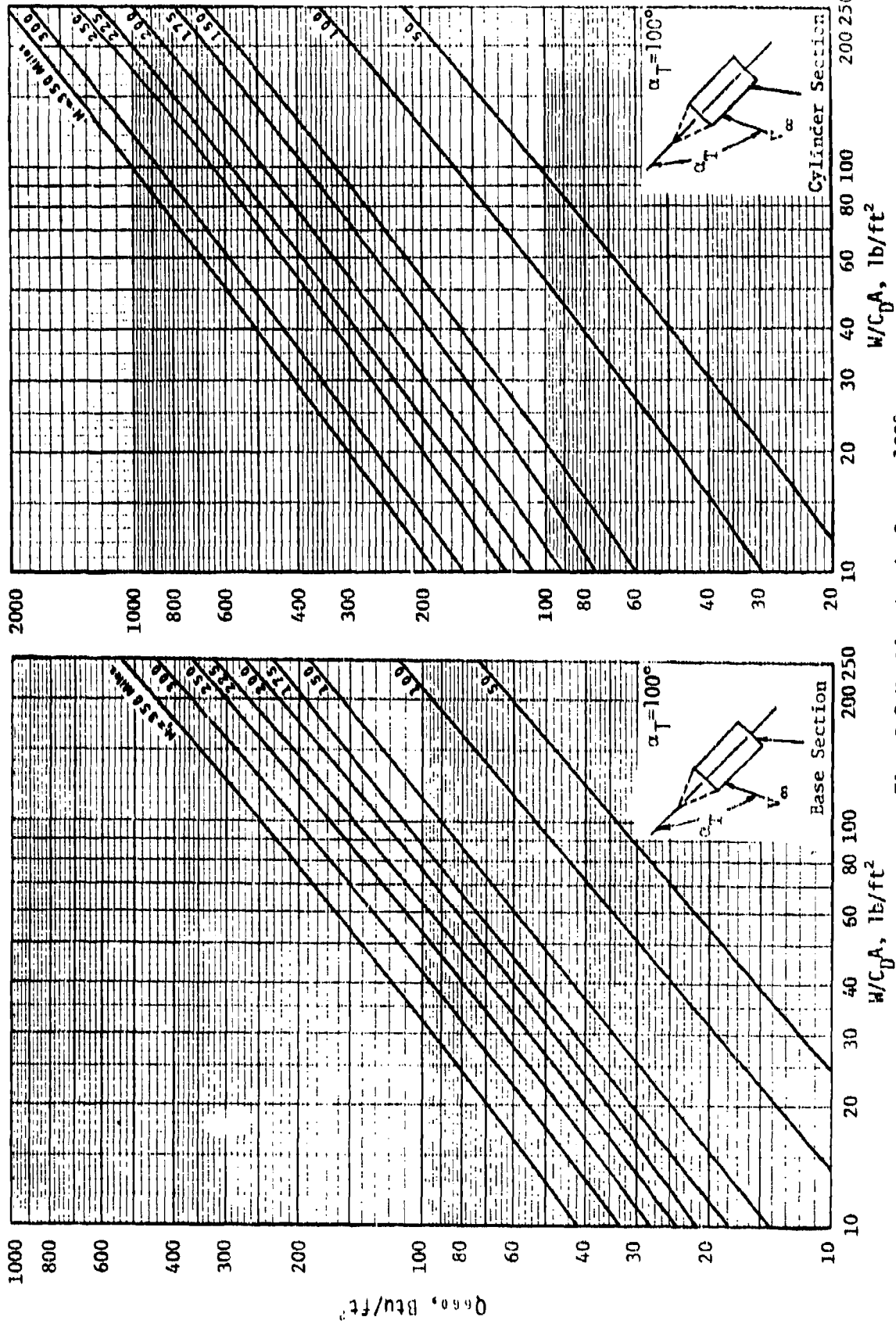


Fig. 3.2 Heating Loads for $\alpha_T=100^\circ$

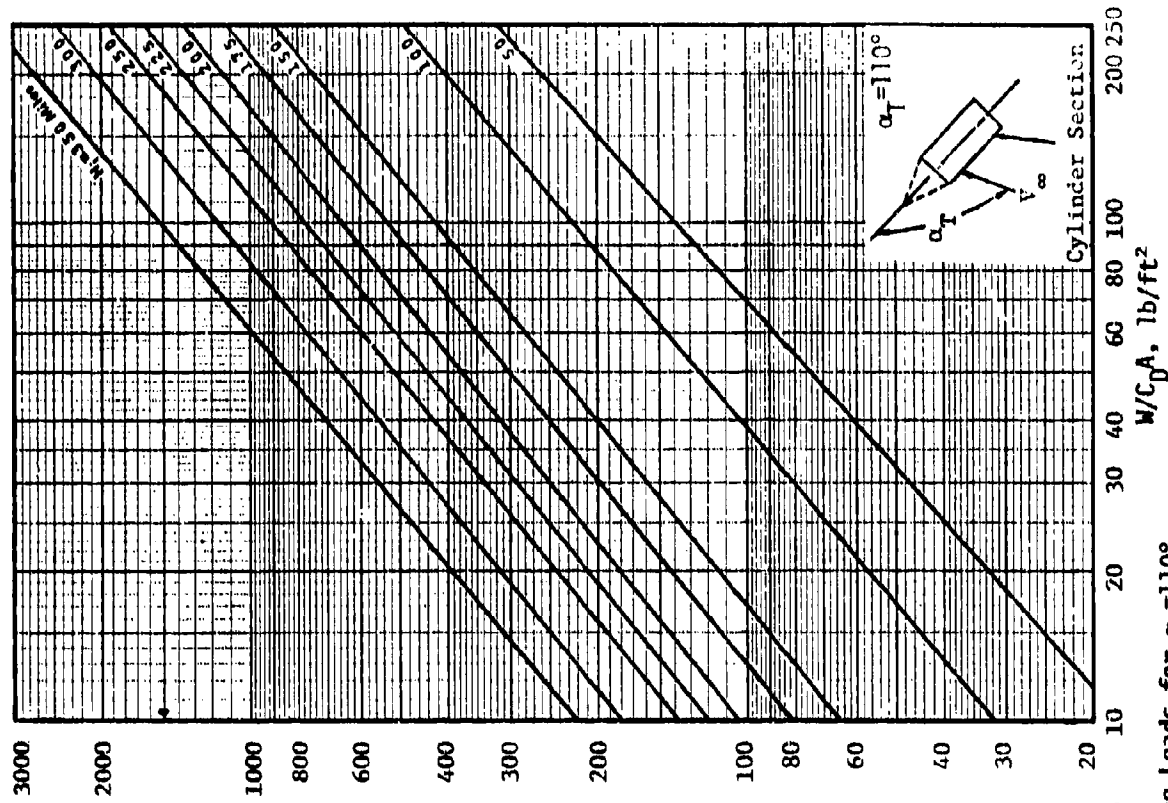
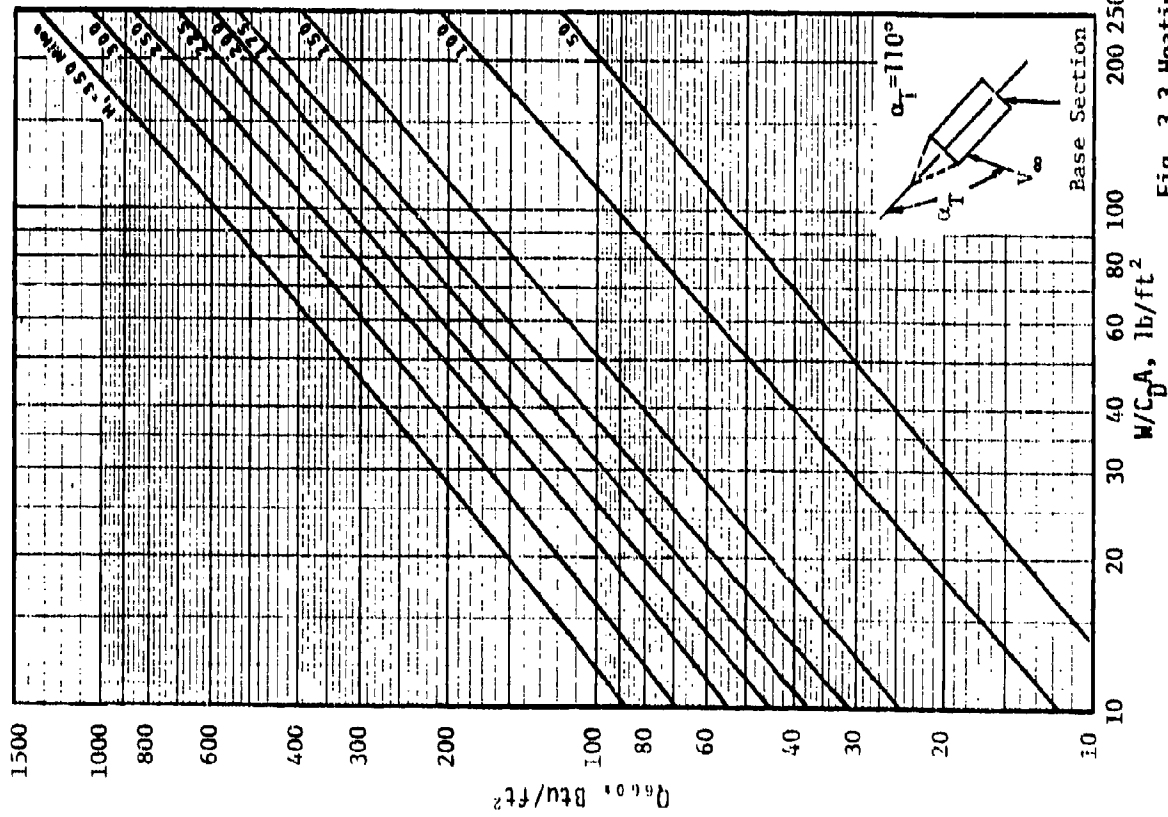


Fig. 3.3 Heating Loads for $\alpha_T = 110^\circ$

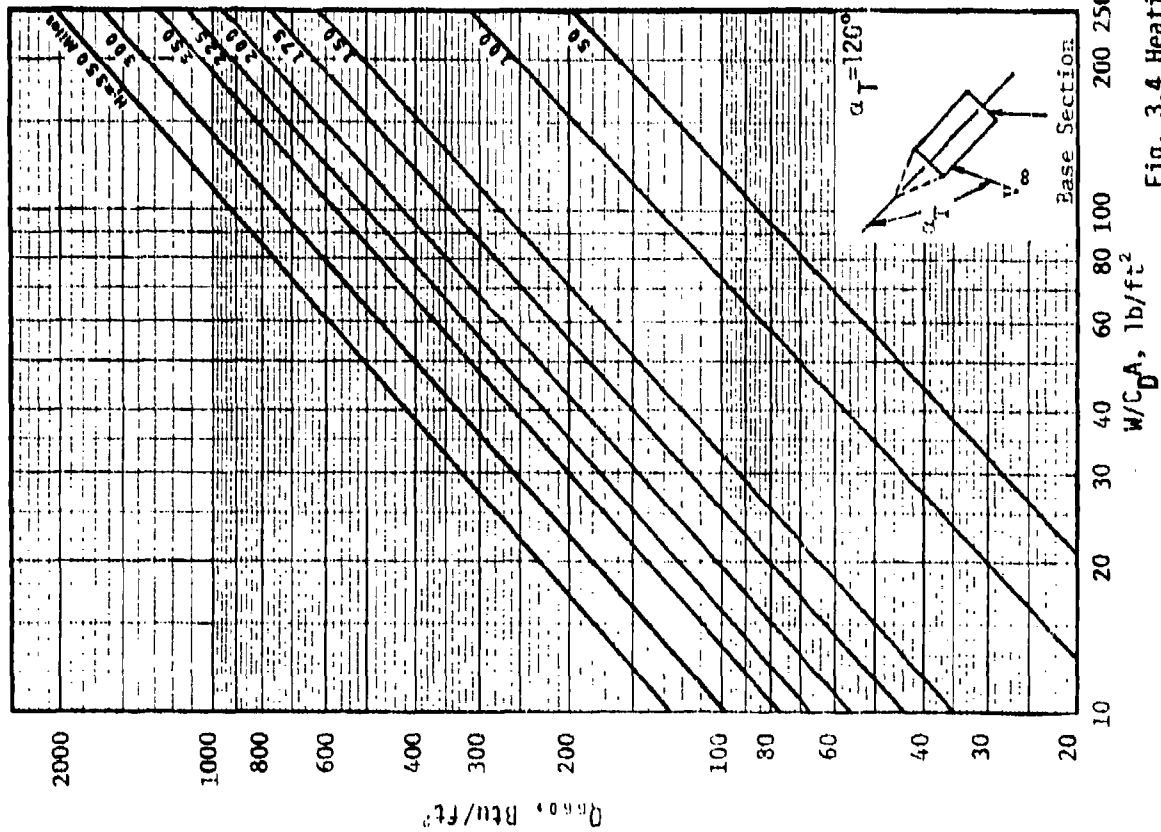
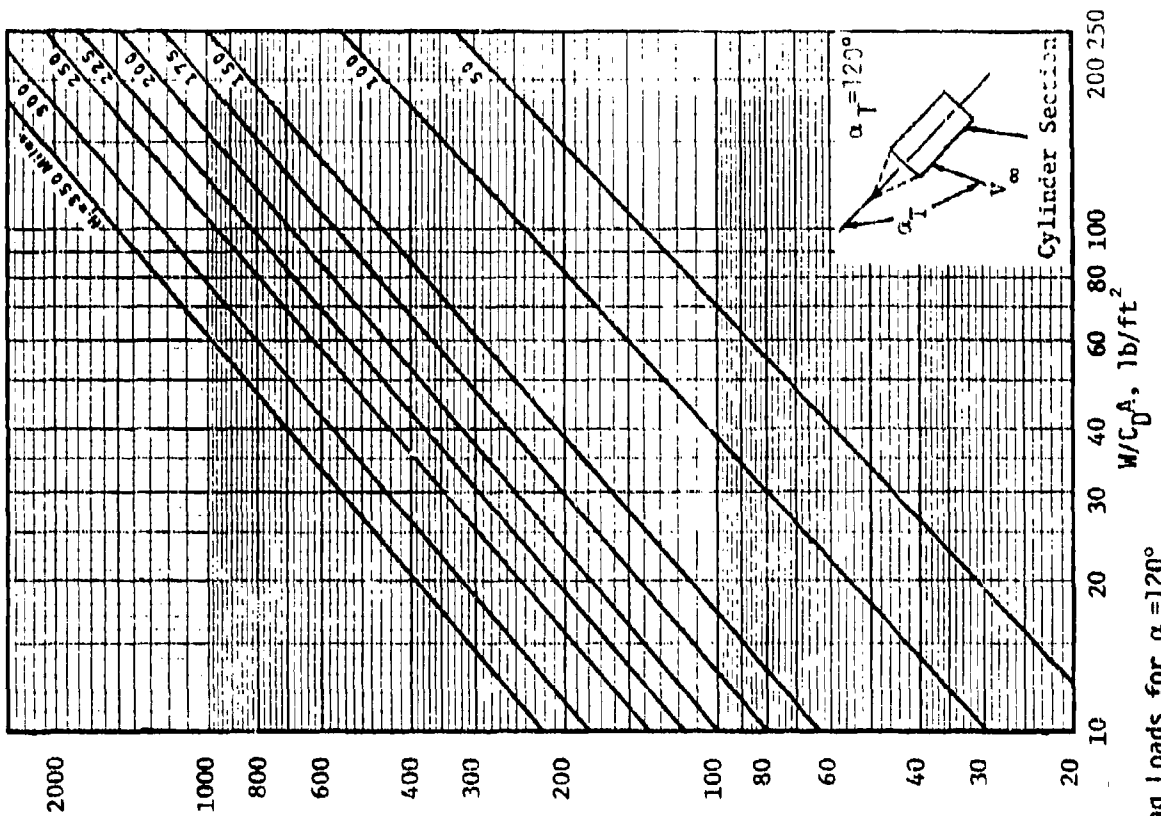


Fig. 3.4 Heating Loads for $\alpha_T = 120^\circ$

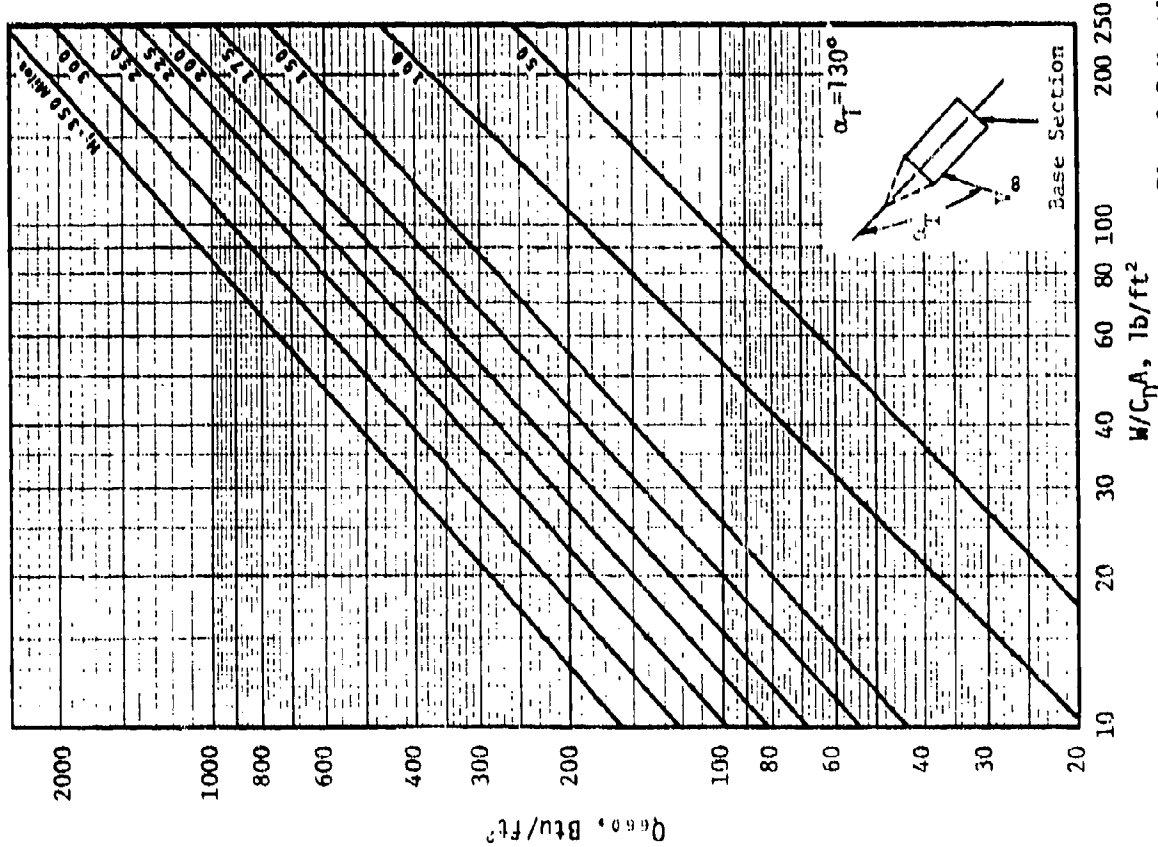
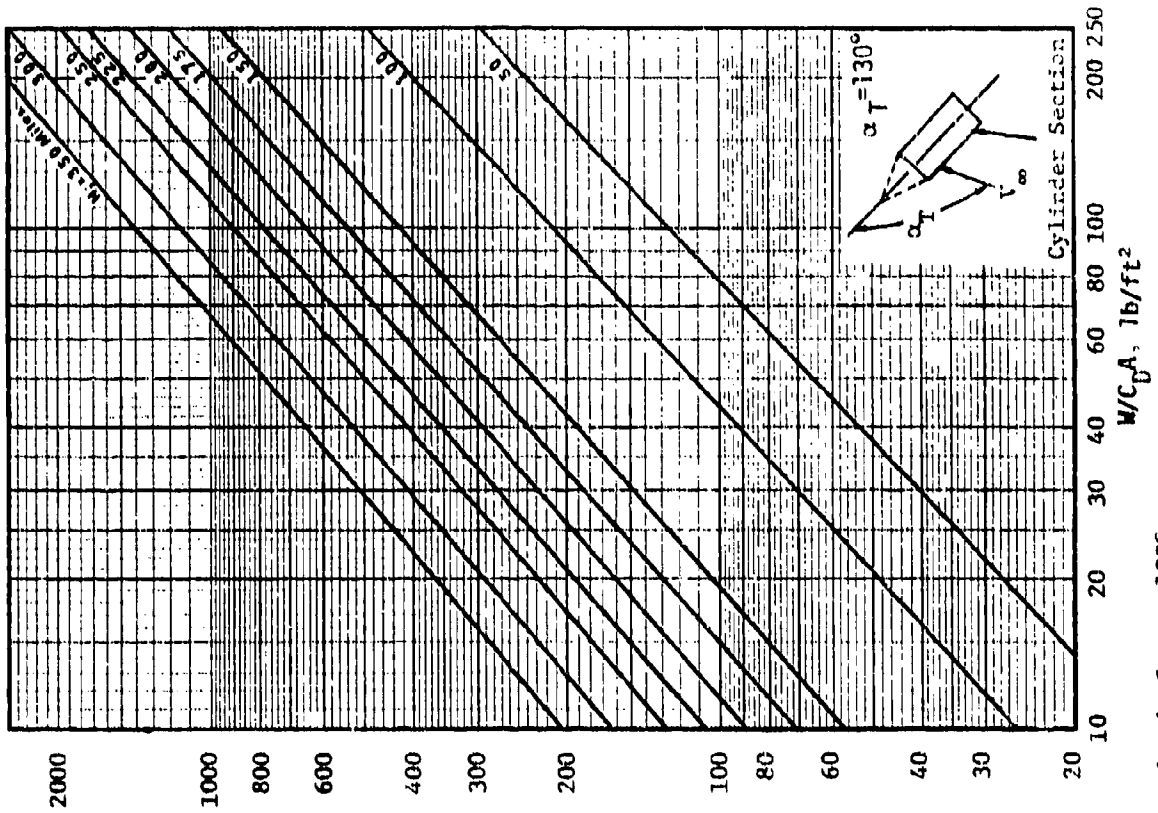


Fig. 3.5 Heating Loads for $\alpha_T = 130^\circ$

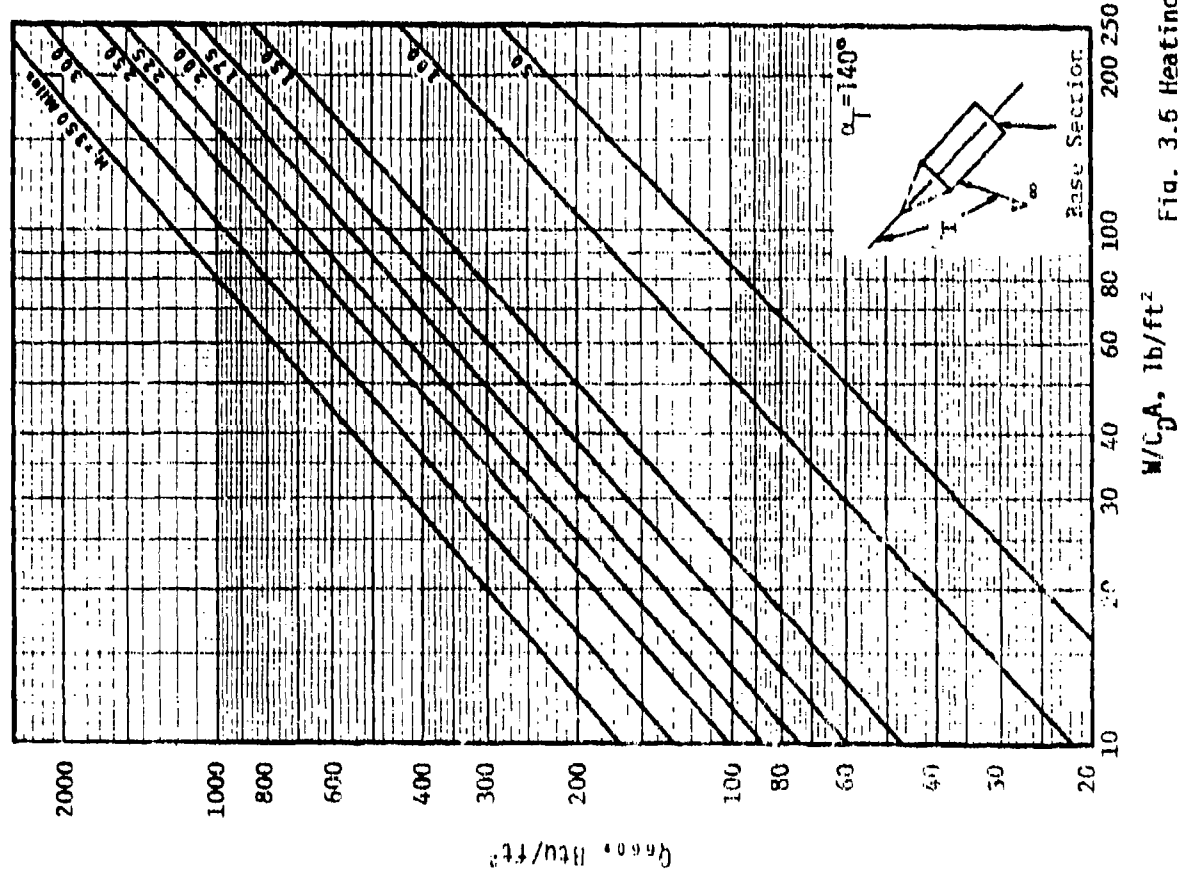
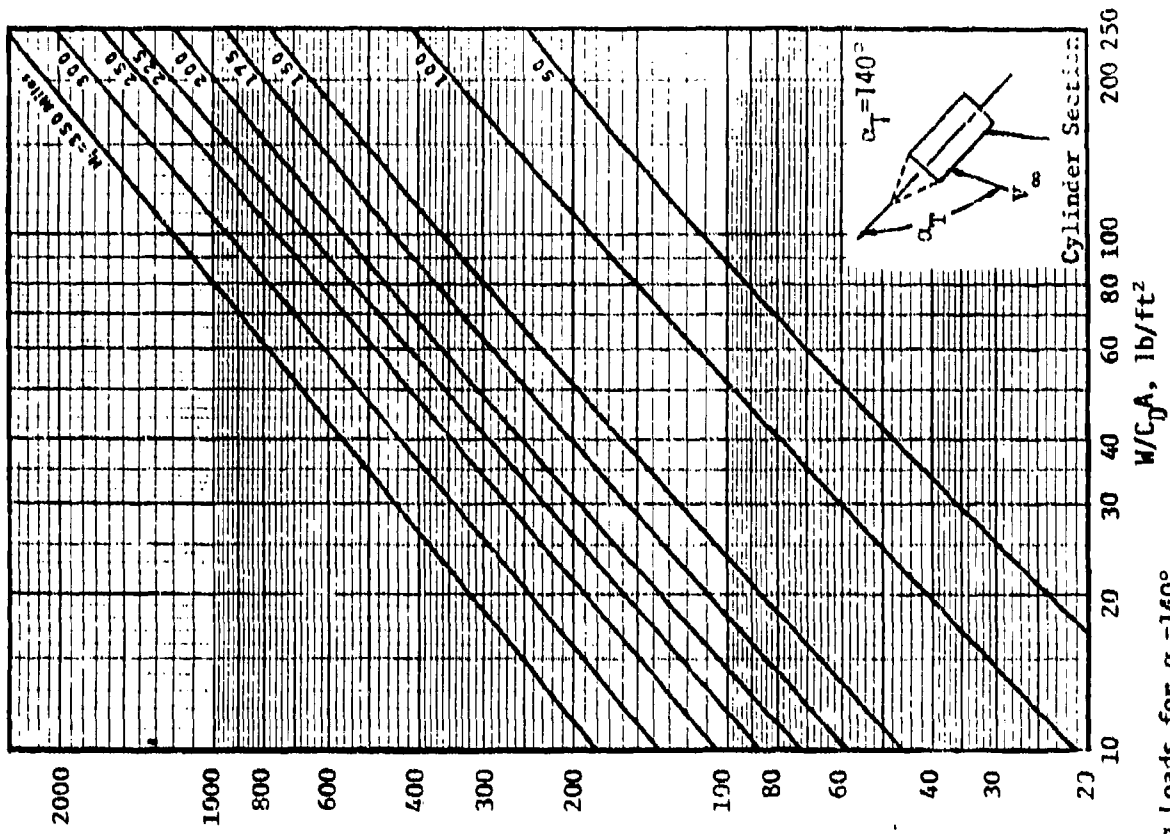


Fig. 3.5 Heating Loads for $\alpha_T = 140^\circ$

Q_{conv}, Btu/ft²

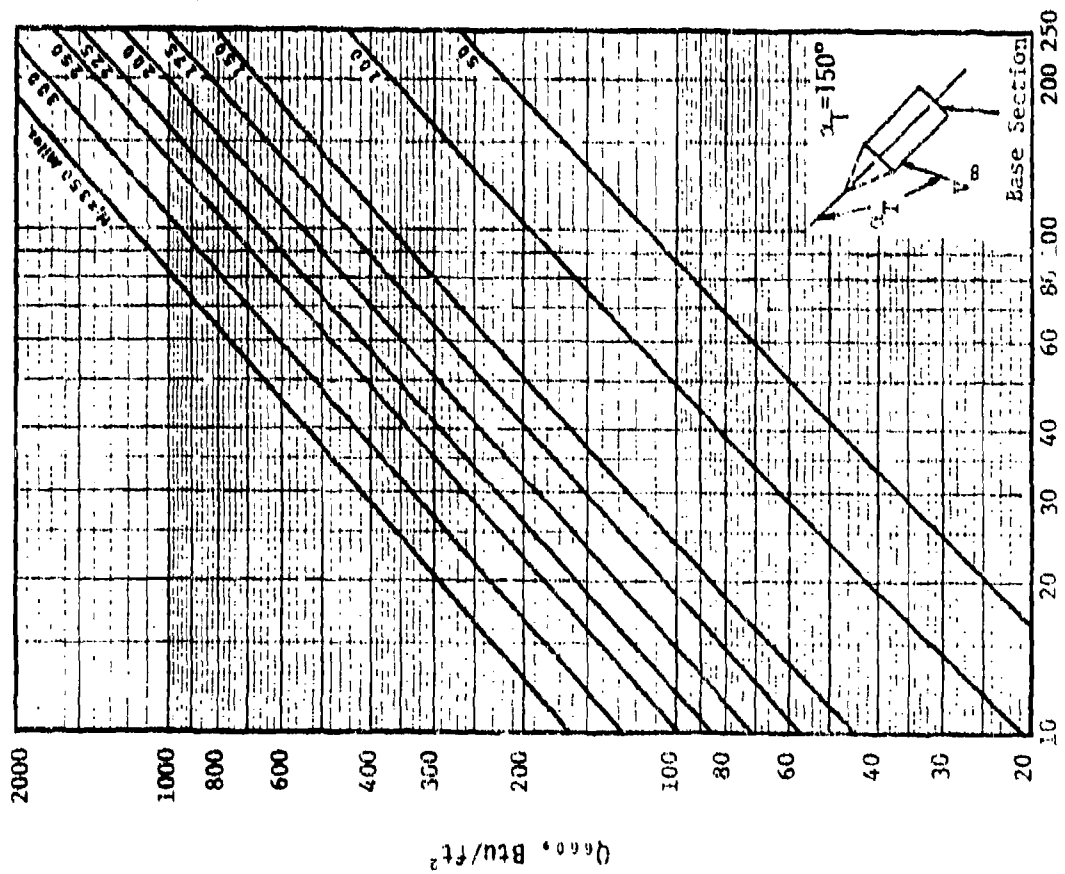
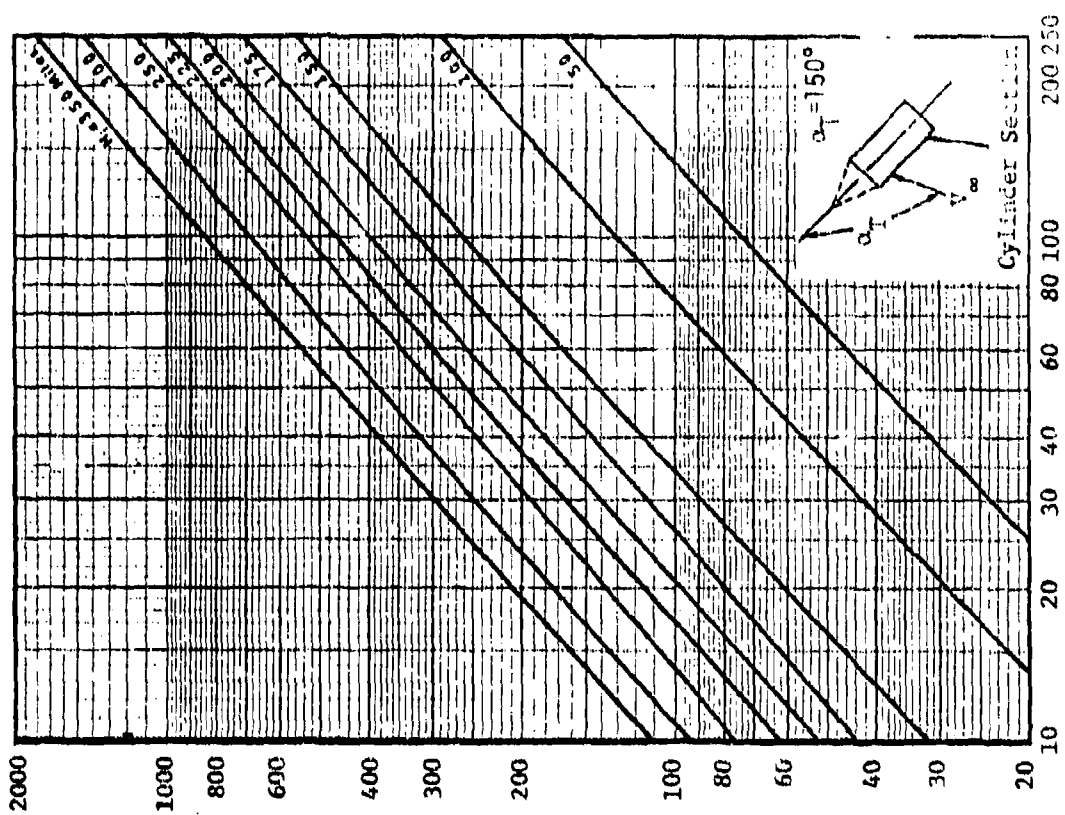


Fig. 3.7 Heating Loads for $\alpha_T = 150^\circ$

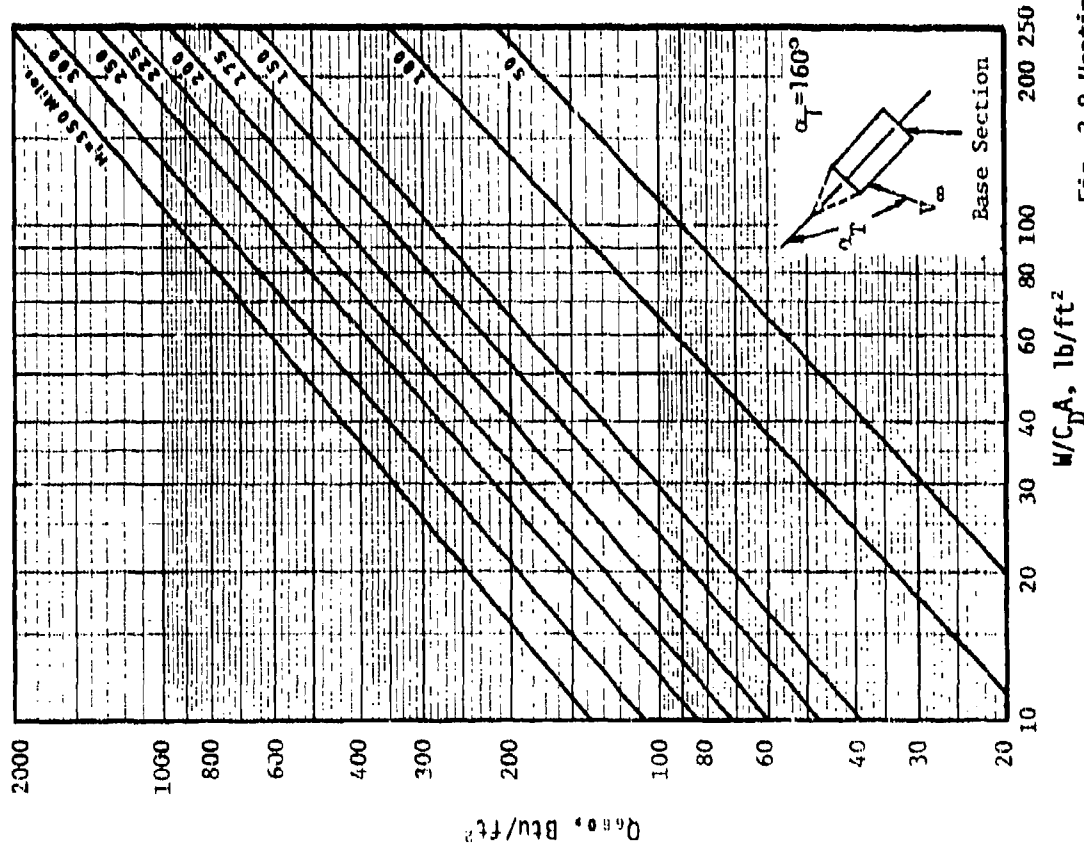
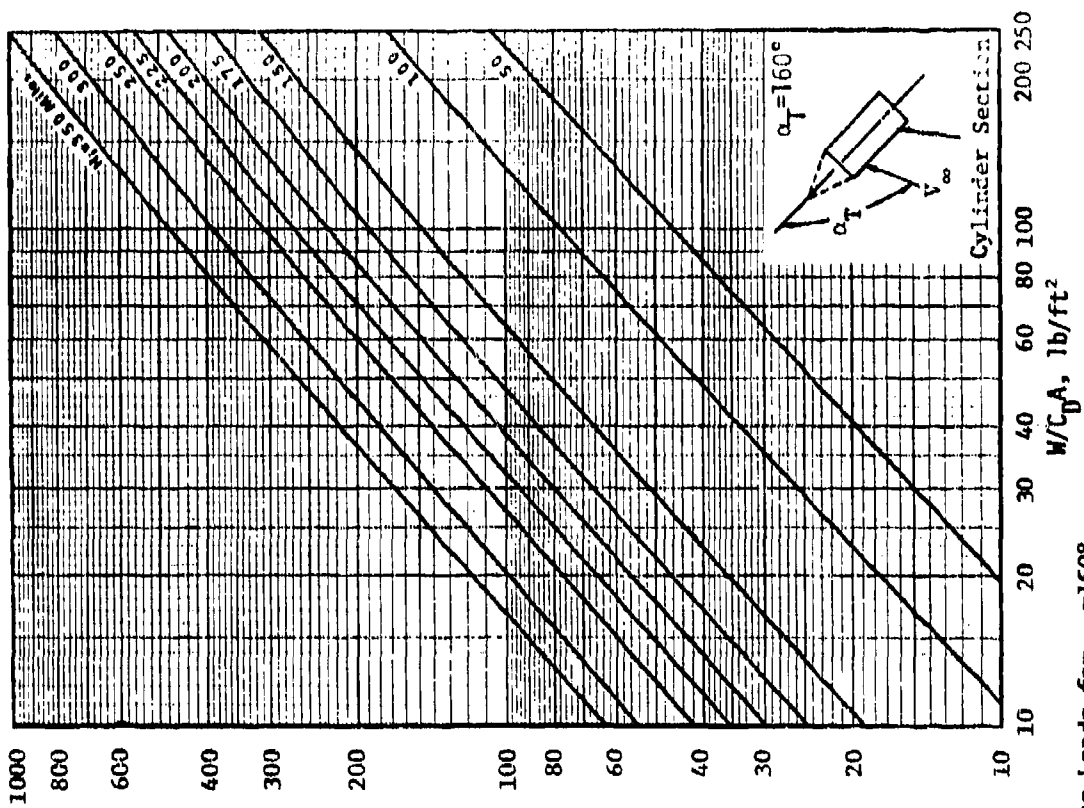


Fig. 3.8 Heating Loads for $\alpha_T = 160^\circ$

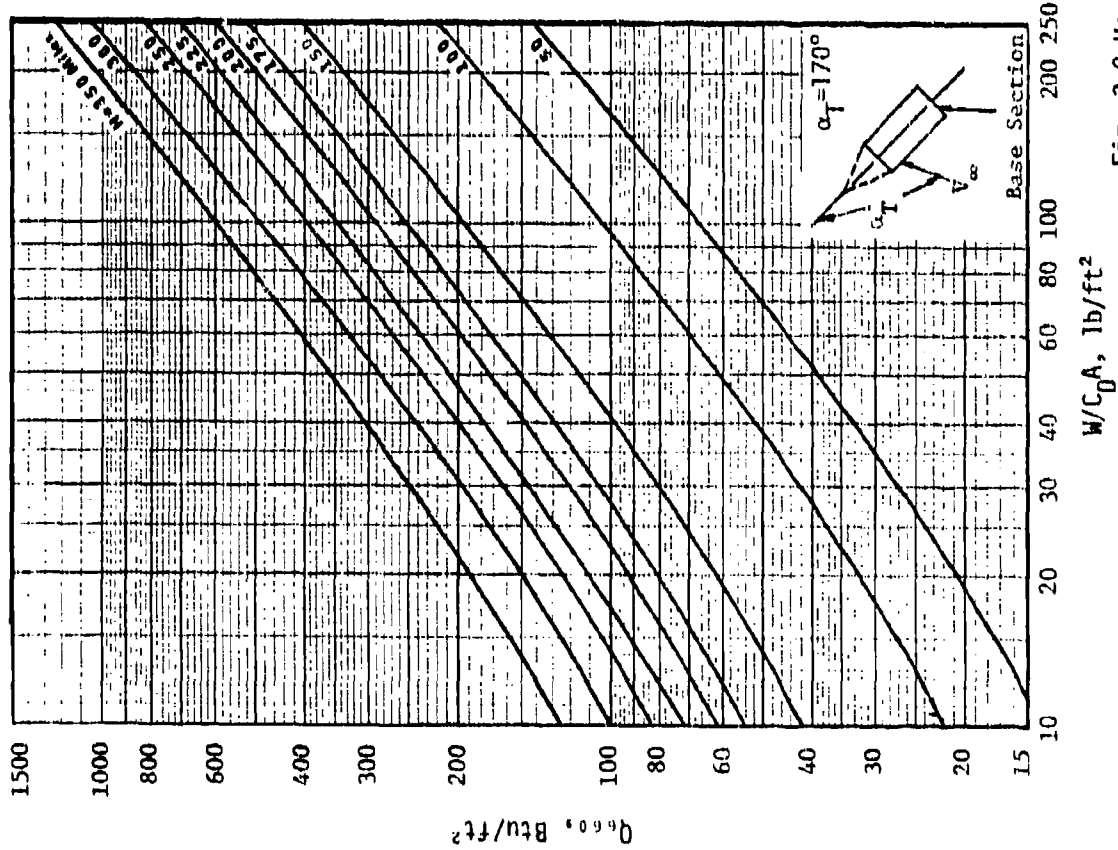
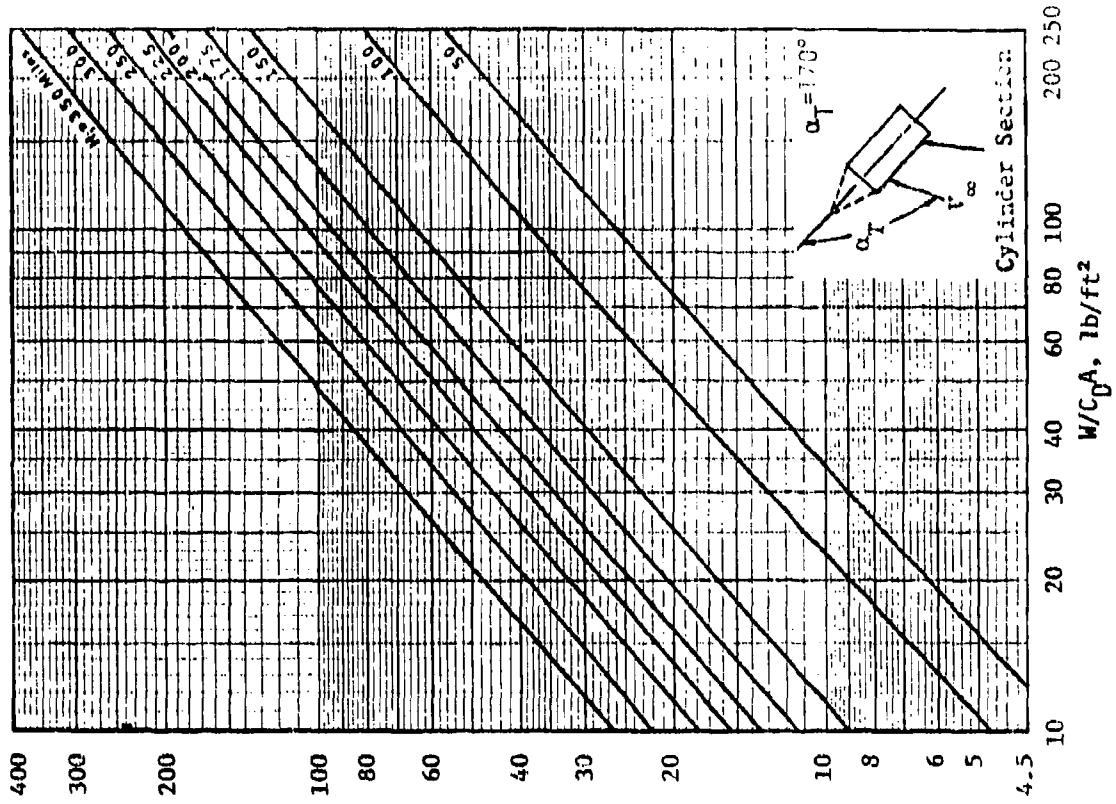


Fig. 3.9 Heating Loads for $\alpha_T=170^\circ$

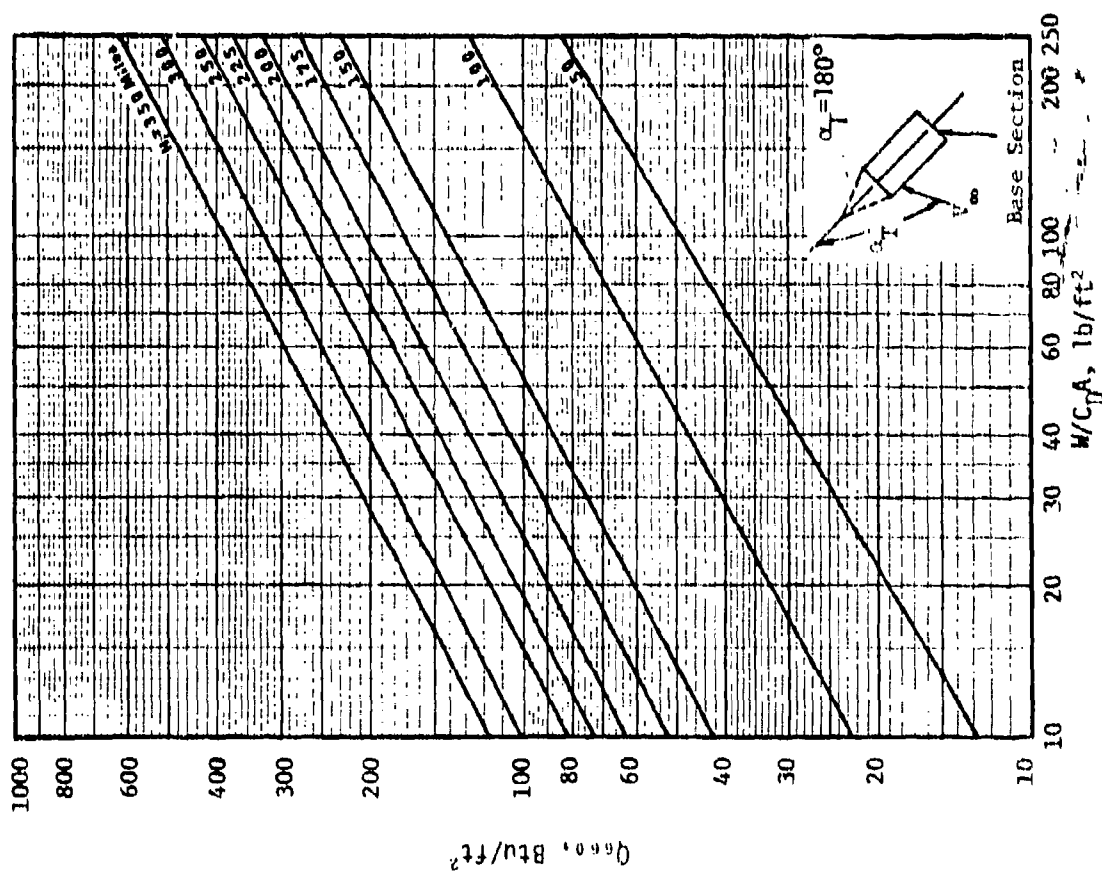
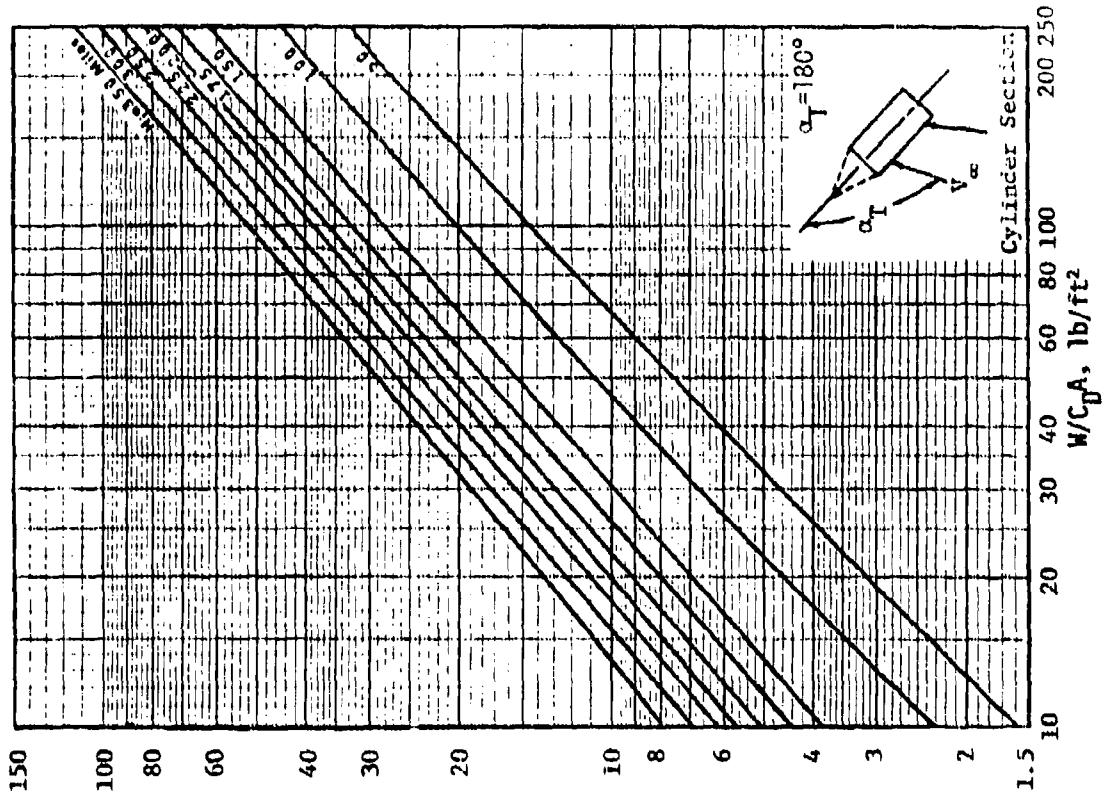


Fig. 3.10 Heating Loads for $\alpha_T = 180^\circ$

SECTION 4

OSCILLATING AND TUMBLE CORRECTION FACTORS

As discussed in previous sections, various C. G. locations and initial release attitude combinations cause large vehicle oscillations and tumbling during reentry for the types of geometric configurations being considered in this analysis. The effects of these types of dynamics on the vehicle's entry trajectory as to its altitude, velocity, and time history were discussed in Section 6. The aerodynamic heating on a reentry vehicle is determined not only by the vehicle's velocity and altitude, but also its attitude. Although the variations in the vehicle's descent velocity changes the heating load, the variations in attitude have a more pronounced effect. This can be seen by examining the heating load plots given in Figs. 3.1 - 3.10 in Section 5 for the range of 90 to 180 degrees in reentry angle of attack.

During typical large oscillating trajectories, the angle of attack may vary 180° for one complete oscillation of the reentry vehicle. This variation could be 360° when the vehicle completely tumbles. The heating rate on the reentry vehicle can vary from a very small rate to a tremendously large rate during one complete oscillation. Therefore, in order to adequately perform a heating analysis, the integrated heating load must be determined which considers this large variation in vehicle attitude. This is the rationale in using a tumbling entry heating program such as the Reentry Computer Program for the heating analysis.

Tables 3.1 and 3.2 in Section 3 present the relative levels of heating for the configuration types and C. G. offset and attitude combinations considered in this analysis. The trajectories, for which these loads were obtained, cover

practically all possible types of constant trim, oscillating, and tumbling reentry trajectories. The heating loads computed with the Bentry Program for these trajectories were non-dimensionalized by the loads obtained for a constant trim ballistic reentry. These non-dimensionalized values which are called tumble correction factors were plotted versus attitude offset parameter, P, and presented in Figs. 4.1 - 4.14. The attitude offset parameter is defined by equation 4.1

$$P = \frac{\alpha_i - \alpha_T}{\alpha_T} \quad 4.1$$

where

α_i = The initial vehicle release attitude (Deg.)

α_T = The vehicle trim attitude determined from Section 2 (Deg.)

It is obvious from equation 4.1 that P is equal to 0 if the vehicle were released at its trim attitude and that the value of P becomes larger the further the release attitude is from the vehicle trim attitude.

It is important, in order to correctly apply the tumble correction factors, that the philosophy behind the development of these factors be discussed. A trim attitude can be established for a reentry vehicle by the methods presented in Section 2 if the aerodynamic force center and C. G. location is known for the vehicle. If the vehicle trims, it will always trim at this attitude and if the vehicle oscillates or tumbles, it will always oscillate or tumble about this trim attitude. Therefore, regardless of what type of vehicle attitude dynamics are involved, a reference heating load can be computed as if the vehicle were trimmed at its theoretical trim attitude. This is precisely the manner in which the constant trim loads were computed in order to non-dimensionalize the heating loads computed with the Bentry Program and to form the tumble correction factors presented in this section.

The tumble correction factors presented in Figs. 4.1 - 4.14 were determined for all the cases and configurations considered in this analysis. If the fineness ratio, C. G. location, or initial release attitude for a flight case varies from the cases considered, linear interpolate in order to determine the tumble correction factors for that case.

Tumble correction factors of 20 are not uncommon for a number of cases considered. Even though these factors are large, the resultant tumble corrected heating loads obtained when using these factors are small. This is due to the fact that the constant trim load, Q_{ct} , is very small. For instance, notice in Fig. 4.1 that a factor of 21 is obtained for the base region of a 7 fineness ratio cone-cylinder configuration with a 2.5% offset forward in C. G. location released at an attitude of 180°. The constant trim load for this case is 9 Btu/ft². The tumble corrected load is then equal to this load times the tumble correction factor of 21 which is equal to 189 Btu/ft² which is a comparatively small heating load. This is usually the case when large factors are obtained.

Even though the tumble correction factors are presented for use in the section, one should exercise great care in their application. This is especially true in applying tumble correction factors less than one. For engineering design purposes, the following guidelines are recommended. Apply the correction factors only when they are greater than one. Use a factor of one in situations where the tumble correction factor is less than one. In this way a certain amount of conservatism is maintained in the results since the heating load is never reduced to a value less than the constant trim heating load.

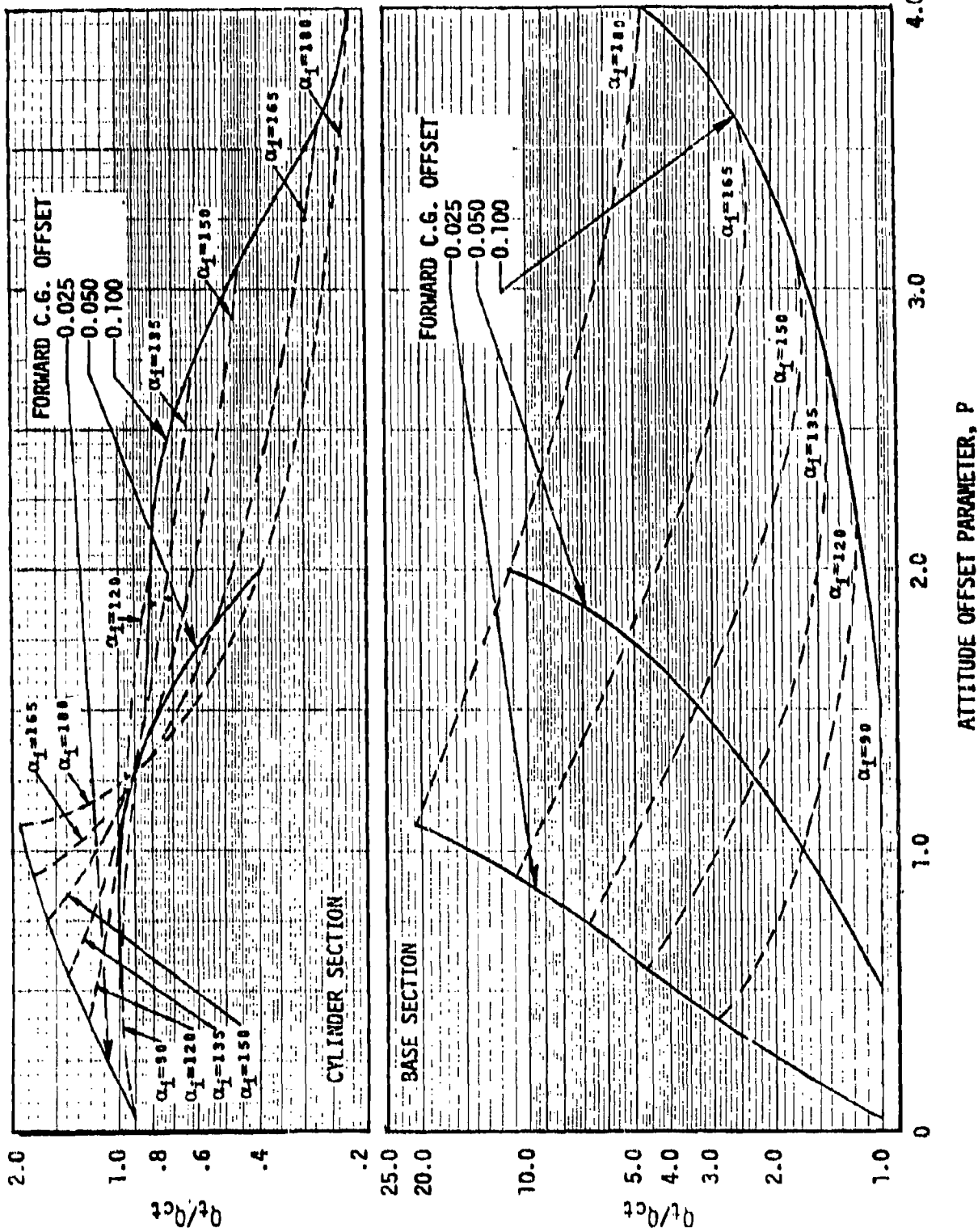


Fig. 4.1 Tumble correction factors, Q_t/Q_{ct} , for base and cylindrical sections of cone-cylinder configuration fineness ratio, l/d , of 7 versus offset parameter, P .

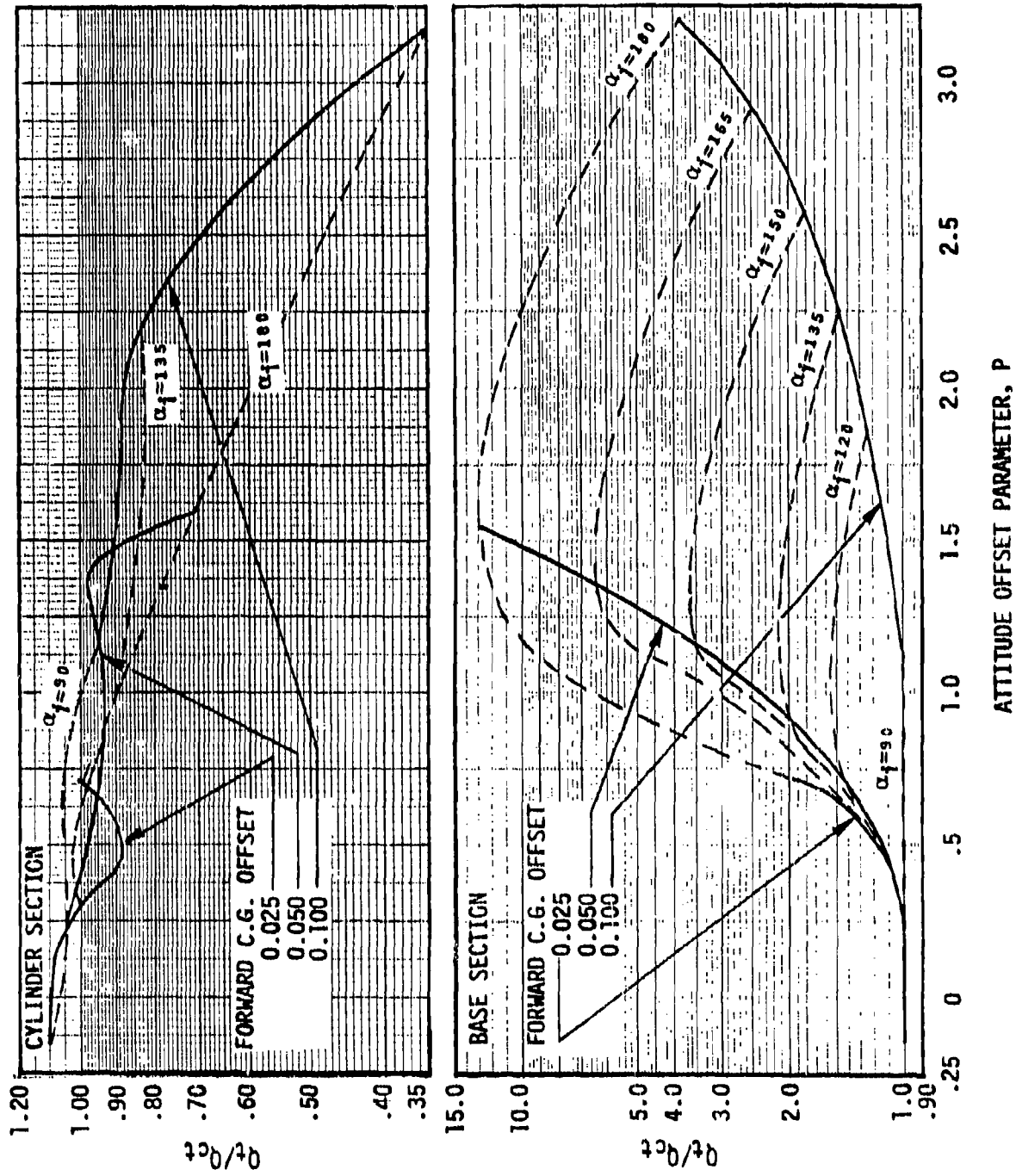


Fig. 4.2 Tumble correction factors, Q_t/Q_{ct} , for base and cylindrical sections of cone-cylinder configuration fineness ratio, z/d , of 5 versus attitude offset parameter, P .

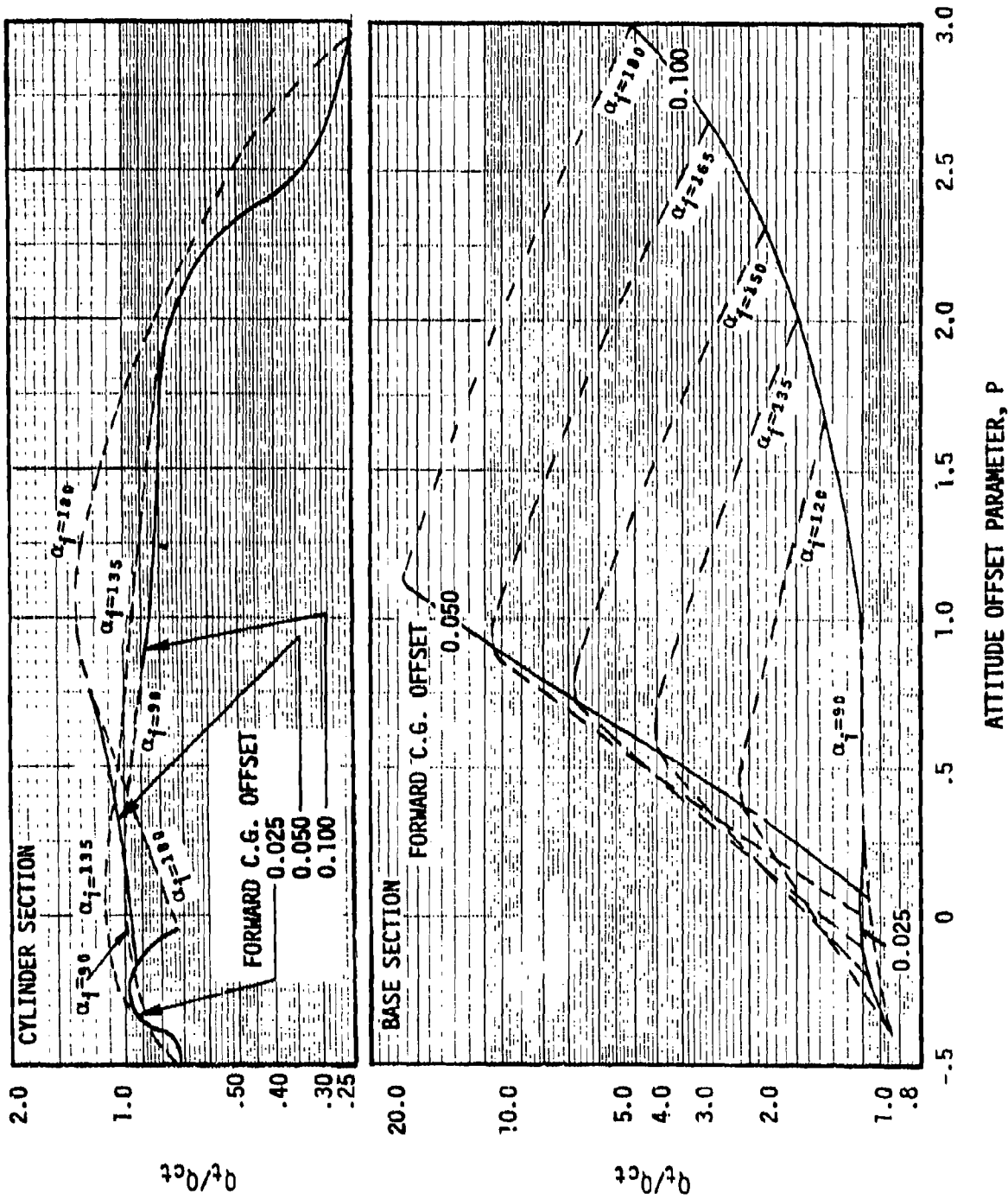


Fig. 4.3 Tumble correction factors, Q_c/Q_{ct} , for base and cylindrical section of cone-cylinder configuration fineness ratio, l/d , of 4 versus attitude offset parameter, P.

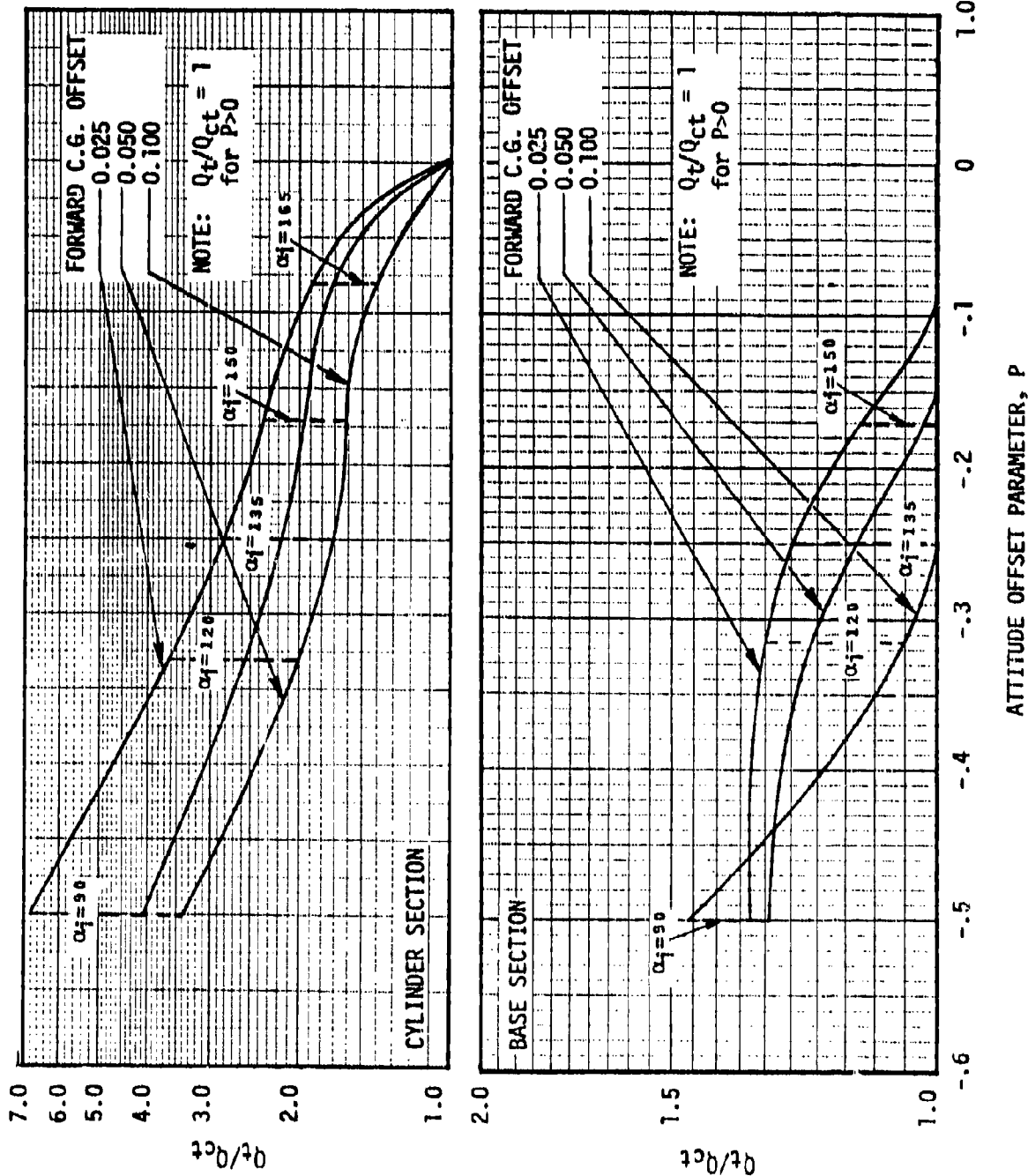


Fig. 4.4 Tumble correction factors, Q_t/Q_{ct} , for base and cylinder sections of cone-cylinder configuration fineness ratio, l/d , of 3 versus attitude offset parameter, P .

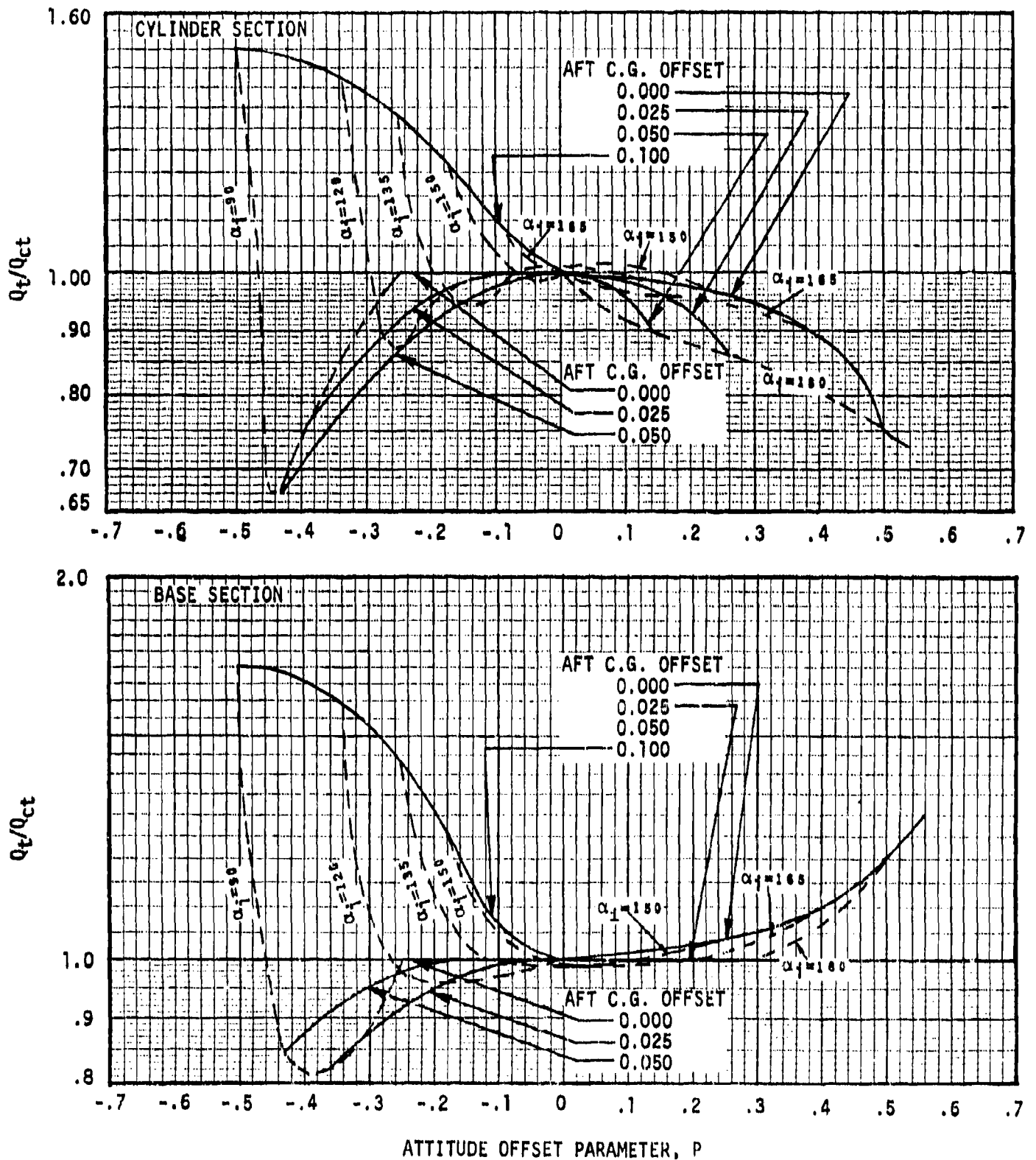


Fig. 4.5 Tumble correction factors, Q_t/Q_{ct} , for base and cylindrical sections of cone-cylinder configuration fineness ratio, ℓ/d , of 7 versus attitude offset parameter, P .

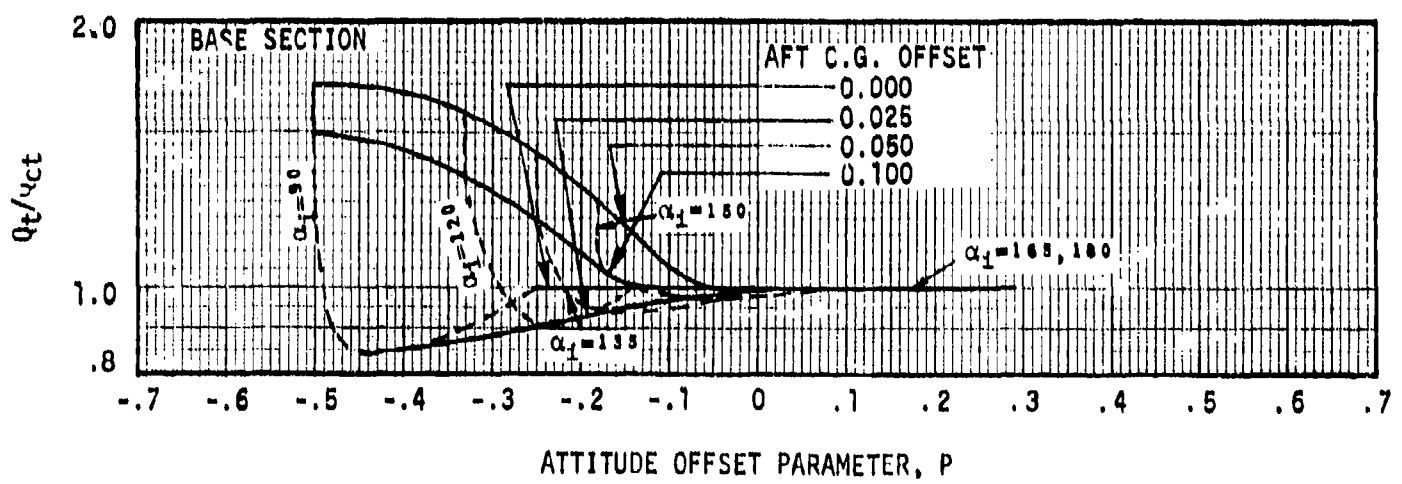
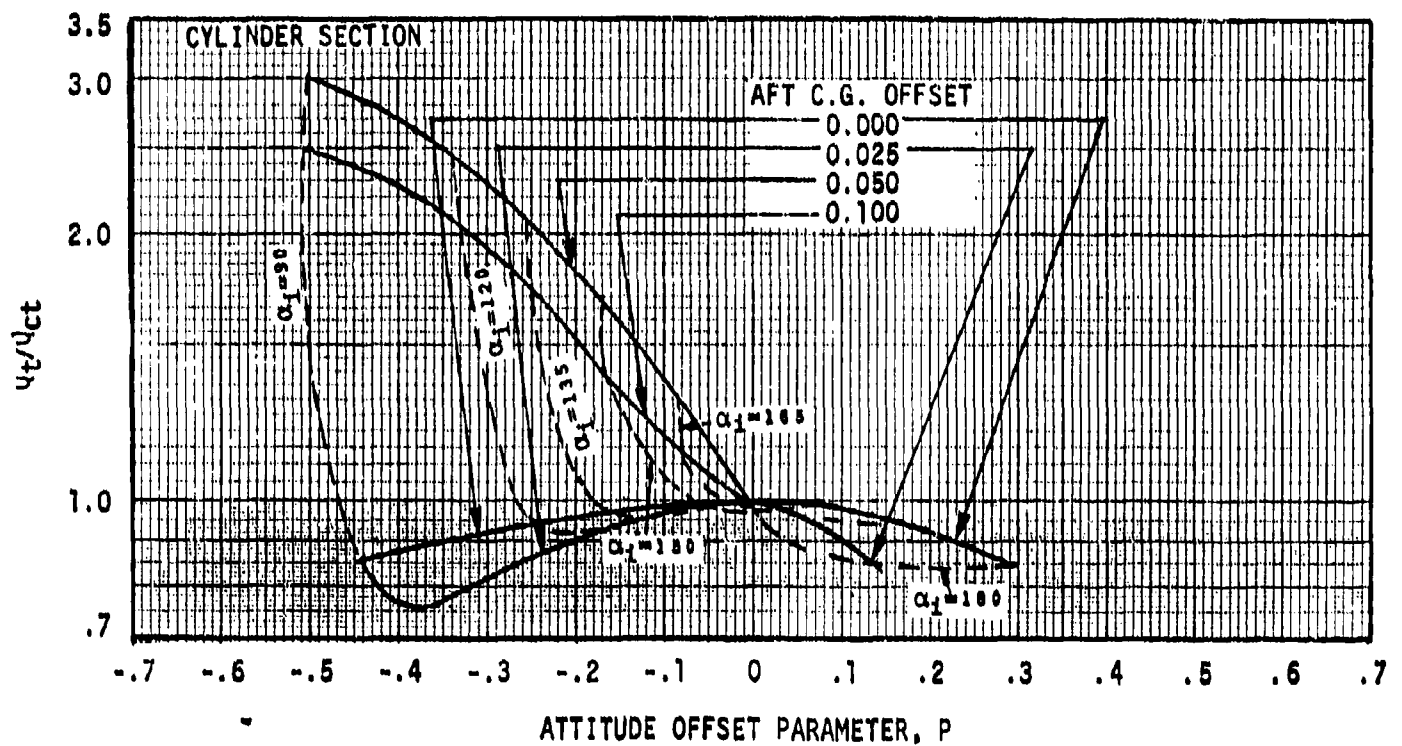


Fig. 4.6 Tumble correction factors, Q_t/Q_{ct} , for base and cylindrical sections of cone-cylinder configuration fineness ratio, λ/d , of 5 versus offset parameter, P.

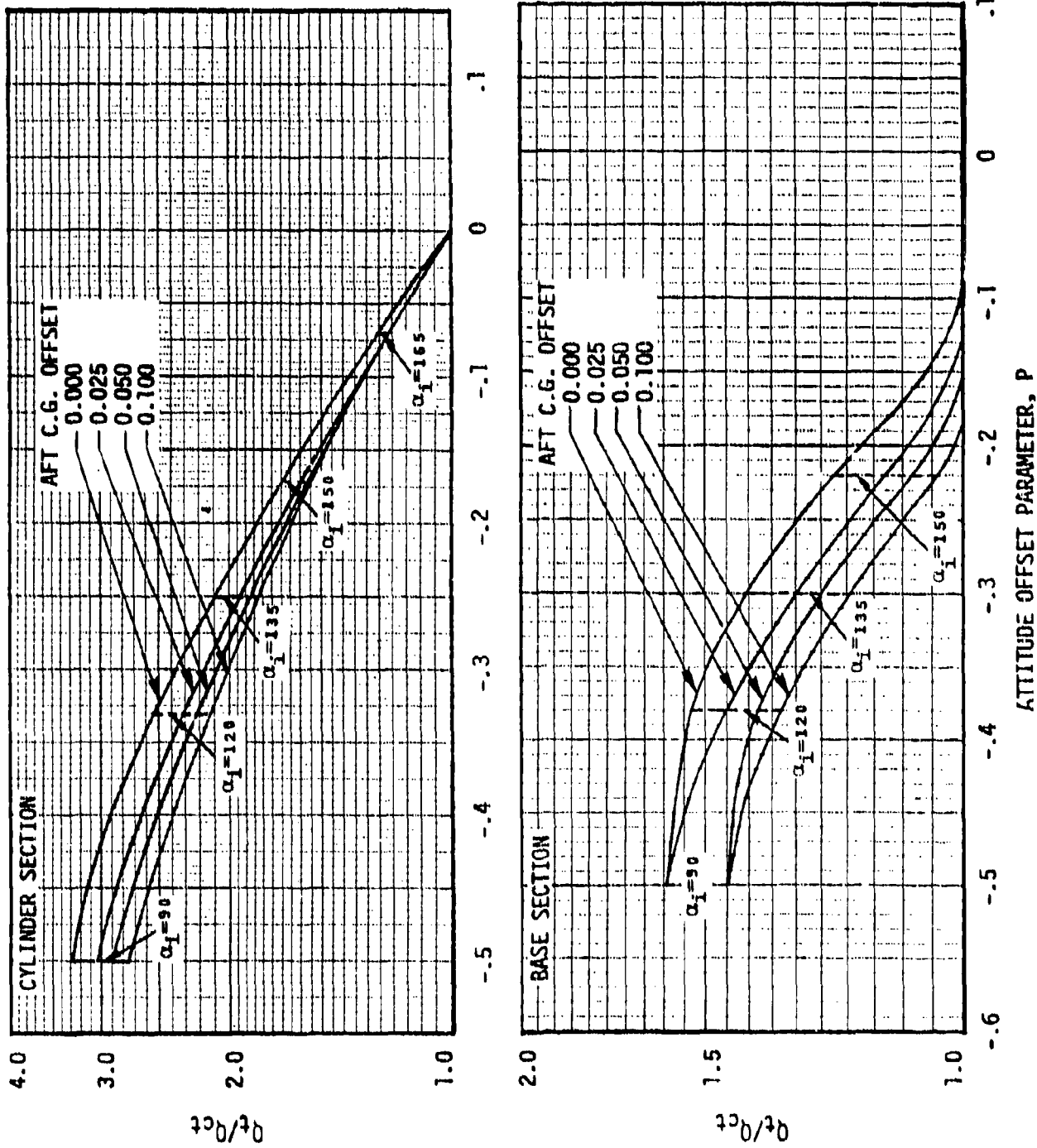


Fig. 4.7 Tumble correction factors, Q_t/Q_{ct} , for base and cylindrical sections of cone-cylinder configuration fineness ratio, λ/d , of 4 versus offset parameter, P .

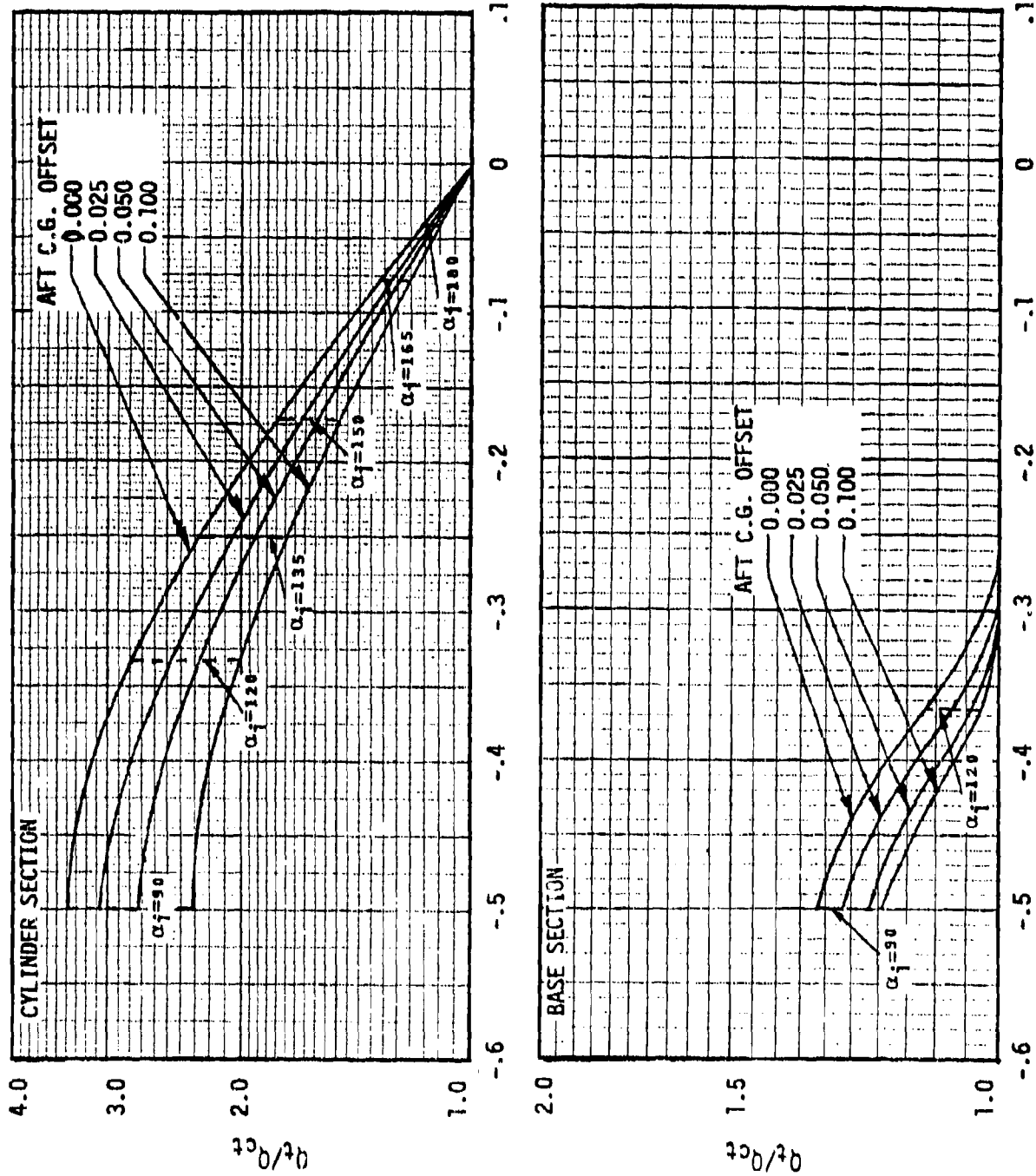


Fig. 4.8 Tumble correction factors, Q_t/Q_{ct} , for base and cylindrical sections of cone-cylinder configuration fineness ratio, λ/d , of 3 versus attitude offset parameter, P .

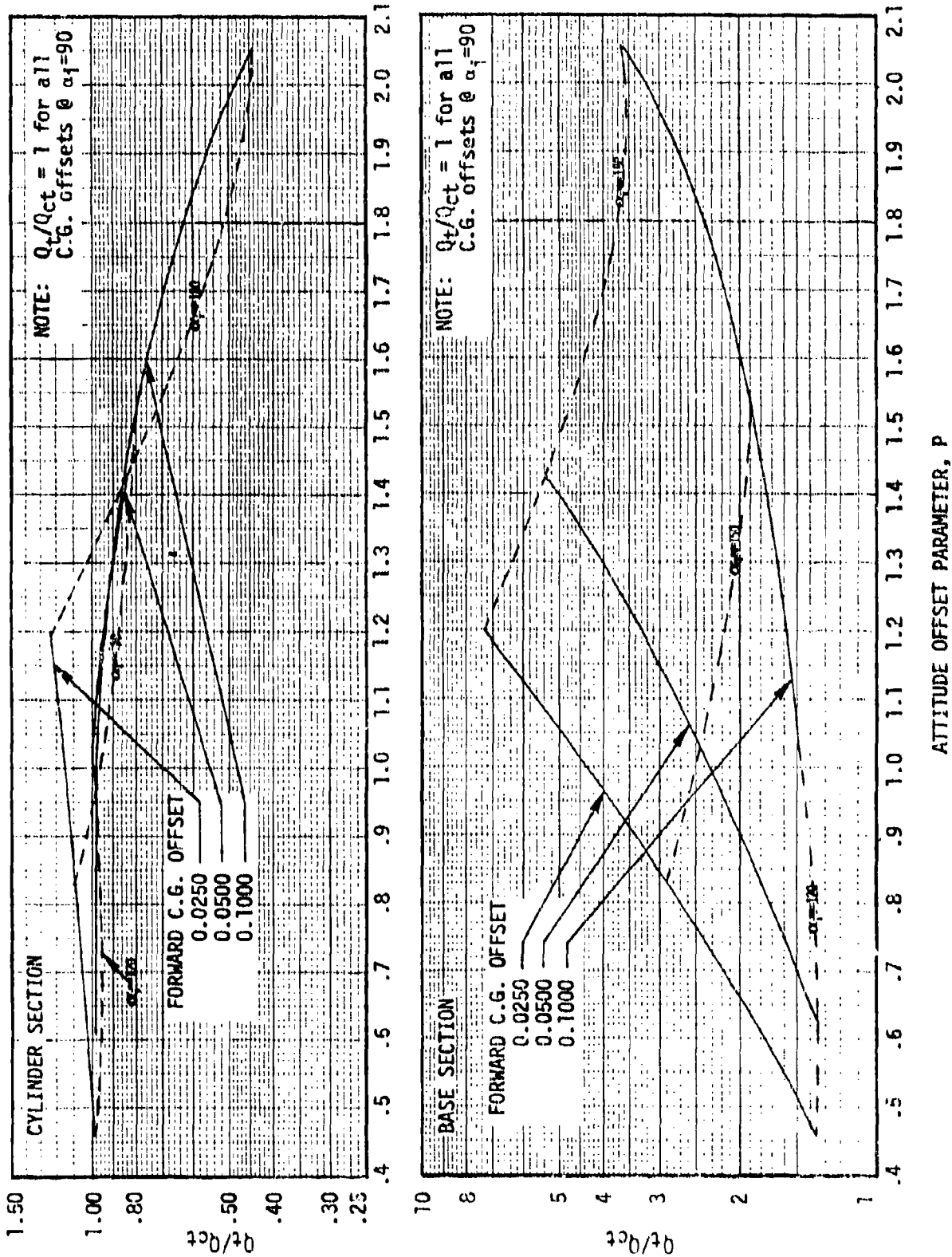


Fig. 4.9 Tumble correction factors, Q_t/Q_{ct} , for base and cylindrical sections of cylinder configuration fineness ratio, z/d , of 2.5 versus attitude offset parameter, P.

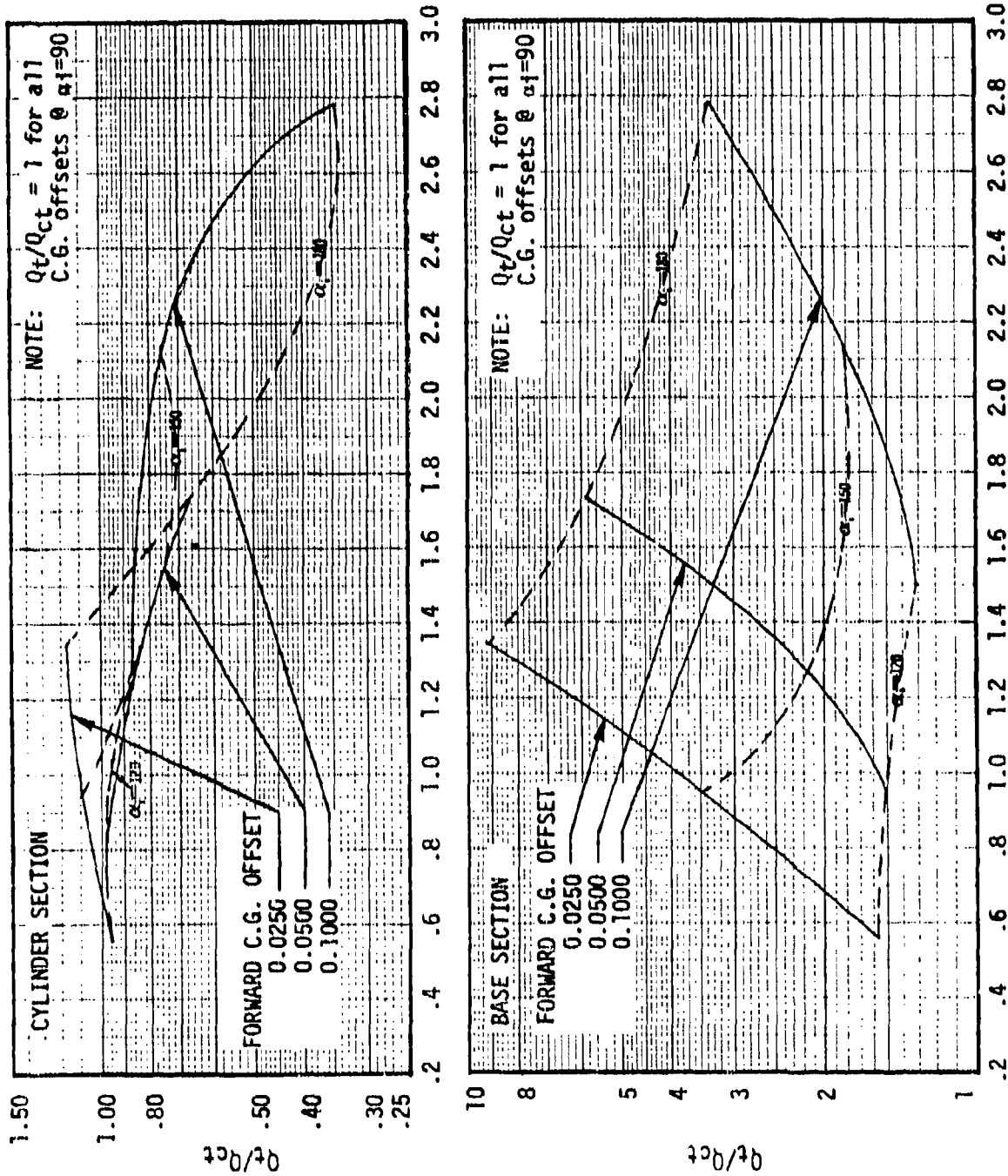


Fig. 4.10 Tumble correction factors, Q_t/Q_{ct} , for base and cylindrical section of cylinder configuration fineness ratio, ϵ/d , of 4 versus attitude offset parameter, P.

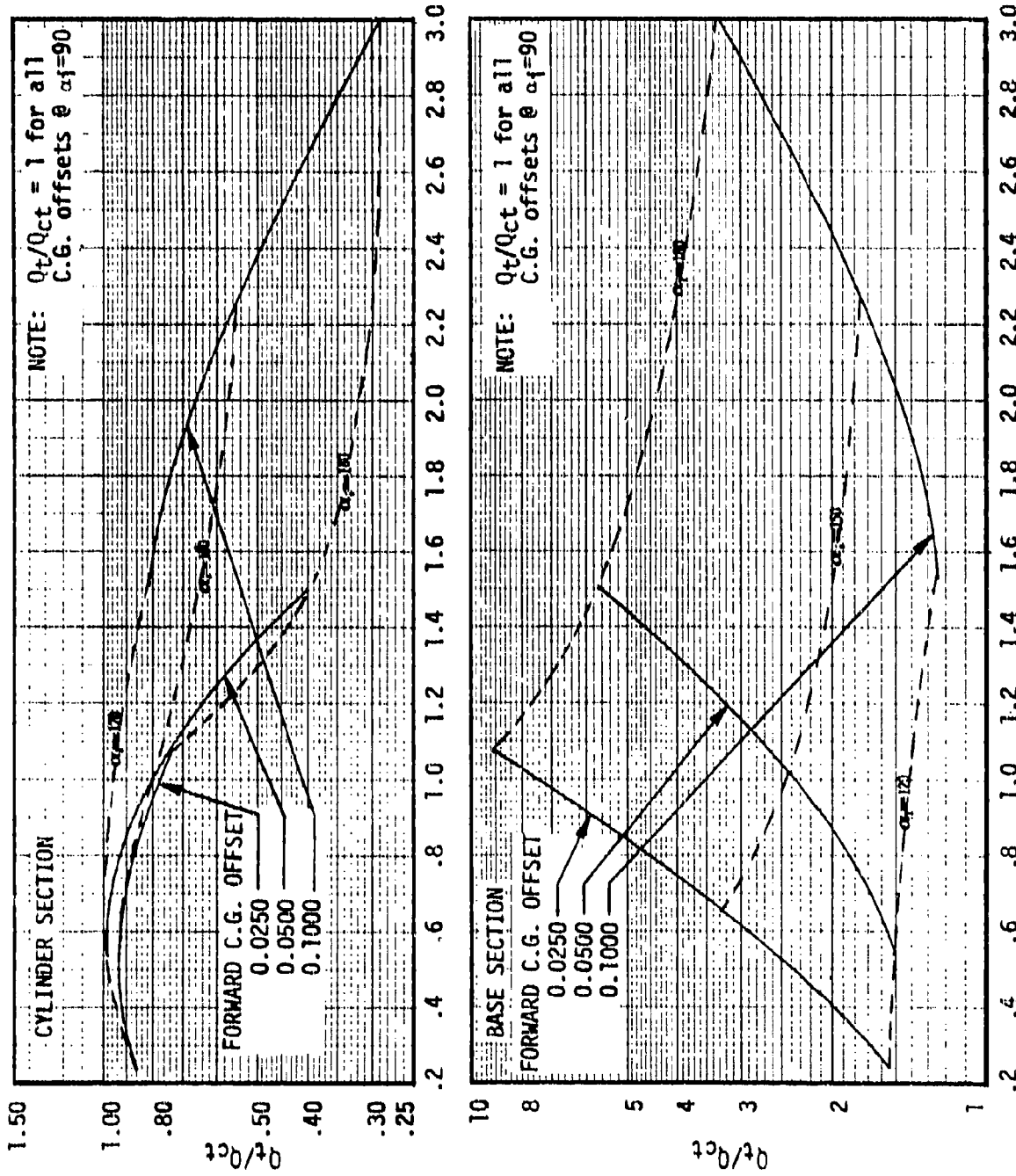
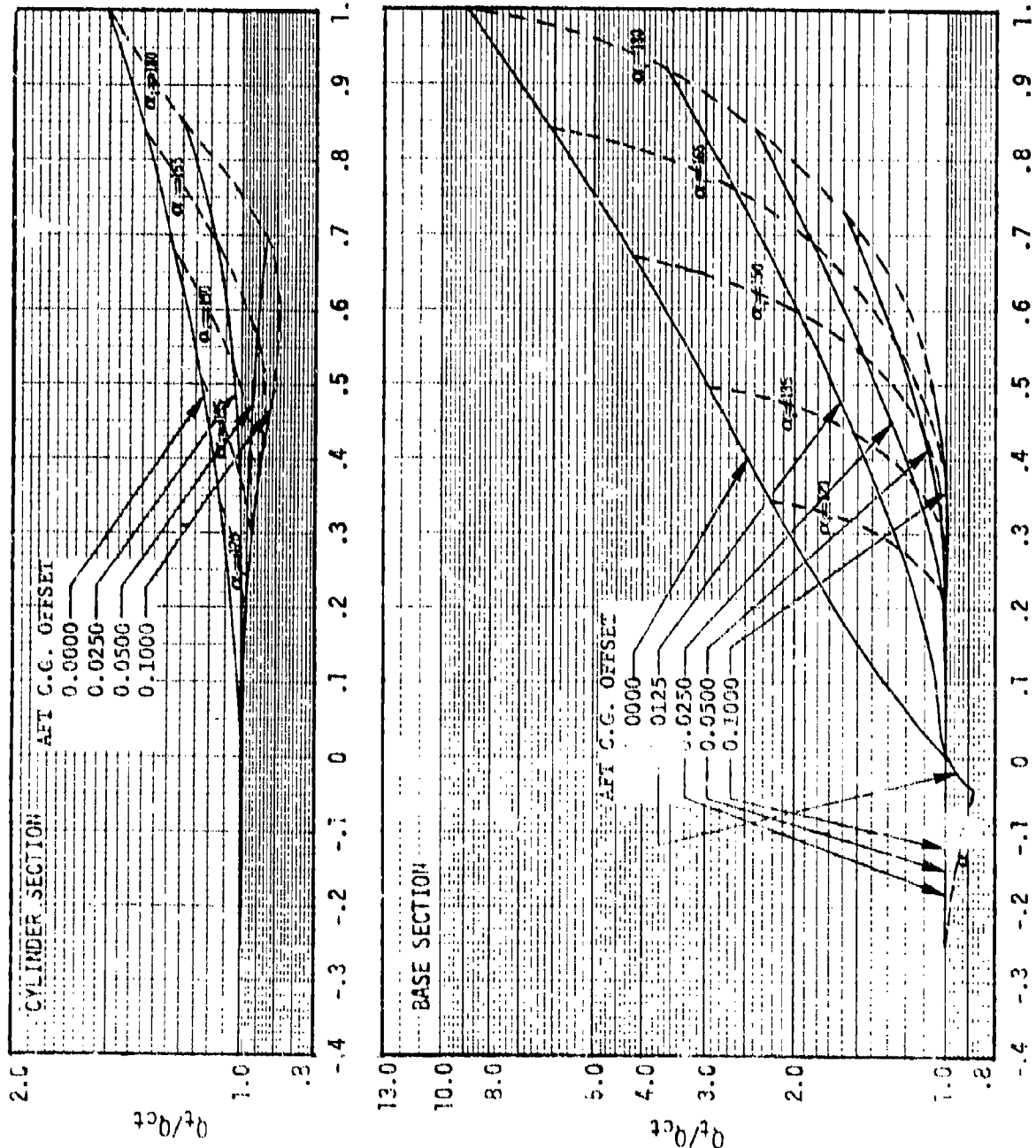


Fig. 4.11 Tumble correction factors, Q_t/Q_{ct} , for base and cylindrical sections of cylinder configuration fineness ratio, 1/d, of 5 versus attitude offset parameter, P.



ATTITUDE OFFSET PARAMETER, P

Fig. 4.12 Tumble correction factors, Q_t/Q_{ct} , for base and cylindrical sections of cylinder configuration fineness ratio, z/d , of 2.5 versus attitude offset parameter, P.

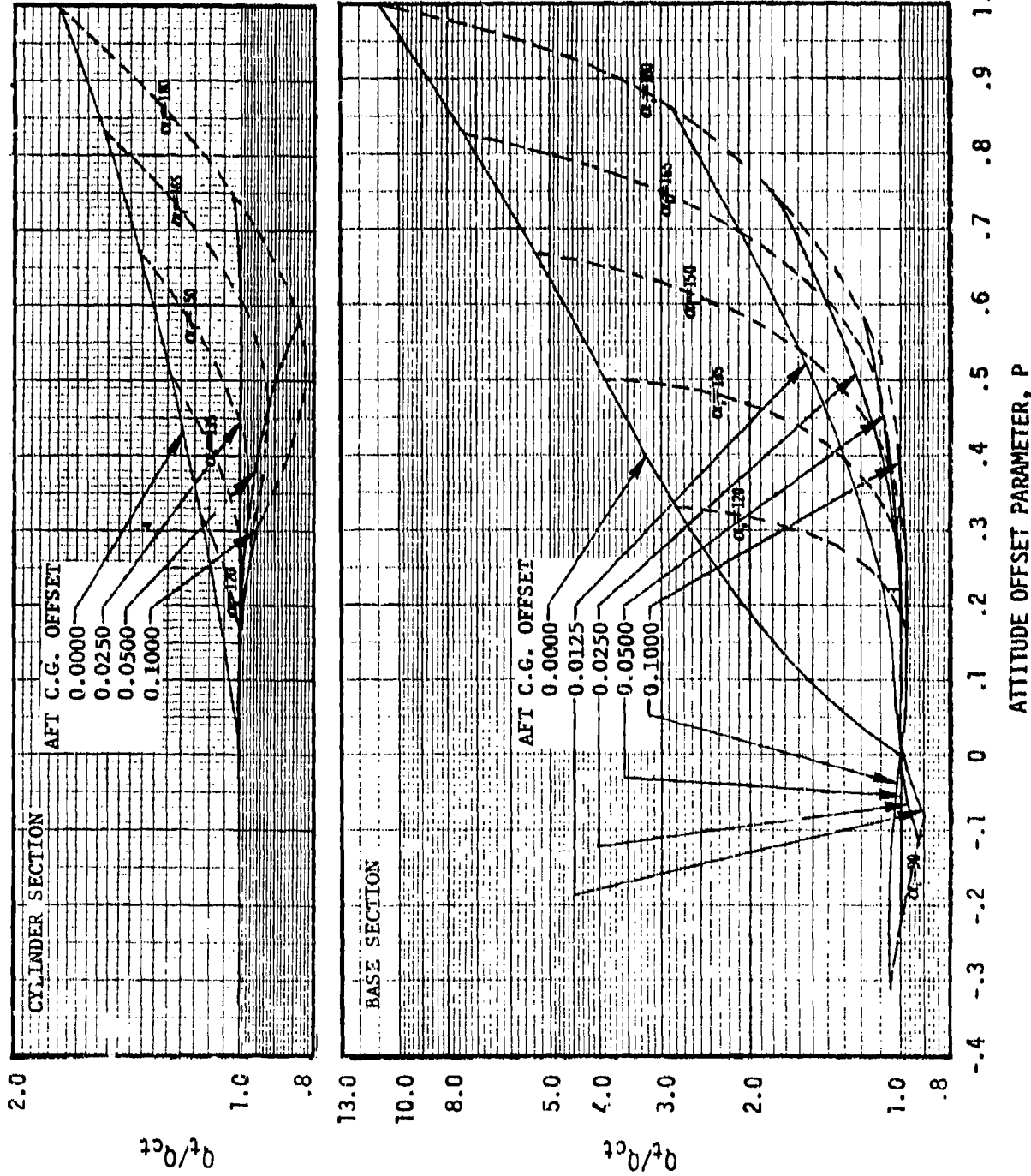


Fig. 4.13 Tumble correction factors, Q_t/Q_{ct} , for base and cylindrical section of cylinder configuration fineness ratio, ϵ/d , of 4 versus attitude offset parameter, P .

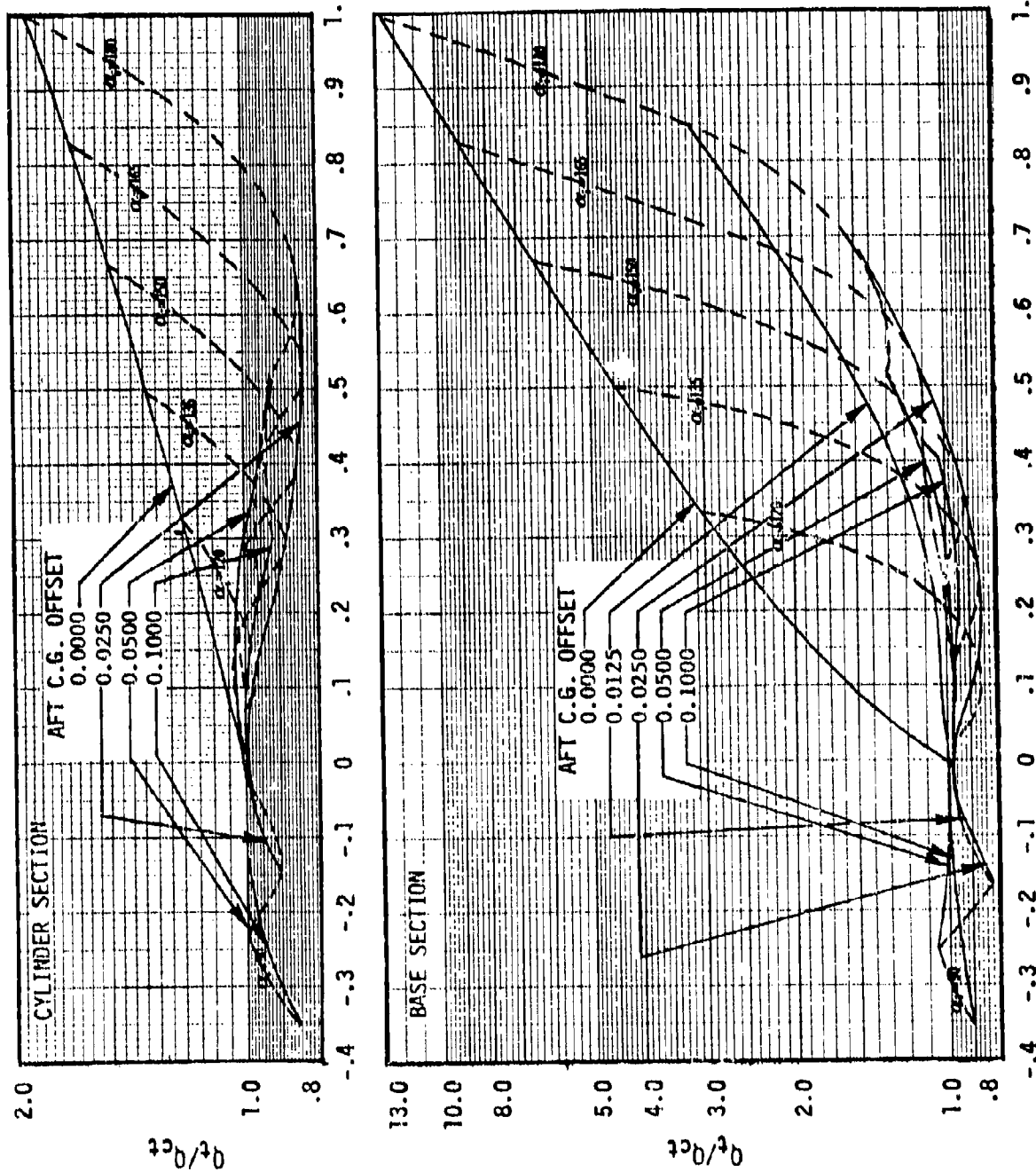


Fig. 4.14 Tumble correction factors, Q_t/Q_{ct} ; for base and cylindrical sections of cylinder configuration fitness ratio, z/d , of 5 versus attitude offset parameter, P.

SECTION 5

SURFACE TEMPERATURE CALCULATIONS

A considerable amount of discussion concerning reentry trajectories and heating rates, and loads on reentry vehicles has been presented in the preceding sections. This section deals with the methods and procedures involved in using the heating loads determined in these sections to obtain vehicle surface temperatures during reentry. The maximum vehicle surface temperatures are of main concern to the design engineer. From these temperatures he can determine whether the vehicle structure and skin can withstand the reentry environment. He could also determine if the surface temperatures would be of great enough magnitude that the vehicle could not be safely reused in future missions.

As discussed in Section 3, and more thoroughly discussed in Appendix C, the integrated loads presented in Figs. 3.1 - 3.10 consider a reference surface temperature of 660°R in the load calculation procedures. In reality, the actual heating load varies with vehicle surface temperature. Since the surface temperature is a function of the vehicle skin thickness, the heating load becomes a function of skin thickness. Fig. 5.1 presents the actual heating load (Q) versus the heating load computed at the reference temperature of 660°R (Q_{660}) for wall thicknesses of .125, .250 and .500 inches. After a heating load is obtained in Section 3 and then corrected for a possible oscillating or tumbling reentry in Section 4, the variable surface temperature correction can be made and the actual load determined by using Fig. 5.1.

The aerodynamic heating rates and subsequent loads on reentry vehicles are dependent on the vehicle radius or diameter. In general, the heating analysis was performed for a cylinder diameter of 24 inches for both the cylinder and cone-cylinder configurations. Both the laminar and turbulent diameter correction factors versus cylinder diameter are presented in Fig. 5.2. The difference in the laminar and turbulent curves stems from the fact that the laminar heating methodology is a function of the cylinder diameter to the 0.5 power, whereas the turbulent heating is a function of the diameter to 0.2 power. An adjustment is made to the corrected heating load obtained from Fig. 5.1 for the cylinder diameter variation by multiplying this value times the adjustment factor presented in Fig. 5.2. In order to determine which curve, whether laminar or turbulent, is to be used for the adjustment factor, use the following procedure. For the cylindrical sections of both configuration types, use the laminar curve for the constant trim attitude range $85^\circ \leq \alpha_T \leq 95^\circ$. The turbulent curve is used for all other trim attitudes. For the base section, use the laminar curve for the range $175^\circ \leq \alpha_T \leq 180^\circ$ and the turbulent curve for the remaining trim attitudes.

In many situations it may be determined that the payload rolls during reentry. If this is the case the heating load may be reduced to the cylinder section of the configuration by multiplying the factor \bar{r}/h_{SL} from Fig. 5.3 times the diameter adjusted heating obtained using Fig. 5.2. This factor is to be applied only to cylinder section of the configuration since vehicle roll does not reduce base region heating.

After the cylinder diameter adjustment has been made, the vehicle surface temperature can then be determined using Fig. 5.4. Fig. 5.4 presents the vehicle surface temperature versus the corrected heating load. This surface

temperature assumes no variation with temperature in the heat capacity of the vehicle's skin material). Although the variable heat capacity correction is not very significant, these corrections can be made for the surface temperature using Fig. 5.5.

Although the methods and procedures for determining surface temperatures on reentry vehicles from heating loads presented in this section seem comparatively simple, an in-depth analysis was performed to verify these methods. The method presented in the form of Fig. 5.4 is a "heat dump method" in which the vehicle surface, because of the material type and thickness, is assumed to react instantaneously to a heat load input by an increase in surface temperature. A conduction heating analysis using a thermal analyzer was performed to verify the validity of this assumption. Detailed discussions of this analysis are presented in Appendix D.

This section presents the explanations and procedures for determining vehicle surface temperatures from the heating loads obtained in previous sections. The value of the surface temperatures obtained after the variable heat capacity correction is made is the best estimate for the surface temperature on a reentry vehicle that can be obtained using the results presented in this handbook.

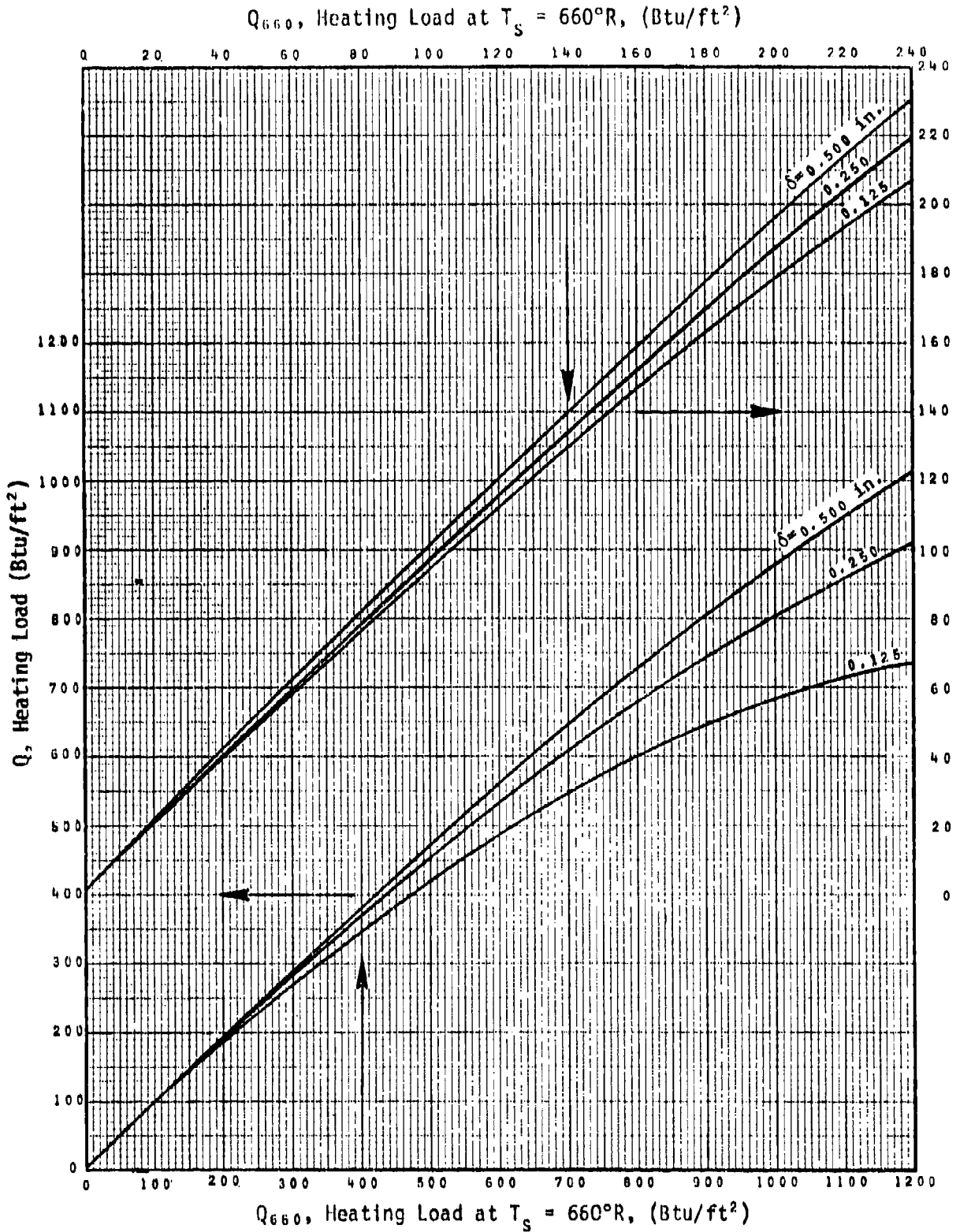


Fig. 5.1 Variable Surface Temperature Correction at Constant Wall Temperature Load, Q_{660} , for Three Wall Thicknesses (δ).

Cylinder: $35 < \alpha < 95$ Laminar
 $\alpha > 95$ Turbulent
 Base: $\alpha < 85$ Laminar
 $\alpha \geq 175$ Laminar
 $\alpha < 175$ Turbulent

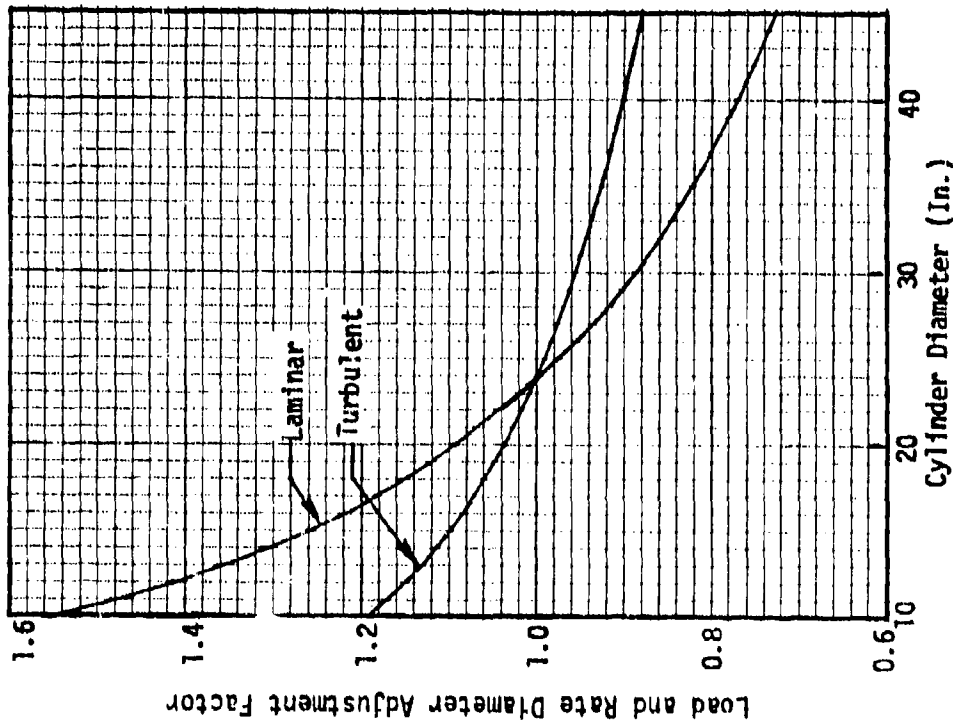


Fig. 5.2 Cylinder Diameter Adjustment Factor for Heating

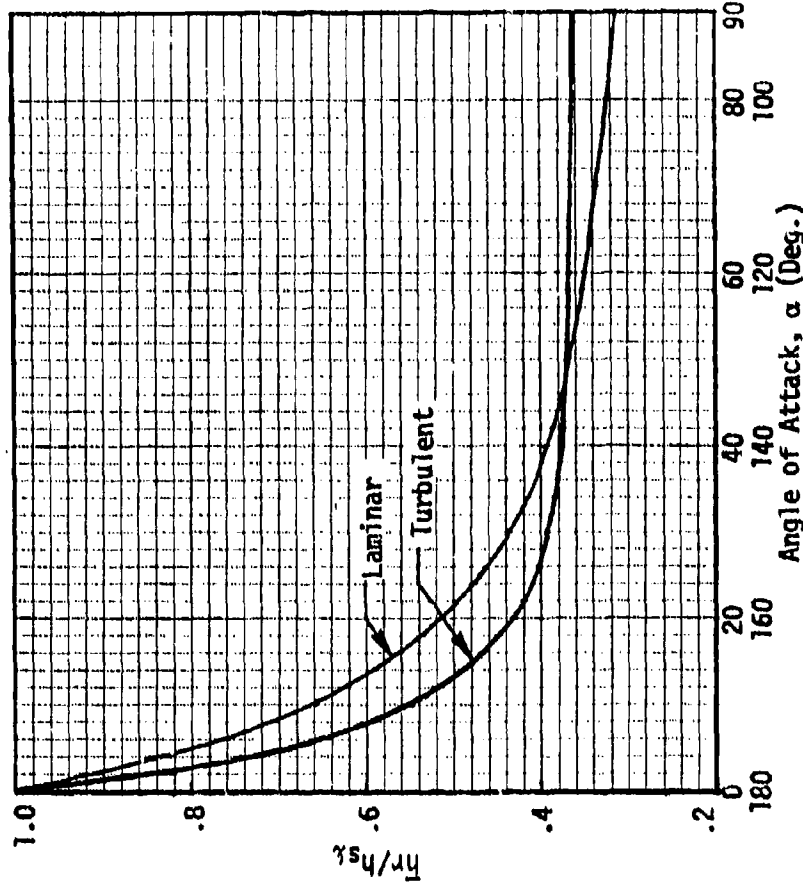


Fig. 5.3 Roll Average Heat Transfer Coefficient to Stagnation Line Coefficient Ratio Versus Angle of Attack (Apply these results to the cylinder section only)

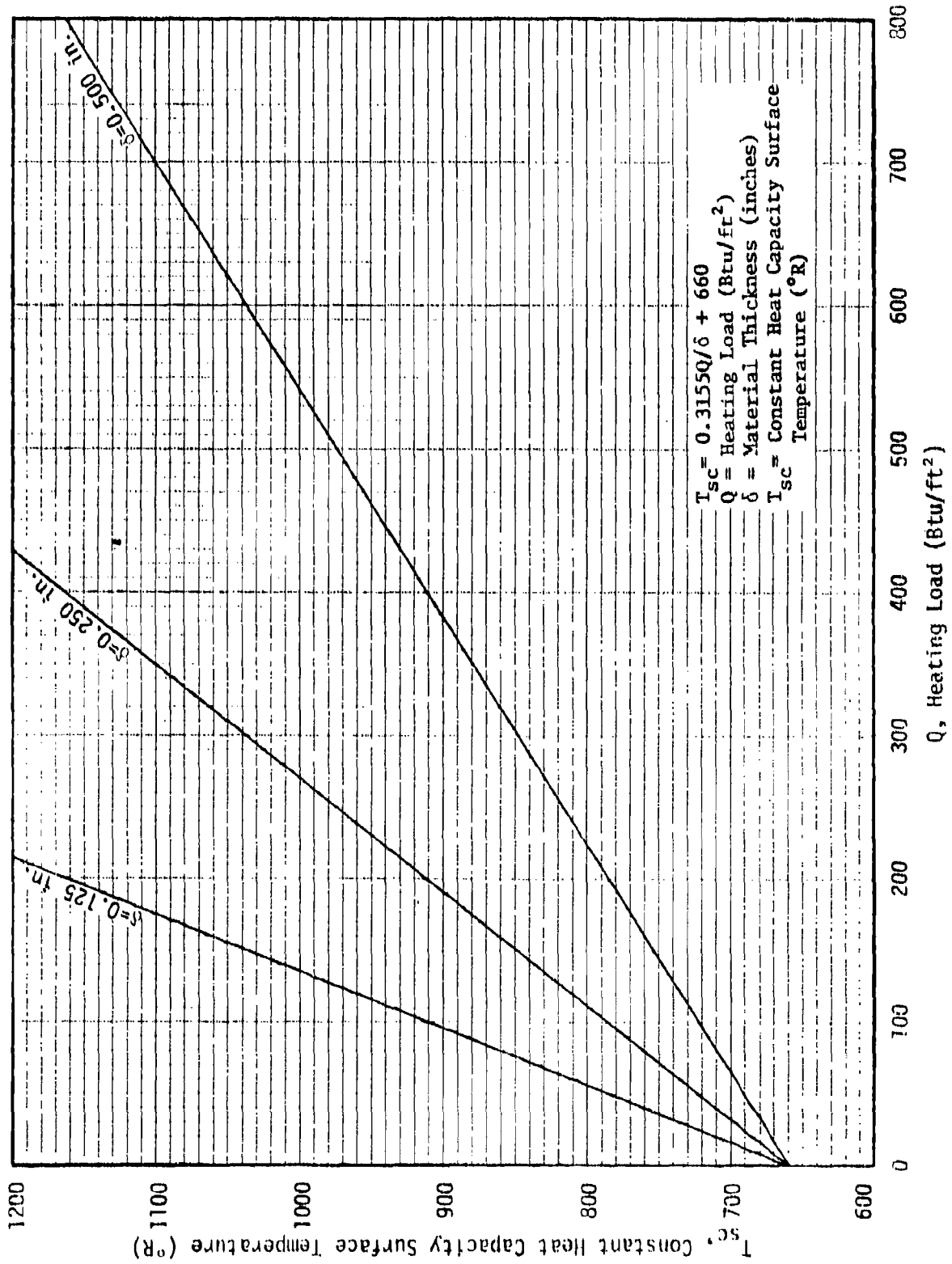


Fig. 5.4 Surface Temperature, T_{sc} , Versus Heating Load Q

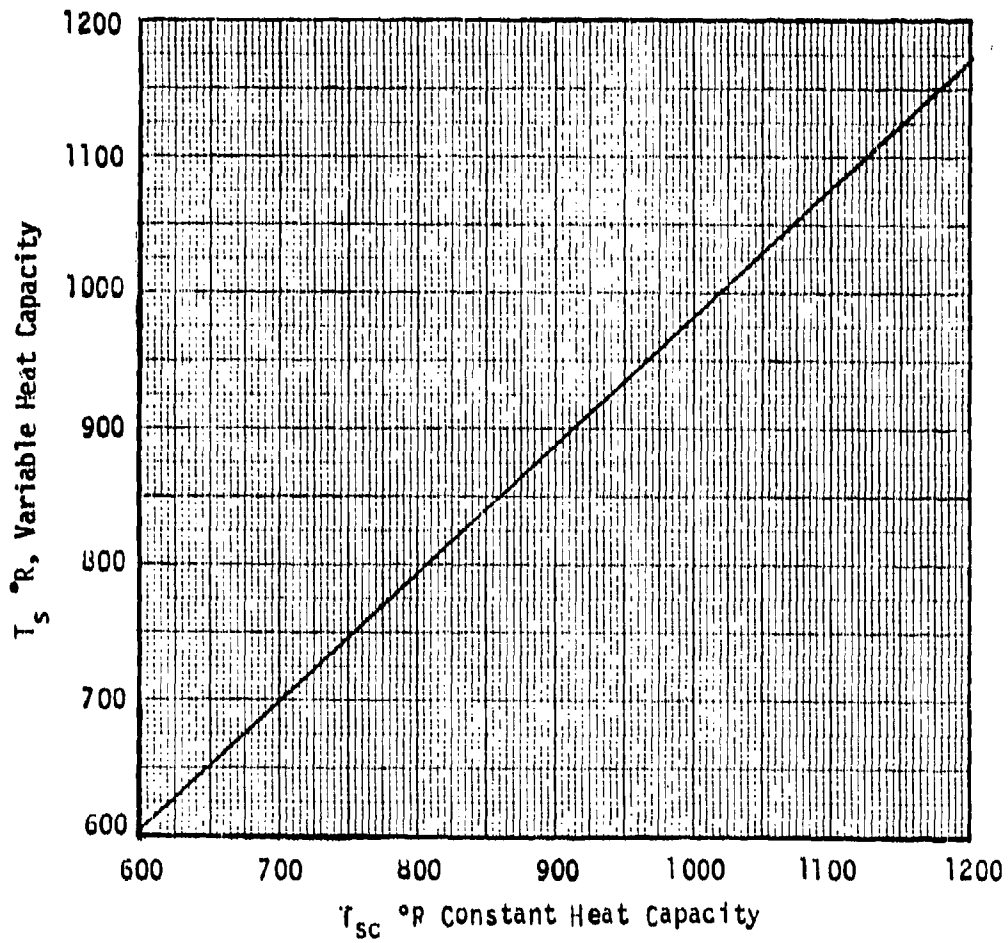


Fig. 5.5 Variable heat capacity adjustment to constant heat capacity surface temperature, T_{sc} .

SECTION 6

PAYLOAD REENTRY DYNAMICS

The payload configurations considered in this analysis may either tumble and oscillate or exhibit normal stable flight at some constant attitude. Neither roll nor yaw type autorotative motions were considered in the results presented in this section since the geometry and initial conditions of the payload at release did not indicate that these types of motions would occur. In Section 6.1, ballistic reentry (reentry at a constant trim attitude) is discussed while the oscillating and tumbling trajectories are discussed in Section 6.2.

6.1 Ballistic Reentry Trajectories

The most important concept behind ballistic reentry is that the trajectory of a ballistic reentry body is a function only of the body's ballistic coefficient and its initial altitude. If a reentry body's weight to drag ratio, $W/C_D A$, (commonly defined as ballistic coefficient) is known as well as the release altitude, then the body's reentry trajectory can be determined from Figs. 6.1 - 6.9. These figures present the reentry trajectories for ballistic coefficients ranging from 10 to 250 lb/ft² for the initial release altitudes of 75 to 350 statute miles.

A given payload's geometry (either cylinder or cone-cylinder) with a specific fineness ratio, diameter, and C. G. location specifies a constant trim attitude (See Section 2) for ballistic reentry. A number of trim attitudes and ballistic coefficients are presented in Table 6.1. This information is to be used along with the information provided in Tables 6.2 and 6.3 to compute the equivalent ballistic coefficients for the cases considered in the analysis.

This coefficient then specifies the ballistic reentry trajectory for the specific configuration type and case.

6.2 Oscillating and Tumbling Trajectories

In many situations, a certain C. G. location combined with an initial release attitude will promote large and small amplitude oscillations about a trim attitude which can be predicted. In many other situations certain combinations will result in a complete tumbling of the vehicle. Ballistic trajectories can be used in situations where the vehicle oscillations are small. Although these are not constant trim attitude entries, the ballistic trajectories closely approximate the small amplitude oscillating trajectories without inducing any appreciable error. In the other situations, however, where the vehicle oscillations are large or where the vehicle tumbles, a ballistic trajectory approximation can result in significant errors in the actual trajectory. Large vehicle oscillations or tumbling result in large variations in the vehicle drag force. Since the descent velocity of a vehicle is dependent on its drag force, this results in large variations in the vehicle's descent velocity and thus its entry trajectory. This section addresses the problem of determining the reentry trajectories for the payload configurations considered in the analysis whose variety of C. G. locations and initial release attitudes result in large vehicle oscillations and tumbling during reentry.

A six-degree-of-freedom trajectory simulation computer code (Ref. 2) was used extensively in determining the effects of variations in C. G. location and initial release attitudes for the various payload configurations. This computer code is discussed in detail in Appendix B. Graphical presentation

of the results of the total matrix of 6 DOF runs is not practical since the total number of graphs describing this matrix are too numerous. The results from a condensed form of the matrix of runs will be presented, however, in tabular form in Tables 6.2 and 6.3. From the 6 DOF trajectory runs, an equivalent ballistic coefficient was obtained in situations where the trajectory varies from a constant trim entry ballistic trajectory. The percent of variation of equivalent ballistic coefficients from the constant trim ballistic coefficients were determined. These results are shown in Table 6.2. While Table 6.1 gives the ballistic coefficients for normal stable constant trimmed entries of the payload configurations and cases being analyzed, Table 6.2 gives the variations from these coefficients when initial vehicle attitudes combined with various C. G. offsets are considered. If this variation is positive, zero, or negative, this indicates that the equivalent ballistic coefficient for the specific case is either greater than, the same, or less than the constant trim ballistic coefficient by the magnitude of the percent shown. Table 6.3 specifies the payload dynamics as to whether it tumbles, oscillates, or is trimmed during entry. From Table 6.3, it is possible to determine if the vehicle is reentering forward or aft end first. If a payload is oscillating, it is also possible to determine the degree of severity of these oscillations, i.e., whether the payload oscillations have small amplitudes or whether the amplitudes are large and unstable.

Perhaps the main criticism in presenting data in a tabular fashion as in Tables 6.2 and 6.3 is how the data is supposed to be applied when the payload geometry, C. G. location, or initial release attitudes vary from the cases presented. It is possible, for instance, although unlikely, that a cone-cylinder configuration of fineness ratio 4 1/2 may exhibit reentry dynamics which are drastically different from the dynamics exhibited by the cone-cylinder geometries

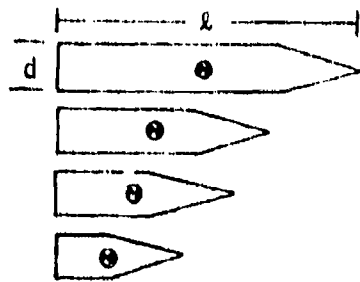
with fineness ratios of 4 and 5 which are presented in the tables. Of course, this will always be a possibility since there is no way to increase the 6 DOF run matrix to include all fineness ratios. It is possible to observe certain trends in Tables 6.2 and 6.3 when considering different fineness ratios. Notice that, in general, C. G. locations aft of the volume C. G. promote reduced ballistic coefficients for the cone-cylinder configurations whereas forward C. G. locations tend to increase the ballistic coefficients. This is, of course, with the exception of the l/d equal to 3 configuration which is essentially identical to stable ballistic reentry no matter what combination of C. G. offset or initial release attitude is being considered. With the exception of the 10% forward C. G. offset and the 180° initial release attitude combination, C. G. locations from the volumetric C. G. to 10% forward for the initial release attitudes of 150° to 180° in general, promote the largest increase in ballistic coefficients for the cone-cylinder geometries. The reason for the large increase in ballistic coefficients for these combinations is due primarily to the large increase in descent velocity which results from large decreases in drag force. Large variations in the vehicle attitude during a vehicle oscillating entry allow the vehicle to fly at some attitudes where the drag force is very small, thus, creating large descent velocity.

Similarly, decreases in ballistic coefficients can be understood when considered in this manner. A number of other trends can be established and rationalized for both the cylinder and cone-cylinder configurations. The data, although not necessarily linear between fineness ratios, C. G. offsets, and initial release attitudes, is consistent and can be applied in situations when a flight case and a case presented in Table 6.2 do not coincide. When this

situation occurs, first determine the bounds for the flight case. These include the configuration type, and the upper and lower bounds on fineness ratio, C. G. location, and release attitude. The percent of variation of the ballistic coefficient is then determined for these bounds. The percent of variation should be weighted more strongly to the results which are closest to the flight case. This weighting can be performed by using linear interpolation or by considering the case in more detail and determining a weighting factor based on engineering judgement.

The equivalent ballistic coefficients discussed in this section relate only to the dynamics of the vehicle. They are not to be confused with or applied to the heating environment for a vehicle during an oscillating or tumbling reentry. In addition to the figures and tables presented in this section to determine trajectories for reentry vehicles, Fig. 6.10 has been provided in order to assist the engineer in the aerial recovery of payloads. The maximum decent velocity of a vehicle is presented versus ballistic coefficient and release altitude for two recovery altitudes. This should provide the engineer with a quick indicator of possible dynamic problems that could arise and effect the successful recovery of the vehicle.

Geometry of Cone-Cylinder Configurations

Body 1, $l/d = 7$ Body 2, $l/d = 5$ Body 3, $l/d = 4$ Body 4, $l/d = 3$

● Volumetric C. G. Location

Conditions: Density assumed constant and = 23.23 lb/ft³; diameter = 2.5 ft.

Body	C.G. Location	Trim Attitude (α_T)°	Weight (lb)	Drag Coef. (C_D)	Ballistic Coef. (lb/ft ²)
1	10% F	37	1614	2.35	140
2	10% F	44	1044	2.40	89
3	10% F	45	759	1.95	79
4	10% F	30	474	0.7	138
1	5% F	64	1614	7.2	46
2	5% F	73	1044	5.7	37
3	5% F	85	759	5.0	31
4	5% F	180	474	1.6	60
1	2.5% F	90	1614	10.1	33
2	2.5% F	107	1044	6.3	34
3	2.5% F	147	759	2.6	59
4	2.5% F	180	474	1.6	60
1	Vol C.G.	115	1614	8.2	40
2	Vol C.G.	137	1044	3.7	57
3	Vol C.G.	180	759	1.6	97
4	Vol C.G.	180	474	1.6	60
1	2.5% Aft	138	1614	4.6	71
2	2.5% Aft	158	1044	2.1	101
3	2.5% Aft	180	759	1.6	97
4	2.5% Aft	180	474	1.6	60
1	5% Aft	156	1614	2.5	132
2	5% Aft	168	1044	1.8	118
3	5% Aft	180	759	1.6	97
4	5% Aft	180	474	1.6	60
1	10% Aft	168	1614	1.7	193
2	10% Aft	180	1044	1.6	133
3	10% Aft	180	759	1.6	97
4	10% Aft	180	474	1.6	60

Table 6.1a Information for determining the Ballistic Trajectories for particular cone-cylinder configurations

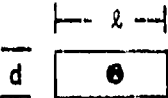
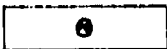
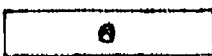
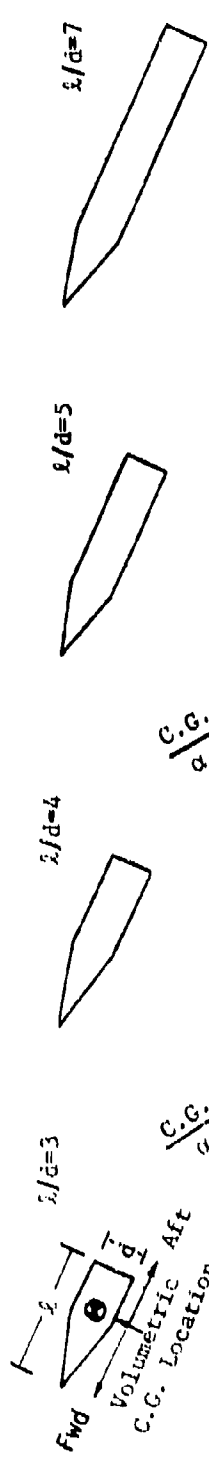
GEOMETRY OF CYLINDER CONFIGURATIONS					
		Body 5, $l/d = 2.5$			
		Body 6, $l/d = 4$			
		Body 7, $l/d = 5$			
● Volumetric C. G. Location					
Conditions: Density assumed constant and = 23.23 lb/ft ³ ; diameter = 2.5 ft.					
Body	C.G. Location	Trim Attitude (α_T)°	Weight (lb)	Drag Coef. (C_D)	Ballistic Coef.
5	10% F	59	499	3.6	28
6	10% F	48	980	4.0	50
7	10% F	42	1225	3.9	64
5	5% F	74	499	4.2	24
6	5% F	66	980	5.9	34
7	5% F	62	1225	6.6	38
5	2.5% F	82	499	4.3	24
6	2.5% F	78	980	6.5	31
7	2.5% F	75	1225	8.0	31
5	Vol C.G.	90	499	4.4	23
6	Vol C.G.	90	980	6.7	30
7	Vol C.G.	90	1225	8.4	30
5	2.5% Aft	98	499	4.3	24
6	2.5% Aft	102	980	6.5	31
7	2.5% Aft	105	1225	8.0	31
5	5% Aft	106	499	4.2	24
6	5% Aft	114	980	5.9	34
7	5% Aft	118	1225	6.6	38
5	10% Aft	121	499	3.6	28
6	10% Aft	132	980	4.0	50
7	10% Aft	138	1225	3.9	64

Table 6.1b Information for determining the ballistic trajectories for particular cylinder configurations.

C.G. (%) α ₁ (°)	Fwd → ← Aft						
	10	5	2.5	0	2.5	5	10
90	-13	-13	-13	-7	0	0	0
120	-11	-10	-10	0	0	0	0
135	-7	0	0	0	0	0	0
150	0	0	0	0	0	0	0
165	0	0	0	0	0	0	0
180	0	0	0	0	0	0	0

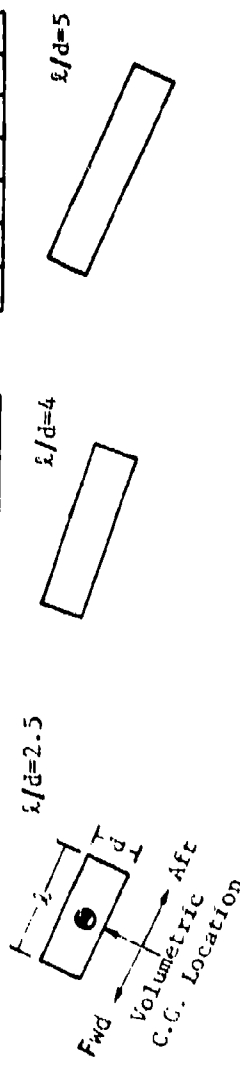
C.G. (%) α ₁ (°)	Fwd → ← Aft						
	10	5	2.5	0	2.5	5	10
90	0	-3	-4	-15	-15	-15	-15
120	7	-3	7	-15	-13	-7	-7
135	7	-3	0	-4	-4	-4	-4
150	13	-3	0	0	0	0	0
165	0	0	0	0	0	0	0
180	-22	44	0	0	0	0	0

C.G. (%) α ₁ (°)	Fwd → ← Aft						
	10	5	2.5	0	2.5	5	10
90	0	0	6	10	0	-22	-17
120	10	4	0	0	0	-13	-10
135	7	8	6	0	0	-24	-2
150	10	17	5	0	0	-10	0
165	4	30	12	0	0	0	0
180	-35	97	39	2	0	0	0



C.G. (%) α ₁ (°)	Fwd → ← Aft						
	10	5	2.5	0	2.5	5	10
90	N/D	N/D	N/D	0	-2	7	2
120	13	8	-5	0	-2	5	5
135	N/D	N/D	N/D	5	1	5	5
150	13	13	-2	6	2	5	5
165	N/D	N/D	N/D	11	8	10	7
180	-6	31	17	26	16	15	5

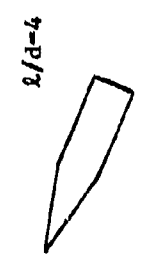
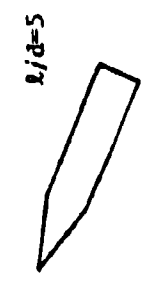
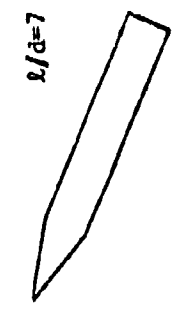
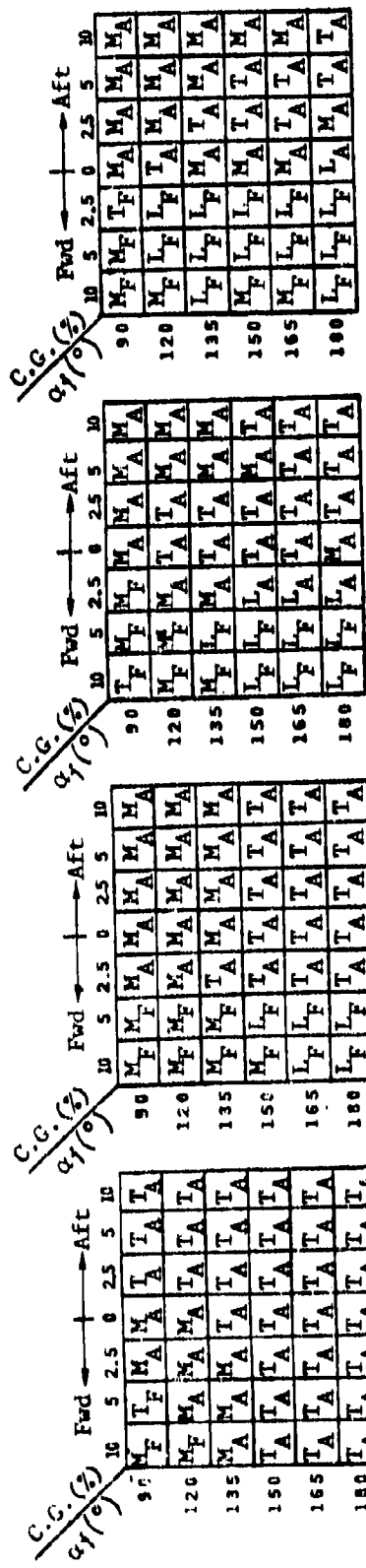
C.G. (%) α ₁ (°)	Fwd → ← Aft						
	10	5	2.5	0	2.5	5	10
90	N/D	N/D	N/D	0	-2	2	3
120	15	9	10	0	-15	0	6
135	N/D	N/D	N/D	6	-7	-1	-6
150	33	38	-3	12	-4	2	-6
165	N/D	N/D	N/D	16	-4	4	-3
180	-10	35	98	32	5	9	-3



* C. G. (%) - The percentage of the vehicle's axial length that the C. G. location is offset from the volumetric center of gravity.

** α₁(degrees) - The initial vehicle release attitude.
 N/D - No data available.

Table 6.2 The percent variation of an equivalent ballistic coefficient from a constant trim entry ballistic coefficient versus initial attitude and C. G. offset.



* C. G. (Z) - The percentage of the vehicle's axial length that the C. G. location is offset from the volumetric center of gravity.

** α_i (degrees) - The initial vehicle release attitude.

- T - vehicle is trimmed (oscillations < 5° about α_t)
- M - mild oscillations (α_t oscillations < 25° about α_t)
- L - large oscillations (oscillations > 25° about α_t)
- TU - vehicle is tumbling
- A - AFT
- F - Forward
- 90 - oscillating about 90°
- N_D - No data available

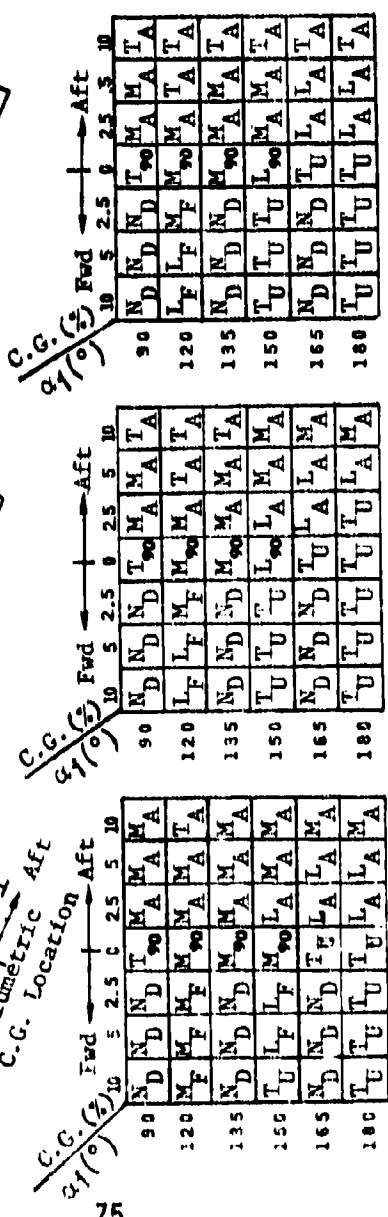


Table 6.3 Vehicle attitude dynamics versus C. G. location and release attitude.

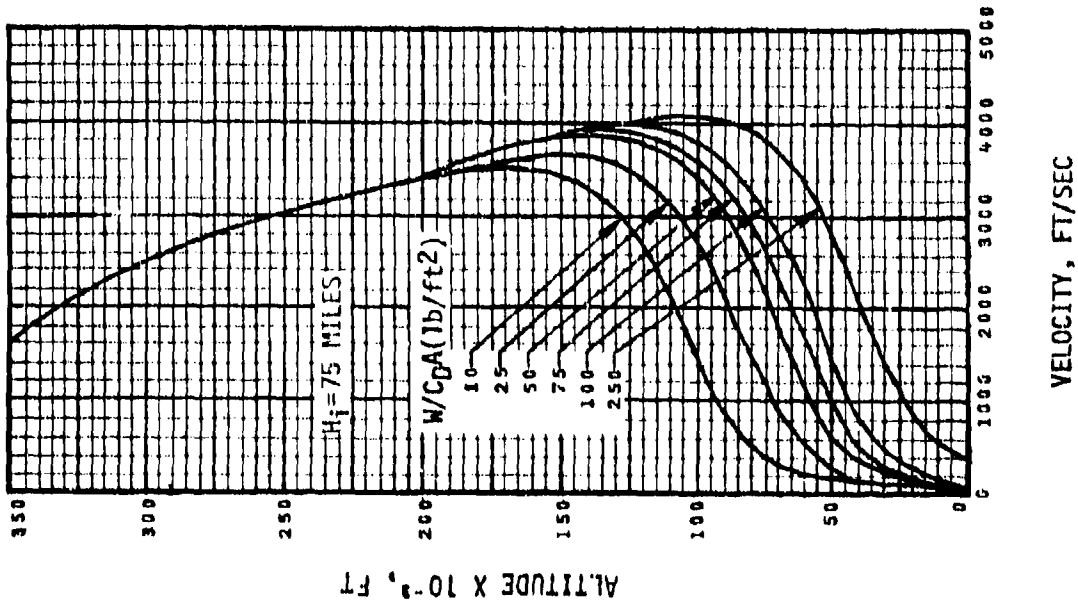
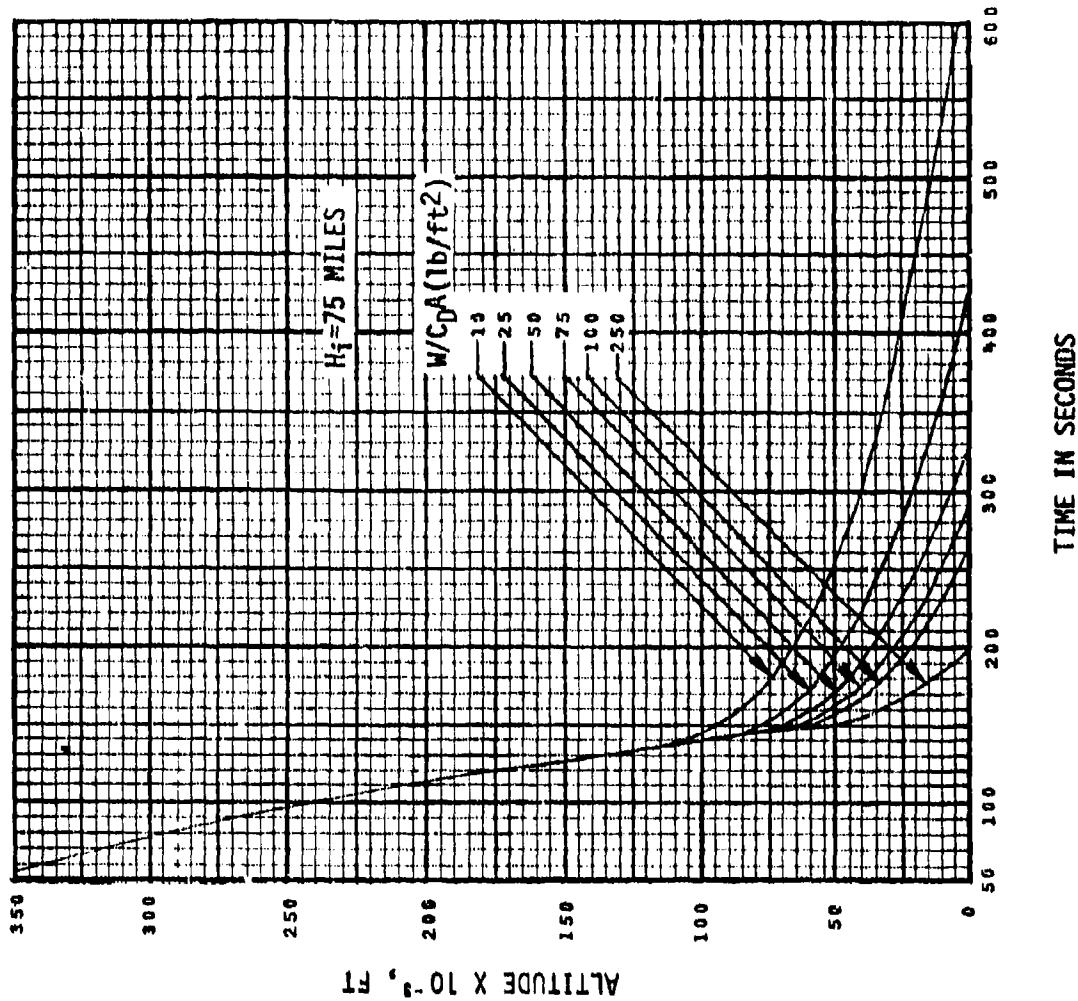


Fig. 6.1 Ballistic trajectories for an initial release altitude (H_i) of 75 miles.

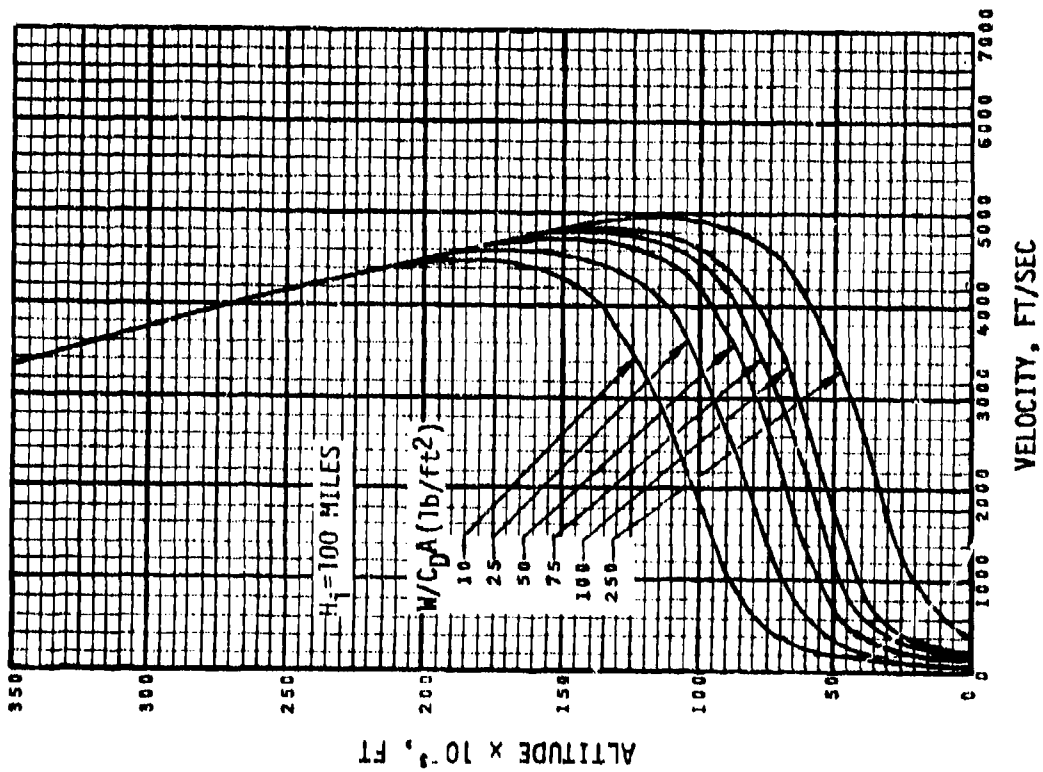
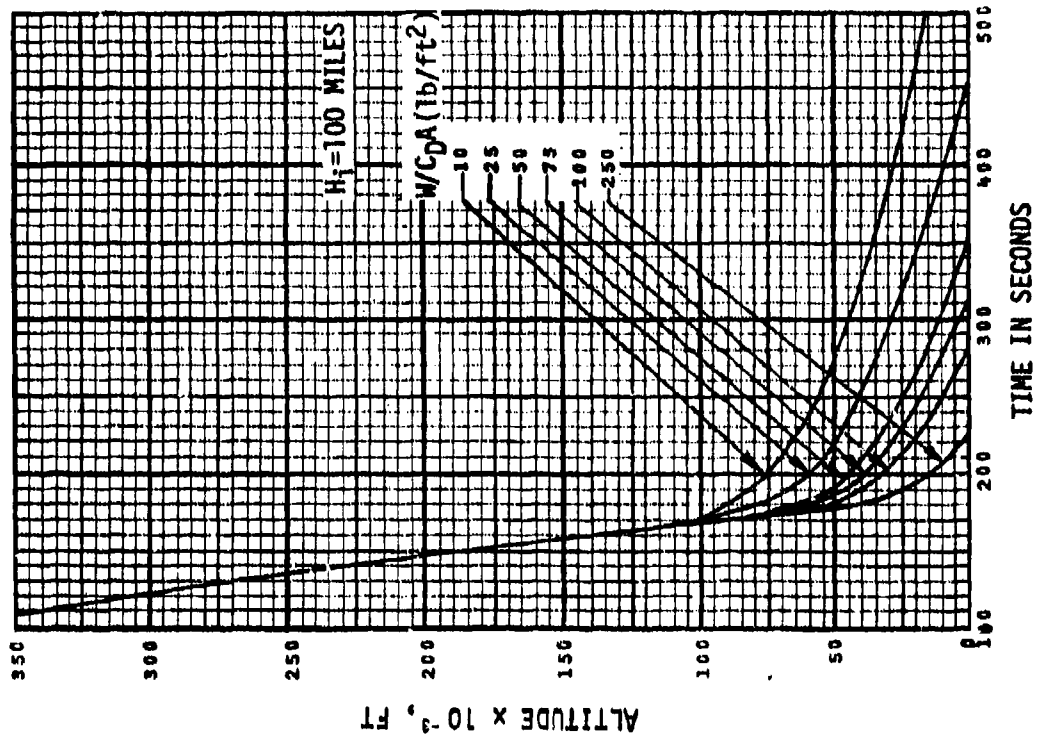


Fig. 6.2 Ballistic trajectories for an initial release altitude (H_i) of 100 miles.

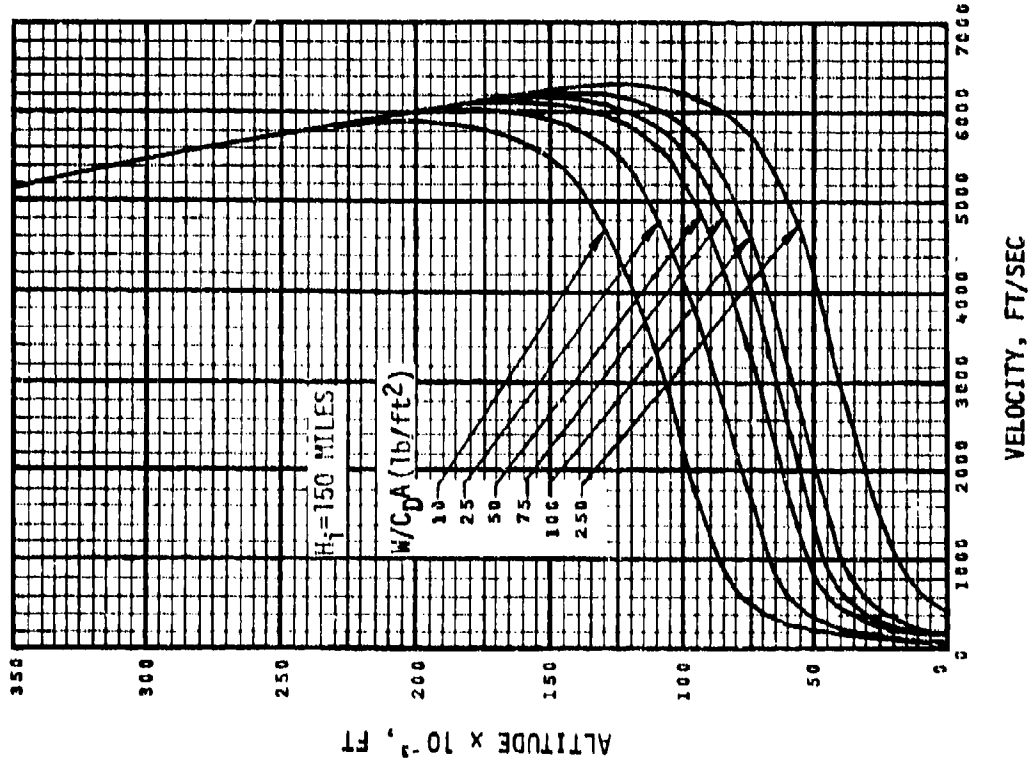
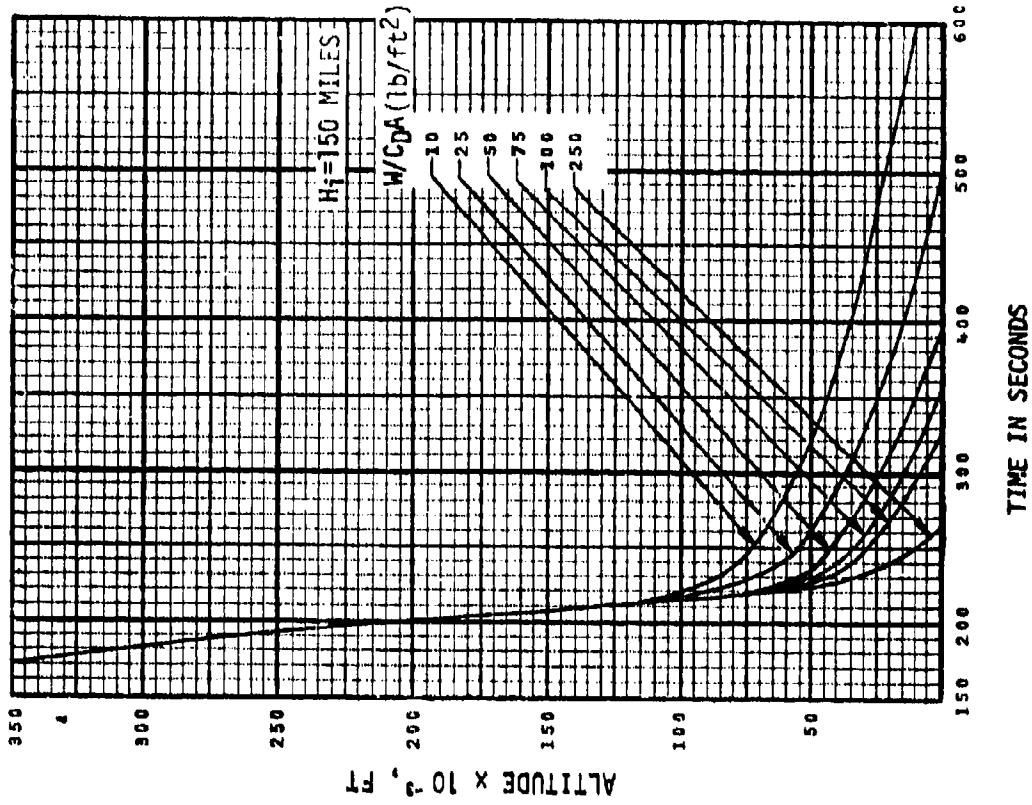


Fig. 6.3 Ballistic trajectories for an initial release altitude (H_1) of 150 miles.

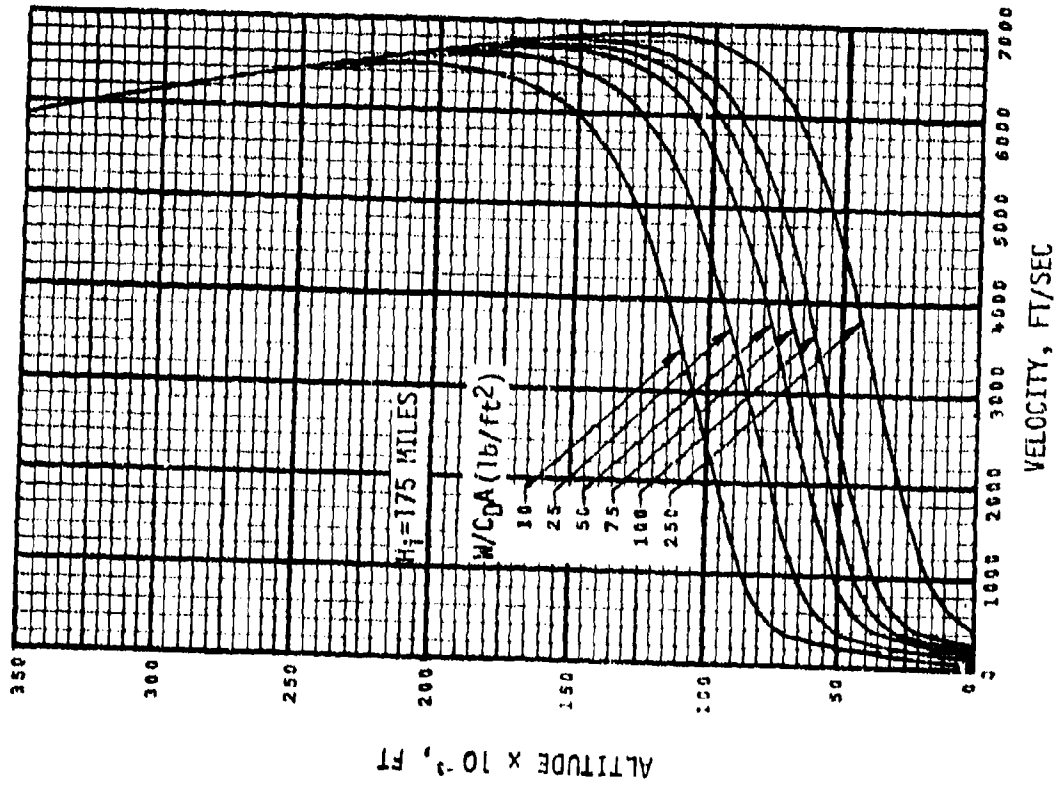
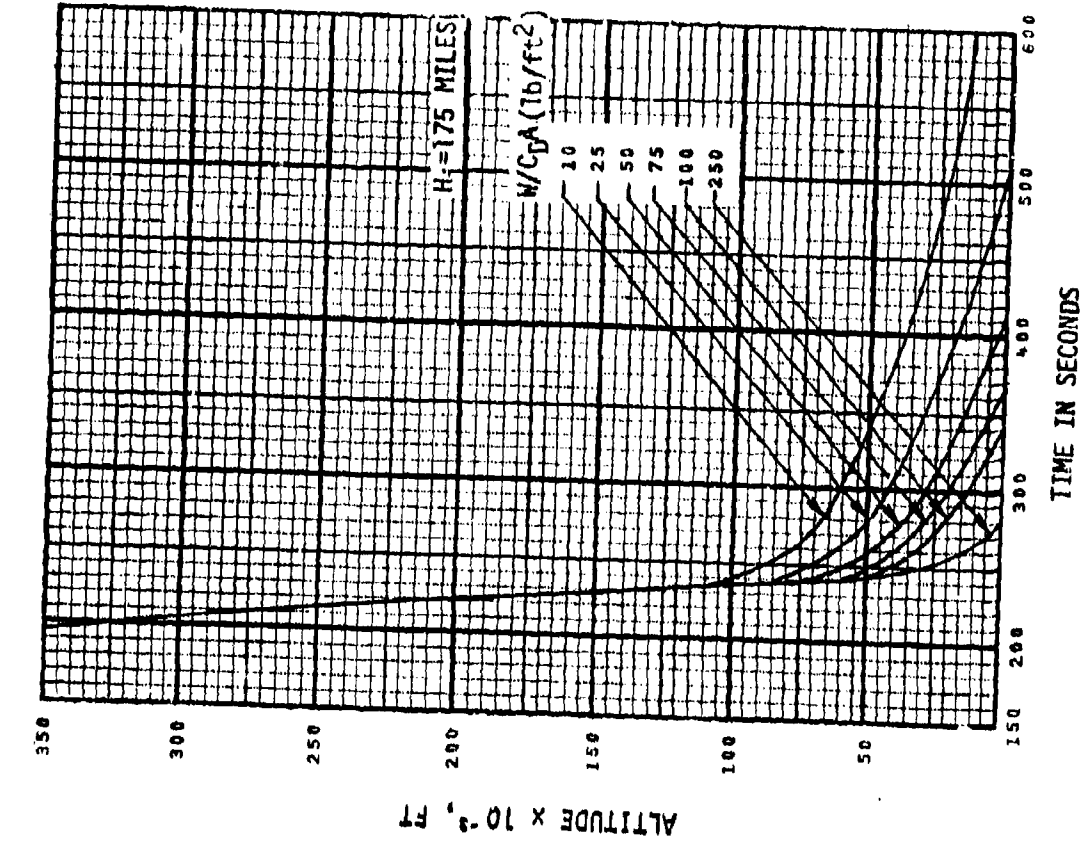


Fig. 6.4 Ballistic trajectories for an initial release altitude (H_i) of 175 miles.

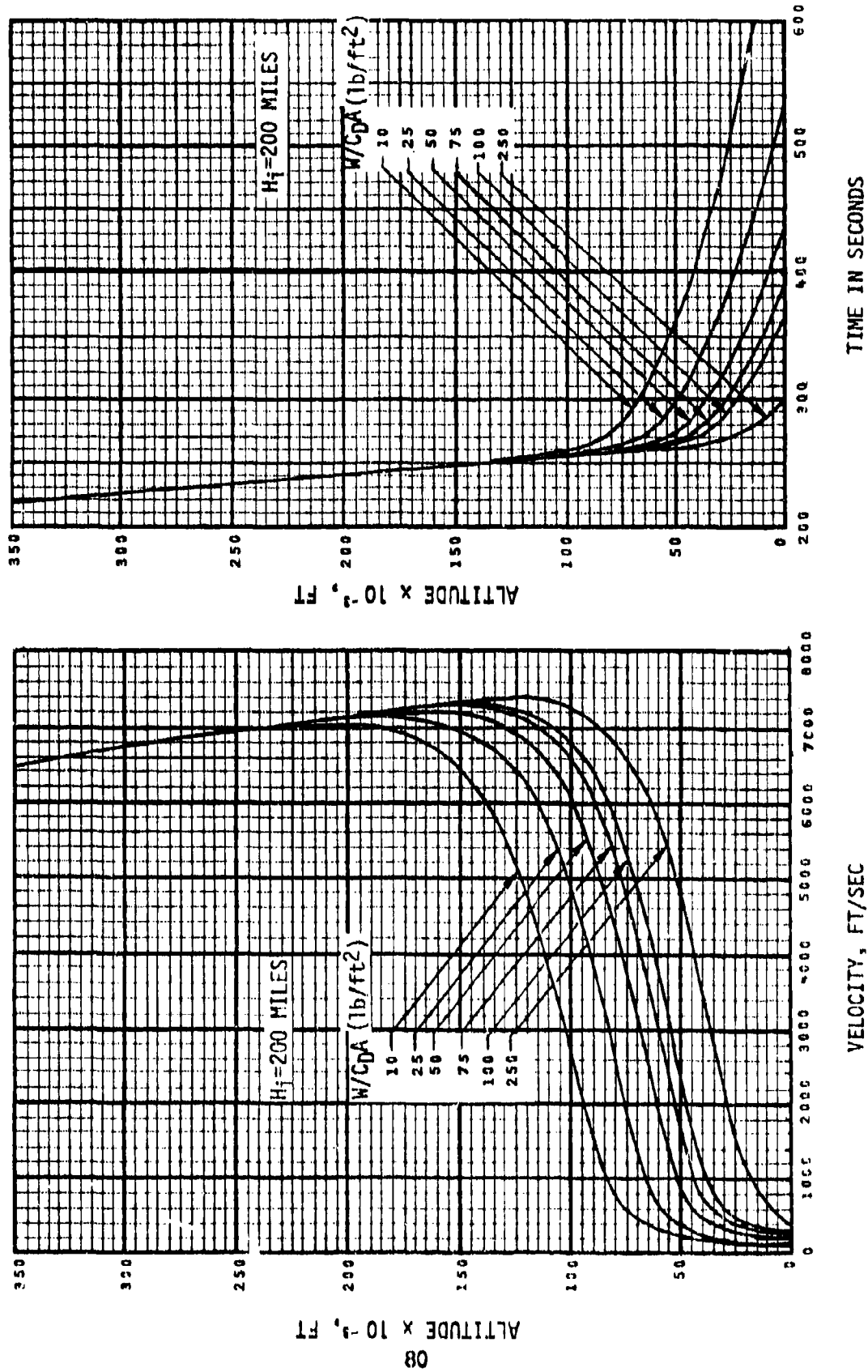


Fig. 6.5 Ballistic trajectories for an initial release altitude (H_i) of 200 miles.

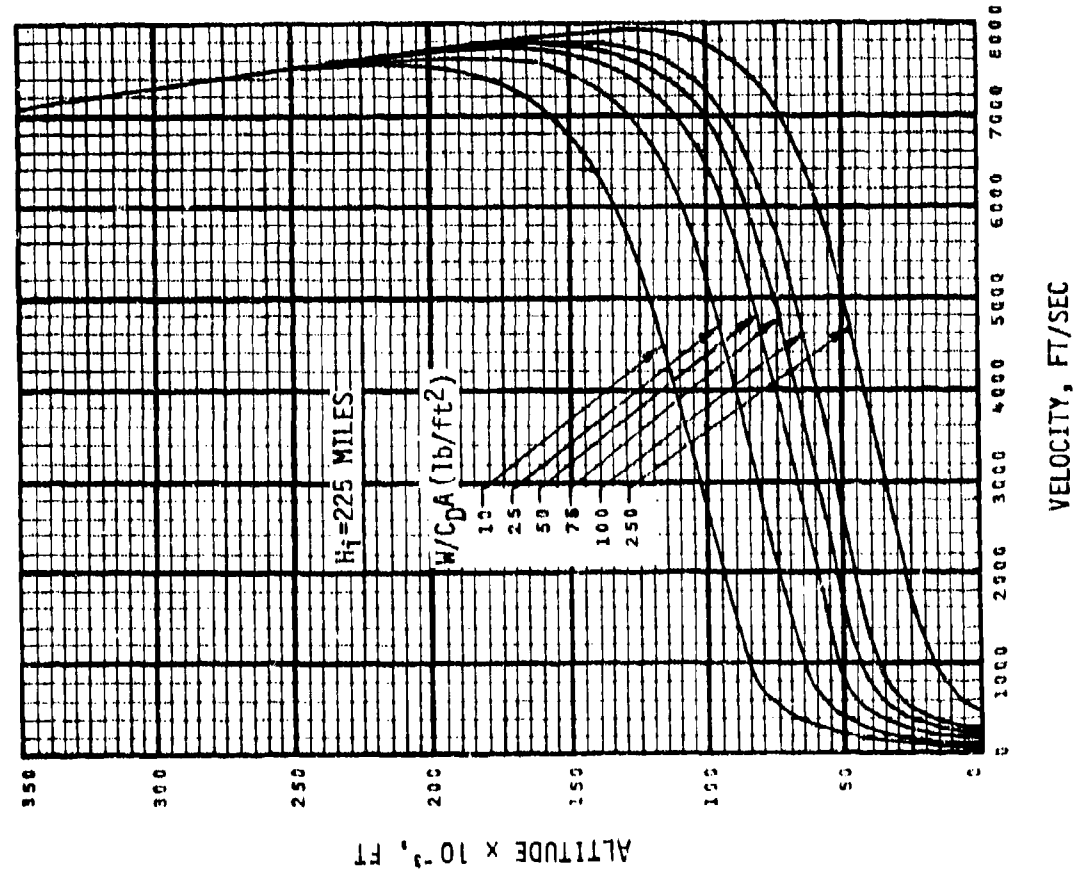
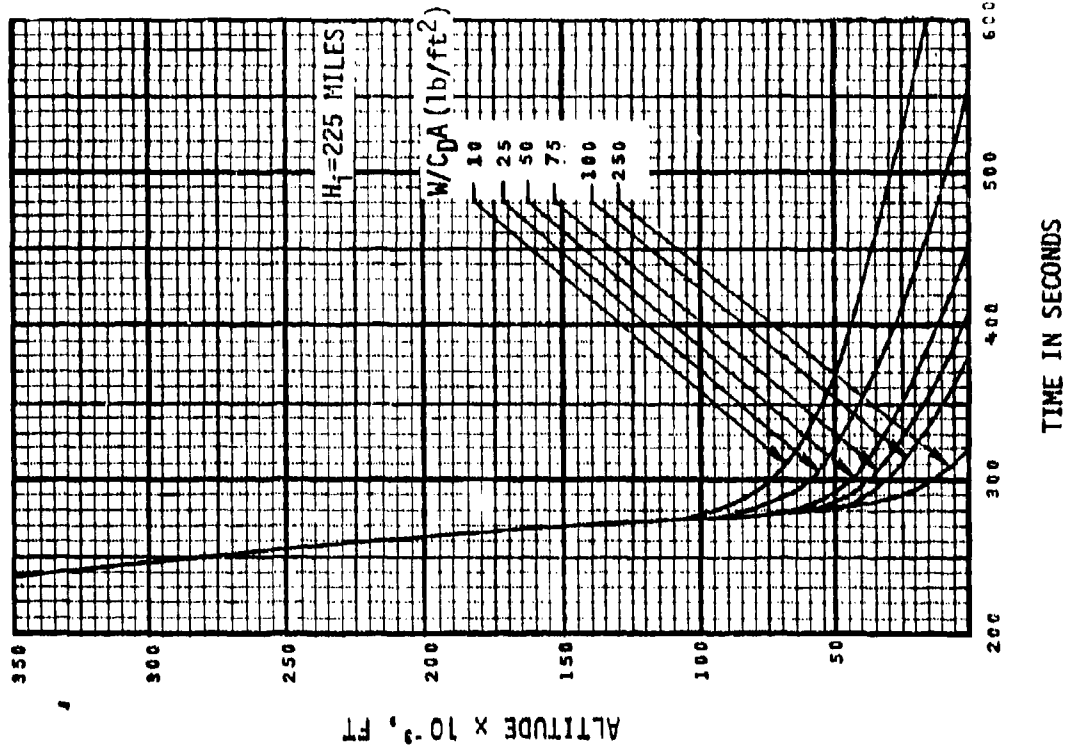


Fig. 6.6 Ballistic trajectories for an initial release altitude (H_i) of 225 miles.

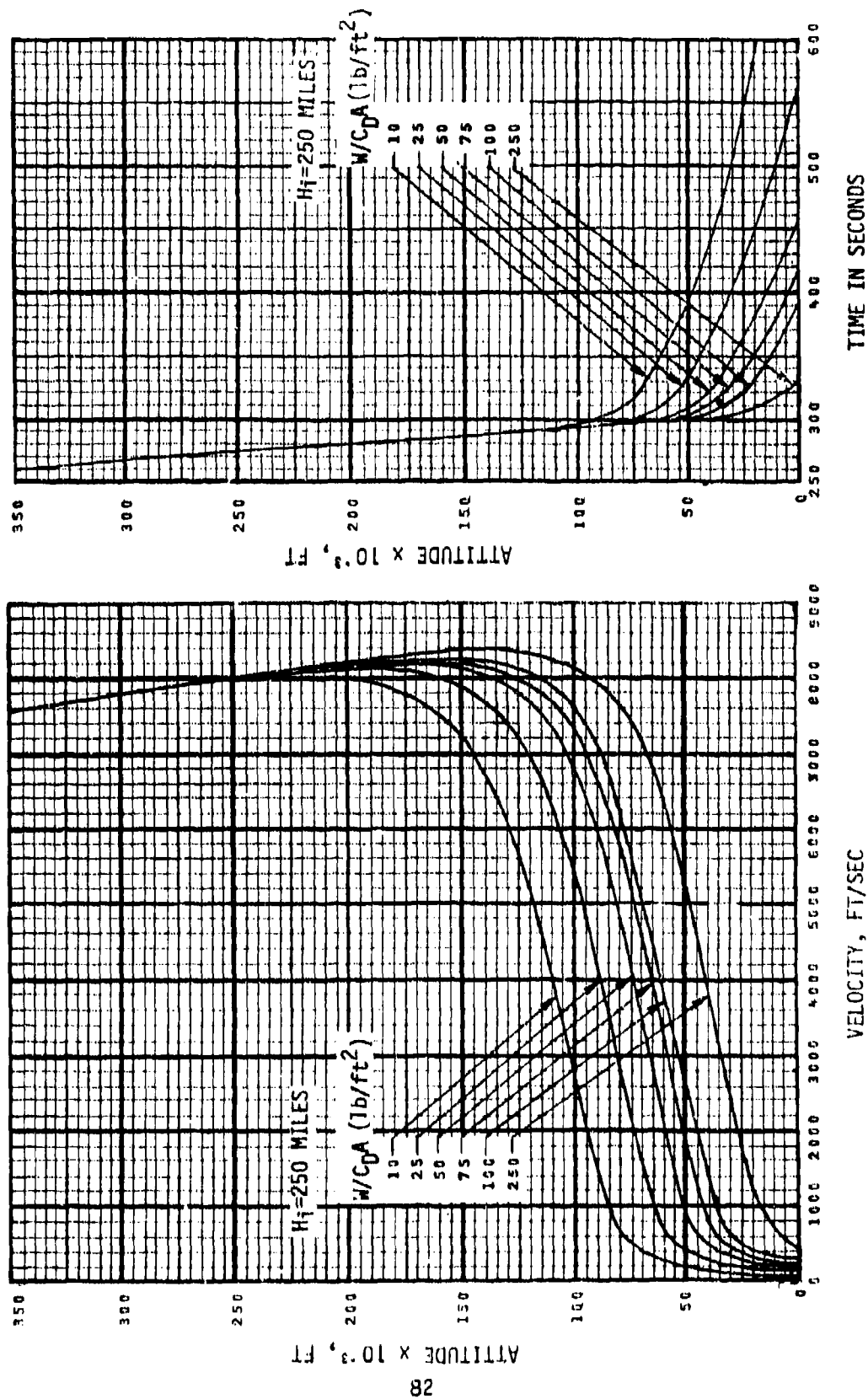


Fig. 6.7 Ballistic trajectories for an initial release altitude (H_i) of 250 miles.

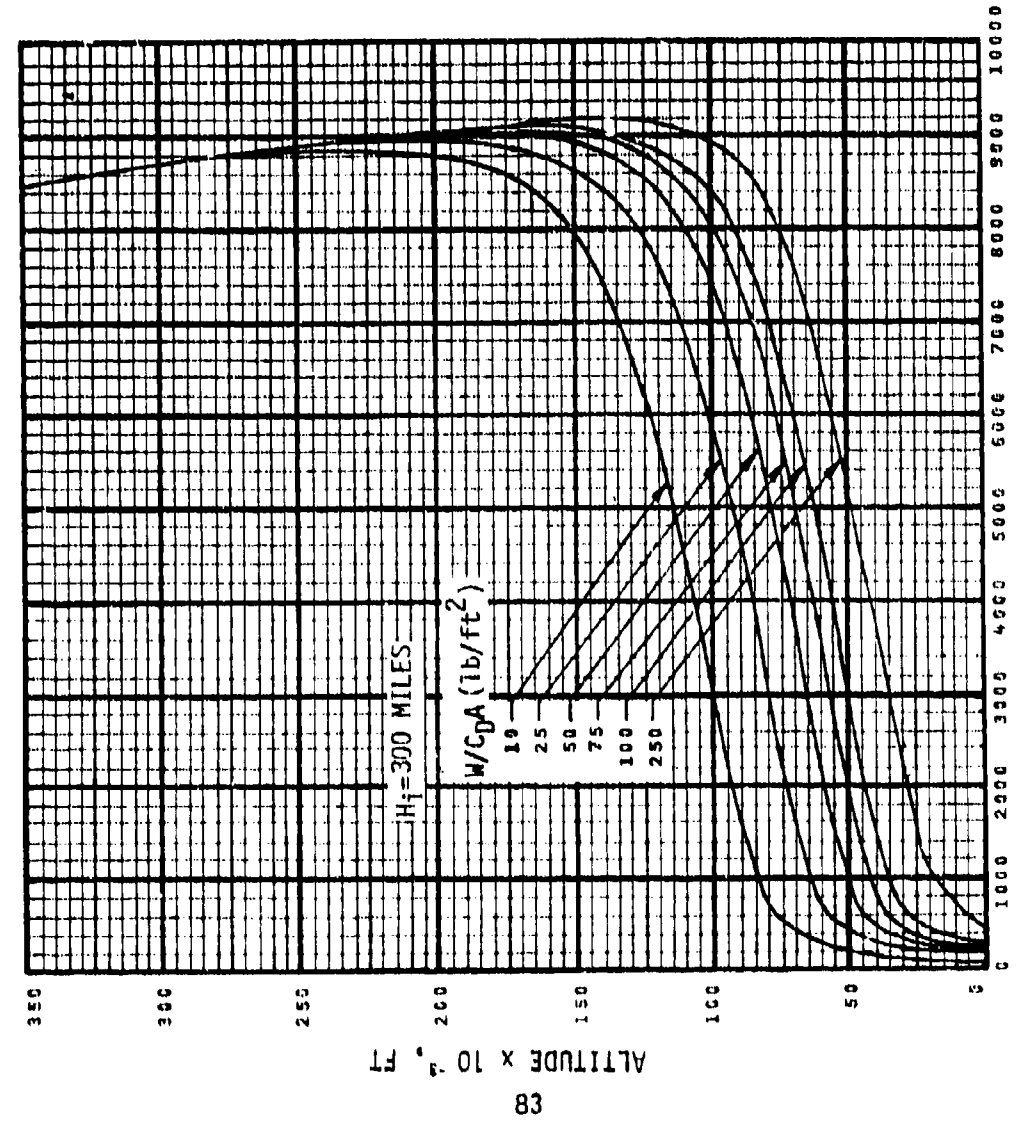
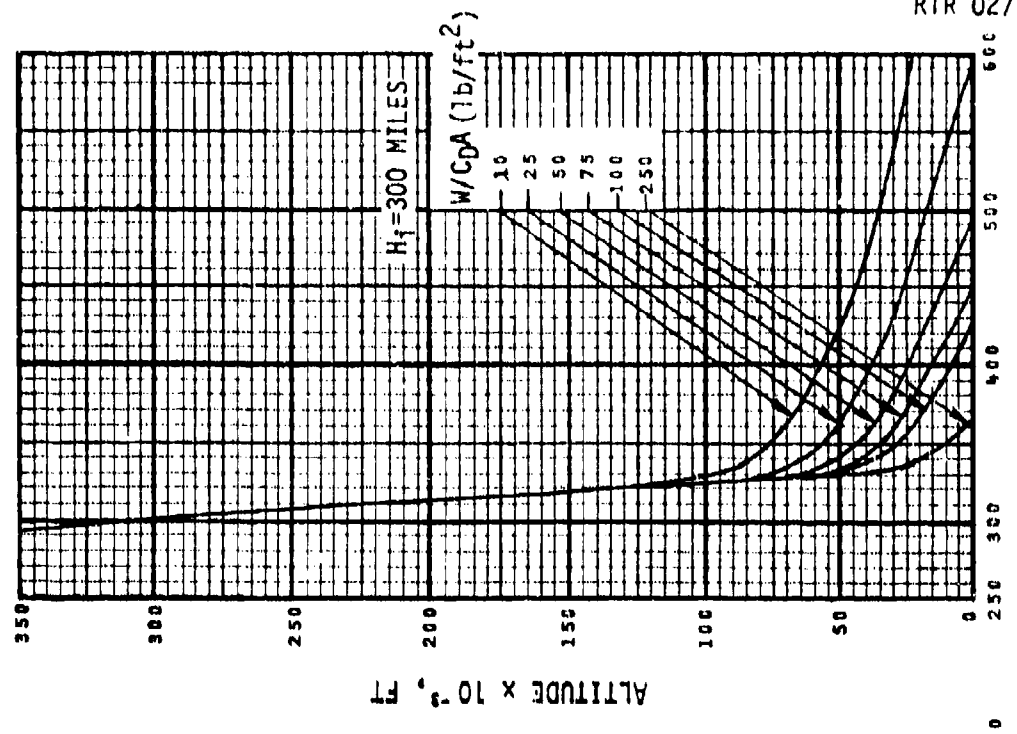


Fig. 6.8 Ballistic trajectories for an initial release altitude (H_i) of 300 miles.

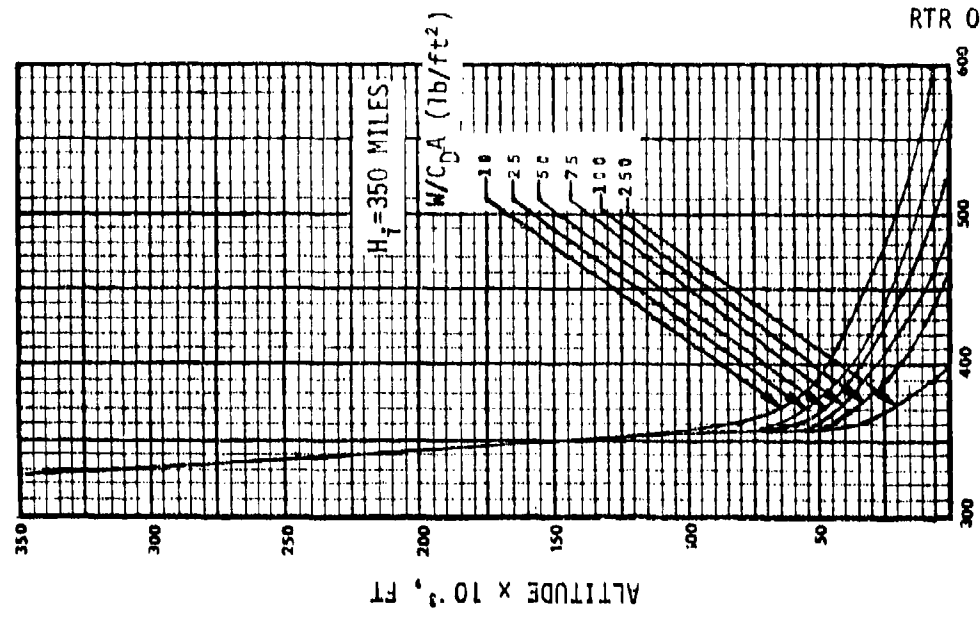
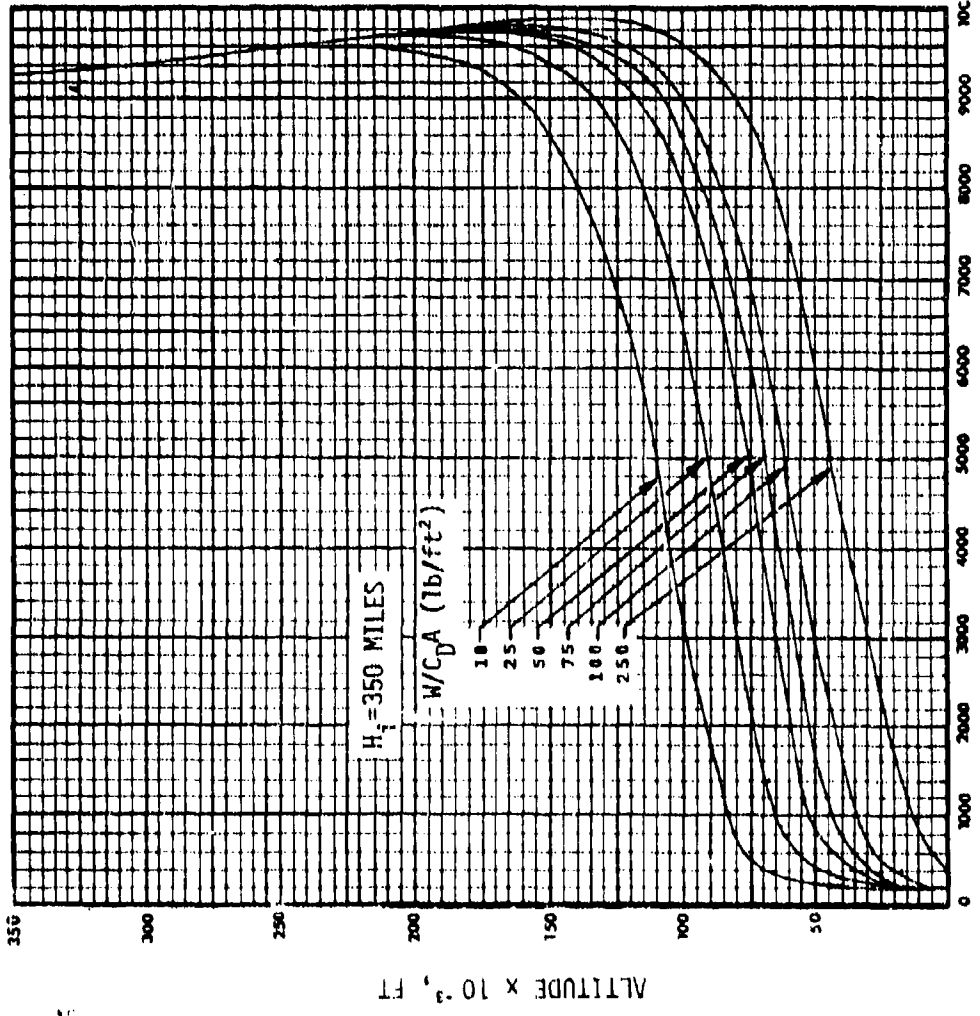


Fig. 6.9 Ballistic trajectories for an initial release altitude (H_i) of 350 miles.

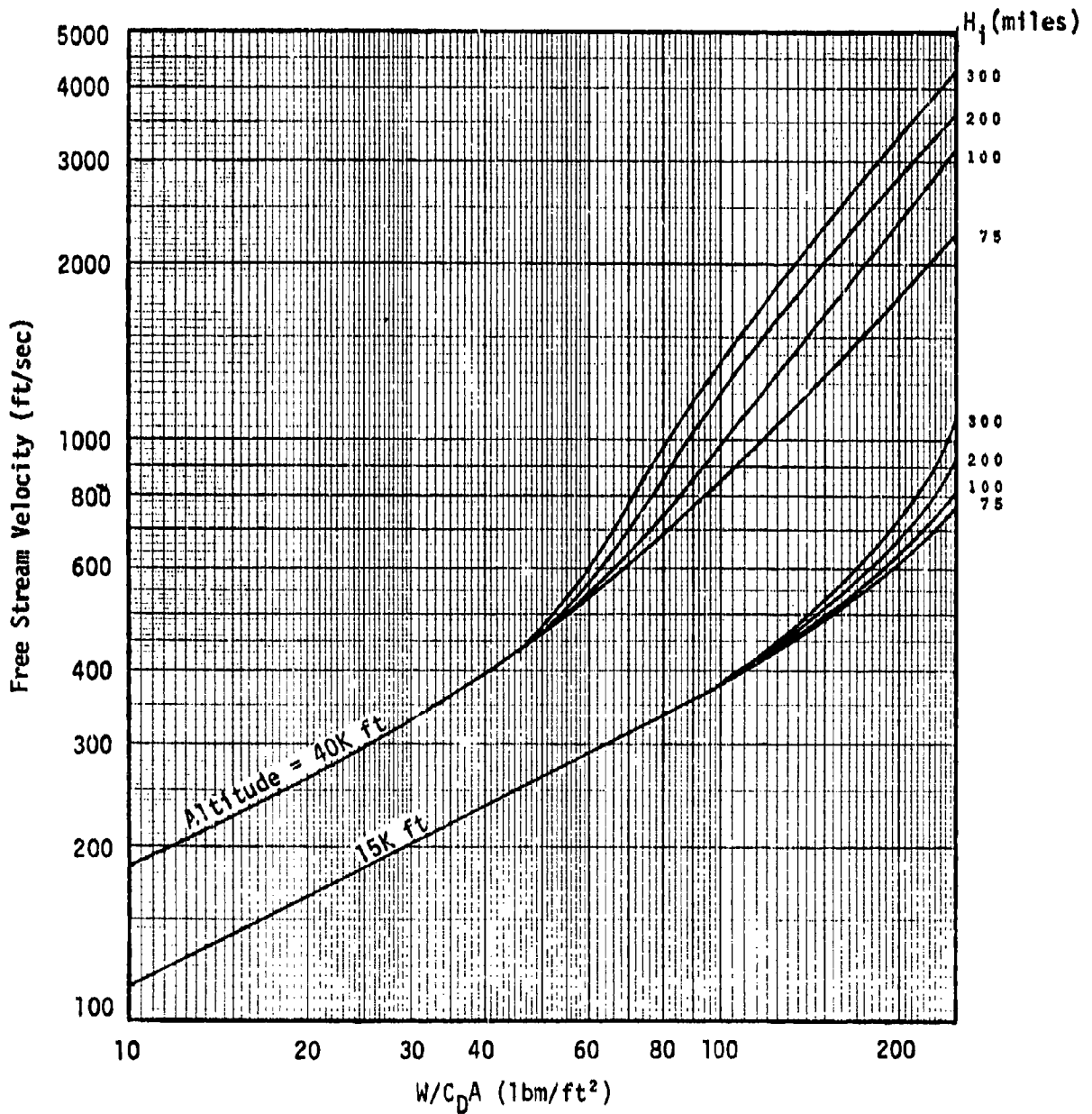


Fig. 6.10 Maximum Descent Velocity Versus Ballistic Coefficient and Release Altitude at Two Vehicle Recovery Altitudes

SECTION 7

CONVECTIVE HEATING RATES

Convection heating rates versus altitude and velocity for angles of attack ranging from 90 to 180 degrees are presented in Figs. 7.1 - 7.10. These heating rates are applicable to the base and cylindrical sections of both the cylinder and cone-cylinder configurations. A method for using the plots for the cylinder heating rates to compute heating rates for the cone of the cone-cylinder configurations is given in Table 7.1. Detailed discussions of the convection heating methodologies used in the analysis are presented in Appendix C.

These heating rates are presented in this section in order to familiarize the design engineer with heating rate environments for reentry payloads. It is entirely feasible that certain pieces of hardware on board a reentry payload could be heating rate sensitive, i.e., the piece of hardware is unable to withstand an extremely high heating rate for a short time period. Certain types of instrumentation could possibly fall into the category of being rate sensitive when subjected to high reentry heating rates.

There is an additional benefit to the design engineer in being able to determine the heating rate history for a vehicle. If the altitude, velocity, time and angle of attack history are known for a reentry payload, an integrated heating load calculation can be performed. A surface temperature for the reentry payload can then be determined from the integrated heating load. If the vehicle is reentering at a constant angle of attack, a heating rate at specific time points can be obtained by superimposing the payload trajectory onto the correct angle of attack figure (Figs. 7.1 - 7.10). A numerical integration of the heating

rate over a certain time interval can be performed in order to determine an integrated heating load. This is essentially the same method by which heating loads were computed in Section 3 of this handbook except, of course, the methods were computerized in order to cut down on the amount of work required and increase the accuracy of the calculation. If the payload is not trimmed during entry, but rather oscillating or tumbling, an integrated load can still be determined in similar fashion provided the vehicle attitude is known at a number of selected time points during the peak heating portion of the entry trajectory.

The heating rate history of a reentry vehicle can also be useful in other areas. The conduction heating from the surface to various structural members inside the vehicle reduces the surface temperature. This reduction in surface temperature can be determined using a thermal analyzer conduction program once the heating rate history and a model of the structural members are obtained. This type of analysis is recommended when the handbook results indicate excessive surface temperatures beyond the safe limits of the material. The analysis is difficult, time consuming, and requires a thorough knowledge of conduction heat transfer and thermal analyzer computer programs. Even though this is the case, the analysis should be considered in these situations.

During a vehicle reentry there is an altitude at which the aerodynamic heating ends and cooling begins. Fig. 7.11 presents this altitude versus ballistic coefficient for three release altitudes of the vehicle. The altitudes presented in Fig. 7.11 provide cutoff limits for the heating rate analyses. These same limits were used in determining the loads presented in Section 3.

The heating rate plots (Figs. 7.1 to 7.10) are based on a 24-inch reference diameter. The flow regime transition from laminar to turbulent flow is built in the plots since the transition criterion is independent of diameter. The

heating rate from the figures (Fig. 7.1 to 7.10) may be corrected for diameter changes using

$$q = q_{Fig} \left(\frac{d}{24 \text{ inches}} \right)^a$$

where

$$\begin{aligned} q_{Fig} &= \text{heating rate from Figs. 7.1 - 7.10} \\ a &= 0.5 \text{ laminar} \\ a &= 0.2 \text{ turbulent} \end{aligned}$$

In order to determine a value for the constant, a , in the above expression the flow regime must be established. The free stream Reynolds number per foot (Re_{∞}/ft) will be used to indicate whether the flow is laminar or turbulent at the particular altitude velocity point where the heating rate is desired. The expression for Re_{∞}/ft is

$$Re_{\infty}/ft = \frac{\rho_{\infty} V_{\infty}}{\mu_{\infty}}$$

where

$$\begin{aligned} \rho_{\infty} &= \text{free stream density (lbm/ft}^3\text{)} \\ V_{\infty} &= \text{free stream velocity (ft/sec)} \\ \mu_{\infty} &= \text{free stream viscosity (lbm/ft-sec)} \end{aligned}$$

The free stream velocity in the Reynolds number expression is known. The free stream density can be obtained at the given altitude from Fig. 7.15. In order to determine μ_{∞} , Sutherland's law for viscosity will be used along with the free stream temperature from Fig. 7.14. The expression for Sutherland's law is

$$\mu_{\infty} = 7.3035 \times 10^{-7} \frac{T_{\infty}^{3/2}}{T_{\infty} + 198.6} \text{ lbm/ft-sec (} T_{\infty} \text{ in } ^{\circ}\text{R)}$$

Once Re_{∞}/ft has been computed the flow regime (laminar or turbulent) may be determined from Fig. 7.12. In general, the flow regime will be laminar for altitudes greater than 300K feet and turbulent for altitudes less than 50K feet. Certain angles of attack will promote laminar or turbulent flow regardless of the altitude and velocity.

Cylinder: $85 \leq \alpha_T \leq 95$ Always laminar

Base: $\alpha_T \geq 175$ Always laminar

If angle of attack, α_T , is less than 90 degrees, the following procedure is used

Cylinder: If $\alpha_T < 90$, compute the heating using $180 - \alpha_T$

Base: If $\alpha_T < 90$, compute the heating using $\alpha_T = 90$.

Once the heating rate is computed using the preceding procedure, a surface temperature correction may be required. The results presented in Fig. 7.1 to Fig. 7.10 are for a wall temperature of 660°R . The heating rate may be corrected for wall temperature by using the following equation.

$$q = q_{660} \frac{(T_{aw} - T_s)}{(T_{aw} - 660)}$$

where

$$T_{aw} = T_\infty + \frac{RV_\infty^2}{2C_p gJ} \quad (^\circ\text{R})$$

$$2C_p gJ = 12019.2 \text{ (ft}^2/\text{sec}^2\text{ }^\circ\text{R)}$$

R = Recovery factor from Fig. 7.13

T_∞ = Free stream temperature from Fig. 7.14

T_s = Surface temperature ($^\circ\text{R}$)

Thus, Fig. 7.1 to 7.10 may be used by making angles of attack, diameter, and wall temperature adjustments to the reference conditions for a large variety of problems.

TABLE 7.1
CONE HEATING RATES

The procedure for computing heating rates to the cone of a cone-cylinder configuration is as follows:

- (1) Determine the angle of attack of the cone's windward surface

$$\alpha_{\text{cone}} = \alpha_{\text{cyl}} + \theta_c$$

α_{cyl} = Angle of attack of cylinder

θ_c = Semi-vertex angle of the cone

NOTE: If $\alpha_{\text{cone}} > 180^\circ$, $\alpha_{\text{cone}} = 180^\circ$

- (2) Determine the heating rate for a cylinder at α_{cone} from Fig. 7.1 to 7.10.

- (3) Determine the cone radius at the midlength of the cone, and cone-cylinder radius ratio. The reference radius for the cylinder is $r_{\text{cyl}} = 12$ inches in Fig. 7.1 to 7.10.



- (4) Correct the heating rate for the radius effect.

$$q = q_{\text{cyl}} \left(\frac{r_c}{r_{\text{cyl}}} \right)^a$$

where $a = .5$ laminar

$a = .2$ turbulent

and where the type of flow can be determined from Fig. 7.12 based on altitude and velocity. If the angle of attack, α_c , is between 85 and 95 degrees the flow is laminar regardless of the altitude and velocity.

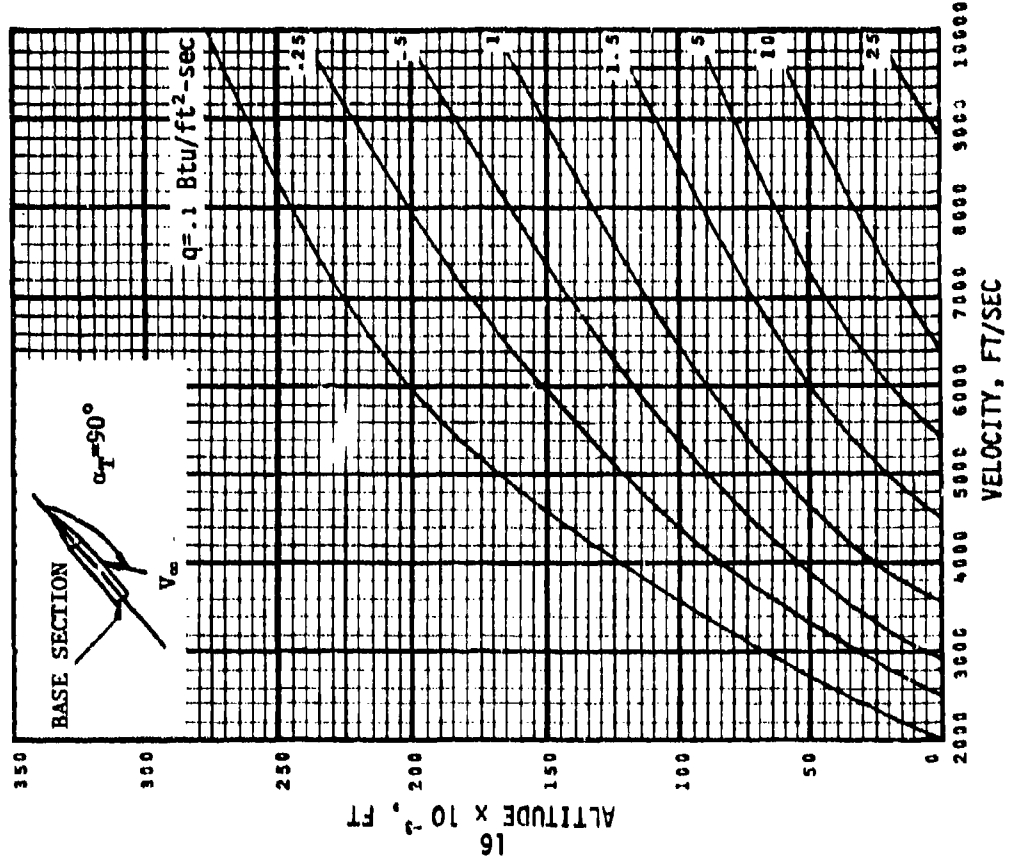
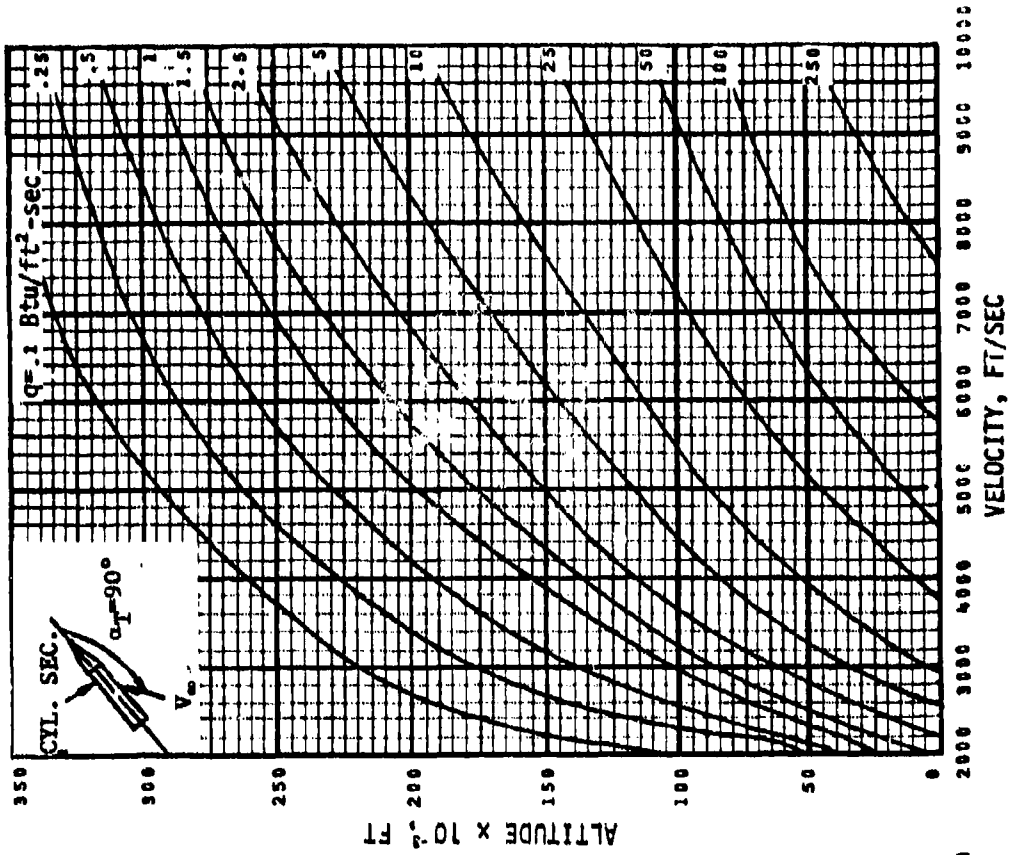
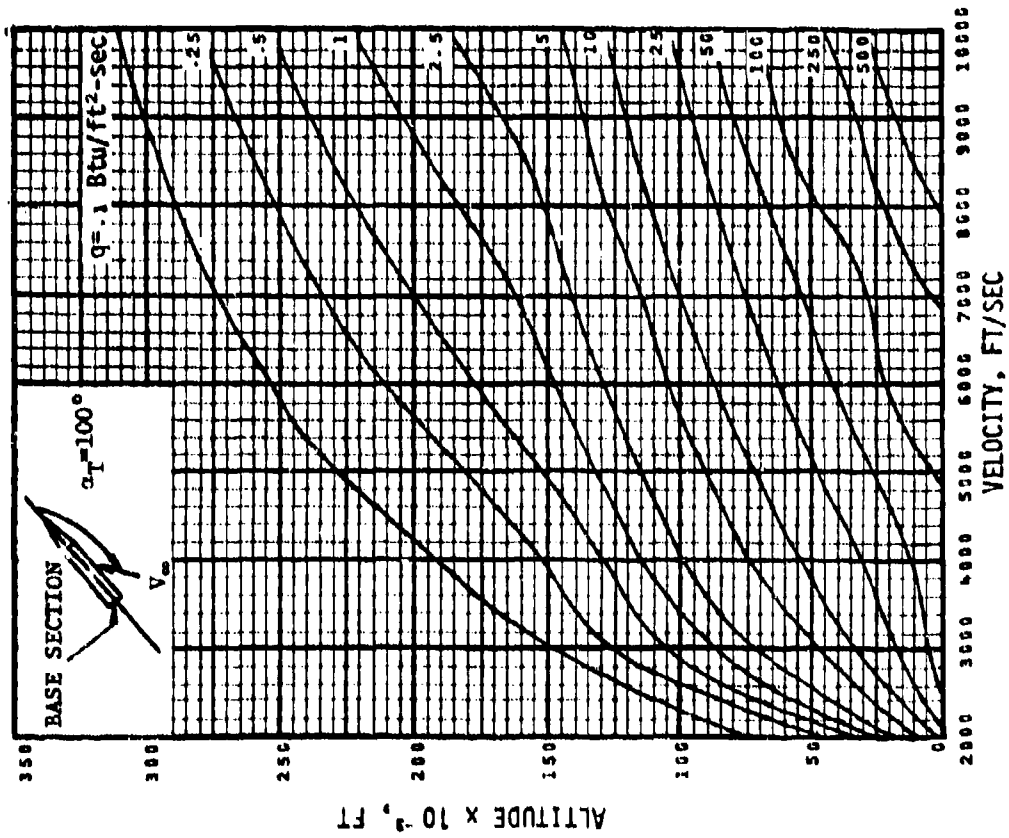
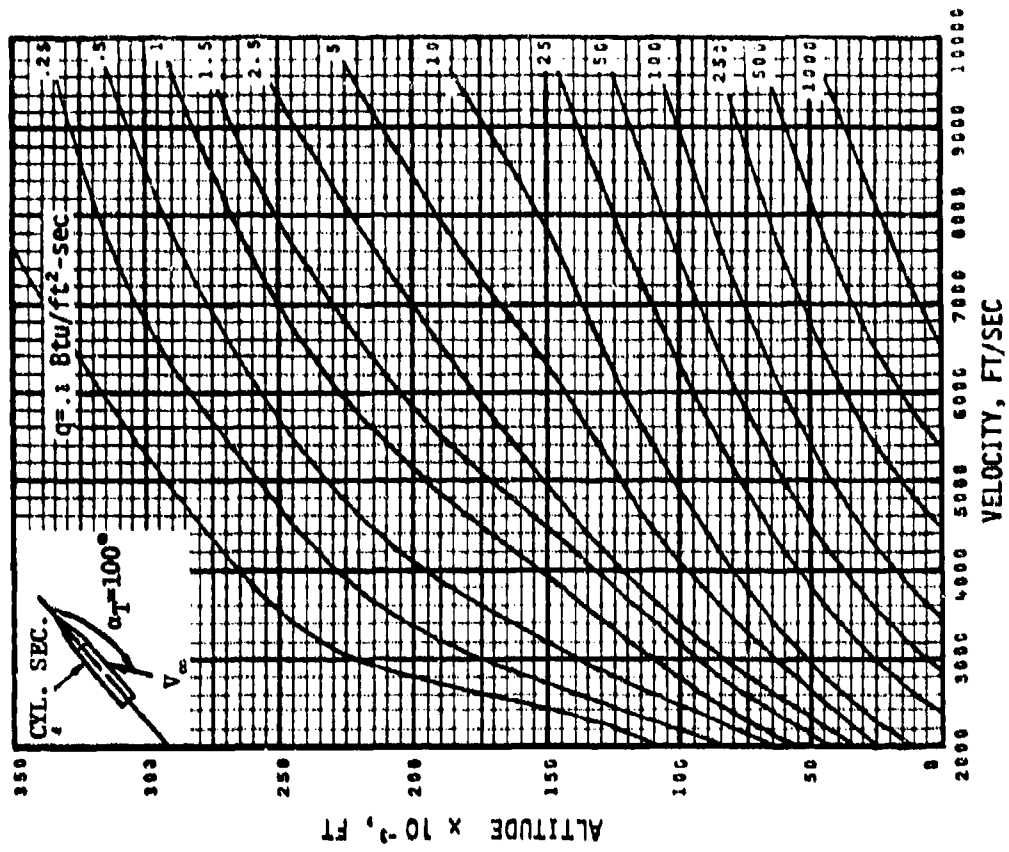


Fig. 7.1 Convection heating rates for $\alpha_T = 90$ degrees.

Fig. 7.2 Convection heating rates for $\alpha_T = 100$ degrees.

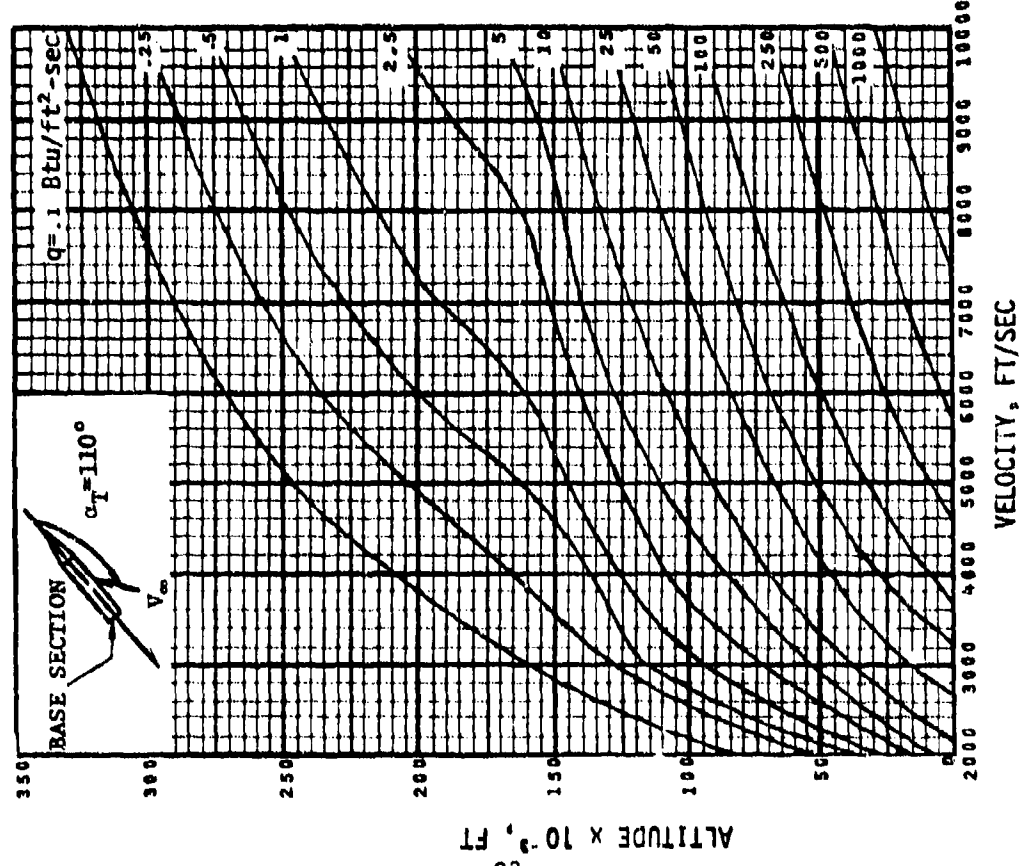
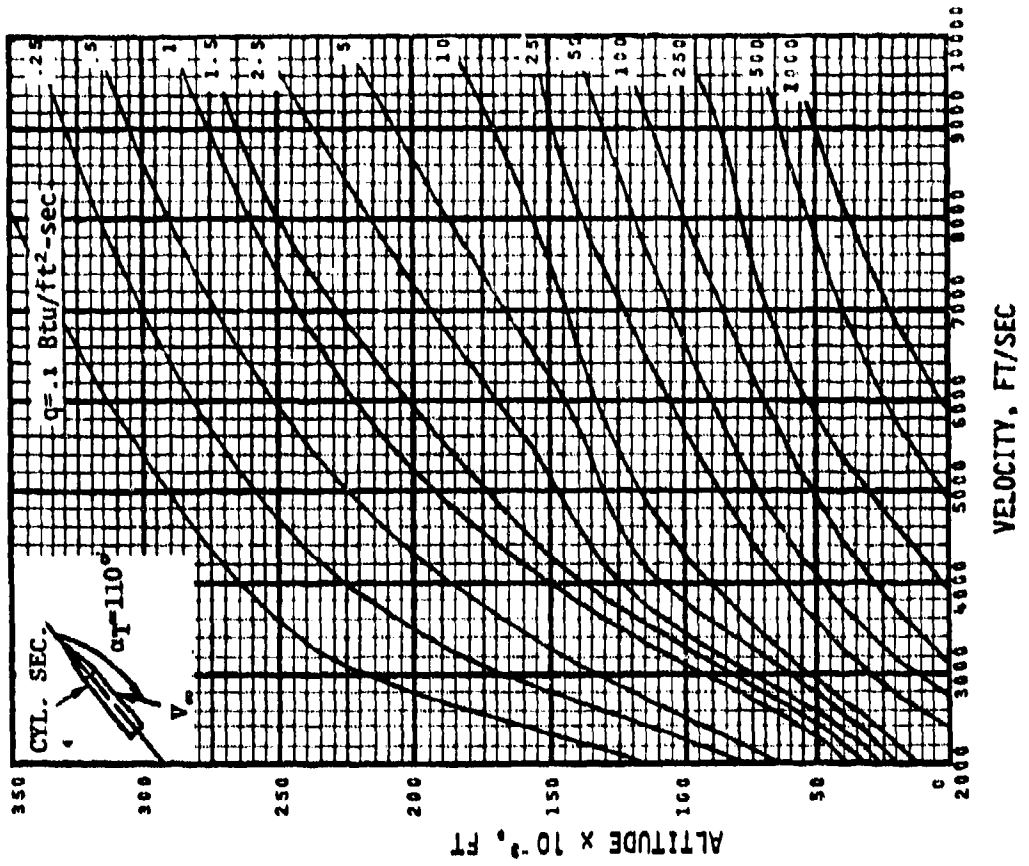


Fig. 7.3 Convection heating rates for $\alpha_T = 110$ degrees.

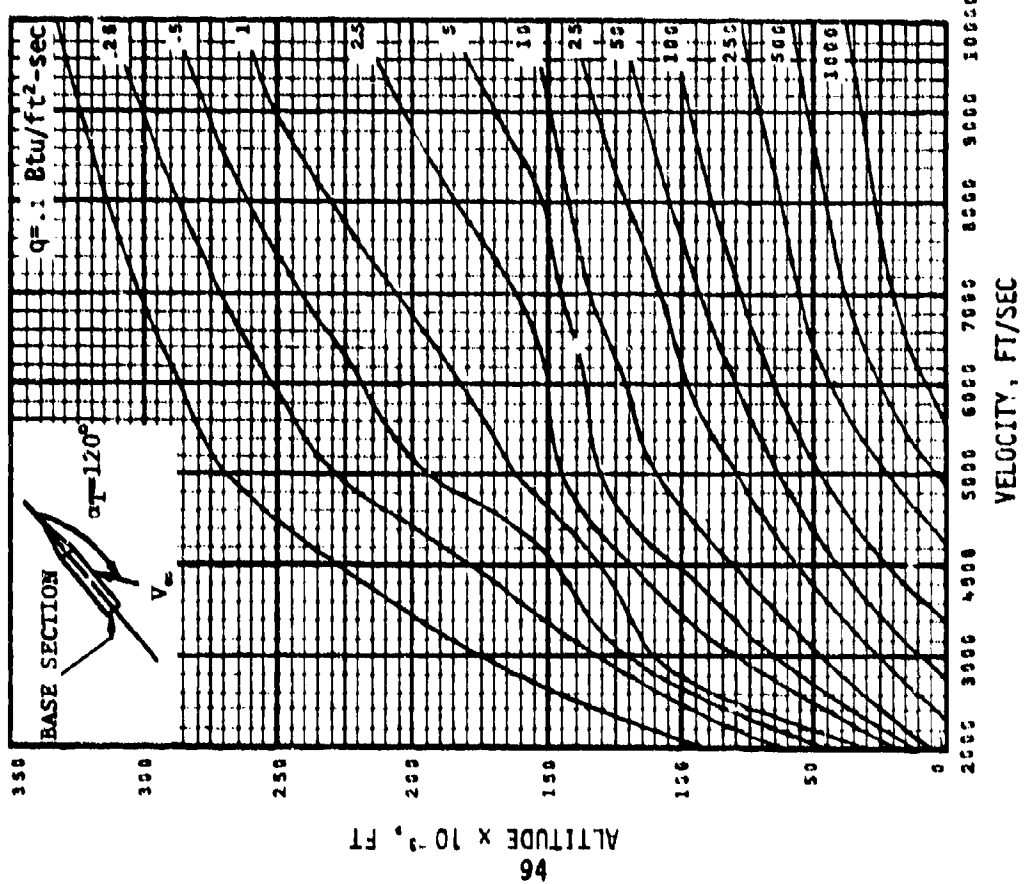
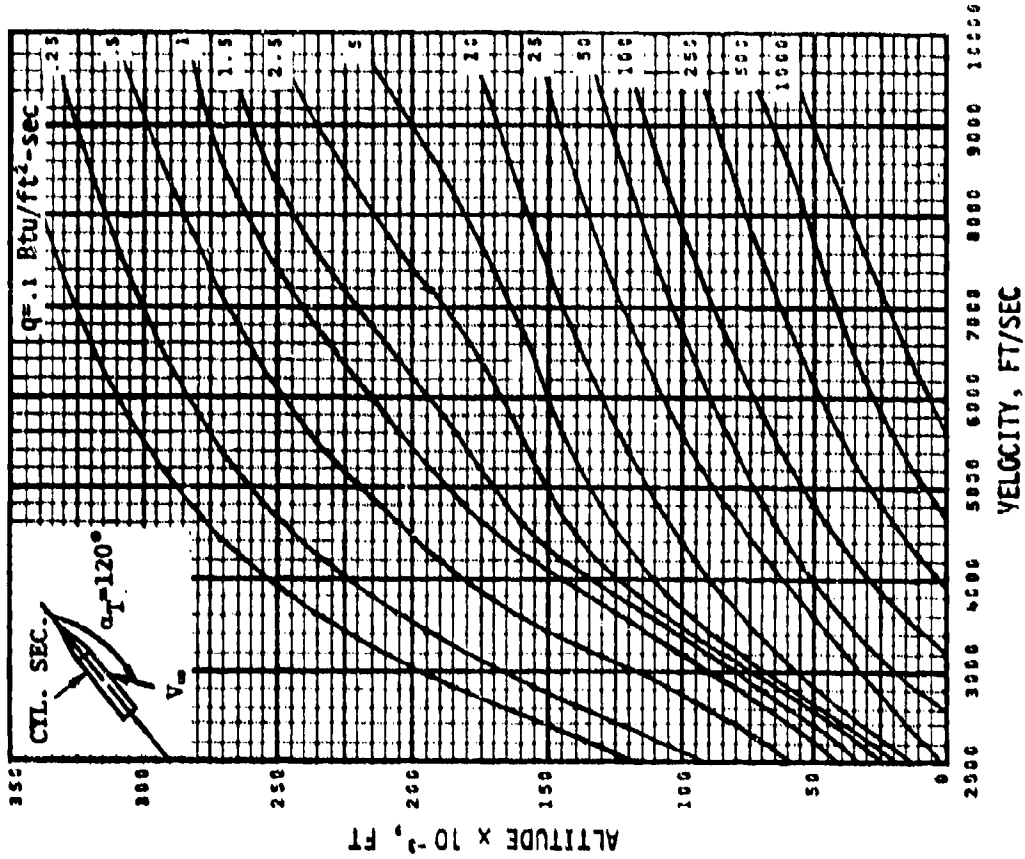


Fig. 7.4 Convection heating rates for $\alpha_T = 120$ degrees.

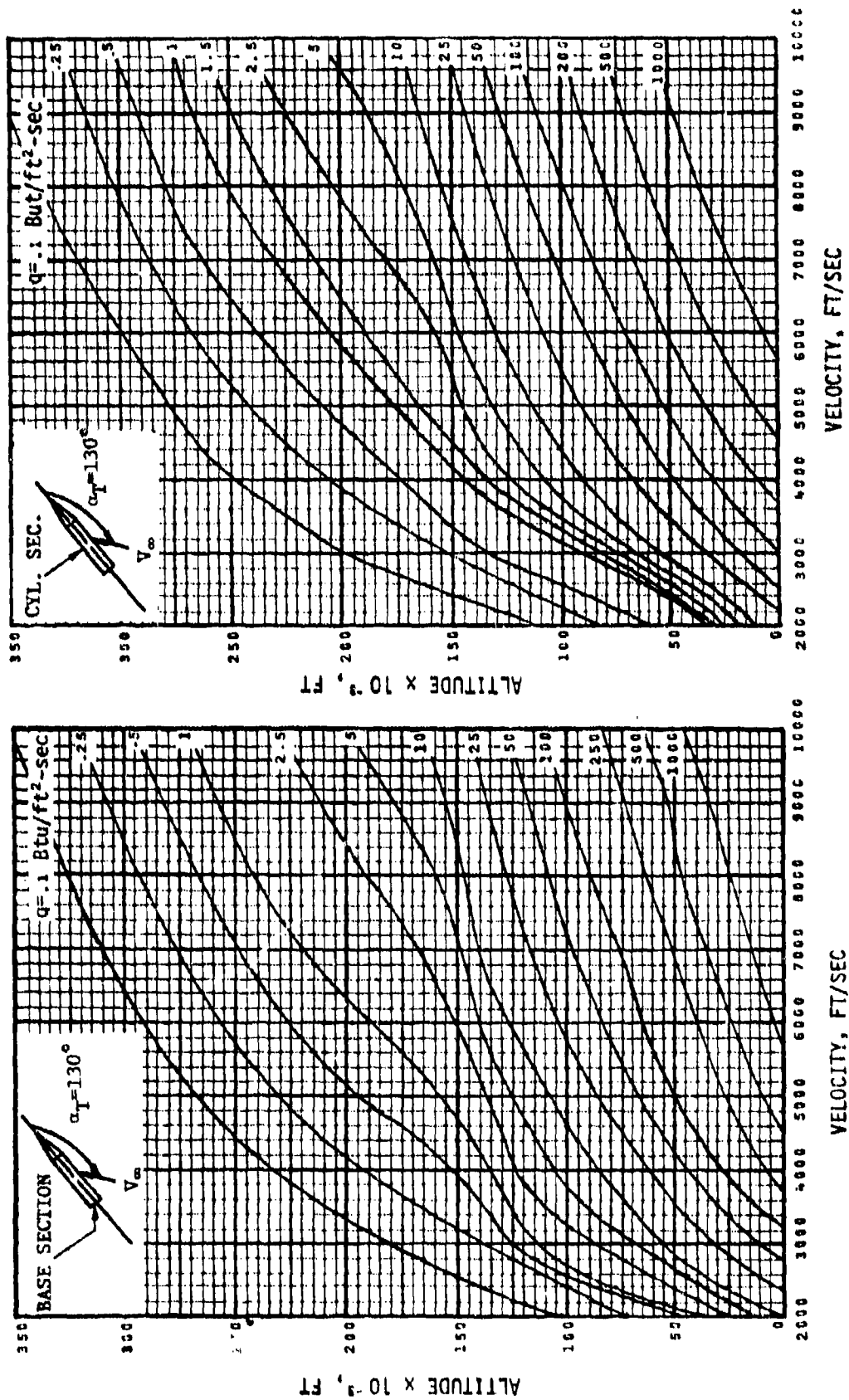


Fig. 7.5 Convection heating rates for $\alpha_T = 130$ degrees.

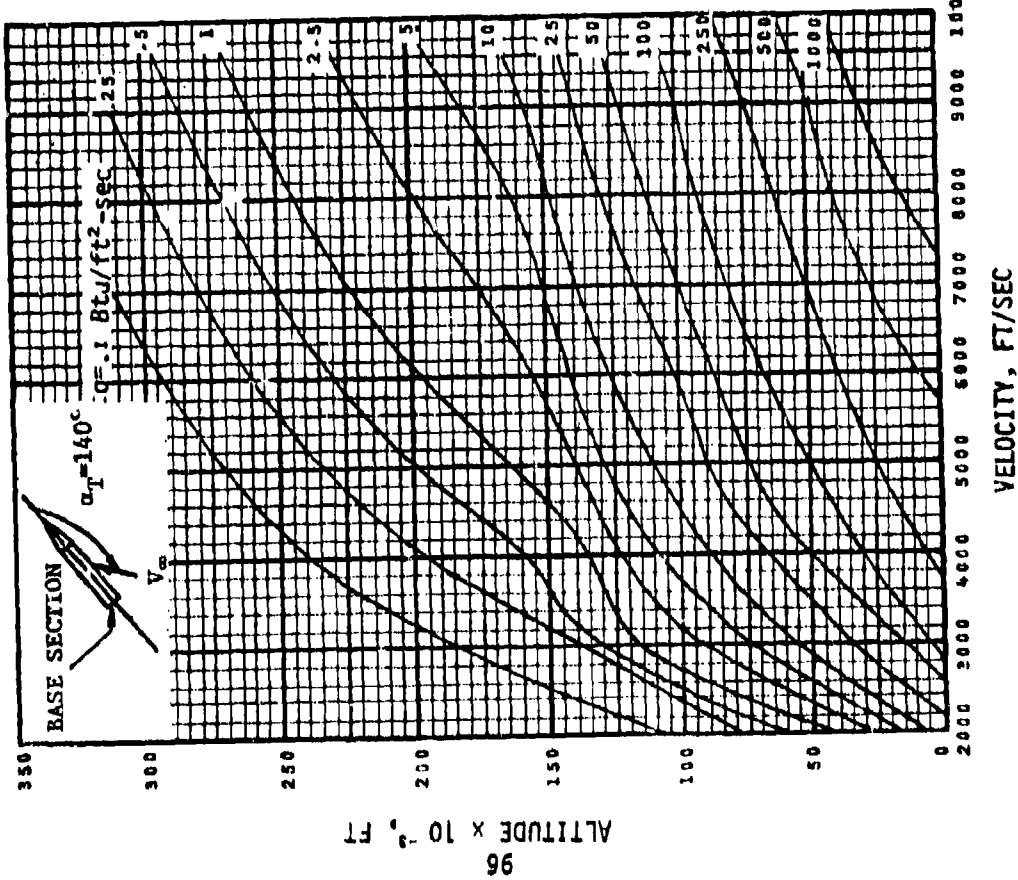
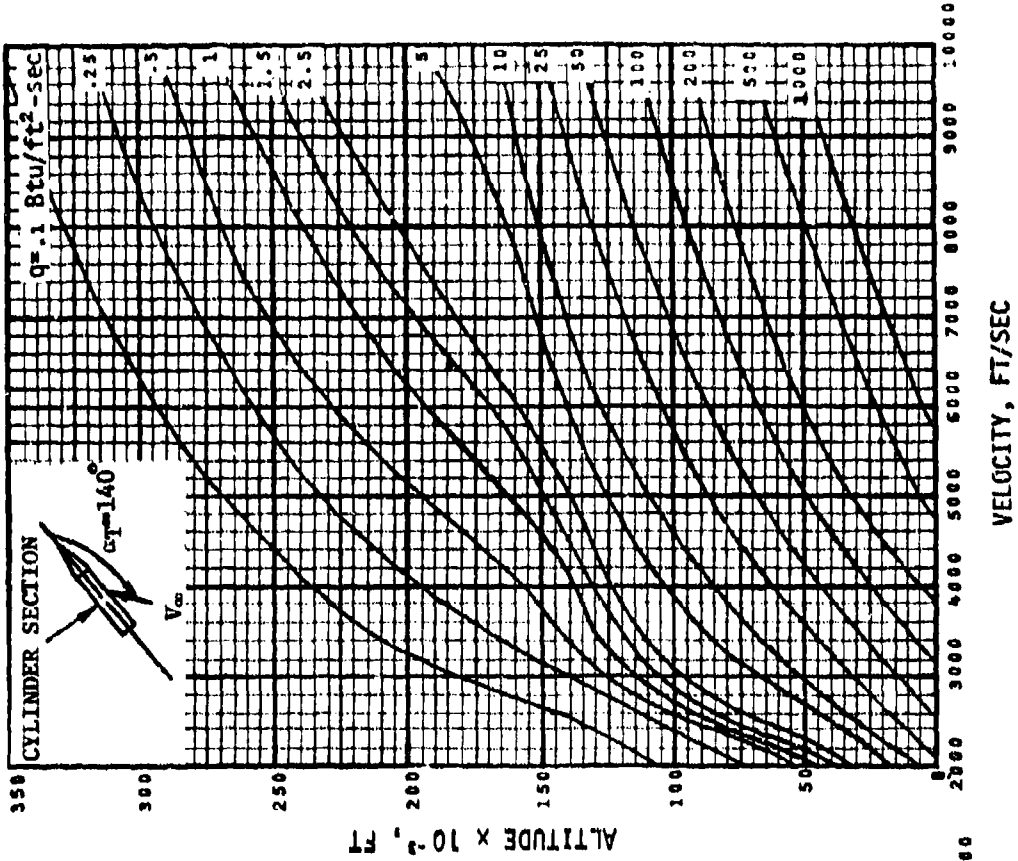


Fig. 7.6 Convection heating rates for $\alpha_T = 140$ degrees.

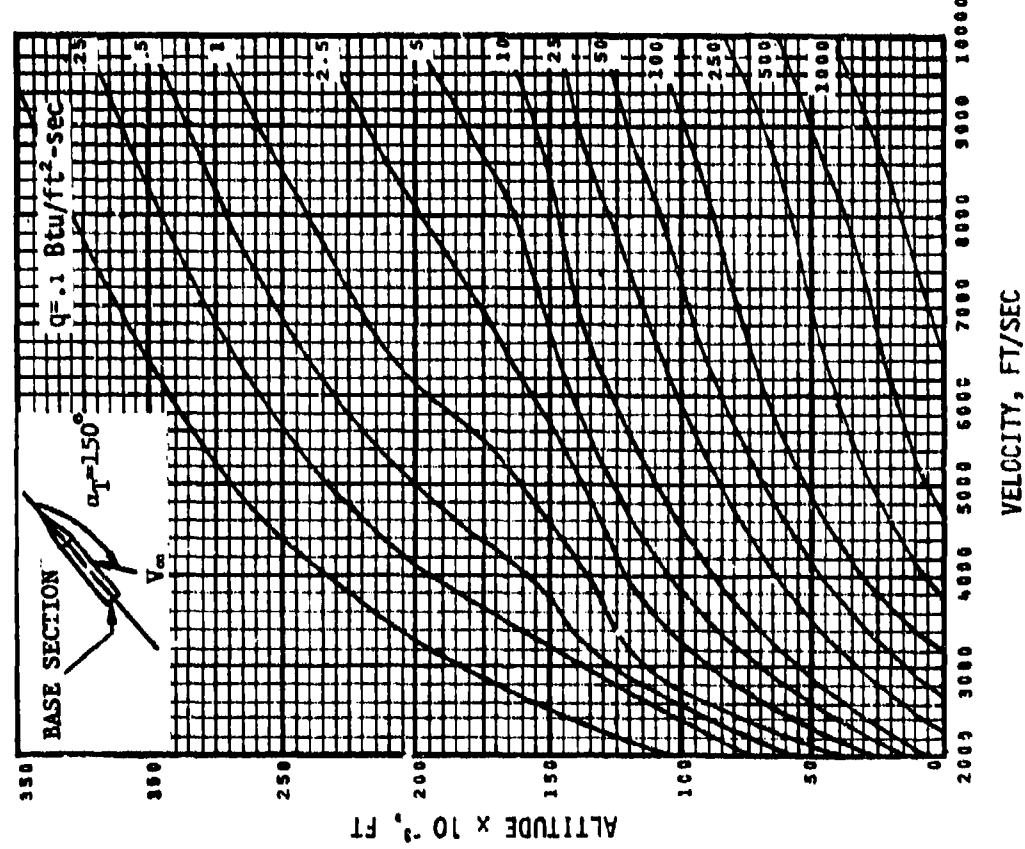
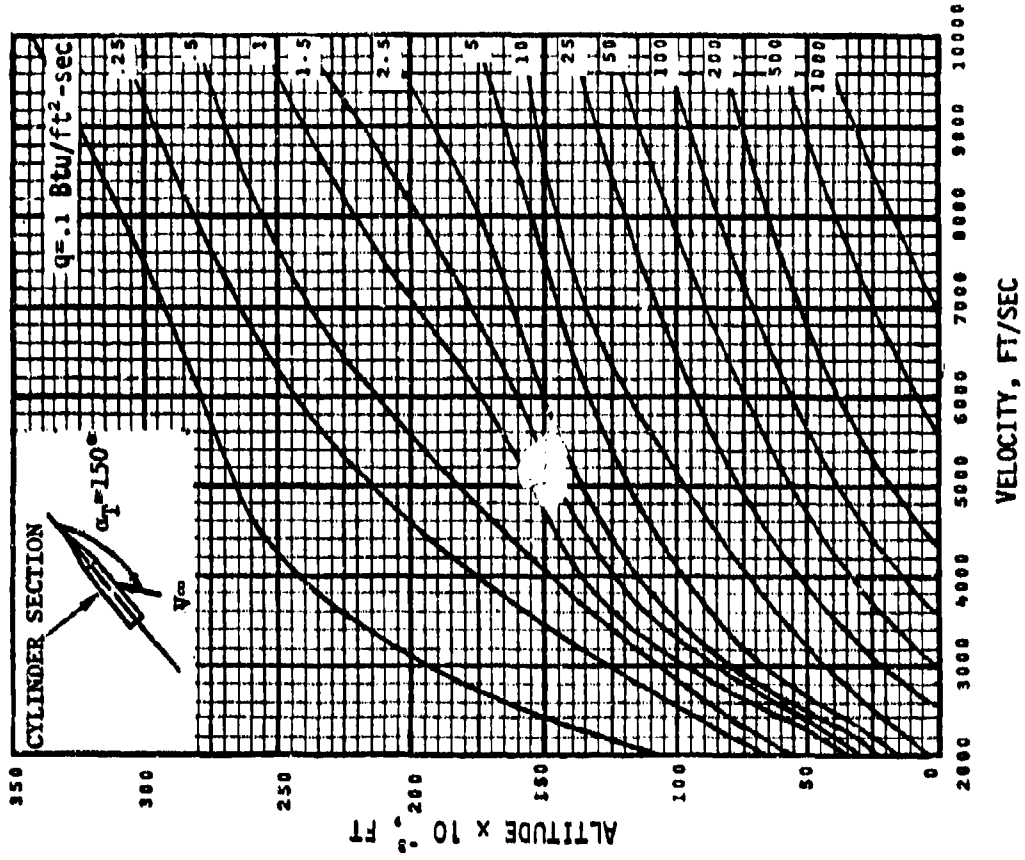


Fig. 7.7 Convection heating rates for $\alpha_T = 150$ degrees.

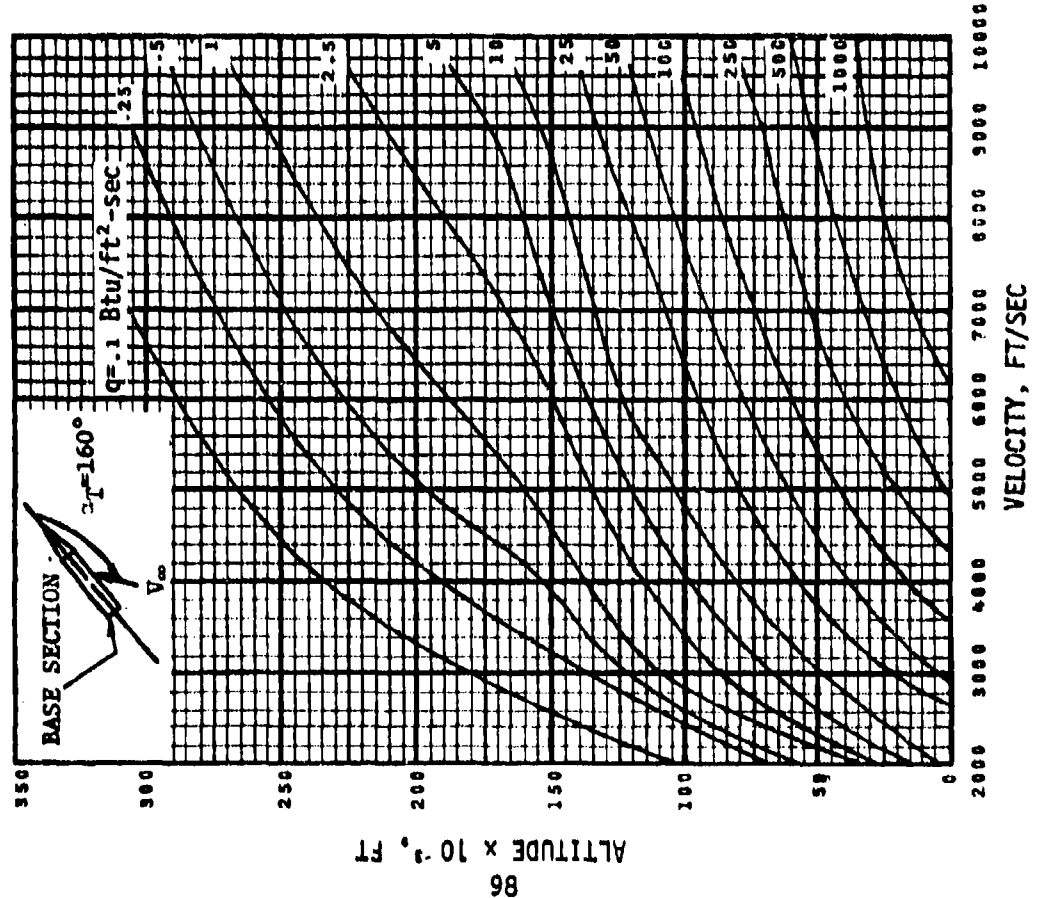
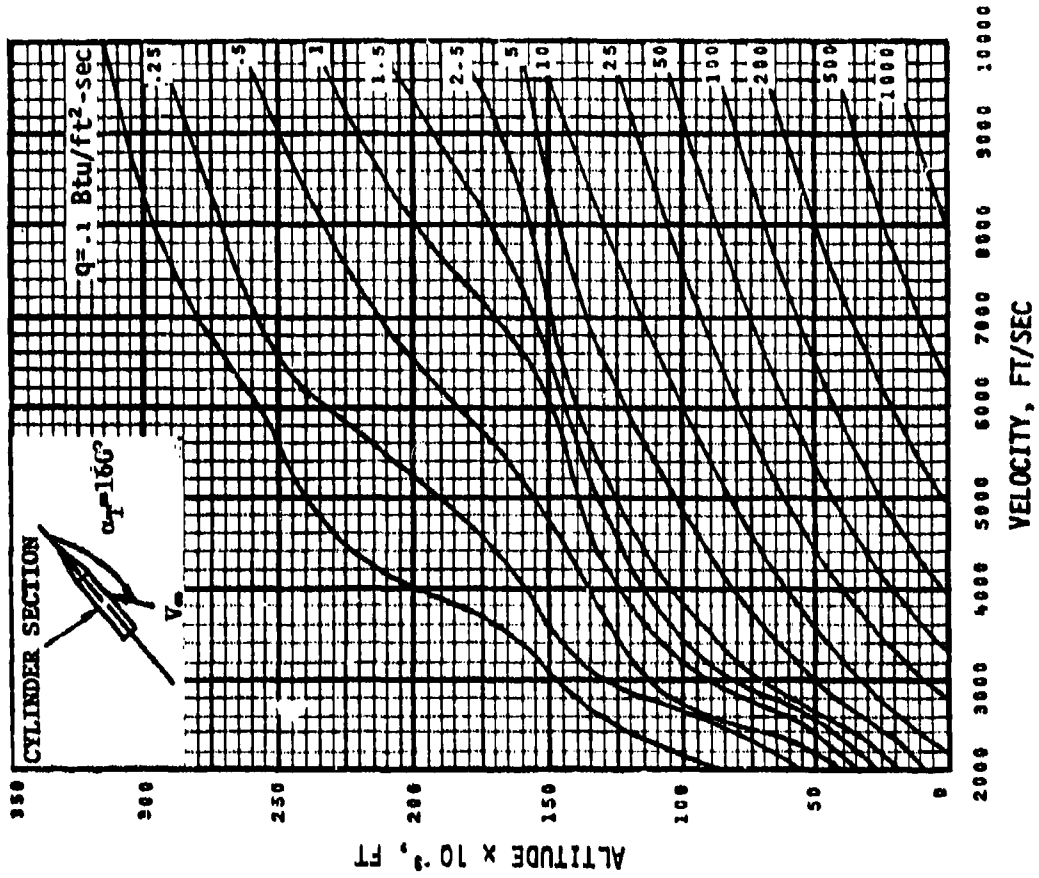


Fig. 7.8 Convection heating rates for $\alpha_T = 160$ degrees.

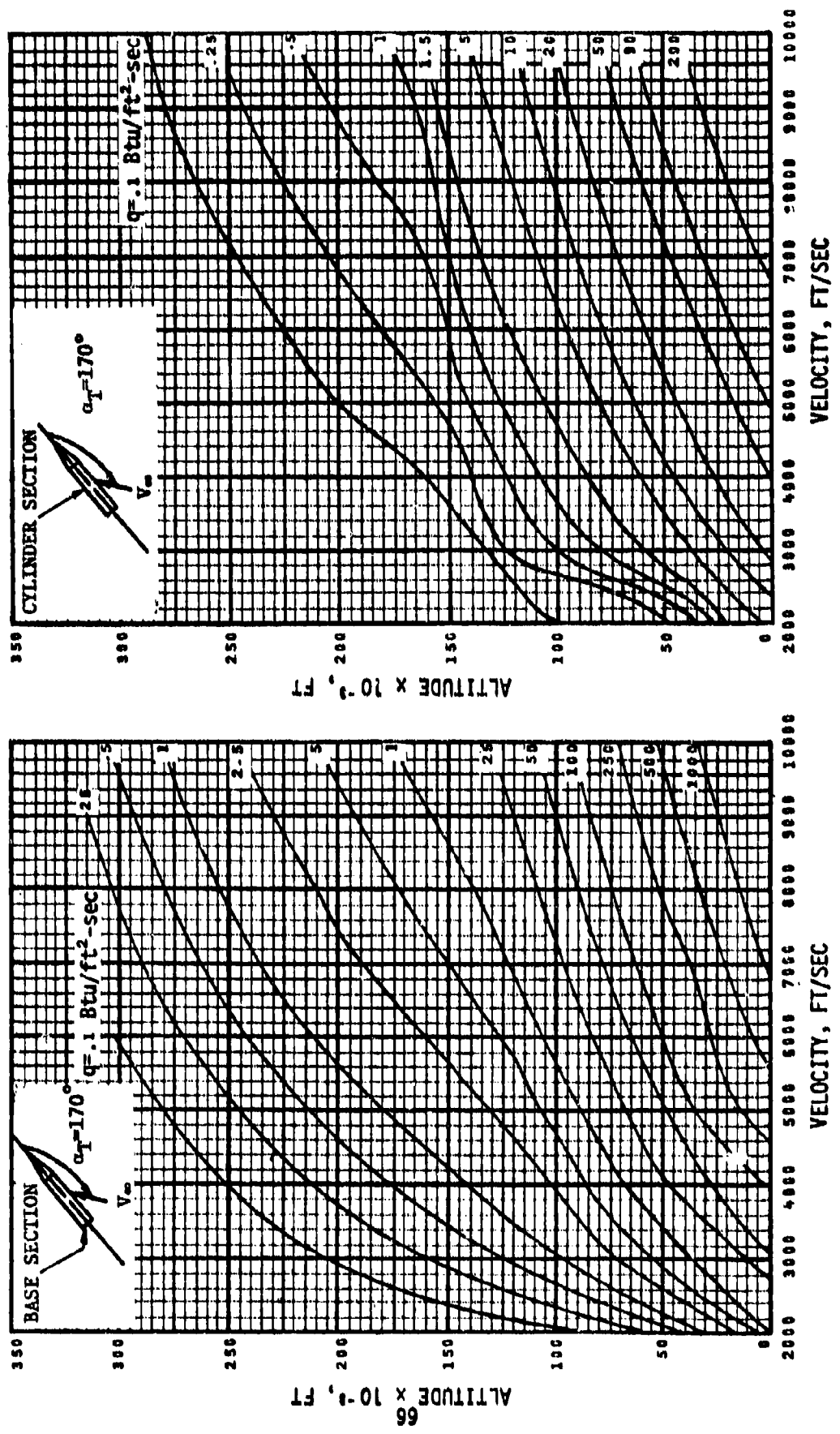
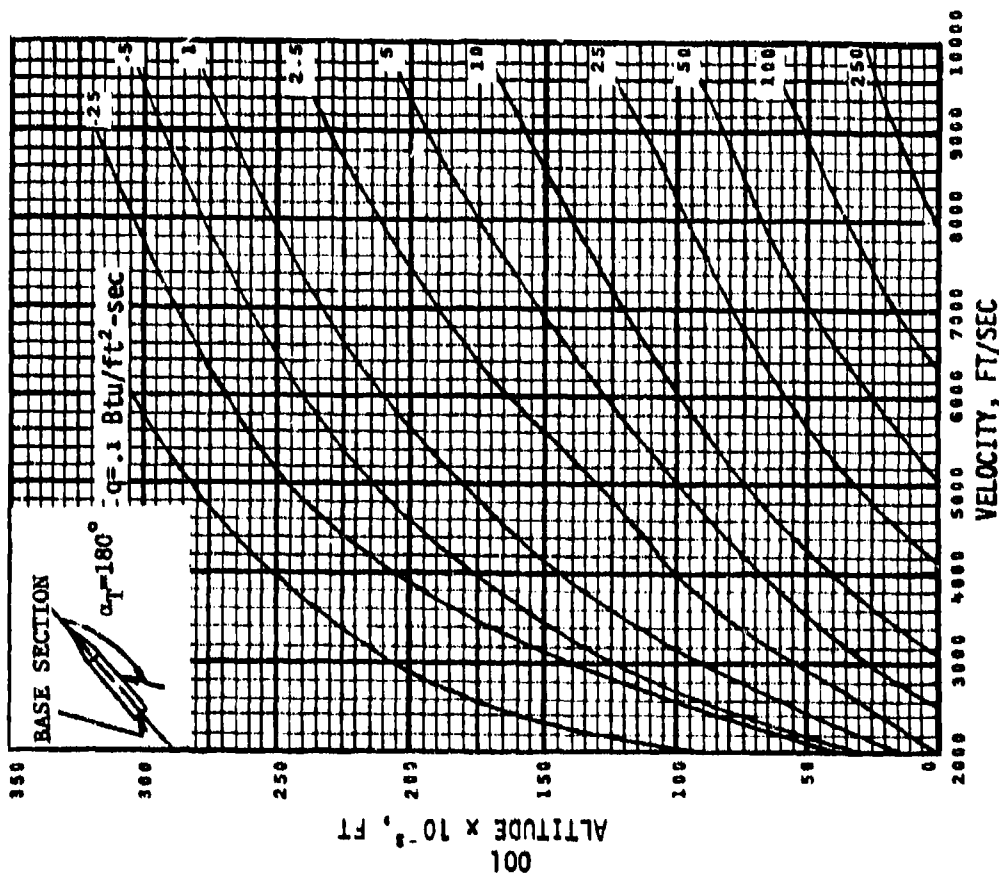
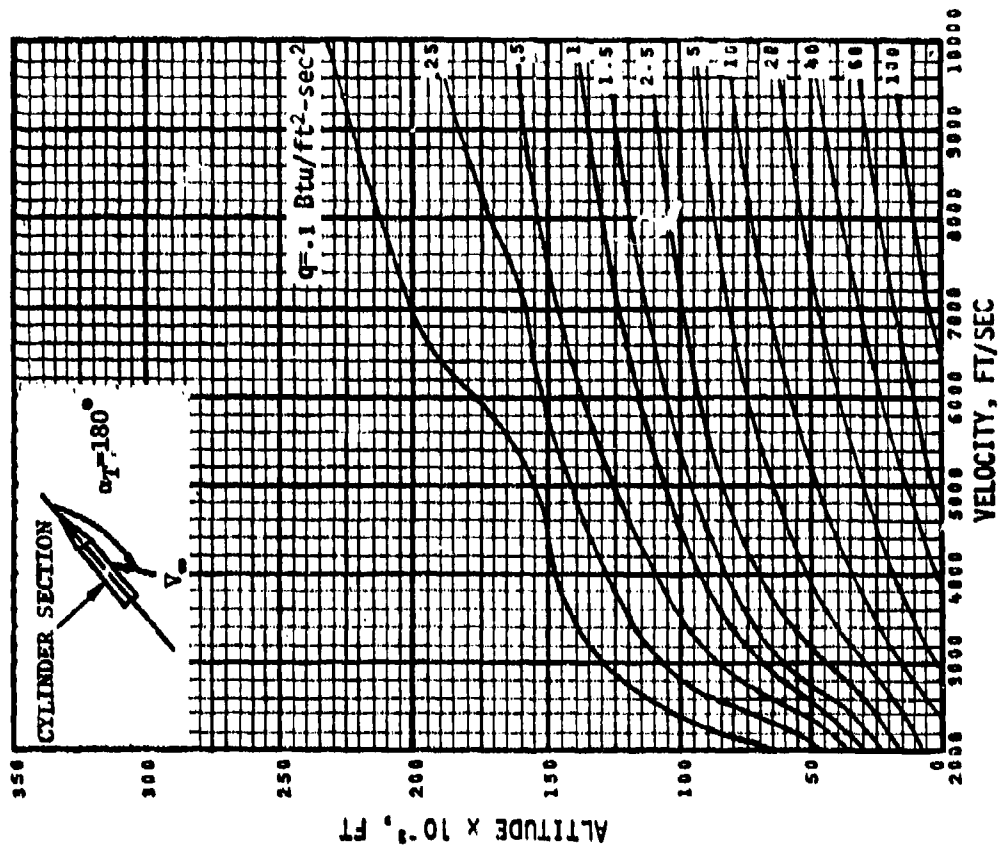


Fig. 7.9 Convection heating rates for $\alpha_T = 170$ degrees.

Fig. 7.10 Convection heating rates for $\alpha_T = 180$ degrees.

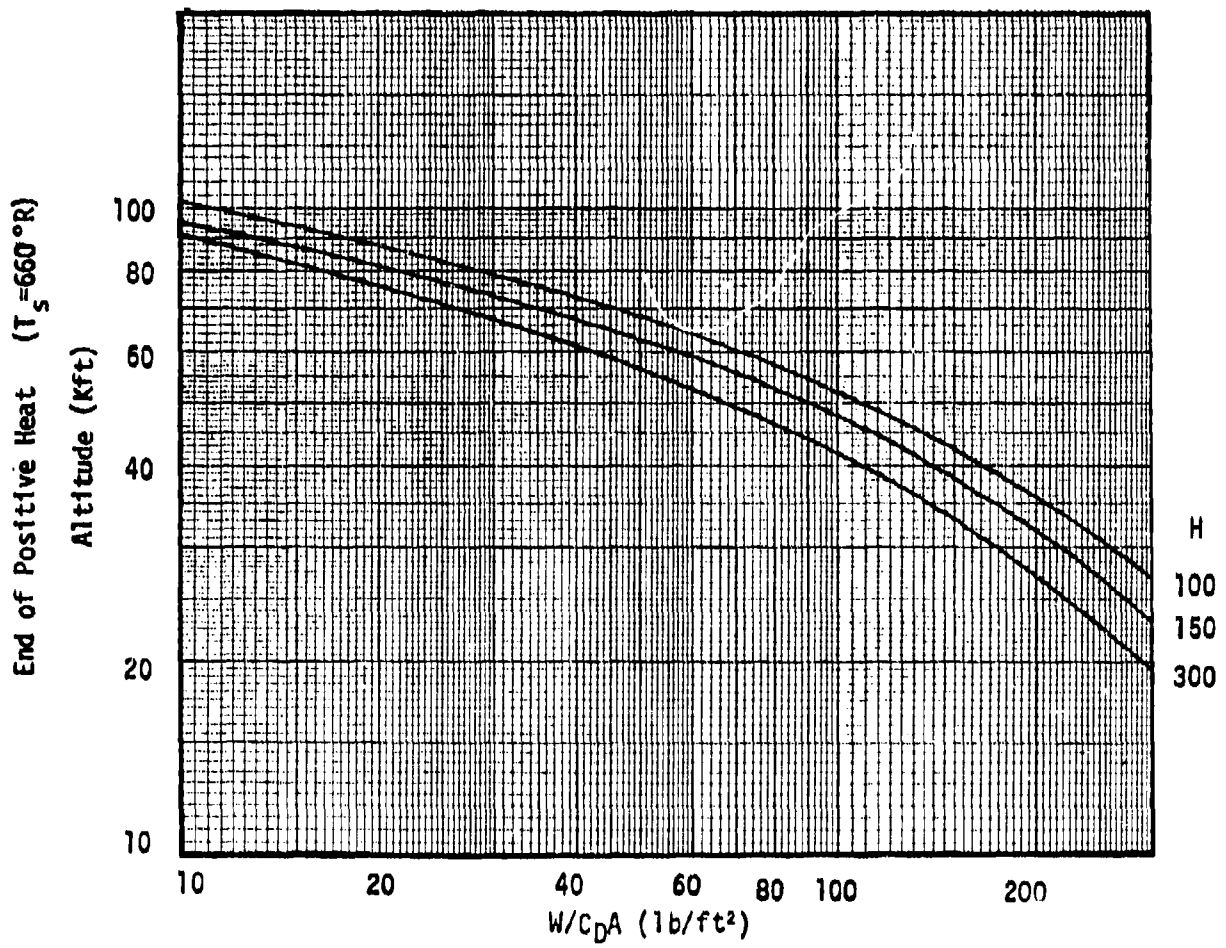


Fig. 7.11 End of positive heating altitude versus ballistic coefficient

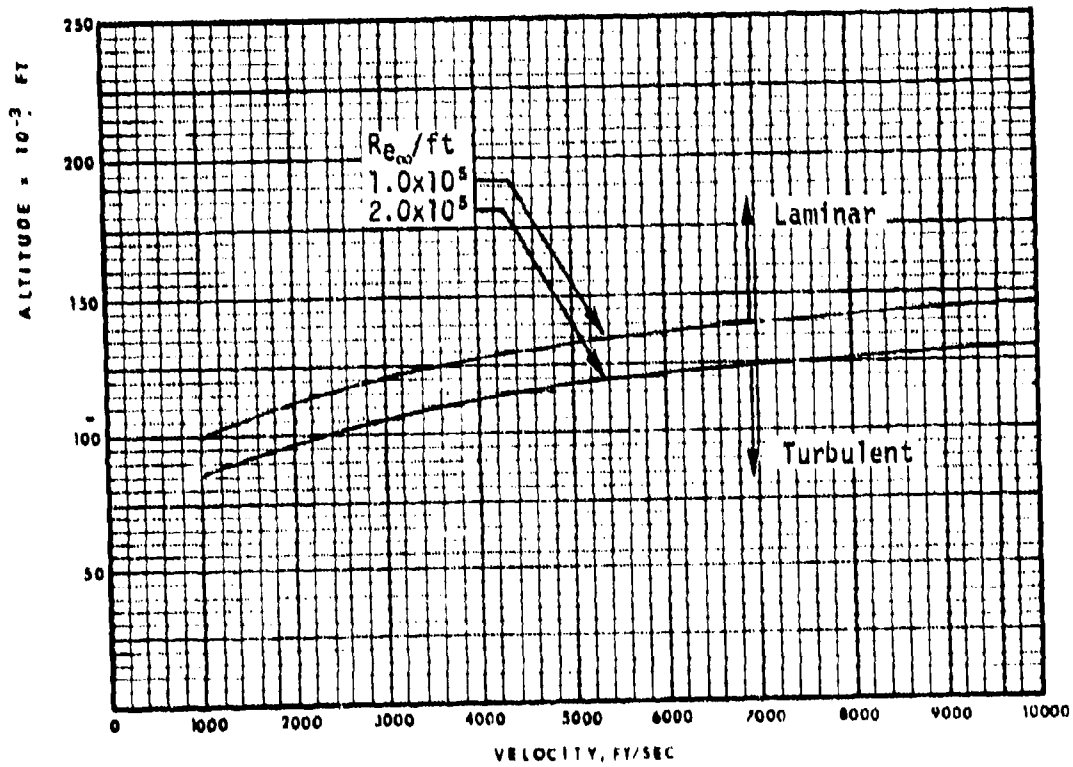


Fig. 7.12 Flow regime transition criterion for cone-cylinders at large angle of attack.

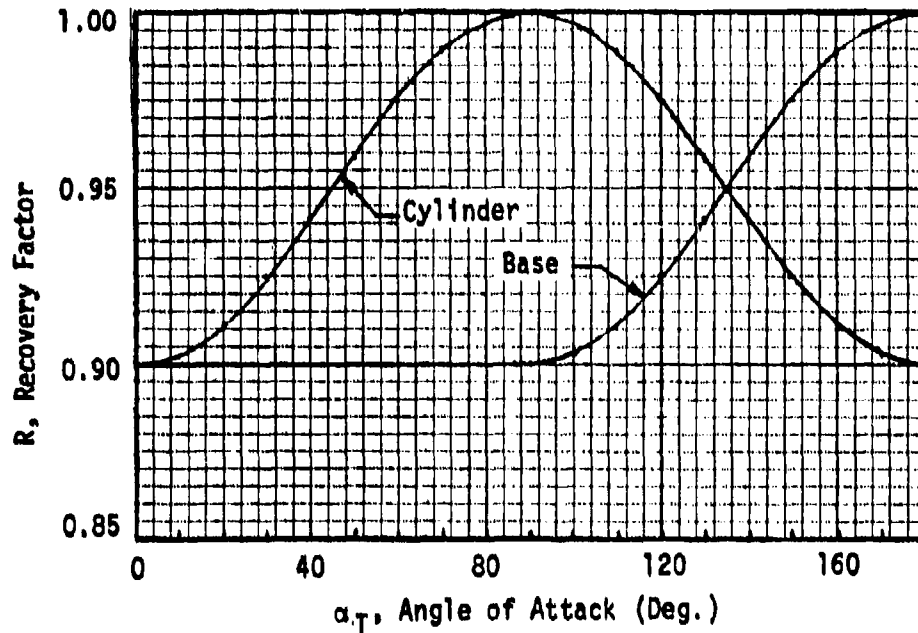


Fig. 7.13a Turbulent Recovery Factor

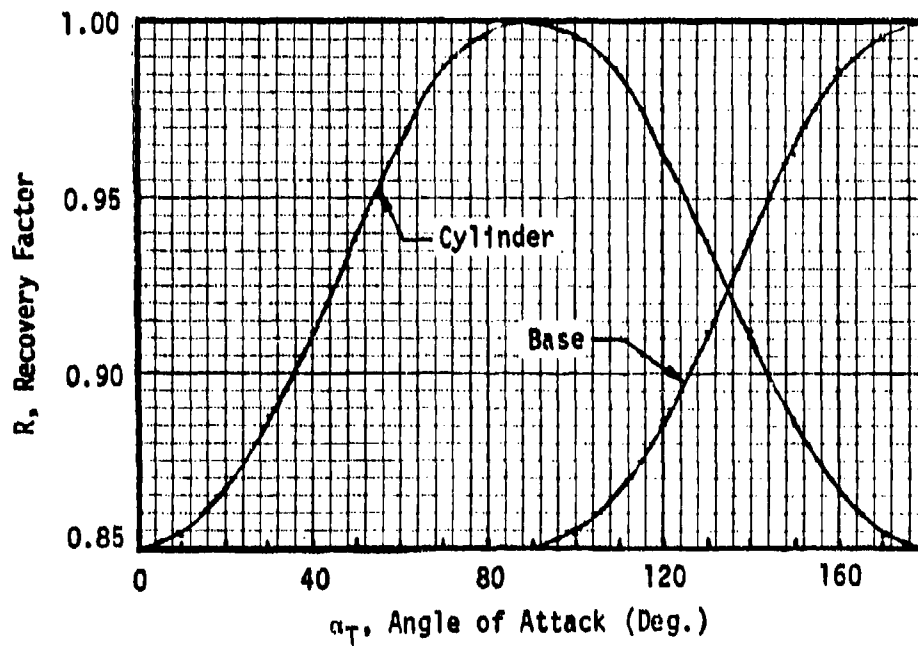


Fig. 7.13b Laminar Recovery Factor

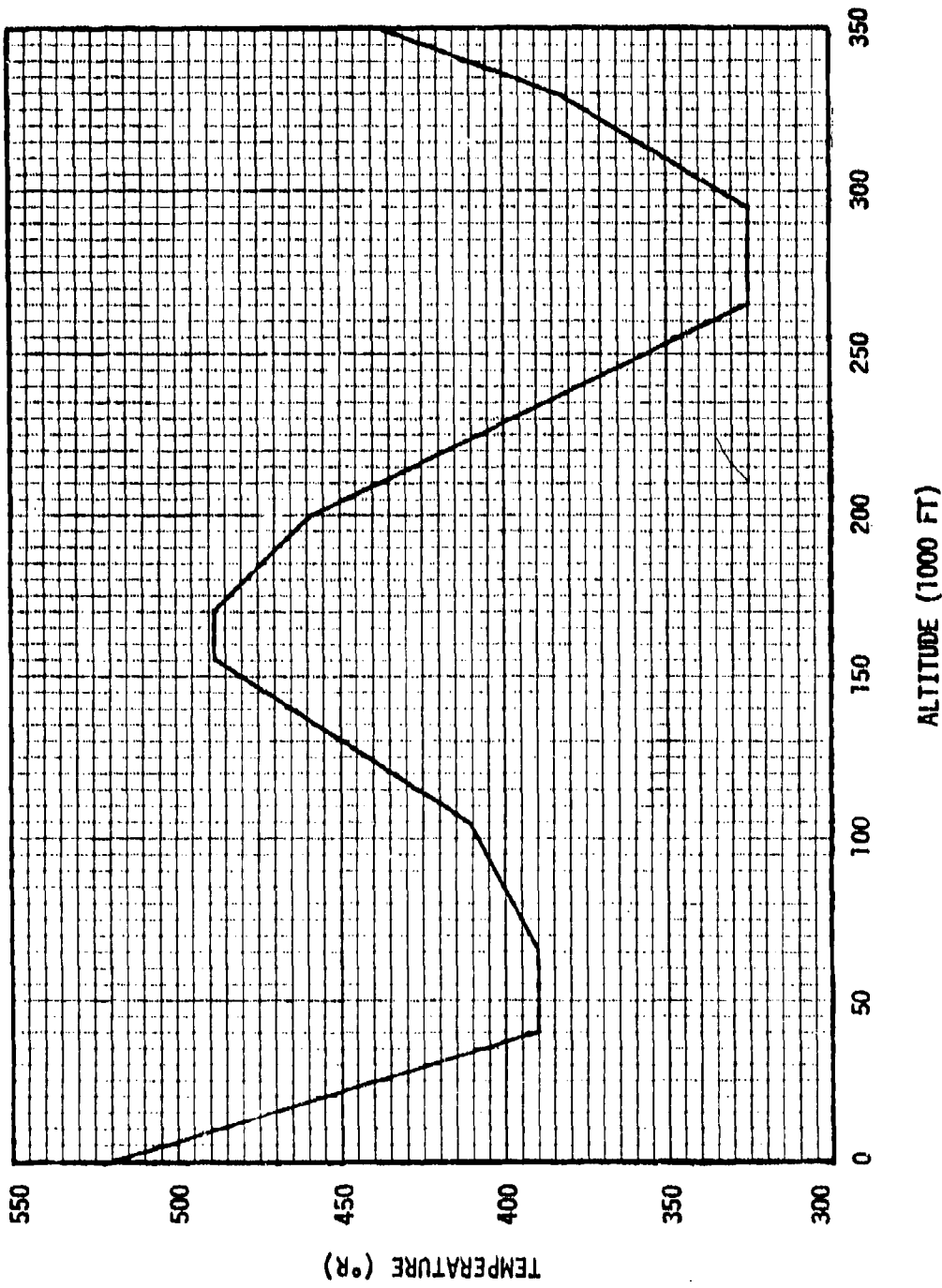


Fig. 7.14 1962 Standard Atmosphere Temperature

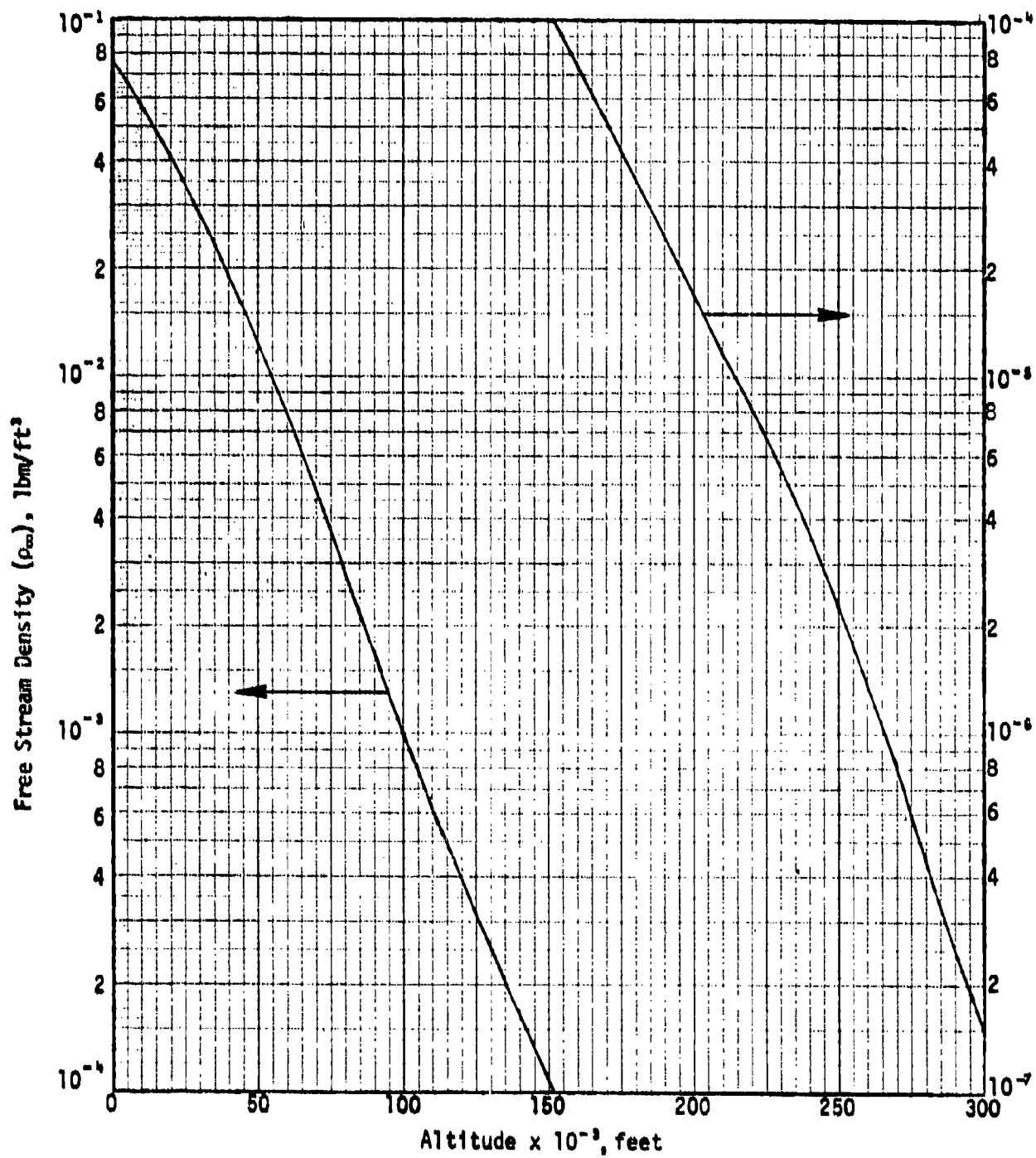


Fig. 7.15 Free Stream Density Versus Altitude

SECTION 8

REENTRY GUIDELINES

In general, reentry problems are coupled problems in that it is impossible to separate and analyze only the dynamics or heating aspect without considering the other. This is especially true when considering missions with high initial release altitudes. The higher the release altitude the more coupled the dynamics and heating becomes. This is the reason that certain restraints and guidelines must be followed when considering a change in the design of a reentry vehicle to solve a dynamics or heating problem.

8.1 Mission and Configuration Dependent Effects

There are a number of mission and configuration dependent effects associated with the dynamics and heating of a reentry payload. These include the effects of (1) C. G. location, (2) release attitude, (3) release altitude, (4) geometric configuration, (5) skin thickness, (6) weight, and (7) external protuberances. The mission usually dictates which effects can and cannot be controlled. This in turn leaves the engineer in many cases with very little flexibility in designing around a potential dynamics or heating problem. The initial release altitude, configuration type, weight, and certain external protuberances are generally felt to be mission dependent. The release attitude and the C. G. location of the vehicle are considered to be more flexible and not totally mission dependent. If the weight requirements of the mission are not too stringent, there could possibly be additional flexibility from the design standpoint in being able to increase the skin thickness of the vehicle in certain areas. In

many situations, a potential dynamics or heating problem can be relieved by modifying the C. G. location, controlling the vehicle release attitude, or varying the vehicle skin thickness provided certain guidelines are followed when doing so.

As previously discussed, a reentry problem is a coupled problem in that any change in the reentry dynamics of the vehicle can and usually does cause a corresponding change in the heating environment. The converse is also true. Because of this, the dynamics and heating problems should be solved simultaneously by an iterative type procedure. In order to demonstrate this procedure, consider the case in which a dynamics problem has been indicated by the results in the previous sections. A shift in the C. G. location is a possible solution to problems since each vehicle has a C. G. location which promotes a vehicle trim attitude at which maximum drag occurs. This results in a minimum descent velocity for the vehicle. If this velocity is acceptable for the recovery system being used then the heating environment for the vehicle should be determined based on the maximum drag attitude. If the resultant heating environment does not create any difficulties, then the total reentry problem has been solved by modifying the vehicle C. G. location. In the event that a severe heating environment results, then iterate until an optimum C. G. location is determined which will satisfactorily solve both problems. For a number of missions, particularly the higher altitude missions, there will be no optimum solution to the combined problem of reentry dynamics and heating. When a C. G. location is varied to solve a dynamics problem, a severe heating problem will be created. Conversely, proposed solutions to the heating problem will create severe dynamic problems. When this situation arises, serious consideration should be given to performing a complete theoretical analysis for the particular mission including a 6 DOF

trajectory analysis and a tumbling heating analysis. These results will be more accurate than the generalized results obtained from the handbook. If these results still indicate severe dynamic and heating problems, then another option should be considered such as inducing some effect by initiating a roll, yaw, or tumble motion to the vehicle. The induced effects will be discussed in the following section. If it is not possible to induce certain effects, or if it is generally felt that these effects will not satisfactorily solve the problem, then serious consideration should be given to changing the vehicle design or the method used in recovering the vehicle.

The surface temperature of a reentry payload can be reduced by increasing the skin thickness. If the skin thickness is increased in a uniform manner, or such that the vehicle C. G. location is not changed, this will cause an increase in the descent velocity of the vehicle due to the added weight. The attitude dynamics of the payload will remain essentially unchanged. In general, increases in the skin thickness of a payload such that the vehicle C. G. location remains unchanged will have the net effects of decreasing the surface temperature and increasing the maximum descent velocity of the vehicle. If the vehicle skin thickness is increased in a fashion such that it causes a shift in the C. G. location, this changes the vehicle attitude, descent velocity and also the heating environment. When an increase in the vehicle skin thickness is being considered, a complete analyses should be performed using the results presented in the handbook in order to determine the net effect of this increase from both a dynamics and heating standpoint.

The results presented in this handbook apply specifically to clean skin reentry vehicles (i.e. vehicles with no external protuberances). Even though this is the case, a certain amount of information concerning protuberances will be provided in this section since the presence of external protuberances on a

reentry vehicle can drastically alter its reentry characteristics. Protuberances are placed on payloads for many functions. Some are required in order for the payload to perform its mission as would be the case of external equipment used in data acquisition. Other types of protuberances are placed on the payload to induce some desired dynamic effect of the vehicle. These types of protuberances will be discussed in the following section. When external protuberances are attached to a payload, the aerodynamic characteristics of that payload can be significantly changed. The extent to which these characteristics are changed depends upon the size, weight, and location of these protuberances. In addition to changing the aerodynamic characteristics, they can also create additional heating problems because of the increased localized heating in areas on and around the protuberance. If external protuberances are required for a payload, a symmetrical circumferential distribution of these protuberances is desired if at all possible. If the protuberances are placed on the payload in an unsymmetric fashion, the vehicle will tend to reach an equilibrium position such that the protuberances are on the leeward side of the vehicle away from the flow. This is a disadvantage in many circumstances. For instance, if an initial roll rate was imposed on the payload at separation in order to relieve the heating load during reentry, an unsymmetrical protuberance distribution could possibly damp out the vehicle roll. This would cause one side of the vehicle to be subjected to maximum stagnation line heating instead of distributing the load which was the original aim in trying to induce vehicle roll. An unsymmetrical distribution of protuberances can also result in extremely complex vehicle dynamics. Various combinations of roll, yaw and tumble motions could result which would have significant effects on the heating environment and the eventual recovery of the vehicle. External protuberances can create a whole host of other problems in the recovery phases of a reentry payload.

In general, the effects of protuberances with heights above the external surface less than approximately 0.5% of the vehicle diameter can be neglected. The effects of external protuberances larger than this should be determined using a separate analysis for the particular configuration and mission.

8.2 Induced Effects for Reentry Payloads

Certain induced effects can be applied to control the dynamics of a vehicle in order to obtain a satisfactory solution to a heating or dynamics problem. Roll, yaw and tumble motions can be imparted to the payload at separation. These types of motions can also result from the addition of selected protuberances placed in specific locations on the vehicle. Roll, yaw and tumble motions and the methods used to initiate and sustain these types of motions are the subjects of this section.

If a payload can sustain a high roll rate during reentry, the heating load to the cone and cylinder sections of the vehicle types considered can be significantly reduced. This roll rate should be a minimum of 1/2 revolution per second as initial roll rate can be imparted to the payload at release. This roll rate should continue and the heat load reduced provided this motion is not damped out by external protuberances. Roll rates can also be initiated and sustained during reentry by attaching aerodynamic vanes or rotors to the external surface of the reentry payload. Reference 1 presents data taken in the University of Maryland wind tunnel which indicates that high roll rates can be obtained by attaching low aspect ratio fins or rib-type rotors to the external surface of the vehicle. No matter what method is selected to initiate and sustain a roll rate, rolling a reentry vehicle is an excellent way to reduce the heating load on the cylinder and cone sections of the configurations being

considered. The heating analyses presented in this handbook assumes that no roll motion has been applied to the vehicle. Accordingly, the heating load is calculated for the stagnation line. Since the precise roll orientation of the body is not known during reentry, the entire vehicle must be designed for this maximum condition. If, however, a roll rate can be initiated and sustained during reentry, the heating load may be reduced by considering the information provided in Fig. 5.3. This figure gives the roll averaged heat transfer coefficient ratioed to the stagnation line value. This ratio can be used as a multiplication factor times the stagnation line load computed from the previous sections. It should be noted that rolling the vehicle will not yield a heating relief to the base. It is more desirable to induce a rolling motion as opposed to a yaw or tumble motion in that this type of motion is easier to induce and sustain. It should be noted also that a roll motion will have no effect on the descent velocity of the vehicle and should be considered only to reduce the heating environment.

An excellent way to reduce the descent velocity of a reentry vehicle is by initiating a yawing or flat spinning autorotative motion of the vehicle. This motion will allow the vehicle to maintain a high angle of attack during reentry. This high angle of attack will create a maximum drag force which will significantly reduce the descent velocity and aid in the recovery of the vehicle. Recently, experiments have shown that flaps and fins strategically placed on cylinder and cone-cylinder type configurations allow a vehicle to sustain this type of motion during reentry. Even though these types of motions could greatly aid in the recovery of a payload, consideration must be given to the heating environment which results from the vehicle flying at these angles of attack during reentry. Consideration must also be given to the increase in

localized heating due to addition of flaps and fins to the external surface of the vehicle.

Another method of reducing the heating environment is to initiate a tumbling motion of the vehicle. If no vehicle roll is considered, a tumbling motion results in distributing the heating load to both sides of the vehicle instead of only heating one side which is the case for a constant trim entry with no roll. The descent velocity of a vehicle cannot, in general, be reduced significantly with tumble unless the trim attitude of the vehicle is such that minimum or near minimum drag force results. A tumble motion can create additional problems from the standpoint of parachute deployment for recovery. These possibilities must be considered before initiating a tumble motion to relieve a heating problem.

8.3 Material Selection

The handbook procedures and tables for computing a surface temperature in Section 7 are based on using aluminum as the vehicle skin. If another material is used or the heating load is sufficiently high to require a different material, an alternate procedure is required. In these events, the surface temperature may be estimated using the following equation.

$$T_s = \Delta T + 660 \quad 8.1$$

$$\Delta T = Q/\rho C \delta \quad 8.2$$

where

Q = heating load

C = specific heat

ρ = material density

δ = material thickness

Equations 8.1 and 8.2 are applicable only to homogeneous materials and should not be applied to any type of nonhomogeneous material such as a honeycomb

structure for instance. This relation also assumes that the material is sufficiently thin to respond instantaneously to the heating rate input and negligible surface reradiation.

TABLE 8.1 TYPICAL HEAT SINK MATERIALS				
Material	Melting Point $^{\circ}$ R	Density lbm/ft	Specific Heat Btu/lbm $^{\circ}$ R	(Tw) _{max} $^{\circ}$ R
Aluminum	1680.1	168.7	0.215	1020
St. Steel (301)	3030	494.2	0.108	2310
Magnesium	1662	108.8	0.25	1002
Copper	2441.1	559.	0.092	1781

Alternate heat sink materials are listed in Table 8.1. If the material thickness for any of those listed in Table 8.1 exceeds 0.50 inches, the temperature lag through the surface may be significant. This would violate the assumptions inherent in using Equations 8.1 and 8.2. A transient analysis is then required.

8.4 Initial Vehicle Surface Temperature

The maximum surface temperature of a reentry vehicle is dependent upon its initial surface temperature due to ascent. A heating analysis was performed on an Aries I payload (cone-cylinder configuration) for three typical ascent trajectories. These trajectories, obtained from Ref. 3, were typical of

future missions to be flown. They also represent extreme cases from an ascent velocity and heating standpoint. The ascent heating results are presented in Table 8.2 below.

Mission	Heating Region	$T_{1/8} (^{\circ}\text{R})$	$T_{1/4} (^{\circ}\text{R})$	$T_{1/2} (^{\circ}\text{R})$
Light	Cylinder	723.	637.	590.
Intermediate	Cylinder	710.	630.	586.
	Cone	883.	723.	635.
	Hemisphere	1002.	790.	665.
Heavy	Cylinder	696.	623.	583.

Table 8.2 Initial surface temperatures on an Aries I payload for three ascent trajectories

The three typical trajectories are designated as light, heavy, and intermediate missions. The light mission considers higher ascent velocities and heating while the heavy mission considers ascent velocities and heating which are significantly lower. The intermediate trajectory results are between these two extremes. The initial surface temperatures denoted at $T_{1/8}$, $T_{1/4}$, and $T_{1/2}$ are for wall thicknesses of 1/8, 1/4 and 1/2 inches respectively. It is apparent from Table 8.2 that the initial surface temperature is more highly dependent on the vehicle skin thickness than its ascent trajectory. From Table 8.2 it is also apparent that the intermediate results provide adequate nominal estimates of the initial surface temperatures attained during ascent for each section of the reentry vehicle.

The surface temperatures provided in Table 8.2 consider no cooling due to radiation losses from the vehicle surface that would occur when the vehicle

is outside the sensible atmosphere. Calculations were performed which indicate that these losses are negligible. The ascent analysis also considers no reduction in the initial surface temperature due to conduction heat transfer from the surface to various structural members and bulk heads located inside the vehicle. The reduction in the initial as well as the maximum surface temperature can be considerable dependent upon the size, placement and material characteristics of these structural members.

It is recommended that adjustments to the maximum surface temperature of the reentry vehicle be made based on the initial surface temperatures provided in Table 8.2. The results presented in Section 7 assumes a 660°R initial surface temperature. Determine the initial temperature from the intermediate results for the particular region and skin thickness. Compute the difference between this value and 660°R . If the initial temperature is less than 660°R , then subtract this difference from the maximum surface temperature determined from Section 7. Accordingly, if the initial temperature is greater than 660°R then add this difference to the maximum surface temperature.

SECTION 9

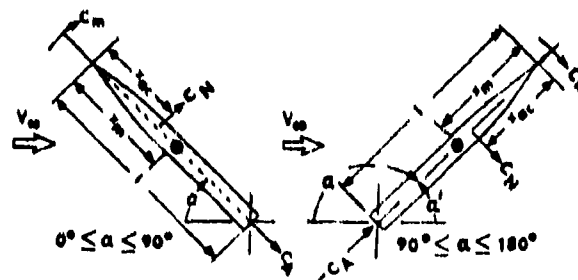
REFERENCES

1. Brunk, E. James, "The Dynamics and Aerodynamics of Self-Sustained Large Angle of Attack Spinning Motions," Alpha Research Report 63-1158-1, February 1963.
2. Shuford, W. David, "Users Guide for Program REENTR; Space Shuttle External Tank Reentry Simulation Program", Northrop Services Report M-250-1303, August 1974.
3. Personal Communications with Mr. Edward McKenna, Air Force Geophysics Lab, Hanscom Air Force Base, Boston, Mass.

APPENDIX A
METHODS AND PROCEDURES FOR
CALCULATING AERODYNAMIC COEFFICIENTS

The basic theory used in determining the aerodynamic characteristics used in this study can be attributed to the methods and procedures proposed by Allen (Ref. A.1). Jorgensen (Ref. A.2) used Allen's methods in computing the normal force, axial force, and pitching moment coefficients for certain missile type configurations flying at angles of attack between 0 and 180 degrees.

The equations for determining the normal-force, axial-force, and pitching moment coefficients are presented in Equations A. 1 - A. 5. Sketch (a) is presented in order to clarify the sign convention used.



Sketch (a)

$$C_N = \frac{A_b}{A} \sin 2 \alpha' \cos \frac{\alpha'}{2} + \eta C_{d_n} \frac{A_p}{A} \sin^2 \alpha'; \quad 0^\circ \leq \alpha \leq 180^\circ \quad A.1$$

$$C_A = C_{A_{\alpha=0^\circ}} \cos^2 \alpha'; \quad 0^\circ \leq \alpha \leq 90^\circ \quad A.2$$

$$C_A = C_{A_{\alpha=180^\circ}} \cos^2 \alpha'; \quad 90^\circ \leq \alpha \leq 180^\circ \quad A.3$$

$$C_m = \left[\frac{V - A_b (\ell - x_m)}{A d} \right] \sin 2 \alpha' \cos \frac{\alpha'}{2} + \eta C_{d_n} \frac{A_p}{A} \left(\frac{x_m - x_c}{d} \right) \sin^2 \alpha'; \quad 0^\circ \leq \alpha \leq 90^\circ \quad A.4$$

and

$$C_m = -\left(\frac{V-A_b x_m}{Ad}\right) \sin 2\alpha' \cos \frac{\alpha'}{2} + \eta C_{d_n} \frac{A_p}{A} \left(\frac{x_m - x_c}{d}\right) \sin \alpha';$$

90° ≤ α ≤ 180° A.5

where

$$\alpha' = \alpha \text{ for } 0^\circ \leq \alpha \leq 90^\circ \text{ and } \alpha' = 180^\circ - \alpha \text{ for } 90^\circ \leq \alpha \leq 180^\circ$$

The aerodynamic force center is given by

$$x_{ac} = \left(\frac{x_m}{d} - \frac{C_m}{C_N}\right) d \quad \text{A.6}$$

The first terms in Equations A.1, A.4 and A.5 come from slender-body potential theory. The second terms represent the viscous crossflow or crossflow attributed to flow separation.

Crossflow drag coefficient - In the expressions for C_N and C_m (equations A.1, A.4 and A.5) C_{d_n} is the crossflow drag coefficient for a section of an "infinite" length cylinder placed normal to an airstream. It is a function of both the Mach number and Reynolds number components that are normal to the cylinder longitudinal axis, and hence, for a body at angle of attack it is a function of

$$M_N = M_\infty \sin \alpha \quad \text{A.7}$$

and

$$Re_N = Re \sin \alpha \quad \text{A.8}$$

M_N is commonly called the crossflow Mach number and Re_N the crossflow Reynolds number.

For circular cylinders, plots have been prepared for the variation of C_{d_n} with M_N and Re_N . Figure A.1 gives the variation of C_{d_n} with M_N over the Mach number range of 7 or 8 down to almost 0.

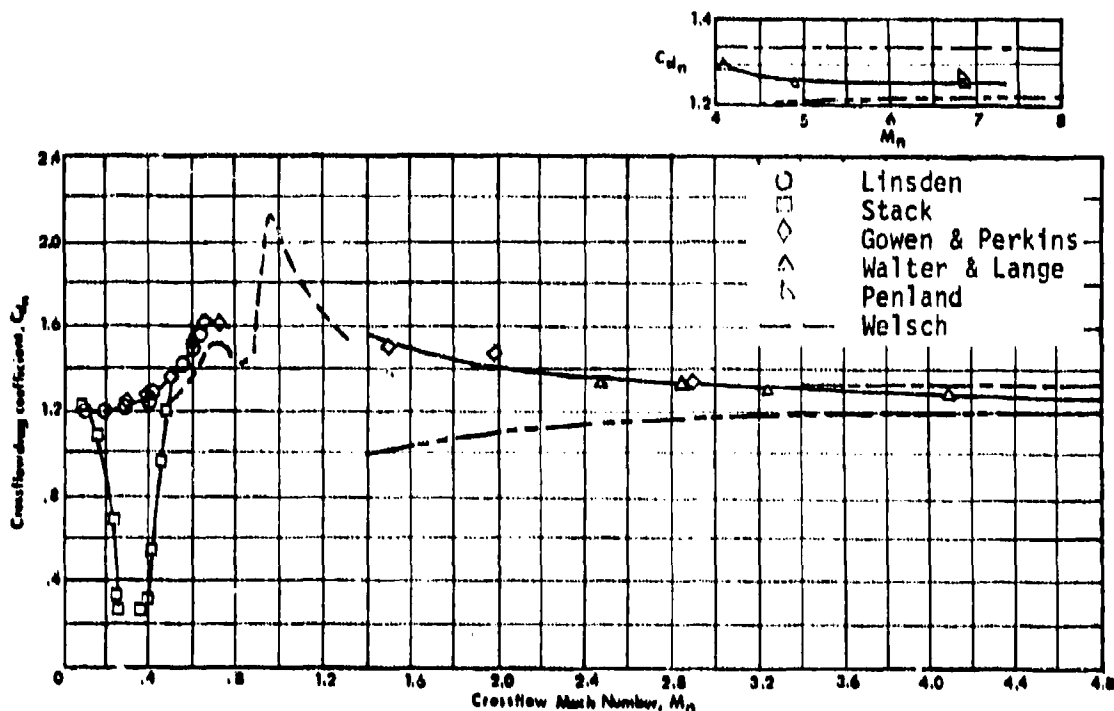


Fig. A.1 Variation of crossflow drag coefficient with crossflow Mach number for circular cylinders. (Ref. A.2)

Crossflow drag proportionality factor - In Equations A.1, A.4 and A.5 η is the crossflow drag proportionality factor, that is, the ratio of the crossflow drag coefficients for a finite length cylinder to that for an infinite length cylinder. Cylinder drag coefficients from which values of η can be determined have been measured only at low subsonic Mach numbers. In Fig. A.2, values of η are plotted as a function of length-to-diameter ratio. For reference, η 's for flat plates are also presented (plotted as a function of plate length-to-width ratio). In spite of a dearth of η data throughout the subsonic Mach number regime, the results given in Fig. A.2 have been

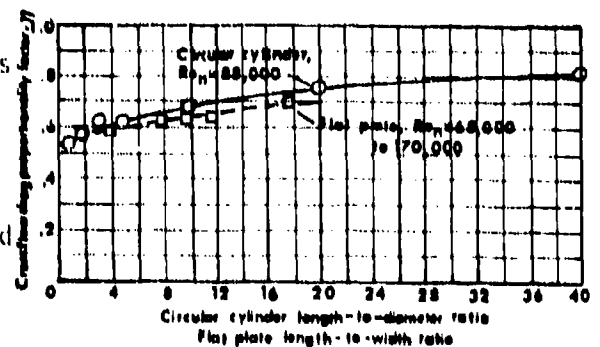


Fig. A.2 Ratio of crossflow drag coefficient for a finite length cylinder (or flat plate) to that for an infinite length cylinder (or flat plate), from reference A.2.

used to successfully predict, for most engineering purposes, the aerodynamic characteristics of bodies of revolution at subsonic Mach numbers. For bodies at supersonic and hypersonic Mach numbers, η probably can be assumed to be unity, an assumption indicated as being essentially correct from past investigations.

Axial-force coefficients at angles of attack of 0° and 180° - To predict the variation of C_A with angle of attack by Equations A.2 and A.3, either computed or measured values of axial-force coefficient at $\alpha = 0^\circ$ or 180° can be expressed by

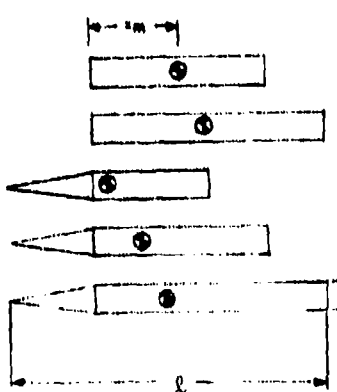
$$C_A = C_{A_W} + C_{A_{SF}} + C_{A_B} \quad A.9$$

where C_{A_W} represents the wave or pressure contribution from the nose or forward-facing base; $C_{A_{SF}}$ is the skin-friction contribution; and C_{A_B} is the base-pressure contribution. There are theoretical expressions presented in Ref. A.2 that can be used to determine C_{A_W} , $C_{A_{SF}}$, C_{A_B} . For this study however, the experimental data presented in Figs. A.3 and A.4 were used to determine the axial-force coefficients at 0° to 180° . These values were used in place of Equations A.2 and A.3 because of the discrepancy between the theoretical predictions and the experimental measurements.

For the six-degree-of-freedom trajectory analysis, the aerodynamic coefficients were computed for supersonic Mach numbers only. Since the variation in coefficients with Mach number in this range was very slight, a constant coefficient assumption allowed for many more cases to be considered with the trajectory program. This was due to the decrease in computer run time because of not having to consider Mach number dependent coefficients. This approach was entirely valid for the heating analysis since any significant heating would occur at the higher

Mach numbers. The approach was also valid for the vehicle dynamics at supersonic Mach numbers. When the crossflow Mach number (M_N) becomes less than one, the approach starts becoming less valid since the aerodynamic coefficients will vary considerably in subsonic flow.

In Figs. A.3 and A.4, the computed values of C_N , C_A , and C_M as a function of angle of attack α are compared with the experimental results for the two fineness ratio cylinder configurations and the three fineness ratio cone-cylinder configurations shown below in Table A.1.



Body No.	l	x_m	$\frac{A_D}{d^2}$	$\frac{V}{d^3}$	$\frac{x_c}{d}$	$\frac{A_s}{d^2}$	Nose Shape
1	6	3	6.000	4.710	3.000	19.63	Flat
2	8	4	8.000	6.280	4.000	25.92	Flat
3	7	3.5	5.500	3.925	4.183	17.31	Cone
4	9	4.5	7.500	5.495	5.200	23.62	Cone
5	11	5.5	9.500	7.065	6.211	29.91	Cone

Table A.1

Bodies For Which The Aerodynamic Characteristics Were Computed

Generally, there is good agreement between the computed and measured results, especially for the variation of C_N and C_M with α . The agreement between the values of C_A were not nearly as good, however. Further comments on this disparity is made in Ref. A.2.

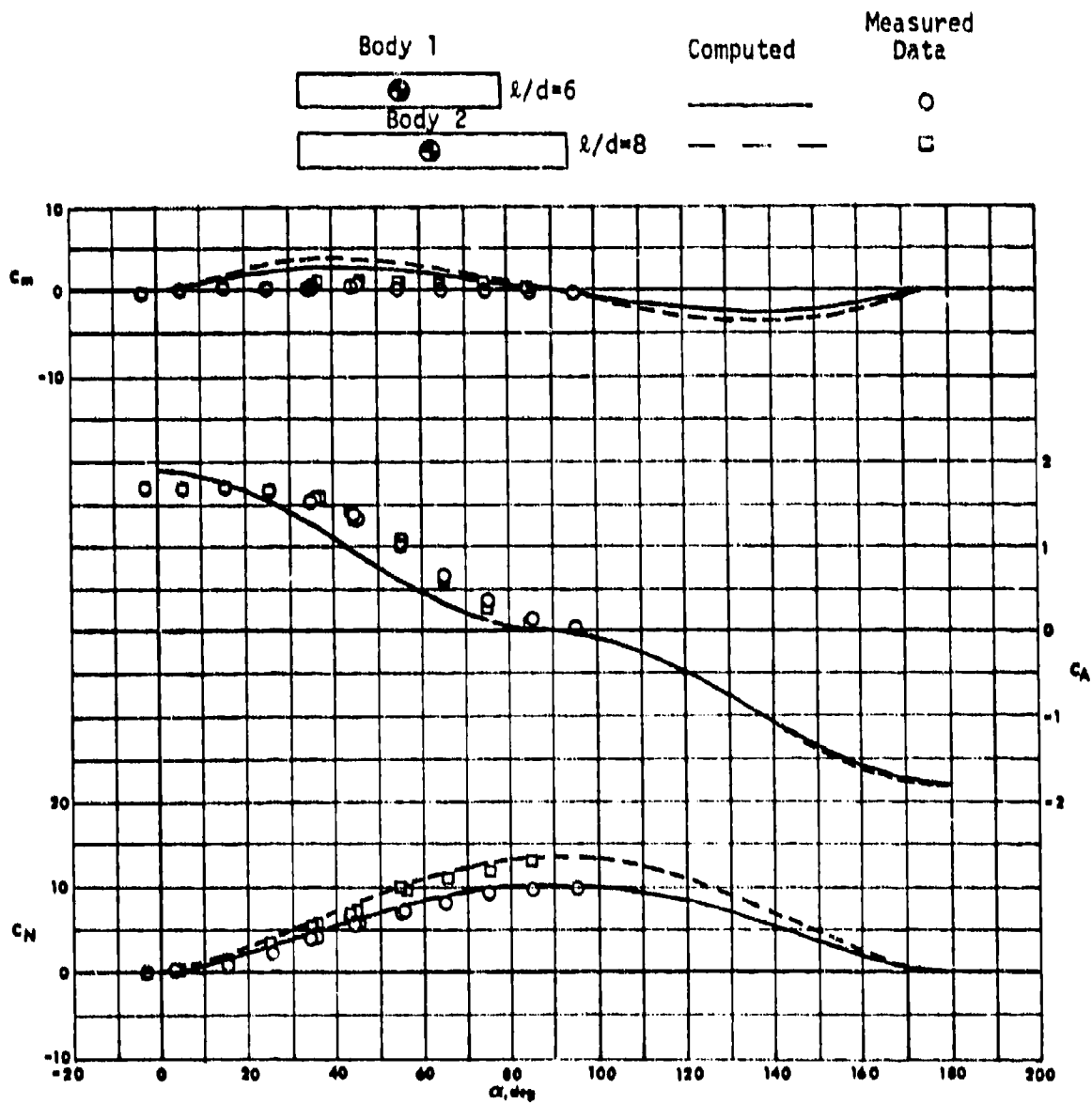


Fig. A.3 Comparison of computed with measured aerodynamic characteristics for cylindrical bodies with completely blunt noses; $M_\infty = 2.86$.

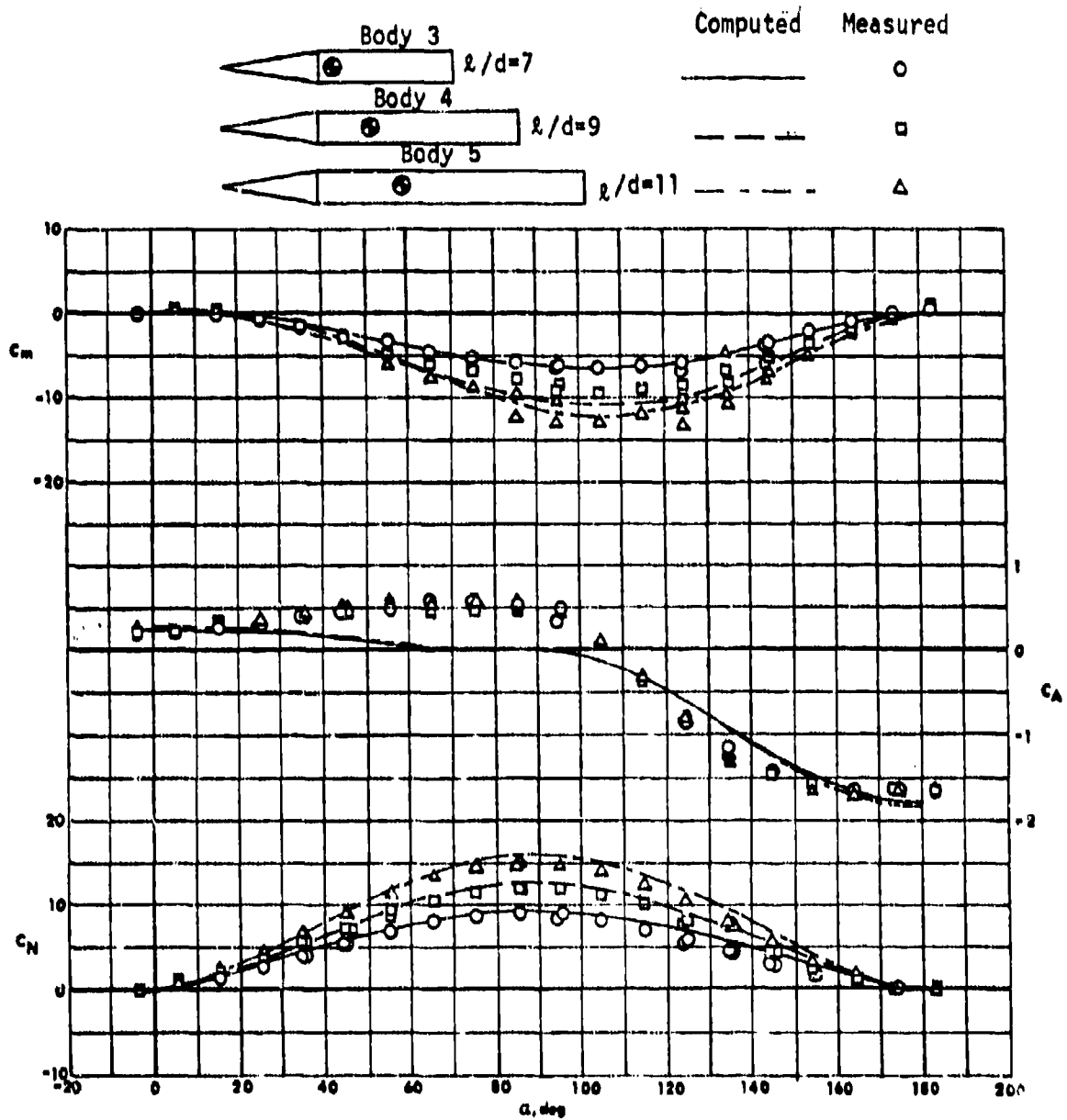


Fig. A.4 Comparison of computed with measured aerodynamic characteristics for cylindrical bodies with conical noses of fineness ratio 3: $M_\infty = 2.86$.

NOMENCLATURE

A	cross-sectional (reference) area of cylindrical portion of body
A_b	body base area (at $x = 0$)
A_p	planform area
A_s	surface wetted area
C_A	axial-force coefficient, $\frac{F_a}{q_\infty A}$
C_a	axial-force coefficient, $\frac{F_a}{q_a A}$
C_{d_n}	crossflow drag coefficient of cylinder section, $\frac{F_n}{q_n (\Delta x_{cy}) d_{cy}}$
C_{m_i}	pitching-moment coefficient about station at x_m from nose, <u>pitching moment</u> $\frac{\quad}{q_\infty A d}$
C_N	normal-force coefficient, $\frac{F_N}{q_\infty A}$
C_p	pressure coefficient, $\frac{p - p_\infty}{q_\infty}$
d	body cross-section diameter
x	body length
x_N	nose length
x_A	aftersection length
M_N	Mach number component normal to body axis, $M_\infty \sin \alpha$
M_∞	free-stream Mach number
p	pressure
p_∞	free-stream static pressure
q_a	dynamic pressure component in body axis direction, $q_\infty \cos^2 \alpha$
q_N	dynamic pressure component normal to body axis, $q_\infty \sin^2 \alpha$
q_∞	free-stream dynamic pressure, $1/2 \rho V_\infty^2$
r_b	nose or body cross-section radius at base
Re	free-stream Reynolds number based on body cross-section diameter, $\frac{\rho V_\infty d}{\mu}$
Re_n	Reynolds number component normal to body axis, $Re \sin \alpha$
V	body volume
V_∞	free-stream velocity

x	axial distance from body nose
x_{ac}	distance from nose to aerodynamic force center
x_c	distance from nose to centroid of body planform area
x_m	distance from nose to pitching-moment reference center
α	angle of attack
η	crossflow drag proportionality factor

SUBSCRIPTS

B	base
W	wave or pressure

REFERENCES

- A.1 Allen, H. Julian, "Estimation of the Forces and Moments Acting on Inclined Bodies of Revolutions at High Fineness Ratio," NACA RM A9126, 1949.
- A.2 Jorgensen, H. Leland, "Prediction of Static Aerodynamic Characteristics for Space-Shuttle-Like and Other Bodies at Angles of Attack from 0° to 180° ," NASA TN D-6996, 1973.

APPENDIX B
6 DOF TRAJECTORY PROGRAM DESCRIPTION
(Program REENTR)

Program REENTR is a versatile six-degree-of-freedom digital simulation providing a means of investigating the reentry characteristics of uncontrolled aerodynamic bodies. The program was first developed for and used in an in depth study of the Space Shuttle External Tank for NASA. It is highly versatile in that it employs several major program options including:

- a. Choice of computers with minimal changes
- b. Machine plot option
- c. Choice of spherical, oblate, or Fischer ellipsoid earth models
- d. Print format option
- e. Random variable selection

In order to streamline the program, increase its speed and still provide the needed accuracy, the program was simplified by eliminating the option on the earth models and choosing a spherical earth, and by locking in the print and plot option, to reduce computer time in checking each option for each loop.

In this Appendix a brief theoretical overview of the program will be presented followed by a brief description of the 3 degrees-of-freedom program which was derived from it.

B.1 Program Organization

Program REENTR is organized into three basic parts: (1) initialization of parameter (2) Dynamic loop computation, and (3) loop and program derivation. Each part will be presented in some detail in the following sections.

B.2 Initialization

The program is initialized by first storing all necessary data. This includes atmosphere model, vehicular aerodynamic coefficients, and initial

position state vector. The atmosphere and aerodynamic coefficients are normally input in tabular form and are used by table readouts as required throughout the simulation. Position data is input for each case and either re-input with changes or re-verified for each subsequent case.

The initialization portion is geared to determine the state of the vehicle at $t = 0$ in altitude, direction, and velocity. This is determined from the following data inputs:

Altitude (h_0)
 Latitude (ψ_0)
 Longitude (λ_0)
 Relative Velocity Magnitude $|\overline{V}_{rel_0}|$
 Relative Heading (σ_{rel_0})
 Relative Flight Path Angle (δ_{rel_0})
 Bank Angle (ϕ_{BK_0})
 Aerodynamic Roll Angle (ϕ_{α_0})
 Total Angle of Attack (α_{T_0})

Since a spherical earth is assumed, the initial position vector \overline{R}_0 is determined as follows:

$$|\overline{R}_0| = R + h_0$$

where R is the radius of the earth, then

$$\overline{R}_0^I = \begin{pmatrix} |\overline{R}_0| \cos \psi_0 \cos \lambda_0 \\ |\overline{R}_0| \cos \psi_0 \sin \lambda_0 \\ |\overline{R}_0| \sin \psi_0 \end{pmatrix} = \begin{pmatrix} R_{X_0}^I \\ R_{Y_0}^I \\ R_{Z_0}^I \end{pmatrix} \quad (\text{See Fig. B.1})$$

The earth centered inertial (I) frame is thus established and a translational vector to the center-of-gravity of the body determined.

A body centered reference frame is determined as a reference point for the velocity vector. This reference frame is termed the geodetic (D) frame and is defined as a reference frame with a north pointing horizontal (X) axis with respect to the inertial (I) frame and having its Z-axis pointing toward the center of the earth. This frame is always centered on the body and is always maintained horizontal to the surface of the earth and oriented as defined.

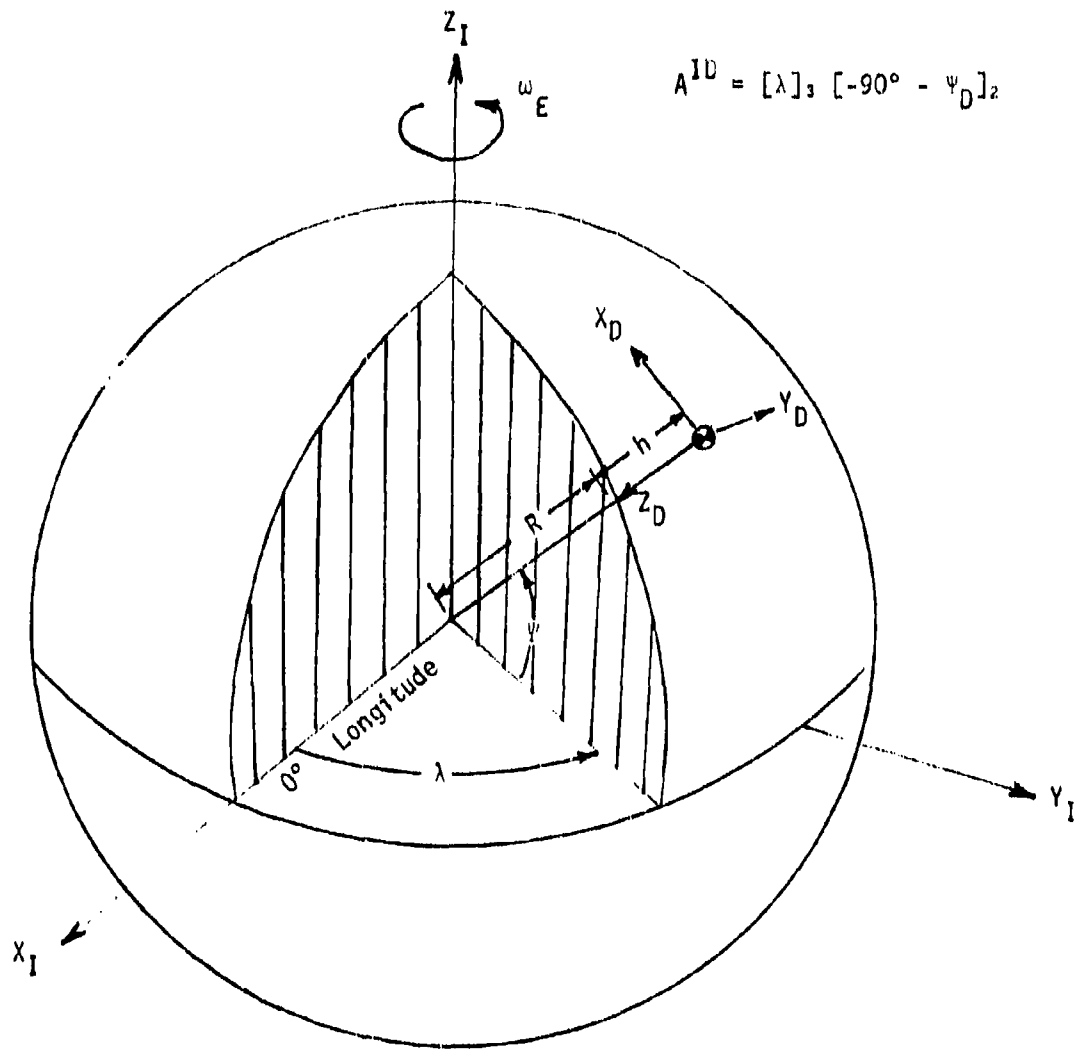


Fig. B.1 Inertial and Geodetic Reference Frames

This is shown in Fig. B. 1.

The direction cosine matrix which transforms points in the D frame to the I frame is determined from

$$A_0^{ID} = [\lambda_0]_3, [-90^\circ - \psi_0]_2$$

The relative velocity vector (R) frame is determined from $|\vec{V}_{rel_0}|$, σ_{rel_0} , and γ_{rel_0} . The vector is determined by:

$$\vec{V}_{rel_0} = \left\{ \begin{array}{l} |\vec{V}_{rel_0}| \cos \gamma_{rel_0} \cos \sigma_{rel_0} \\ |\vec{V}_{rel_0}| \cos \gamma_{rel_0} \sin \sigma_{rel_0} \\ -|\vec{V}_{rel_0}| \sin \gamma_{rel_0} \end{array} \right\} \quad \text{See Fig. B-2}$$

In order to transform this to inertial velocity, the rotation of the earth must be accounted for. Therefore,

$$\vec{V}_0^D = \vec{V}_{rel_0} + \omega_E \begin{pmatrix} -R_{y_0}^I \\ R_{x_0}^I \\ 0 \end{pmatrix}$$

Where ω_E is the rotational velocity of the earth, the total inertial velocity vector is then:

$$V_0^I = A_0^{ID} V_0^D$$

The orientation of the body is determined by the given body angles with respect to the velocity vector. A body (B) to relative velocity vector (R) frame direction cosine matrix is determined from:

$$A_0^{RB} = [\phi_{BK}]_3, [\alpha_{T_0}]_1, [\phi_{\alpha_0}]_1 \quad (\text{See Fig. B.3})$$

The R frame can be related to the D frame by:

$$A_0^{DR} = [\sigma_{rel_0}]_3, [\gamma_{rel_0}]_2$$

The body to inertial transformation then becomes:

$$A_0^{IB} = A_0^{ID} A_0^{DR} A_0^{RB}$$

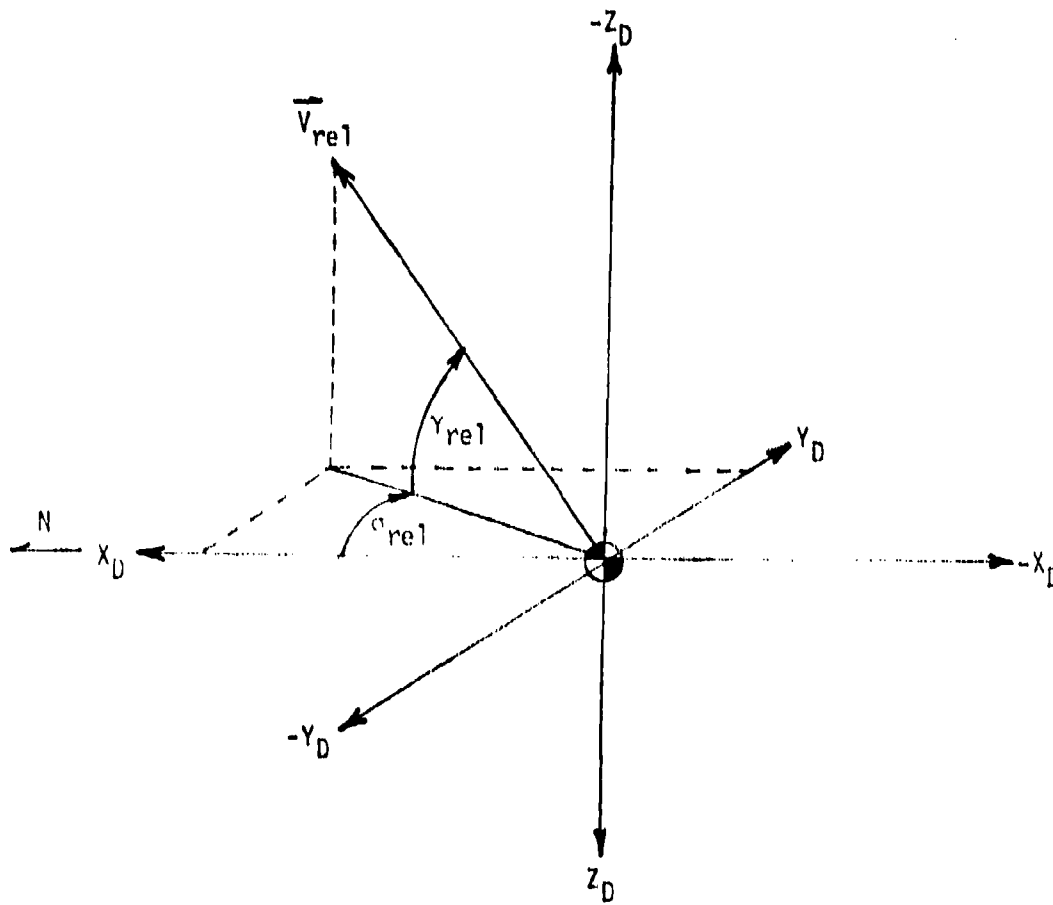


Fig. B.2 Relative Velocity in the Geodetic Frame

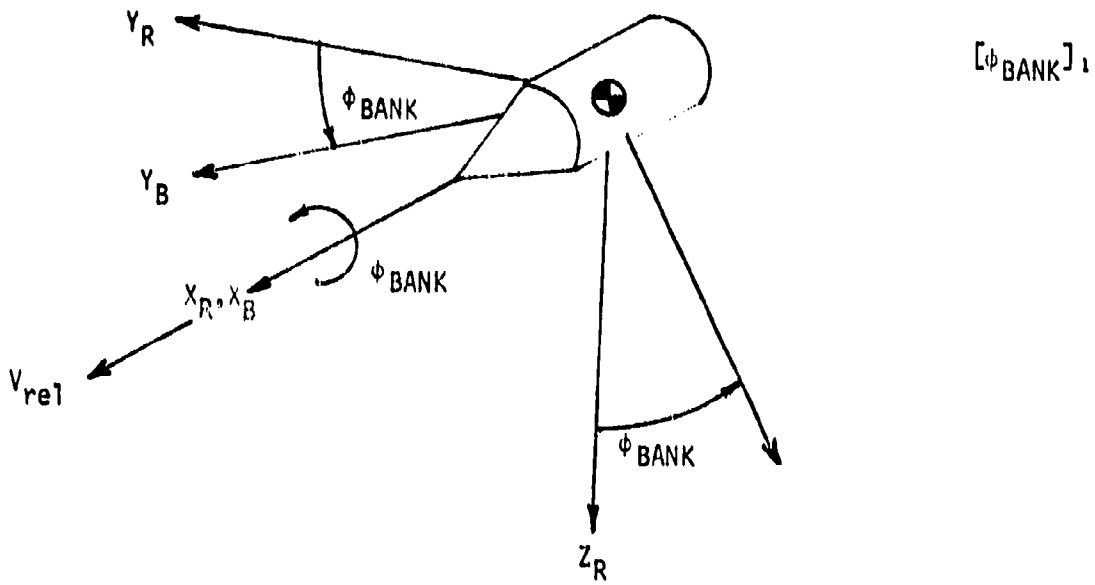


Fig. B.3a Body Orientation 1

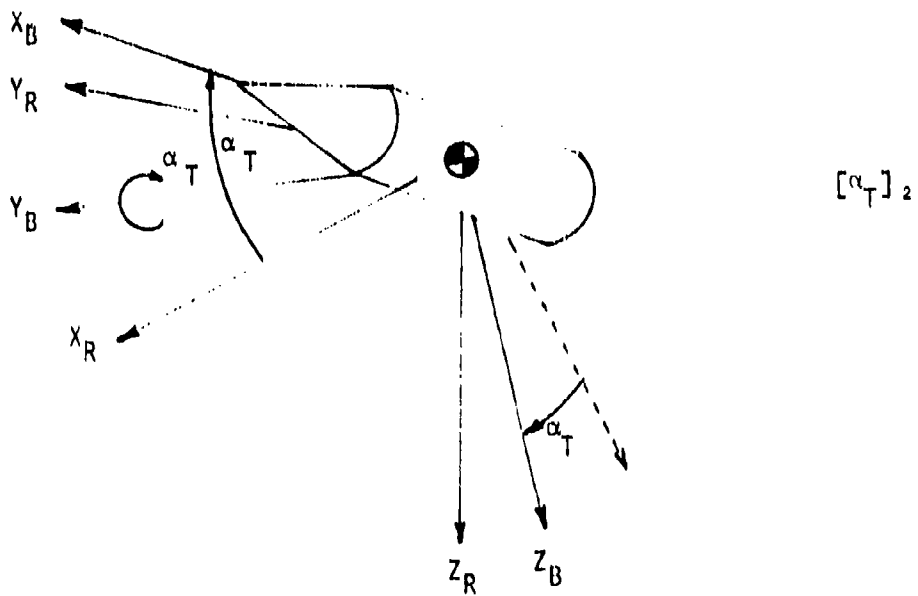


Fig. B.3b Body Orientation 2

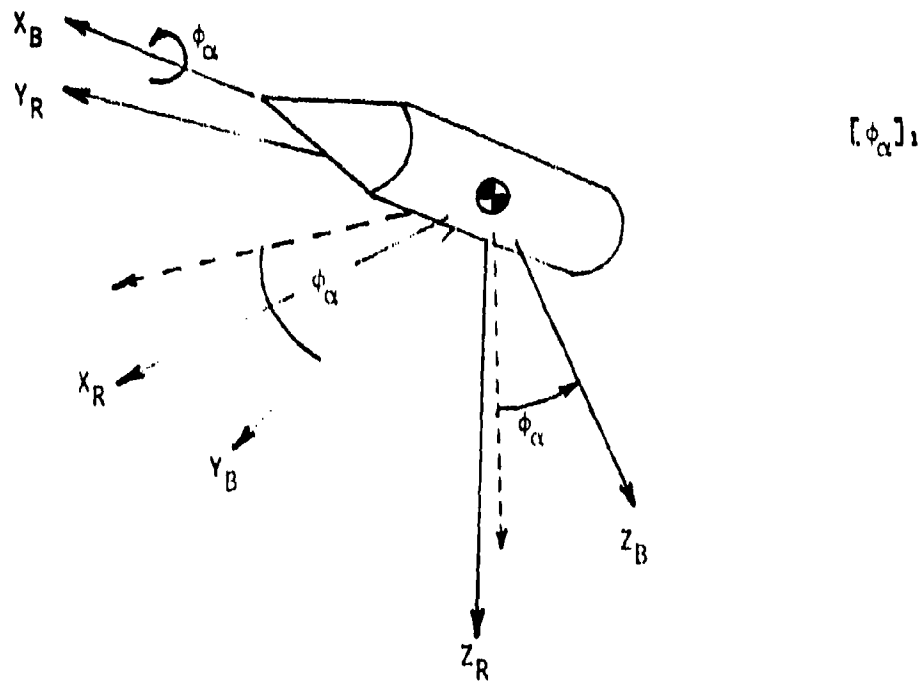


Fig. B.3c Body Orientation 3

With the body orientation determined, the only other data required is the mass characteristics of the reentry body including:

Mass

Center-of-gravity location with respect to a known body point

Moment-reference point (for aerodynamics) from same body point

Body dimensions and body rates

The A_0^{IB} matrix is converted to quaternion (to be discussed in more detail later) and the dynamic moment arm determined:

$$\vec{r}_{mrp}^B = \begin{pmatrix} (x_{mrp} - x_{cg}) / D_{ref} \\ (y_{mrp} - y_{cg}) / D_{ref} \\ (z_{mrp} - z_{cg}) / D_{ref} \end{pmatrix}$$

The dynamic loop can now commence.

B.3 Dynamic Loop Computations

As the body reenters the atmosphere, gravitation, atmosphere, and motion effects must all be updated on a frequent basis. The dynamic loop updates by determining the derivatives of the primary parameters and then integrating to determine the updating increment. The integration method used is a four pass Runge Kutler method. The critical derivatives are:

Rotational acceleration	$\dot{\omega}$
Translational acceleration	\dot{V}^I
Position change	\dot{R}^I
Quaternions	\dot{Q}

In the first pass through the loop on each case, all of the initial parameters are reverified. In order to simplify and compact the simulation, a set of

parameters known as Quaternion, from Hamiltonian calculus, are used. The quaternions are used to represent the main direction cosine matrix A^{IB} and are defined from the initial parameters of that matrix. The calculation of these parameters is tedious and will not be shown here. Basically they are defined by:

$$Q_1 = \alpha \sin (\phi/2)$$

$$Q_2 = \beta \sin (\phi/2)$$

$$Q_3 = \gamma \sin (\phi/2)$$

$$Q_4 = \cos (\phi/2)$$

where $\alpha, \beta,$ and γ are eigenaxis direction cosines and ϕ is the eigenaxis rotation angle. Integration and recomputation of components of the A^{IB} matrix allows continual update of vehicle body orientation and rotation.

Using the above, the program updates on a frequent basis updating position, velocity, and rates of each body in contact. The forces on the body are determined based on atmospheric characteristics, aerodynamic characteristics, etc. and force coefficients and moment coefficient determined. The final body torques and forces are:

$$\vec{T}_A^B = \bar{q} S_{ref} D_{ref} \vec{C}_{\text{mom}_T}$$

where \vec{C}_{mom_T} is the torques on the body based on all forces supplied.

$$\vec{F}_A^B = \bar{q} S_{ref} \vec{C}_{xyz}$$

where \vec{C}_{xyz} is the forces on the body. The derivatives then are

$$\dot{\vec{\omega}} = I^{-1} (\vec{T}_A^B - \vec{\omega} \times I \vec{\omega})$$

I is the inertia matrix for the body

$\vec{\omega}$ is the rotational rate of the body

$$\dot{\vec{Q}} = 1/2 \begin{bmatrix} Q_4 & -Q_3 & Q_2 \\ Q_3 & Q_4 & Q_1 \\ -Q_2 & Q_1 & Q_4 \\ -Q_1 & -Q_2 & -Q_3 \end{bmatrix} \vec{1}_3$$

$$\vec{V}^I = \frac{1}{m} \vec{F}_A^I + \vec{g}^I$$

where

m is vehicle mass

\vec{g}^I is the gravitational vector

All derivatives are converted to inertial frame for integration.

B.4 Loop and Program Termination

At the completion of each integration step, all parameters are updated and the program continues until stopped. The computer program checks to determine print and plot intervals and stores all required data or prints it. At program termination, the final data is printed and plotted as required.

B.5 Three Degree-Of-Freedom Program

A 3 degree-of-freedom program was also developed for the Shuttle studies and used in this study. This program is an adaptation of the six degree-of-freedom program employing a point mass lift/drag model based on vehicle aerodynamics.

The primary advantage to the use of this model is its high speed (Approx. 1 second per 100 seconds of trajectory) thus allowing the run of large numbers of similar cases, perhaps varying one parameter over a large range. Where the reentry bodies trim, this becomes a high speed way of studying the changes in reentry characteristics with eight variations in atmospheric conditions, etc.

B.5 CONCLUSION

The two programs described in this Appendix were modified slightly to provide data useful in computing aerodynamic heating data. Direct type output of many trajectories could be fed directly into heating calculation programs to determine heating characteristics. Program REENTR and its derivatives are currently available in REMTECH's files for future studies of this type.

MATHEMATICAL NOTATION

NOTATIONDEFINITION \vec{x}^I

Vector resolved into I-frame coordinate axes. Axes systems used are:

- I - Earth centered inertial
- D - Local normal, north pointing
- G - Geocentric local normal, north pointing
- R - Relative velocity vector, local horizontal
- B - Body fixed

 A^{xy}

Direction cosine matrix which transforms vectors from the y-frame to the x-frame

 x_0

Initial value of X

 \dot{x}

dx/dt

$$[O]_1 = \begin{bmatrix} 1 & 0 & 0 \\ 0 & \cos\theta & -\sin\theta \\ 0 & \sin\theta & \cos\theta \end{bmatrix} \quad \text{Direction cosine matrix for x-axis rotation through angle } \theta$$

$$[O]_2 = \begin{bmatrix} \cos\theta & 0 & \sin\theta \\ 0 & 1 & 0 \\ -\sin\theta & 0 & \cos\theta \end{bmatrix} \quad \text{Direction cosine matrix for y-axis rotation through angle } \theta$$

$$[O]_3 = \begin{bmatrix} \cos\theta & -\sin\theta & 0 \\ \sin\theta & \cos\theta & 0 \\ 0 & 0 & 1 \end{bmatrix} \quad \text{Direction cosine matrix for z-axis rotation through angle } \theta$$

NOTE: All direction cosine matrices used herein transform from the new coordinate frame to the original coordinate frame.

LIST OF SYMBOLS

<u>SYMBOL</u>	<u>COMPUTER SYMBOL</u>	<u>DEFINITION</u>
C_A	CA	Aerodynamic axial force coefficient
C_m	CM	Aerodynamic pitching moment coefficient
C_N	CN	Aerodynamic normal force coefficient
$C_{\dot{\alpha}p}$	CLP	Rolling moment damping coefficient
$C_{m\dot{q}}$	CMQ	Pitching moment damping coefficient
C_{nr}	CNR	Yawing moment damping coefficient
$\vec{C}_{\dot{\alpha}mnT}$	CLMNT	Total aerodynamic moment coefficient vector with respect to c.g.
$\vec{C}_{\dot{\alpha}mnT}$	CPLMN	Total aerodynamic moment coefficient vector less c.g. offset effect
\vec{C}_{xyz}	CXYZ	Total aerodynamic force coefficient vector
D_{ref}	DREF	Vehicle diameter
\vec{F}_A^B	FAB	Aerodynamic force vector
$ \frac{A}{g} $	GMAG	Magnitude of acceleration-of-gravity
\vec{g}	G	Acceleration-of-gravity vector
GM	GM	Earth gravitational constant
h	H	Altitude
I	IXYZ	Vehicle moment of inertia
I^{-1}	IXYZI	Inverse moment of inertia
L_{ref}	LRLF	Vehicle length
m	GMASS	Vehicle mass
Mach	MACH	Mach number (V_{rel}/V_s)
p	PQR(1)	Roll rate ($=\dot{\alpha}_x$)
q	PQR(2)	Pitch rate ($=\dot{\alpha}_y$)

<u>SYMBOL</u>	<u>COMPUTER SYMBOL</u>	<u>DEFINITION</u>
r	PQR(3)	Yaw rate ($=\omega_z$)
q	QBAR	Dynamic pressure
Q_1, Q_2, Q_3, Q_4	Q(1), Q(2), Q(3), Q(4)	Quaternion parameters
R	R	Earth's radius
R_s	RS	Kennedy Space Center earth radius
S_{ref}	SREF	Vehicle reference area
\vec{T}_B	TAB	Aerodynamic torque vector
$ \vec{v}_{rel} $	VRMAG	Magnitude of relative velocity vector
\vec{v}_{rel}^x	VRELX	Relative velocity vector in X-frame
V_s	VS	Speed of sound
\vec{v}_w^x	VWX	Wind velocity vector in x-frame
x_{cg}, y_{cg}, z_{cg}	XCG, YCG, ZCG	Reference location of c.g.
$x_{mrp}, y_{mrp}, z_{mrp}$	XMRP, YMRP, ZMRP	Moment reference point location with respect to c.g.
α_T	ALPHT	Total angle-of-attack
γ_{rel}	GAMR	Relative flight path angle
λ	LAMDA	Longitude
ρ	RHO	Atmospheric density
σ_{rel}	SIGR	Relative heading
ϕ_α	PHIA	Aerodynamic roll angle
ϕ_{BK}	PHIBK	Bank angle
ψ_D	PSID	Geodetic latitude
ω_E	OMGE	Earth rotational velocity
$\vec{\omega}$	PQR(I)	Vehicle rotational rates

APPENDIX C
REENTRY HEATING METHODOLOGY

The aerodynamic heating methods used in this study were those contained in the BENTRY computer code (Ref. C.1) and modifications for this specific class of problems. A discussion and definition of the aerodynamic heating methods used for each part of the payload geometry is given in this appendix. The geometries considered were flat face right circular cylinders and cone-cylinder-flat face bodies. The heating methods for each geometry is described.

Free stream properties were obtained for each trajectory point using the 1962 standard atmosphere. All thermodynamic and transport properties of air were obtained using the method of Hansen (Ref. C.2). Equilibrium thermodynamic properties of air which include its major components (O_2 , N_2 , O , N , O^+ , N^+ , e^-) were obtained in closed form from a set of approximate partition functions. The partition functions and thermodynamic relations were programed such that the total enthalpy, entropy, speed of sound, average molecular weight, heat capacity and species concentration can be found for a given temperature and pressure. The calculation of transport properties by Hansen's method is based on simple kinetic theory of hard spheres. The viscosity is a function of species density, mean velocity and mean free path. The thermal conductivity is computed accounting for energy transfer by molecular collision and for energy transfer by specie diffusion.

A boundary layer transition criterion which is simple and appropriate for design work was used. The criterion can be stated as:

Transition Criterion	}	Laminar if $Re_{\omega d} < 100000$
		Transitional if $100000 < Re_{\omega d} < 200000$
		Turbulent if $Re_{\omega d} > 200000$

The atmospheric properties, air thermodynamic and transport properties and transition criterion were applied to all geometries.

CYLINDER GEOMETRY

The specific calculations procedure for the cylinder is determined by the angle of attack and the transition criterion. The following bar chart gives reference to the heating methods used.

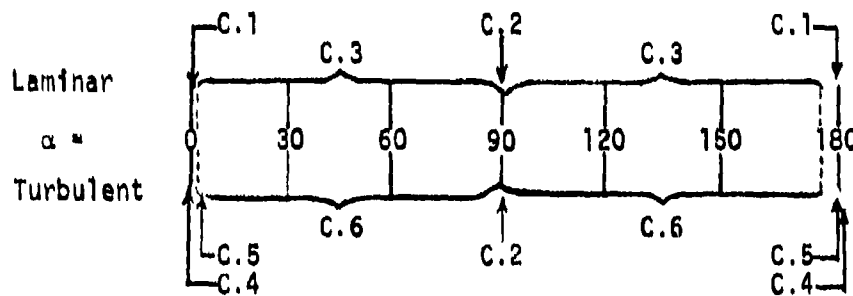


Fig. C.1 Stagnation Line Cylinder Heating Methods

The numbers in Fig. C.1 refer to tables which define the heating method.

All the methods require a recovery enthalpy calculation. The recovery factor is computed using the Newtonian type theory presented in Table C.7.

In order to utilize these heating methods the local flow conditions are required. The following steps are used to compute the flowfield.

Zero Angle of Attack Flow Fields

1. Normal shock calculation is made.
2. Total post shock conditions are computed.
3. Using the stagnation entropy, the flow is expanded to free stream pressure.
4. Edge conditions are determined from the stagnation entropy and edge pressure.

Angle of Attack Flow Fields

If the angle of attack plus the body angle is greater than 1.0 degrees an angle of attack calculation is made using the following steps:

1. An oblique shock calculation is made for a shock parallel to the local body angle if the normal component of free stream Mach number is greater than one.
2. If the normal component of Mach number is less than one, the edge enthalpy and pressure are computed by

$$\text{Edge enthalpy } h_e = h_\infty + U_\infty^2 n / 2gJ$$

$$\text{Edge Pressure } P_e = P_\infty (1 + .2M_\infty^2 n)^{3.5}$$

where the subscript n means normal component. Based on these two properties the remaining edge conditions are computed.

3. If an oblique shock calculation was made (step 1), the edge conditions are computed by isentropically compressing the normal component of velocity

$$\text{Edge enthalpy } S_e = S_\delta$$

$$\text{Edge enthalpy } h_e = h_\delta + U_\delta^2 n / 2gJ$$

δ = post shock

Typical results using the preceding heating methods and flow field methods are compared with experimental data in Fig. C.1.

Heating Distributions

In order to compute the heat transfer coefficient distribution for a tumbling or rolling case a method based on data was used. This distribution is given in Table C.8. Thus with the stagnation line value from the previous methods and the local to stagnation line heat transfer coefficient ratio, the local value can be obtained. The heating is then computed using

$$q = h(H_r - H_w)$$

where

q = local heating rate
 h = local heat transfer coefficient
 H_r = local recovery enthalpy
 H_w = wall enthalpy

BASE GEOMETRY

The base geometry was approximated as a flat face of a right circular cylinder. The specific calculation procedure for the base is determined by the angle of attack and transition criterion and is shown pictorially below:

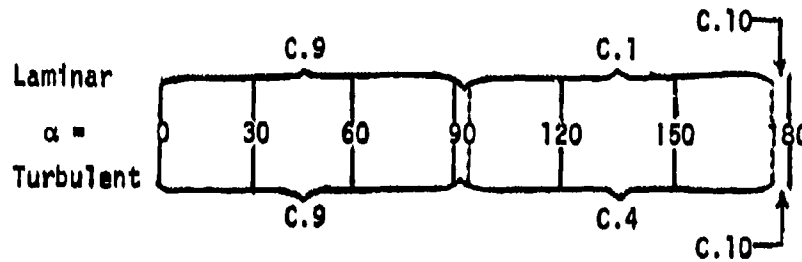


Fig. C.3 Base Flow Heating Methods

The flow field calculations for the different heating methods were made as described below:

Flow Fields for $\alpha < 95^\circ$ and $\alpha > 175^\circ$

1. Normal shock calculation is made.
2. Total post shock calculations are computed and used as edge conditions

Flow Fields for $95^\circ < \alpha < 175^\circ$

1. An oblique shock calculation is made for a shock parallel to the base surface if the normal component of free stream Mach number is greater than 1.0.
2. If the normal component of Mach number is less than one, the edge enthalpy and pressure are computed by

$$\text{Edge enthalpy } h_e = h_w + (u_w^2)_n / 2g_c$$

$$\text{Edge pressure } P_e = P_w (1 + .2M_w^2)_n^{3.5}$$

where the subscript n means normal component. Based on these two properties the remaining edge conditions are computed.

3. If an oblique shock calculation was made (step 1), the edge conditions are computed by isentropically compressing the normal component of velocity

The heating is computed to the center of the base and assumed to be constant over the entire base.

CONE GEOMETRY

A separate cone calculation methodology was not required since the cone heating may be related to cylinder calculations. The Stanton number data and theory presented by Ref.C.3, shown in Fig. 3, demonstrates that swept cylinder heating theory can be used for cone heating calculations. The heating rate for a cone related to the cylinder is simply a function of the radius ratio.

$$\frac{q_{\text{cone}}}{q_{\text{cyl}}} = \left(\frac{R_{\text{cyl}}}{R_{\text{cone}}} \right)^a$$

$$a = 0.5 \text{ laminar}$$

$$a = 0.2 \text{ Turbulent}$$

The local cone radius is used.

All of the heating calculations for this report were made using reference conditions. These are

$$\text{Surface Temperature} = 660^\circ\text{R}$$

$$\text{Cylinder Diameter} = 24 \text{ inches}$$

Procedures are described in the main text to adjust for diameter and surface temperature effects on heating rates and load.

Table C.1

ECKERT'S LAMINAR FLAT PLATE HEATING METHOD

Eckert's laminar flat plate heating relation can be expressed as:

$$h = 0.332 \frac{g_c}{(P_e^*)^{2/3}} \frac{\rho^* u_e}{\sqrt{R_e^*/\tau_m}} \quad (\text{lbm/ft}^2\text{sec})$$

where

$$R_e^* = \frac{\rho^* u_e x}{\mu^*} \quad \text{Reynolds no. evaluated at reference conditions}$$

The reference conditions are obtained from the reference enthalpy

$$H^* = H_e + 0.5 (H_w - H_e) + 0.22 (H_{aw} - H_e)$$

and edge pressure. Other reference properties are evaluated as:

$$\rho^* = f(H^*, P_e)$$

$$\mu^* = f(H^*, P_e)$$

For geometries other than a flat plate, the Mangler transformation may be evaluated as:

$$\begin{aligned} \tau_m &= 1 \quad \text{Flat Plate} \\ &= 2 \quad \text{Cylinder} \\ &= 3 \quad \text{Cone} \end{aligned}$$

Nomenclature

g_c	=	32.174 lbm/slug
h	=	Heat Transfer Coefficient (lbm/ft ² sec)
H_e	=	Edge Enthalpy (Btu/lbm)
H_{aw}	=	Adiabatic Wall Enthalpy (Btu/lbm)
H_w	=	Wall Enthalpy (Btu/lbm)
P_e	=	Edge Pressure (atm.)
u_e	=	Edge Velocity (ft/sec)
x	=	Surface Distance From Origin to Point of Interest
ρ^*	=	Reference Density
μ^*	=	Reference Viscosity
τ_m	=	Mangler Transformation

Table C.2
STAGNATION POINT HEATING

Stagnation point heating is based on the theory of Fay and Riddell (Ref. T1).

$$q = \frac{N_u}{\sqrt{Re}} \sqrt{g_c \rho_w \mu_w} \left(\frac{dU_e}{dx} \right) \frac{(H_t - H_w)}{Pr_w}$$

where

$$\frac{N_u}{\sqrt{Re}} = 0.76 Pr_w^{0.4} \left(\frac{\rho_t \mu_t}{\rho_w \mu_w} \right)^{0.4} \left\{ 1 + (Le^{.52} - 1) \frac{H_d}{H_t} \right\}$$

$$\left(\frac{dU_e}{dx} \right) = \frac{1}{R} \sqrt{2g_c \frac{(P_t - P_\infty)}{\rho_t}} \text{ for a sphere and } M_\infty > 1.22$$

$$= \frac{1}{2R} \sqrt{2g_c \frac{(P_t - P_\infty)}{\rho_t}} \text{ for a cylinder and } M_\infty > 1.12$$

$$= \frac{U_\infty}{R} (1.5 - 0.378M_\infty^2 - 0.02625 M_\infty^4) \text{ for a sphere and } M_\infty \leq 1.22$$

$$= \frac{U_\infty}{R} (2.0 - 0.872M_\infty^2 - 0.328M_\infty^4) \text{ for a cylinder and } M_\infty \leq 1.12$$

and the dissociation enthalpy

$$H_d = C_O h_O^\circ + C_N h_N^\circ$$

$$h_O^\circ = 6636.26 \text{ Btu/Lbm}$$

$$h_N^\circ = 14456.53 \text{ Btu/Lbm}$$

Nomenclature

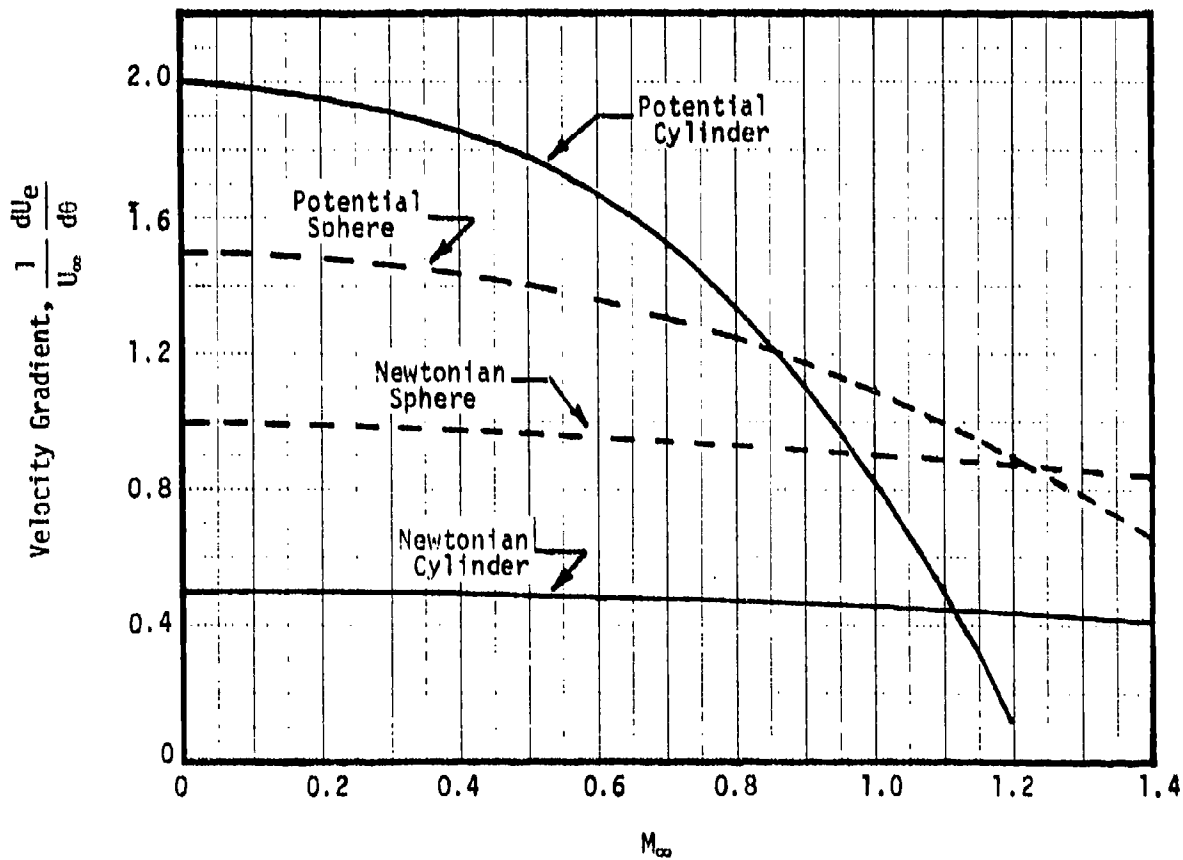
q	=	Heating Rate (Btu/ft ² sec.)
q _c	=	1 (slug ft./lb _f sec. ²)
g	=	32.174 (Lbm/slug)
ρ	=	Density (slug/ft. ³)
μ	=	Viscosity (Lb _f sec/ft ²)
U	=	Velocity (ft./sec.)
P	=	Pressure (Lb _f /ft. ²)
H	=	Enthalpy (Btu/lbm)

Table C.2 (Cont.)

- L_e = Lewis Number
 H_d = Dissociation enthalpy of air (Btu/Lbm)
 C_i = Mass fraction of species i ($i = O$, oxygen and $i = N$, nitrogen)
 R = Nose radius (ft.)
 P_r = Prandtl Number

Subscripts

- e = Edge
 t = Stagnation (post shock)
 w = Wall
 ∞ = Free stream

References

- T1. Fay, J. A. and Riddell, F. R., "Theory of Stagnation Point Heat Transfer in Dissociated Air", J. Aeronaut. Sci., Vol. 25, No. 2, Feb. 1958, pp. 78-85, 121.

Table C.3

LAMINAR STAGNATION LINE HEATING TO YAWED CYLINDERS

The laminar stagnation line heating by the method of Sayano and Greenwald (Ref. T1) is expressed by the following empirical relation.

$$h/h_{\Lambda=0} = \cos^{1.5} \Lambda + (q_{fp}/q_{\Lambda=0}) \sin^2 \Lambda$$

where

$$h_{\Lambda=0} = 0.707 h_{FR}$$

Nomenclature

- h = Heat Transfer Coefficient
- h_{FR} = Fay and Riddell Spherical Stagnation Point Heat Transfer Coefficient
- q_{fp} = Flat Plate Heating Rate
- q = Cylinder Heating Rate at Zero Sweep
- Λ = Sweep Angle

Reference

- T1 Sayano, S. and G. F. Greenwald, "Approximate Method for Calculating Heat Transfer to Yawed Cylinders in Laminar Flow", JSR Vol. 10, No. 2, Feb. 1973.
-

Table C.4

SPALDING-CHI METHOD MODIFIED FOR REAL GAS HEAT TRANSFER
FOR TURBULENT BOUNDARY LAYER FLOW

- (1) Spalding-Chi define F_c , F_{R_0} , F_{R_s} (Ref.T1) which are functions of Mach Number and Temperature alone such that

$$1/2 C_f F_c = \psi_0(F_{R_0} RE_0) = \psi_s(F_{R_s} RE_s)$$

$$(2) F_c = \frac{1}{Z_e T_e} \left[\int_0^1 \left(\frac{1}{ZT} \right)^{1/2} d \left(\frac{u}{u_e} \right) \right]^{-2}$$

$$\text{Where } Z, (T) = f(H, P_e) \text{ \& } H = H_w + (H_{aw} - H_w) \left(\frac{u}{u_e} \right) - (H_{aw} - H_e) \left(\frac{u}{u_e} \right)^2$$

$$(3) F_{R_0} = \left(\frac{H_{aw}}{H_w} \right)^{0.772} \left(\frac{H_e}{H_w} \right)^{0.702} \quad (\text{Ref.T2})$$

$$(4) F_{R_s} = F_{R_0} / F_c$$

$$(5) C_{f1} = 1/2 \exp \left\{ \sum_{i=1}^{10} g(i) \left[\ln \left(F_{R_s} \frac{RE_s}{\tau_{III}} \right) \right]^{i-1} \right\} = 1/2 C_f F_c$$

Where

$g(1) = 9.2808635$
$g(2) = -4.7340248$
$g(3) = 6.6858663 \quad 10^{-1}$
$g(4) = -4.1876614 \quad 10^{-2}$
$g(5) = -5.5054577 \quad 10^{-4}$
$g(6) = 2.8367291 \quad 10^{-4}$
$g(7) = -2.1249608 \quad 10^{-5}$
$g(8) = 8.0162000 \quad 10^{-7}$
$g(9) = -1.5900985 \quad 10^{-8}$
$g(10) = 1.3236350 \quad 10^{-10}$

$$RE_s = \frac{\rho_e u_e^s}{\mu_e}$$

$\tau_{III} = \text{Mangler Transformation (Ref.T3)}$

Table C.4 (Cont. 1)

Nomenclature

C_f	Skin Friction Coefficient
h_{TURB}	Heat Transfer Coefficient For Turbulent Flow
H	Enthalpy
P	Pressure
P_r	Prandtl Number
Re_θ, Re_s	Local Reynolds Number Based on Momentum Thickness θ and Characteristic Lengths Respectively
S	Inverse of Von Karman Reynolds Analogy Factor
St	Stanton Number
T	Temperature
u	Velocity
Z	Compressibility
ρ	Density

Subscripts

aw	Recovery
e	Local
i	Incompressible
w	Wall

References

- T1. Spalding, D.B., and Chi, S.W., "The Drag of A Compressible Turbulent Boundary Layer on a Smooth Flat Plate With and Without Heat Transfer", Journal of Fluid Mechanics, Vol. 18, Part I, pp. 117-143, Jan. 1964.
- T2. Wallace, J.E., "Hypersonic Turbulent Boundary Layer Studies at Cold Wall Conditions", 1967 Heat Transfer and Fluid Mechanics Institute, La Jolla, CA June 1967.
- T3. Komar, J.J., "Improved Turbulent Skin-Friction Coefficient Predictions Utilizing the Spalding-Chi Method", Douglas Aircraft Company, Douglas Report DAC-59801, Nov. 1966.

Table C.5
 TURBULENT STAGNATION LINE HEATING
 NEAR $\alpha = 0$

Beckwith and Gallagher's stagnation line theory predicts zero heat transfer coefficients at an angle of attack of zero. In order to achieve a transition to more realistic value the following approximation for turbulent flow is used.

$0 \leq \alpha \leq 5 \text{ deg.}$

$$\beta = 18 (5 - \alpha)$$

$$h = h_{BG} + h_{\alpha = 0} \sin \beta$$

Nomenclature

- h - Heat transfer coefficient
 - $h_{\alpha = 0}$ - Heat transfer coefficient at $\alpha = 0$, computed using flat plate conditions processed by a normal shock and expanded to edge pressures.
 - α - Angle of attack
 - h_{BG} - Beckwith and Gallagher heat transfer coefficient
-
-

Table C.6

BECKWITH AND GALLAGHER TURBULENT REAL GAS
YAWED CYLINDER STAGNATION LINE HEATING

$$h_{SL} = \frac{0.0323}{Pr^{0.46667}} \left(\frac{u_{\infty} \sin \Lambda}{\mu_0} \right)^{0.5} (g\rho^* \mu^*)^{0.5} \left(\frac{du_e}{dx} \right)_{x=0}^{0.2} \quad (1)$$

$$\left(\frac{du_e}{dx} \right)_{x=0} = \frac{1.414}{R} \left(\frac{P_e - P_m}{P_e} \right)^{0.5} \quad (2)$$

g	32.174	Lbm/slug
h	Heat Transfer Coefficient	Lbm/ft ² sec
P	Pressure	Lbf/ft ²
Pr	Prandtl Number @ edge conditions	Dimensionless
R	Radius of Cylinder	Feet
u	Velocity	Ft/sec
x	Distance from Stagnation Line	Feet
Λ	Sweep Angle	Degrees
μ	Viscosity	Lbm/ft-sec
ρ	Density	Slugs/ft ³

Subscripts:

SL	Stagnation Line
e	Edge Conditions
o	Total

Superscript:

*	Evaluate at Eckert's Reference Enthalpy & edge Pressure
---	---

Reference:

1. Beckwith, I. E., and Gallagher, J. J., "Local Heat Transfer and Recovery Temperatures on a Yawed Cylinder at a Mach Number of 4.15 and High Reynolds Number, NASA TR R-104, 1961.

TABLE C.7
RECOVERY FACTOR DISTRIBUTION

The local recovery factor or recovery enthalpy is computed using the following Newtonian type of distribution (Ref. T1).

$$h_r = h_\infty + [r_L \sin^2 \alpha \cos^2 \theta + r_{\alpha=0} (\sin^2 \alpha \sin^2 \theta + \cos^2 \alpha)] U_\infty^2 / 2gJ$$

where

$$r = r_{\alpha=0} = \left(\frac{(h_e - h_\infty) + P_r^{1/n} U_e^2 / 2gJ}{U_\infty^2 / 2gJ} \right)_{\alpha=0}$$

$$r_L = 1.0 \text{ for } 0 \leq \theta \leq 90$$

$$r_L = \frac{(H_T - A_L^2 / 2gJ - h_\infty) + P_r^{1/n} A_L^2 / 2gJ}{U_\infty^2 / 2gJ}$$

A_L = Leaside speed of sound based on total temperature

$n = 2$ for laminar flow

$n = 3$ for turbulent flow

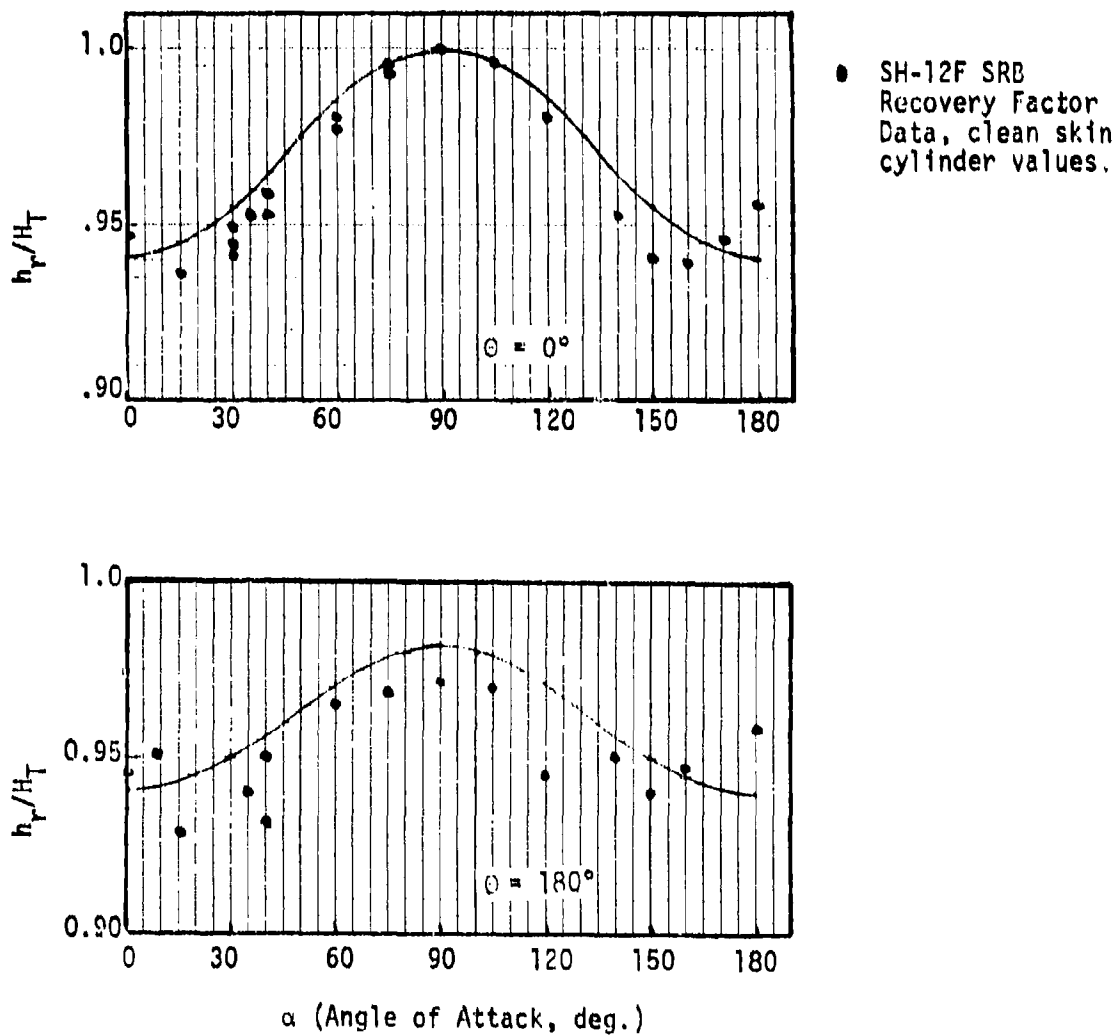
For subsonic flow $r_L = 1.0$ for all θ .

Nomenclature

- h_∞ = Free stream static enthalpy (Btu/lbm)
- h_r = Recovery enthalpy (Btu/lbm)
- H_T = Total enthalpy (Btu/lbm)
- U_∞ = Free stream velocity (ft./sec.)
- g = 32.174 lbm ft./lb_f sec
- J = 778.66 ft. lb_f/Btu
- r = Recovery factor 0.85 laminar flow
0.897 turbulent flow
- α = Angle of attack (degrees)
- θ = Angular position from stagnation line (degrees)

TABLE C.7 (cont.)

The following figures show a comparison of data and the preceding equation.



References

- 11 C. D. Engel, "Tumbling Entry Heating Programs - Teheat and Bentry Users' Manual," RTR 011C-1, NAS8-21810, July 1976.

Table C.8
TURBULENT CIRCUMFERENTIAL HEATING
DISTRIBUTION AROUND A CYLINDER

The circumferential heating distribution around a right circular cylinder has been correlated (Ref. T1) using the following equations

$$\frac{h_U}{h_{s1}} = 1.0 + \frac{(1-K_2)}{2} \cos \Delta + \frac{(K_2 - 2K_1 + 1)}{4} \cos 2\Delta + (2K_1 + K_2 - 3)/4$$

where

$$K_1 = e^{-\alpha} \cosh^2 (3.98 \alpha)$$

$$K_2 = e^{-\alpha} \cosh (\alpha) \text{ for } 0 < \alpha < 0.785398$$

$$K_3 = e^{-\alpha} \cosh (\alpha) [1 + 11.8 / (1 + e^{-10(\alpha - 1.309)})]$$

for $0.785398 < \alpha < \pi/2$

$$h_U = \text{Undisturbed heat transfer coefficient}$$

$$h_{s1} = \text{Stagnation line heat transfer coefficient}$$

$$\alpha = \text{Angle of attack resolved into 90 degrees (radians)}$$

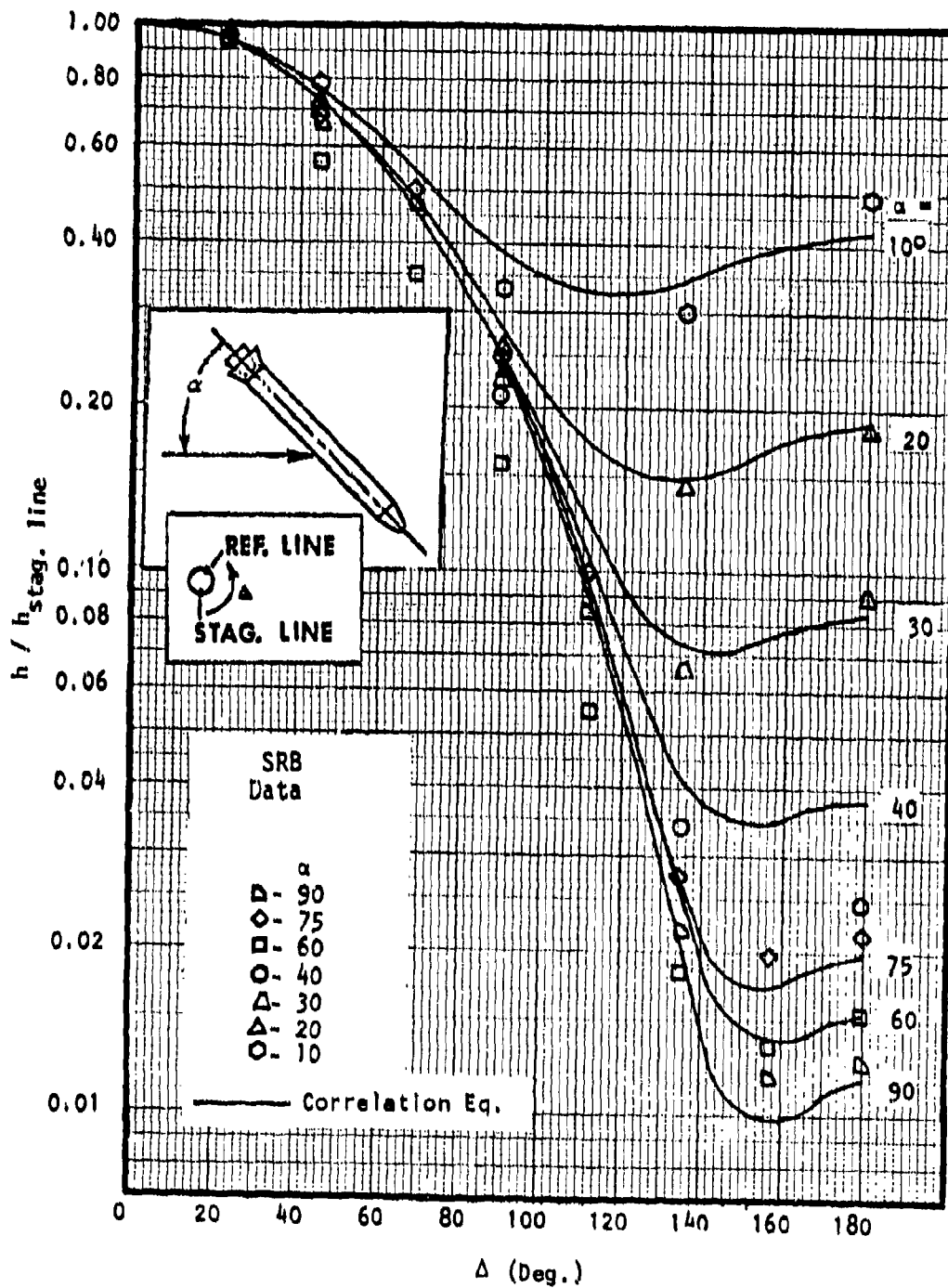
$$\Delta = \text{Circumferential angle from stagnation line resolved into 180 degrees}$$

A comparison of the correlation with data is given in the following figure.

References

- T1. C. D. Engel, J. V. McAnally, B. M. Levine, "SRB Data Book Procedure Documentation", RM 020-2, NAS8-31360, March 1976.

Table C.8 (Cont.)



Comparison of Correlation Equation and SH-12F Test Data for Undisturbed Heating ($M_\infty = 3.75$, $Re_\infty/ft = 3.5 \times 10^6$, $D = 4.38$ in).

TABLE C.9
LEEWARD BASE FLOW

The heating to the base of a cylinder when the base face is leeward is approximated by:

$$q = h (H_{aw} - H_w)$$

where

$$h = 0.05 h_{FR}$$

h_{FR} = Hemispherical stagnation point heating coefficient for cylinder radius (Table C.2)

$$H_{aw} = 0.85 H_t$$

H_w = Wall enthalpy

TABLE C.10
STAGNATION BASE FLOW

The heating to the flat face of right circular cylinder is determined from the theory of Fay and Riddell together with a velocity gradient modification from Boison and Curtiss (Ref. T.1). The heat transfer coefficient is expressed as

$$h = h_{FR} (0.46628) e^{0.4471 M_{\infty}^2}$$

where

h_{FR} = Hemispherical stagnation point heating coefficient for the cylinder radius (Table C.2)

M_{∞} = Free stream Mach number

Reference

- T1. J. C. Boison, H. A. Curtiss, "An Experimental Investigation of Blunt Body Stagnation Point Velocity Gradient," ARS Journal, pp. 130-135, February 1959.
-
-

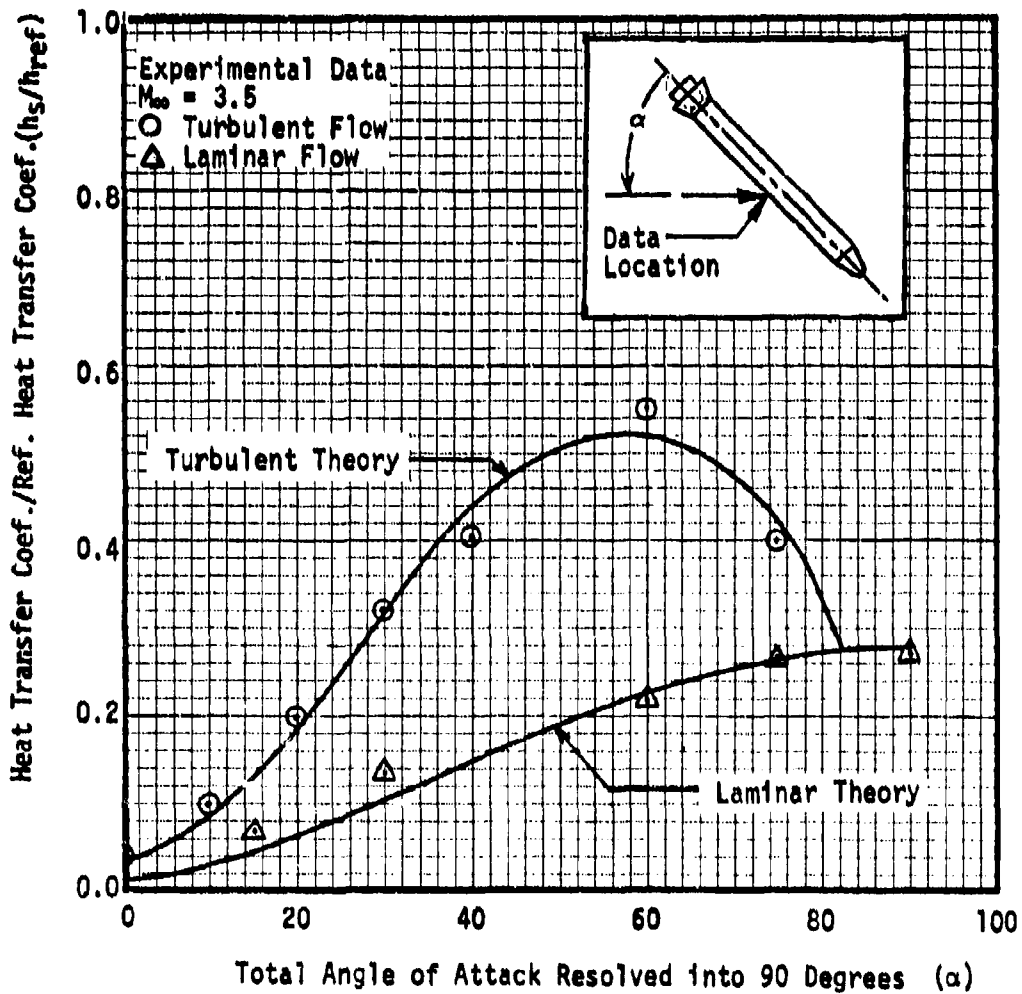


Fig. C.2 Comparison of Laminar and Turbulent Stagnation Line Theory and Data for the Cylindrical Section of a Cone-Cylinder-Flare

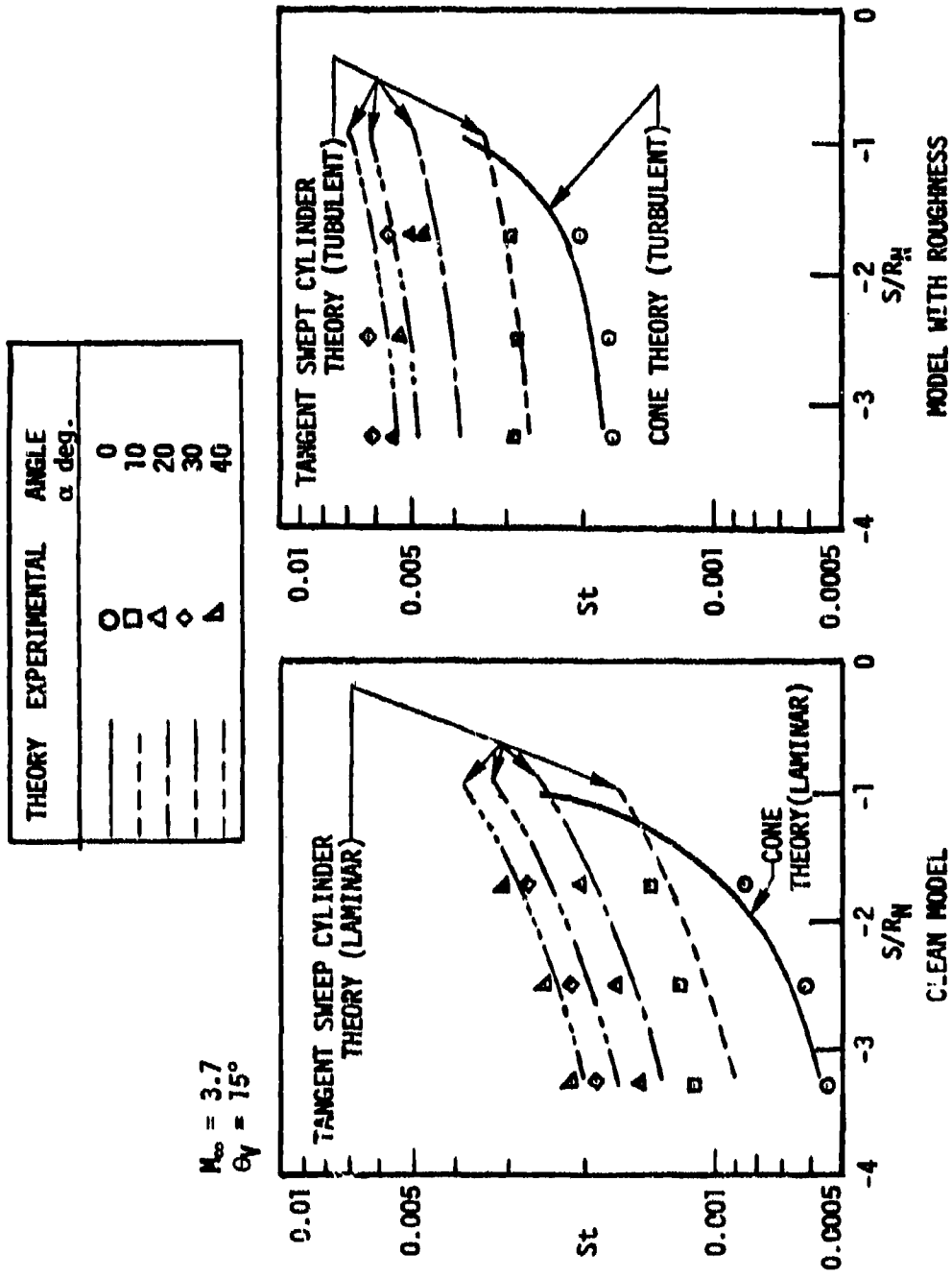


Fig. C.3 Comparison with Theory of Measured Heating Distributions on Half-Cone Surface. (Stallings, Wright, and Collins)

REFERENCES

- C.1 Engel, Carl D., "Tumbling Entry Heating Programs - Teheat and Bentry Users Manual", RTR 011C-1, REMTECH, Inc., July, 1976
- C.2 Hansen, Frederick C., "Approximations for the Thermodynamic and Transport Properties of High-Temperature Air", Technical Report R-50, National Aeronautics and Space Administration, 1959.
- C.3 Nestler, D. E., "Hypersonic Boundary Layers and Selected Heat Flux Problems", General Electric, Philadelphia, Pa., April, 1970.

APPENDIX D
CONDUCTION HEAT TRANSFER ANALYSIS

The first approach to predicting the surface temperature for the cases of interest was to use a heat conduction program which accounted for all possible circumstances such as variable material properties, radiation at the interior and exterior surfaces, transient effects, and variable convective heat transfer coefficients. Reference D.1 documents such a program which uses a finite difference scheme to solve the heat transfer equations:

$$h_e (t_{Re} - t_e) - \epsilon_e \sigma (t_e^4 - t_{ae}^4) = - \left(k \frac{dt}{dx} \right)_e \text{ (exterior surface)} \quad (D1)$$

$$\left(k \frac{\partial t}{\partial x} \right)_e = \left(k \frac{\partial t}{\partial x} \right) \text{ (steady-state) (internal point)} \quad (D2)$$

$$\rho c \frac{\partial t}{\partial \theta} = \frac{\partial}{\partial x} \left(k \frac{\partial t}{\partial x} \right) \text{ (transient) (internal point)} \quad (D3)$$

$$h_i (t_{Ri} - t_i) - \epsilon_i \sigma (t_i^4 - t_{ai}^4) = - \left(k \frac{dt}{dx} \right)_i \text{ (interior surface)} \quad (D4)$$

where

- h - local convective heat transfer coefficient
- t_R - recovery temperature
- t - local material temperature
- ϵ - emissivity
- σ - the Stefan-Boltzmann constant
- t_a - temperature to which the point radiates
- k - conductivity
- x - internal distance from the surface
- ρ - density
- c - specific heat
- θ - time
- i, e - interior and exterior surface

The skin is approximated by an infinite plate and equations D1 - D4 have only one space dimension -x.

Preliminary efforts dealt with choosing finite increments of space and time which would give adequate solutions without using computer time unnecessarily. It was found that use of four internal nodes along with the interior and exterior node gave results almost identical to those achieved using 8 or more internal

nodes. Also time steps of one second produced similar results when compared to more rigorous time steps of 0.5 and 0.1 seconds.

After several test cases were run, it was found that the emissivity of aluminum, $\epsilon = 0.15$, was low enough that radiation losses were very small. It was also found that the temperature gradient through the skin was very small. These facts led to a considerably simplified equation which assumed no radiative heat transfer and no internal resistance to heat flow (high conductivity):

$$q = c\rho V \frac{dt}{d\theta} = h_e A_e (t_R - t) \quad (D5)$$

where

q - heat transfer

V - volume

A - area

For the one-dimensional case, V/A is equal to $A\delta/A$ or δ , the thickness.

Solution of the above equation yields:

$$\frac{t - t_R}{t_0 - t_R} = e^{-Nu\theta} \quad Nu = \frac{h\delta}{k} \quad \theta = \frac{k\theta}{c\rho\delta^2} \quad t_0 = \text{temperature } \theta = 0 \quad (D6)$$

or

$$t = e^{-Nu\theta} (t_1 - t_R) + t_R \quad (D7)$$

This equation is readily solved using a calculator.

To compare the two methods of solution three cases (Table D1) were run using 1/4 inch thick aluminum skin. Each method assumes that h and t_R are constant during the time increment involved. The second method calculated the average h and t_R for the time step and uses these values. The first method integrates h and t_R across the step. A listing of the program used to solve equation D7 with a HP-97 calculator is shown in Table D2.

The results are compared in Fig. D1. The plots for all practical purposes coincide proving that the assumption of negligible internal resistance was correct for 1/4 inch (and therefore thinner) skins.

The effects of thickness on the accuracy of the second method can be seen in Fig. D2 where both methods were used to predict the surface temperature for the worst case (Case 3) when the skin thickness is 3/8 inch. The second method does not respond as quickly as the more correct first method, and it is anticipated that thicker skins would have to be analyzed using the time-consuming first method.

The effects of thickness on the peak surface temperature for the three cases are shown in Fig. D3. As would be expected, the thicker skins provide additional heat sinking so the peak temperature is significantly lowered.

In the second method of calculation it was assumed that the response of the skin to each input of heat during the time step would be slow enough that the skin would not come to steady state before a new time increment and thus a new heat transfer rate began. To check this, an extremely simplified third method was investigated which assumed steady state response at each time step using the equation:

$$q = c_p V (t_s - t_0) \quad (D8)$$

where, t_s is the skin temperature resulting from the cumulative heat transferred, q , to the skin volume, V . The skin volume would be $A\delta$ where A is equal to unity for the one-dimensional assumption made throughout the analysis. Therefore the temperature at anytime is:

$$t_s = t_0 + \frac{q}{c_p \delta} \quad (D9)$$

To compare the first and third method, values of q were obtained using BENTRY (Ref. C.1, Appendix C) which assumed a constant 660°F surface temperature. These values and values of c and ρ at 200°C (1118°R) were used to calculate the peak temperature for the sample cases. The results are shown in Fig. D4 and indicate an almost exact correspondence. Considering that the BENTRY q calculation assumed a constant temperature it was concluded that q had little dependence on surface temperature. It was also concluded that transient conduction effects were negligible.

The surface temperature calculation scheme finally used was a form of the third method. First, using the temperature at the beginning of the trajectory time step, q was calculated for each step. Second, the temperature at the end of each time step (which was also the beginning of the next step) was calculated using equation D9. This process continued until the skin began to cool (negative q) - the last calculated skin temperature was therefore the peak. After several trials were made, it was found that a variable specific heat was needed for accuracy and the equation:

$$c = 0.08697 + 3.586 \times 10^{-4}t - 2.803 \times 10^{-7}t^2 + 8.23 \times 10^{-11}t^3 \quad (\text{D10})$$

evaluated at the beginning of each time step, was used in all subsequent calculations.

The simple method of calculation used is justified by comparison with the rigorous method. The method compares well because thin aluminum skins react quickly to the input heat transfer rates. Use of materials with significantly lower conductivities or thicker skins would invalidate the assumptions implicit in this method, and a more sophisticated approach would have to be used.

REFERENCE

- D.1 Beck, David F., "A Finite Difference Solution to the Problem of One-Dimensional Heat Conduction with Variable Material Properties," Internal Report, Unsteady Aerodynamics and Thermal Environment Branch, Systems Dynamics Laboratory, Marshall Space Flight Center, NASA, June 1976.

TABLE D.1
 CASES USED FOR CONDUCTION HEAT TRANSFER ANALYSIS
 (Cone-Cylinder Configuration with L/D = 4.0)

Case 1				Case 2				Case 3			
75 Mile Initial Release Altitude		200 Mile Initial Release Altitude		350 Mile Initial Release Altitude		75 Mile Initial Release Altitude		200 Mile Initial Release Altitude		350 Mile Initial Release Altitude	
Time from Significant Heating(sec)	$\frac{h \times 10^6}{(\text{ft}^2 \cdot \text{sec} \cdot ^\circ\text{R})}$	t_{re} ($^\circ\text{R}$)	Time from Significant Heating(sec)	$\frac{h \times 10^6}{(\text{ft}^2 \cdot \text{sec} \cdot ^\circ\text{R})}$	t_{re} ($^\circ\text{R}$)	Time from Significant Heating(sec)	$\frac{h \times 10^6}{(\text{ft}^2 \cdot \text{sec} \cdot ^\circ\text{R})}$	t_{re} ($^\circ\text{R}$)	Time from Significant Heating(sec)	$\frac{h \times 10^6}{(\text{ft}^2 \cdot \text{sec} \cdot ^\circ\text{R})}$	t_{re} ($^\circ\text{R}$)
0	1.00	700	0	54.55	4136	0	54.55	4136	0	65.40	7815
10	1.50	650	2	82.08	4193	2	82.08	4193	2	112.90	7889
20	3.00	500	4	119.50	4254	4	119.50	4254	4	193.20	7982
30	4.00	680	6	176.60	4325	6	176.60	4325	6	318.10	8090
35	5.68	750	8	252.8	4412	8	252.8	4412	8	490.6	8225
40	9.32	766	10	346.0	4515	10	346.0	4515	10	738.1	8353
45	14.16	814	12	461.2	4618	12	461.2	4618	12	1074.0	8463
50	21.06	862	14	614.0	4718	14	614.0	4718	14	1542.0	8525
55	32.80	924	16	806.6	4805	16	806.6	4805	16	2203.0	8514
60	51.83	987	18	1046.0	4873	18	1046.0	4873	18	3257.0	8340
65	79.18	1061	20	1395.0	4914	20	1395.0	4914	20	4795.0	7853
70	116.80	1175	22	1867.0	4907	22	1867.0	4907	22	6805.0	6783
75	177.0	1300	24	2488.0	4829	24	2488.0	4829	24	8339.0	5053
80	258.2	1424	26	3306.0	4633	26	3306.0	4633	26	8506.0	3161
85	375.2	1540	28	4448.0	4272	28	4448.0	4272	28	7296.0	1810
90	548.2	1638	30	5473.0	3669	30	5473.0	3669	30	5759.0	1101
95	815.6	1712	32	6724.0	2881	32	6724.0	2881	32	4469.0	764
100	1255.0	1737	34	6299.0	2071	34	6299.0	2071	34	3684.0	599
105	1945.0	1697	36	5729.0	1430	36	5729.0	1430	36	3339.0	525
110	2811.0	1529	38	4798.0	1011	38	4798.0	1011	38	3082.0	474
115	3374.0	1178	40	4067.0	759	40	4067.0	759			
120	3338.0	835	42	3628.0	631	42	3628.0	631			
125	2988.0	618	44	3205.0	538	44	3205.0	538			
130	2772.0	502	46	3010.0	490	46	3010.0	490			

TABLE D2

PROGRAM FOR CALCULATING SOLUTIONS ON HP-97 CALCULATOR
(Negligible Internal Resistance Assumed)

Initialization

Store $\Delta\theta$ \longrightarrow
 Store h_1 \longrightarrow
 Store t_{R1} \longrightarrow

Computation

$\frac{1}{cp\delta}$ \longrightarrow

$\frac{\Delta\theta}{cp\delta}$ \longrightarrow

t_0 \longrightarrow

Enter with t_j ($j=1; t_j-t_0$)* \longrightarrow
 Recall h_1 \longrightarrow
 Enter h_{j+1} , Enter t_{Rj+1} \longrightarrow

Average h for j^{th} time step, $\frac{h_j+h_{j+1}}{2}$ \longrightarrow

$Nu\theta$ \longrightarrow

$e^{-Nu\theta}$ \longrightarrow

Recall t_{Rj} \longrightarrow

Average t_R for j^{th} time step, $\frac{t_{Rj}+t_{Rj+1}}{2}$ \longrightarrow

$(t_j - t_R)$ \longrightarrow

$t_{j+1} = (t_j - t_R)e^{-Nu\theta} + t_R$ \longrightarrow

Go to label B with $t_j = t_{j+1}$ \longrightarrow

Finish

* Temp at beginning of j^{th} time step

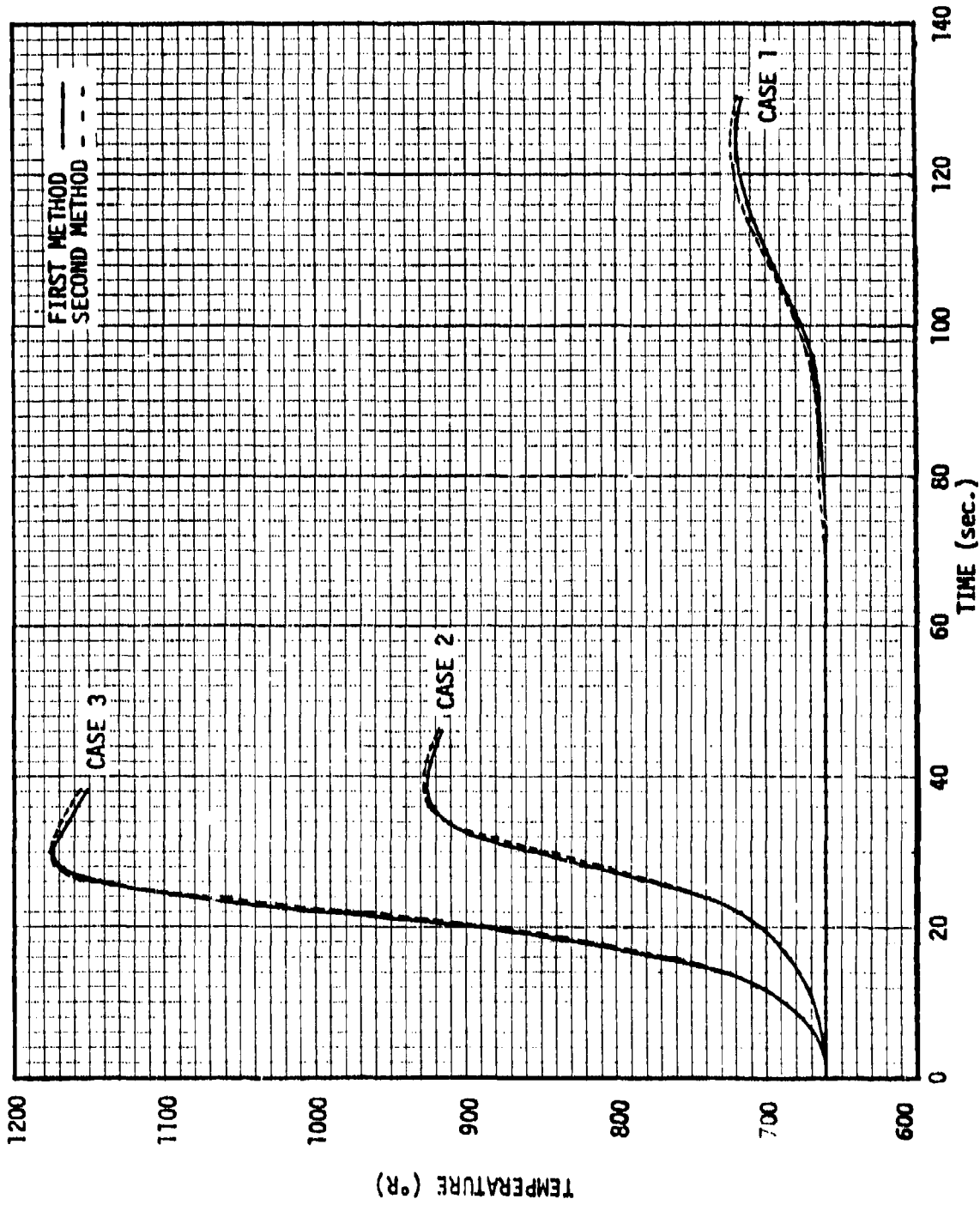


Fig. D1 Comparison of first and second method calculations for 1/4 inch aluminum skin.

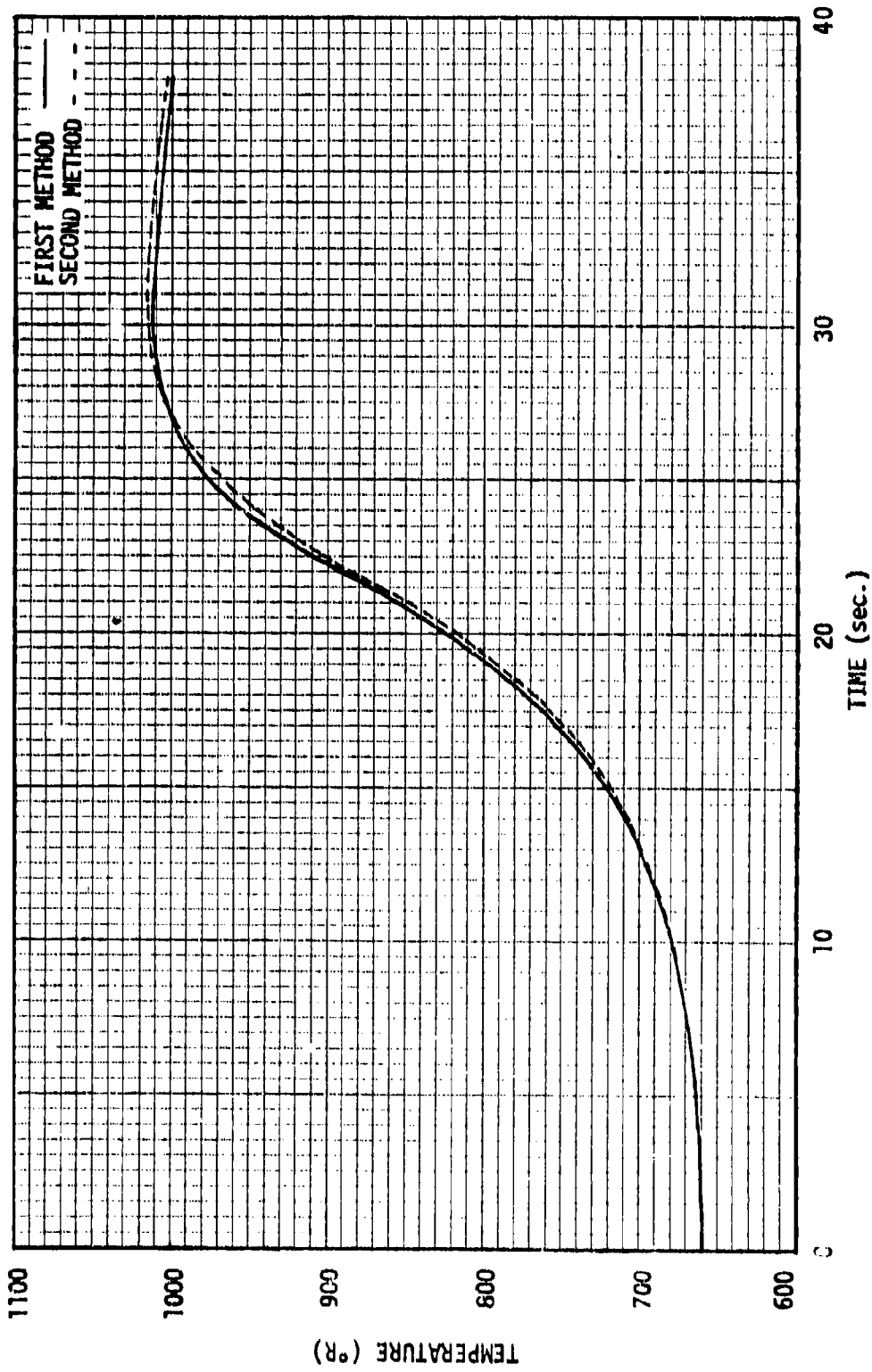


Fig. D2 Comparison of first and second method calculations for 3/8 inch aluminum skin.

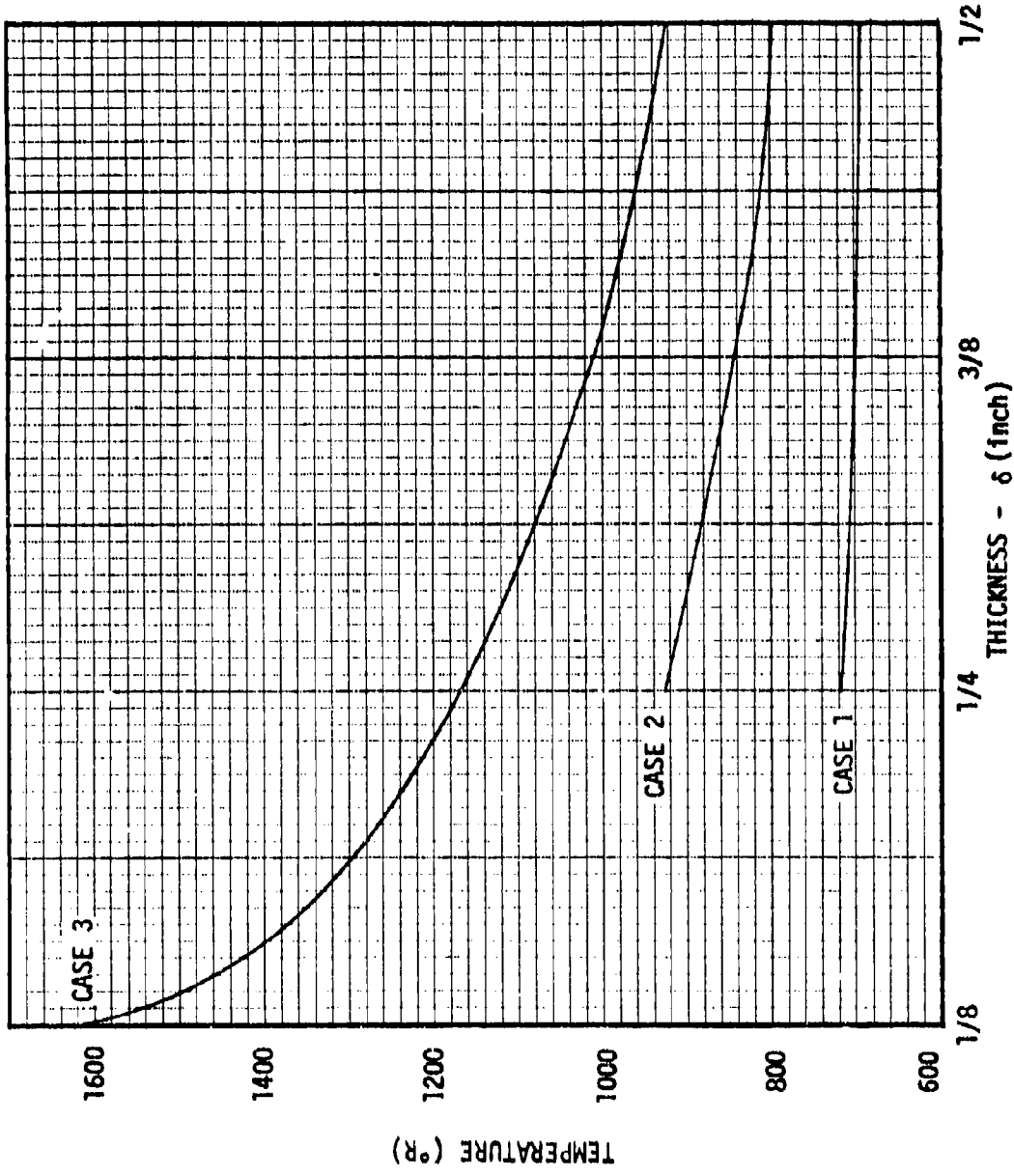


Fig. D3 Effects of thickness on peak surface temperature.

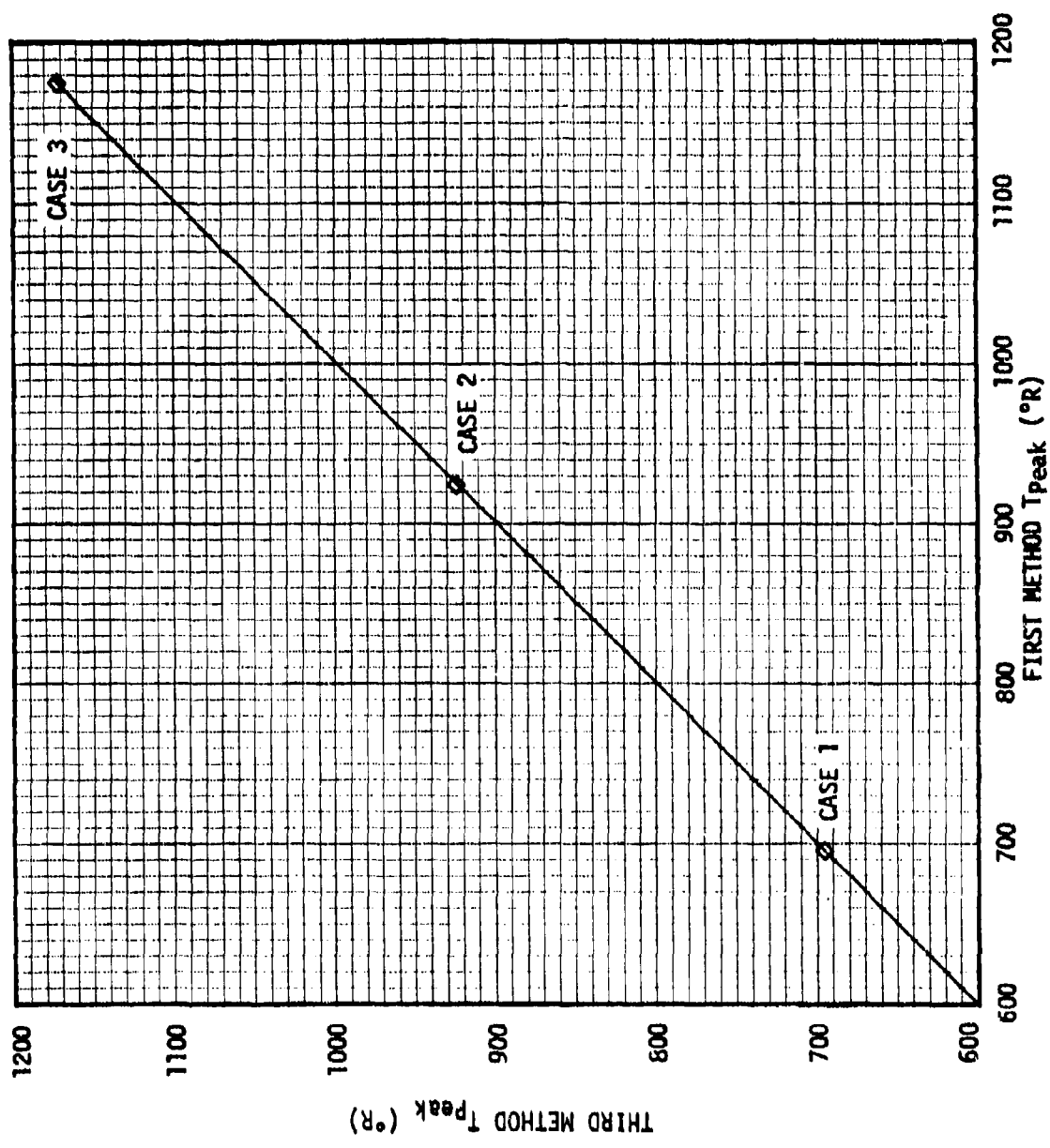


Fig. D4 Comparison of third and first method calculations for the peak surface temperature of 1/4 inch aluminum skin.